Higher order corrections to multijet production in $e(^+)e(^-)$annihilation

John M. Campbell

Higher Order Corrections to Multijet Production in e^+e^- Annihilation

A thesis presented for the degree of
Doctor of Philosophy
by

John M. Campbell

Physics Department
University of Durham
July 1998

Acknowledgements

First and foremost I would like to thank my supervisor, Nigel Glover, for making my Ph.D. such an enjoyable experience. Never knowing whether a collaborative discussion is going to be on the topic of physics or football has kept me on my toes for three years. I'm indebted to him for showing me the tricks of QCD and for steering me clear of the perils of Higgs physics.

To my fellow student collaborators, David Miller and Matthew Cullen, a special thank-you too. By being great friends also, you've made work a pleasure. David I am especially grateful to, for accelerating my learning and keeping me on the right track in my first year in Durham.

The friendly atmosphere on the third floor, due to staff and students both past and present, has made the group an easy one in which to work. There are names too numerous to mention who have illuminated the corridor, but particular thanks to my room-mates Matthias Heyssler, Matt Slater and Ricardo Alves, who have endured discussions in our office with patience. Of those that have now left Durham, a special thank-you to both Kirsten Miller and Claire Fynbo, for friendship and lively conversation both in the department and outside it.

Thanks also to all my friends in Durham who are untainted by the particle physics bug. For clearing my head of physics when it needed to be, thanks to my former house-mates Michelle Keen and Karen Lucas. The whole of the football crew deserve a special mention too, for providing a fun distraction from work and a backdrop to my dubious skills. You have all been a pleasure to play against – especially Amanda, whose close marking I have particularly appreciated over the last couple of months.

Lastly, thanks to my family – Mum, Dad, Peter and Nicola – for supporting me and for giving me the confidence to carry out this research.

Abstract

The analysis of hadronic events in high-energy electron-positron annihilation often relies upon the clustering of individual hadrons into energetic jets. By solving our theory of strong interactions, Quantum Chromodynamics (QCD) perturbatively, we may make theoretical predictions for these multijet configurations.

In this thesis we provide some calculational tools which are useful for evaluating terms in the perturbative series beyond leading order. These include a convenient method of dealing with one-loop integrals containing tensor denominators and universal factorization formulae for matrix elements where two particles are unresolved, which are relevant at the 2-loop (next-to-next-to-leading order) level. In particular we concentrate on the case of the next-to-leading order corrections to 4 jet production (and related processes) and apply our techniques to obtain explicit results in electron-positron annihilation which are then compared with experimental data.

Declaration

I declare that I have previously submitted no material in this thesis for a degree at this or any other university.

The research presented in this thesis has been carried out in collaboration with Dr. E. W. N. Glover, Dr. D. J. Miller and M. A. Cullen. The content of chapters 3–7 is based on the following publications:

- J.M. Campbell, E.W.N. Glover and D.J. Miller,
  'One-Loop Tensor Integrals in Dimensional Regularization',
  Nucl. Phys. **B498** (1997) 397 [hep-ph/9612413].

- J.M. Campbell, E.W.N. Glover and D.J. Miller,
  'The One-loop QCD Corrections for $\gamma^* \to q\bar{q}gg$',
  Phys. Lett. **B409** (1997) 503 [hep-ph/9706297].

- J.M. Campbell and E.W.N. Glover,
  'Double Unresolved Approximations to Multiparton Scattering Amplitudes',
  Nucl. Phys. **B527** (1998) 264 [hep-ph/9710255].

- J.M. Campbell, M.A. Cullen and E.W.N. Glover,
  'Four jet event shapes in electron-positron annihilation',
  in preparation.

Chapter 1

A Review of QCD

1.1 Introduction

The advent of the 1960's saw a revolution in the field of particle physics. Akin to the world of chemistry before Mendeleev, there had been a proliferation in the number of so-called elementary particles, with strongly interacting *hadrons* being produced in many high energy experiments worldwide. Lacking structure and thus predictive power, the subject was revitalized in 1964 by the independent proposals of Gell-Mann and Zweig [1].

The key idea was that hadrons were not themselves fundamental objects, but instead formed as bound states of *quarks*, spin 1/2 point-like particles. By building hadrons from a quark-antiquark pair (mesons, such as the pion) or three quarks (baryons, for example the proton) this new theory was able to bring order to the particle zoo. Just as was the case for its forerunner, this new 'Periodic Table' successfully predicted the existence of hitherto unknown elements of the theory such as the Ω^- baryon. Direct evidence for quarks was to come only a few years later with the deep inelastic scattering experiments of SLAC-MIT in 1968 [2].

Despite the apparent initial success of the quark model, it was still confronted with some puzzling problems, not all of which are well understood today. The most immediately apparent of these was the implicit violation of Fermi statistics. Some of the baryons appeared to be

symmetric under the interchange of two identical quarks, contradicting the anti-symmetric nature of the spin 1/2 constituents. The resolution of this dilemma involved the introduction of a further conserved quantum number – *colour*.

The assignment of colour states to individual quarks led to further postulates. By demanding that we only observe combinations of quarks that are colourless, we obtain strict experimental bounds. As well as predicting the known combinations in mesons and baryons, we also find that we should never discover lone quarks and that they are always *confined*. Although free quarks have never been observed experimentally, the precise mechanism for the confining process is not yet fully understood.

The implementation of the above qualitative description of quarks is of course far from straightforward. In particular, it is necessary to introduce the concept of a *quantum field theory* to describe the quark states, with the strong force mediated by bosonic particles (similar in many respects to the photon) called gluons. Both the quarks and gluons are intrinsically linked by their colour quantum numbers, which are described mathematically with reference to the group $SU(3)$. It is the theory based on this group, commonly referred to as *Quantum Chromodynamics* (QCD), that will be the subject of this thesis.

The aim of this chapter is to proceed from the basic Lagrangian density of QCD, in terms of quark and gluon fields, to a point where we may begin to consider real applications to experiment. In section 1.2 we present the quantum field theory of QCD by outlining the derivation of some of the terms in the Lagrangian and then describing how their interpretation leads to the Feynman rules. The theory that we build requires a further ingredient, that of renormalization. We discuss this, and its relation to the key QCD concepts of a running coupling and asymptotic freedom in section 1.3. In making predictions pertubatively, rather than solving the full theory, we necessarily introduce an ambiguity due to renormalization. The chapter concludes in section 1.4 with a discussion of the choice of resolution of this ambiguity, illustrated by the real example of the average value of 1-Thrust.

1.2 The Gauge Theory of QCD

In this thesis we shall be interested in the application of the perturbative $SU(3)$ model of QCD, working in particular from a direct application of the Feynman rules to physical processes. In this section we shall briefly sketch the development of QCD as a gauge theory, from the Lagrangian containing the fundamental fields through to its perturbative implementation in a diagrammatic form.

1.2.1 Quarks and Gluons

The Lagrangian density which describes the quark content of QCD is expressed simply as,

$$\mathcal{L}_{\text{quark}} = \sum_f \bar{q}_f (i\not{D} - m_f \mathbf{1}) q_f, \tag{1.1}$$

where $\not{a}$ is a shorthand notation for the contraction $a_\mu \gamma^\mu$ and the gamma matrices satisfy the Clifford algebra relation,

$$\{\gamma^\mu, \gamma^\nu\} = 2g^{\mu\nu}. \tag{1.2}$$

In equation (1.1), each flavour of quark is represented by a triplet of fields in colour space,

$$q_f(x) = \begin{pmatrix} q_f^{(r)}(x) \\ q_f^{(g)}(x) \\ q_f^{(b)}(x) \end{pmatrix},$$

with the conventional colour superscripts of r(ed), g(reen) and b(lue). The independence of our physical observations from these internal colour degrees of freedom means that we should be free to perform any rotation of the colour fields into one another. By insisting that this requirement be satisfied at every point separately, we obtain a *local* $SU(3)$ *symmetry.* Mathematically, this means that the Lagrangian density should be invariant under any local $SU(3)$ transformation $V(x)$, which can be parametrized by,

$$V(x) = \exp(i\theta(x) \cdot t),$$

where $\theta(x) \cdot t = \theta^a(x) t^a$ and t^a are the generators of $SU(3)$. Since $V(x)$ is a unitary matrix, it is clear that the generators t^a are traceless and they must also satisfy a set of commutation

relations,

$$[t^a, t^b] = if^{abc}t^c, \tag{1.3}$$

with the coefficients f^{abc} often referred to as the *structure constants* of the group. Under this $SU(3)$ rotation, the quark fields transform as,

$$q_f(x) \to V(x)q_f(x),$$

so unitarity ensures that the quark mass term $-\sum_f m_f \bar{q}_f q_f$ in the Lagrangian (1.1) is invariant. However, the kinetic term requires more subtlety and we must ensure that the *covariant derivative* D_μ transforms in the correct manner to cancel out the rotation of the quark fields,

$$D_\mu(x)q_f(x) \to V(x)D_\mu(x)q_f(x).$$

In order to do this, we must include a new vector *gauge* field A^a_μ (which will eventually represent the gluon degrees of freedom) in the definition of D_μ,

$$D_\mu \equiv \partial_\mu \mathbf{1} + igt^a A^a_\mu.$$

Having thus constructed a Lagrangian representing the matter content of QCD, we now turn to the dynamics of the gauge particles. We can implement a kinetic term by constructing the field strength tensor of the gluon field, $F^a_{\mu\nu}$, which is given by the commutator of two covariant derivatives,

$$\begin{aligned} [D_\mu, D_\nu]q_f(x) &= [\partial_\mu \mathbf{1} + igt \cdot A_\mu, \partial_\nu \mathbf{1} + igt \cdot A_\nu]q_f(x) \\ &\equiv igt \cdot F_{\mu\nu}\, q_f(x), \end{aligned}$$

where $F^a_{\mu\nu}$ is given by,

$$F^a_{\mu\nu} = \partial_\mu A^a_\nu - \partial_\nu A^a_\mu - g f^{abc} A^b_\mu A^c_\nu. \tag{1.4}$$

Note that this is exactly what we would have obtained in constructing a gauge theory for QED, except for the additional non-Abelian third term. We must now form a gauge-invariant quantity from the field strength, which is done by simply taking the trace [1] (with a convenient normalization) to give,

$$\mathcal{L}_{\text{gluon}} = -\frac{1}{4} F^{\mu\nu}_a F^a_{\mu\nu}. \tag{1.5}$$

[1] Unlike in QED, $F^a_{\mu\nu}$ is not itself gauge invariant because of the gluon self-interactions.

1.2.2 Gauges and Ghosts

In order to sensibly define our theory, it is also necessary to add two additional terms to the Lagrangian. The technical reasons for these terms are best understood by performing quantization in the functional integration approach and using the trick due to Faddeev and Popov[3].

Without the addition of the first term, propagation of the gluon field is not well-defined. To solve this ambiguity, we introduce a *gauge-fixing* term, which also contains a free (gauge) parameter ξ,

$$\mathcal{L}_{\text{gauge-fixing}} = -\frac{1}{2\xi}\left(\partial^\mu A^a_\mu\right)^2. \tag{1.6}$$

The parameter ξ specifies the covariant gauge to be used, although other choices of gauge fixing are possible (for example, axial gauges where one also specifies a vector n^μ). This is not specific to QCD: we would perform the same trick in QED for the photon. We may freely work in any gauge that we desire, with any physical observable necessarily being gauge-independent. Some choices of the gauge parameter ξ (and their common names) are,

$\xi = 0,$	$\xi = 1,$	$\xi = \infty.$
(Landau gauge)	(Feynman gauge)	(Unitary gauge)

The final ingredient is the *ghost* term, which represents unphysical degrees of freedom. Without this explicit term, longitudinal gluons would be allowed to propagate, violating our physical observations. To remedy this, we can introduce a complex ghost field η which couples to gluons via the term,

$$\mathcal{L}_{\text{ghost}} = \partial_\mu \eta^{a\dagger}(D^\mu_{bc}\eta^c). \tag{1.7}$$

It suffices to know that η is a scalar field, yet satisfies Fermi statistics, a further sign of its unphysical nature.

1.2.3 The QCD Lagrangian

To summarize, the full Lagrangian density for QCD is given by,

$$\mathcal{L}_{QCD} = \mathcal{L}_{\text{quark}} + \mathcal{L}_{\text{gluon}} + \mathcal{L}_{\text{gauge-fixing}} + \mathcal{L}_{\text{ghost}},$$

where the individual terms are given by equations (1.1), (1.5), (1.6) and (1.7) respectively. Having explicitly written down the Lagrangian, we now proceed to make some remarks about its significance.

- There is no possible gauge invariant mass term for the gluon, but quark masses can be naturally admitted.
- By examining equations (1.4) and (1.5) we see that the Lagrangian includes (non-Abelian) terms which are cubic and quartic in the gluon field A^a_μ. These would not be present in QED and lead to gluon self-interactions.
- To proceed to the calculation of physical observables, we divide the Lagrangian into a free piece $\mathcal{L}_0$ and an interacting one $\mathcal{L}_I$, and consider the action which is defined by,

  $$\mathcal{S} = i \int \mathcal{L}\, d^4x.$$

  The interacting theory can now be solved perturbatively as an expansion in the strong coupling g.
- A convenient book-keeping device for calculating the terms in the perturbative expansion is provided by the *Feynman rules*. One can calculate transition probabilities from initial to final states by summing over the set of topologically distinct diagrams which represents all possible interactions. In this language, terms in the free action $\mathcal{S}_0$ lead to propagators in momentum space (lines in a diagram), whilst $\mathcal{S}_I$ leads to interactions between quarks and gluons via momentum-conserving vertices.

1.2.4 The Feynman Rules

The full Feynman rules for QCD external lines, propagators and interactions are shown in Figure 1.1. In this thesis we shall always work with spin-summed and averaged matrix elements (for final and initial states respectively) so the extra spin label on the spinors and polarization vectors has been omitted.

In addition, when including diagrams with loops one must also:

- integrate over the loop momentum ℓ with the measure $\int d^4\ell/(2\pi)^4$;
- include a factor of -1 for each quark or ghost loop;
- multiply by a factor of $1/n!$ for a loop of n identical gluons.

By using these rules and summing over all the relevant diagrams, one obtains the amplitude $i\mathcal{M}$.

In order to calculate the squared matrix elements for a process, we also require the following sums,

$$\sum_{\text{spins}} u(p)\bar{u}(p) = \not{p} + m, \qquad \sum_{\text{spins}} v(p)\bar{v}(p) = \not{p} - m, \qquad \sum_{\text{pols.}} \epsilon^{\mu}\epsilon^{\nu *} = -g^{\mu\nu},$$

where the gluon polarization sum assumes use of the Feynman gauge ($\xi = 1$). Following these replacements we can simply use the usual rules for the traces of gamma matrices, all easily derived from the Clifford algebra relation (1.2). The rules presented here include a mass for the quark, although in many applications this can be neglected. Working at scales sufficiently high above the quark masses (true for all but the top quark at $Q = M_Z$), the approximation of a zero mass greatly simplifies calculations. We shall adopt this approach throughout the remainder of the thesis. Finally, we note that in the squared matrix elements we always obtain an even power of g, so it is usual to always consider a perturbative expansion in powers of α_S defined by,

$$\alpha_S = \frac{g^2}{4\pi}. \tag{1.8}$$

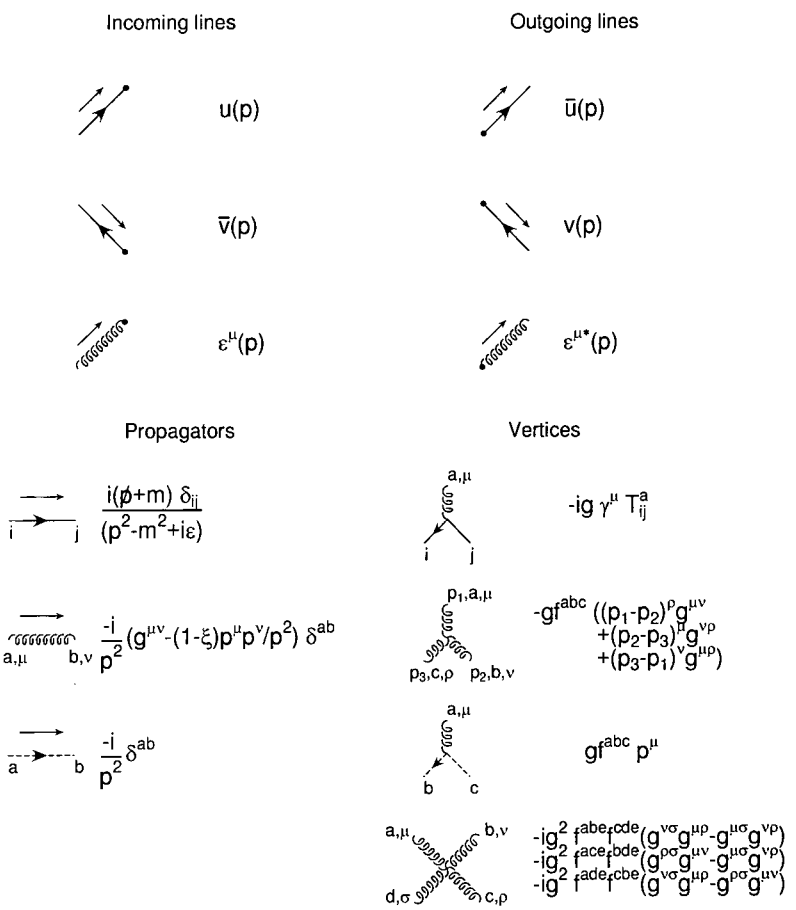

Figure 1.1: The Feynman rules for QCD, using the usual convention of {solid, springy, dashed} lines to represent {quarks, gluons, ghosts}. Unless otherwise stated, the momentum flow along a line is p in the direction indicated by the arrow alongside it. The gluon propagator is given in a covariant gauge specified by the parameter ξ. In the triple gluon vertex, all momenta are outgoing. For fermion lines, the arrow on the line itself indicates the direction of fermion flow.

1.3 Renormalization

Within a quantum field theory such as QCD, we require renormalization to remove ultraviolet divergences that are naturally present. These divergences are associated with higher order terms in the perturbative expansion of any physical observable. For example, consider the one-loop ('bubble') integral with two internal lines and external momentum k,

$$\mathcal{I} = \int \frac{d^4\ell}{\ell^2(\ell+k)^2}.$$

In the ultraviolet limit $\ell \to \infty$ the integral $\mathcal{I}$ is (logarithmically) divergent. We may renormalize by introducing an upper cut-off on the integral, at the momentum scale $\ell^2 = \mu^2$ say, or by dimensional regularization, continuing to $d < 4$ dimensions. Ultimately, either method introduces an additional scale μ – the *renormalization scale* – upon which our observable must depend at any given order in perturbation theory.

By calculating the counterterms to Greens functions – terms in the perturbative expansion – in a particular renormalization scheme we may determine the dependence on the parameter μ. In QCD at the 1-loop order, this amounts to the calculation of the diagrams in Figure 1.2. However, the dependence of an observable R upon the scale μ is entirely spurious – the physical observable cannot be dependent upon the artificially introduced unphysical parameter μ. By truncating the perturbative series rather than solving the whole theory we have introduced this extra dependence. This has the important effect known as the *running coupling*.

1.3.1 The Running of α_S

We shall consider a dimensionless observable R, so that at all scales Q in which we are interested any other scales are small (for instance, the quarks have masses m with $m^2/Q^2 \ll 1$). The independence of R from μ is expressed by,

$$\frac{dR}{d\mu} = \left(\frac{\partial}{\partial\mu} + \frac{\partial\alpha_S}{\partial\mu}\frac{\partial}{\partial\alpha_S}\right) R = 0,$$

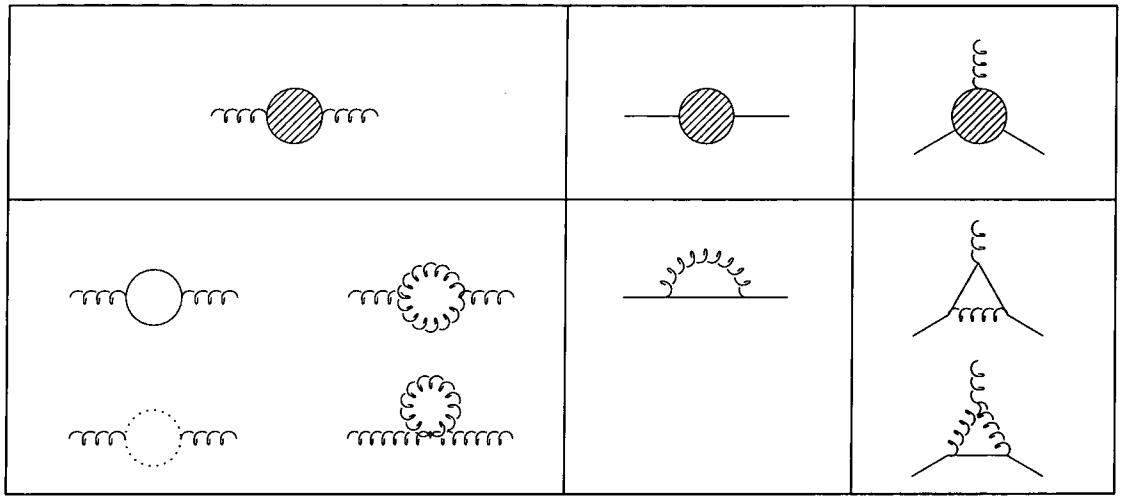

Figure 1.2: The 1-loop contributions to the renormalization counterterms for the gluon and fermion self-energies and the gluon-fermion vertex. These diagrams are sufficient to calculate the renormalization scale dependence of any physical observable at the one-loop level.

where $R = R(Q/\mu, \alpha_S)$ since it can only depend upon the dimensionless ratio Q/μ and the coupling at the renormalization scale, $\alpha_S = \alpha_S(\mu)$. We can re-express this equation in terms of the scale Q and the function $\beta(\alpha_S) = \mu\,\partial\alpha_S/\partial\mu$, yielding,

$$\left(-Q\frac{\partial}{\partial Q} + \beta(\alpha_S)\frac{\partial}{\partial \alpha_S}\right) R(Q/\mu, \alpha_S) = 0.$$

We now introduce a reference momentum scale Q_0 and define the new variables t and η by,

$$\frac{Q}{Q_0} = e^t \quad , \quad \frac{d\eta}{d\alpha_S} = \frac{1}{\beta(\alpha_S)}.$$

Noting that we have $\partial R/\partial\eta = \partial R/\partial t$ we may introduce the new function R' via,

$$R(Q/\mu, \alpha_S) = R'(Q_0/\mu, \eta + t) = R'\left(Q_0/\mu, \int_{\alpha_S^0}^{\alpha_S} \frac{dx}{\beta(x)} + t\right),$$

where α_S^0 is an arbitrary lower limit. By setting $t = 0$ in this formula we also obtain,

$$R(Q_0/\mu, \tilde{\alpha}_S) = R'\left(Q_0/\mu, \int_{\alpha_S^0}^{\tilde{\alpha}_S} \frac{dx}{\beta(x)}\right).$$

By equating these two expressions we find that we may relate the observables at two different energy scales provided that we modify the coupling,

$$R(Q/\mu, \alpha_S) = R(Q_0/\mu, \tilde{\alpha}_S) \qquad \text{subject to} \qquad \int_{\alpha_S^0}^{\tilde{\alpha}_S} \frac{dx}{\beta(x)} = \int_{\alpha_S^0}^{\alpha_S} \frac{dx}{\beta(x)} + t.$$

The constraint can itself be re-cast in the form of a differential equation for the coupling,

$$Q \frac{\partial \tilde{\alpha}_S(Q)}{\partial Q} = \beta(\tilde{\alpha}_S) \qquad \text{with} \qquad \tilde{\alpha}_S = \alpha_S. \tag{1.9}$$

Thus the strong coupling α_S is a function of the energy scale at which it is evaluated and runs according to the function $\beta(\alpha_S)$ which can be calculated from the diagrams in Figure 1.2. Such a calculation yields the result,

$$\begin{aligned} \beta(\alpha_S) &= -\frac{(11N - 2n_F)}{6\pi} \alpha_S^2 + \ldots \\ &\equiv -\beta_0 \alpha_S^2 + \ldots, \end{aligned} \tag{1.10}$$

where $(\ldots)$ represents the terms omitted due to working only at one-loop order. The expression in 1.10 represents the crucial conclusion. In QCD with $n_F < 17$ flavours of light quark, the coupling decreases as the energy scale is increased. This is known as *asymptotic freedom* and has many consequences for experimental observation which will be discussed further in chapter 2. This behaviour is in stark contrast to QED, where the coupling becomes weak at high energies (corresponding to $\beta(\alpha) = \frac{1}{3\pi} \alpha^2 + \ldots$).

α_S from Experiment

In theory then, it should be possible to make a number of experimental observations at different energy scales Q and thus extract measurements of $\alpha_S(Q)$ over a broad range of Q. Such measurements could then be compared with the theoretical prediction of equation (1.9), to confirm that the coupling does indeed run as we expect. At leading order in the perturbative expansion, it is simple to solve (1.9) with equation (1.10) to obtain,

$$\alpha_S(Q) = \frac{\alpha_S(Q_0)}{1 + \beta_0 \log\left(\frac{Q}{Q_0}\right) \alpha_S(Q_0)}. \tag{1.11}$$

Since we know that the coupling diverges as we decrease the energy scale, it is convenient to introduce a parameter Λ equal to this scale, near which perturbation theory becomes unreliable. This enables us to write an alternative form for the running,

$$\alpha_S(Q) = \frac{1}{\beta_0 \log\left(\frac{Q}{\Lambda}\right)}.$$

Although these two forms of the running are equivalent (simply different boundary conditions for the differential equation 1.9), use of each varies from application to application. As a test of the strong coupling, the use of Λ is often disfavoured. This parameter has a definition which changes order-by-order in perturbation theory, takes different values as one changes the number of quark flavours and also has the unphysical interpretation of being the scale at which the coupling diverges. For these reasons, it has become conventional to instead convert all measurements of $\alpha_S(Q)$ into a value at $Q = M_Z$ by running the coupling to this scale. This supposedly provides a more physical observable than Λ. By choosing $\alpha_S(M_Z)$ we are sufficiently far away from quark thresholds (and hence non-zero mass effects) and also close to the asymptotic region where perturbation theory should apply ($\alpha_S \sim 0.1$). Beyond these theoretical considerations, we can also make very accurate measurements due to the very high statistics at LEP on the Z-pole.

A recent compilation of data on measurement of the strong coupling (at varying values of Q) is shown in Figure 1.3. Despite encompassing a wide range of energy scales, from deeply inelastic lepton-nucleon scattering at $Q = 1.6$ GeV up to e^+e^- annihilation at $Q = 133$ GeV, all extracted values are consistent and provide a world average of [4],

$$\alpha_S(M_Z) = 0.118 \pm 0.004. \tag{1.12}$$

1.4 Scale Choice and Uncertainty

In the discussion of the running of the strong coupling above - and in all the determinations mentioned so far - we have assumed that the argument Q in $\alpha_S(Q)$ is the experimental energy

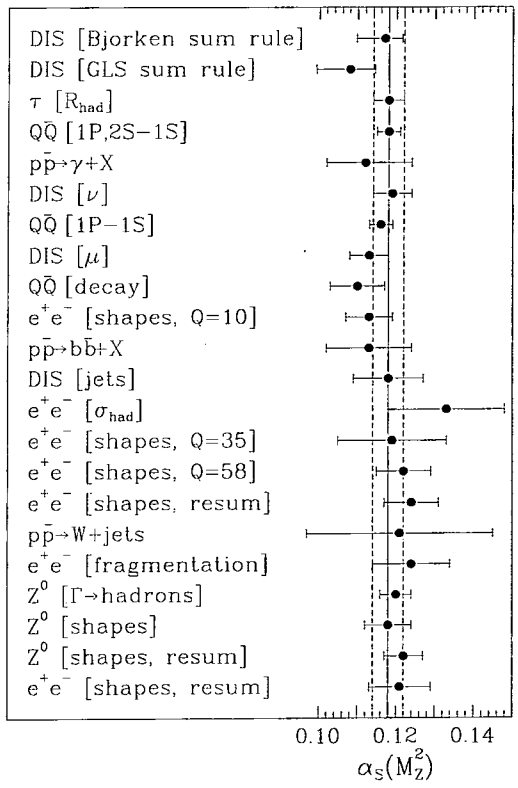

Figure 1.3: Measurements of $\alpha_S(M_Z)$ in the $\overline{MS}$ scheme, extracted from experiments at energy scales in the range 1.6 – 133 GeV. The figure is reproduced from reference [4].

scale of the process. This choice is normally referred to as the *physical scale.* It is usually motivated by naturalness arguments and the fact that if we choose a scale μ far from it then equation 1.11 introduces large logarithms of the form $\log(\mu/Q)$. When comparing values of $\alpha_S(M_Z)$ extracted in this way from the same observable at leading and next-to-leading order, it is clear that there will be some discrepancy. The lowest order determination requires a larger (smaller) value of α_S if the NLO coefficent is positive (negative). In order to try to assess the effect of higher order perturbative terms, the scale is often allowed to vary from $Q/2$ to $2Q$ and this uncertainty dominates all determinations, including the world average in 1.12. As more orders of perturbation theory are included, the dependence upon the renormalization scale should decrease and thus the determination becomes more accurate.

1.4.1 The Thrust Distribution

As an example, consider the 3-jet like observable thrust (T), which is defined by,

$$T = \max_{\vec{n}} \frac{\sum_k |\vec{p}_k \cdot \vec{n}|}{\sum_k |\vec{p}_k|}, \tag{1.13}$$

with the sum running over all particles in the event. Thrust describes the spread of jets within an event, such that $T = 1$ for events with two back-to-back particles and $T = 1/2$ for completely spherical events. Since T is fully inclusive, the averaging means that it is free of the large kinematical logarithms which afflict distributions in jet observables close to the two-jet region.

Since three jet production requires gluon emission from a quark, it is usual to consider the variable $< 1 - T >$, whose perturbative expansion begins with one factor of α_S. At next-to-leading order $< 1 - T >$, measured at centre-of-mass energy $Q^2 = M_Z^2$, is given by,

$$< 1 - T >= A\left(\frac{\alpha_S(\mu)}{2\pi}\right) + \left(B + 2\pi A\beta_0 \log\left(\frac{\mu}{M_Z}\right)\right)\left(\frac{\alpha_S(\mu)}{2\pi}\right)^2, \tag{1.14}$$

where β_0 is given by equation 1.10 and we have written the result as factors multiplying a series in $\alpha_S/2\pi$, the strong coupling with a common normalization. These scale-independent coefficients have the numerical values $A = 2.10$ and $B = 40.74$ for five light quark flavours.

To demonstrate the dependence upon the renormalization scale, the leading order and next-to-leading order variation of $< 1 - T >$ with μ is shown in Figure 1.4. The curves are

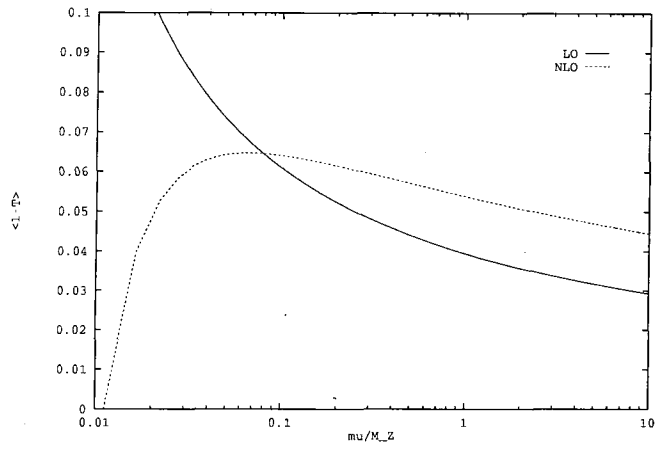

Figure 1.4: The dependence of the average value of 1-Thrust, $< 1 - T >$ upon the renormalization scale μ at leading (solid line) and next-to-leading order (dotted).

shown according to the two-loop running of α_S, which corresponds to an extra term in the β-function, $\beta = -\beta_0\alpha_S^2 - \beta_1\alpha_S^3 + \ldots$, where $\beta_1 = (153 - 19n_F)/12\pi^2$. The value of α_S at $Q = M_Z$ is chosen to agree with the central value of the current world average in 1.12.

It is clear that the lowest order curve is simply a scaled version of the one-loop running of α_S and thus tends to zero as the renormalization scale grows (asymptotic freedom), whilst diverging as $\mu \to 0$. In contrast, at next-to-leading order the additional logarithmic term dominates for small values of μ and we see a characteristic turn over and negative divergence. However, in the region $\mu = 0.05M_Z$ to $\mu = 10M_Z$ the curve is relatively flat and thus any extraction of the strong coupling using the physical scale in the conventional manner will attribute a smaller error to the measurement than at leading order.

We now discuss two other possible methods of choosing the renormalization scale and illustrate them with our example of $< 1 - T >$.

The Principle of Minimal Sensitivity (PMS)

This method of choosing the scale [5] attempts to reproduce the behaviour of the full perturbative series. That is to say, at any given order of perturbation theory we try to choose the scale such that the dependence upon μ is as small as possible. So in our thrust example, we impose,

$$\frac{\partial < 1 - T >}{\partial \log \mu} = 0,$$

where $< 1 - T >$ is given by the NLO expansion in 1.14. Graphically, this corresponds to finding the position of the local maximum in Figure 1.4. It is straightforward to carry out this differentiation and use the running of α_S to determine the scale that this condition picks out. Retaining all the next-to-leading terms (dropping $\mathcal{O}(\alpha_S^4)$) we find that the PMS scale $\mu^{\rm PMS}$ is given by,

$$A\beta_1 + \frac{\beta_0}{\pi}\left(B + 2\pi A\beta_0 \log\left(\frac{\mu^{\rm PMS}}{M_Z}\right)\right) = 0. \tag{1.15}$$

Fastest Apparent Convergence (FAC)

An alternative method of choosing the scale [6] is to stipulate that all the coefficients beyond lowest order in α_S vanish. That is to say, at NLO we choose the scale such that the LO and NLO predictions coincide, ie. the point where the lines cross in Figure 1.4. We notice that this scale appears to be very close to that obtained from the PMS requirement above. From equation 1.14 it is clear that for the FAC scale we simply require the second term in parentheses to vanish. In fact, this is a very similar condition to that for the PMS scale and by combining the two statements we find,

$$\frac{\mu^{\rm PMS}}{\mu^{\rm FAC}} = e^{-\beta_1/2\beta_0^2} \approx 0.85.$$

So in general we find that the FAC and PMS scales are very close to one another at next-to-leading order[2], differing by approximately 15%. However, these scales may be very different from the physical scale (depending on the coefficents A and B for each observable), as is the case for $< 1 - T >$.

[2]It can be shown that the scales also remain similar at next-to-next-to-leading order [7].

1.5 Summary

By tracing the development of QCD from a quantum field theory through to some important consequences of its non-Abelian gauge group, in this chapter we have reviewed some of the most important aspects of the theory of quarks and gluons. Although a proper derivation of the Feynman rules and their implications is beyond the scope of this thesis, we have nevertheless outlined their application and significance.

We have concentrated, as we shall do throughout the remainder of the thesis, on a perturbative solution of QCD in powers of the strong coupling g. An important consequence of this is that we must renormalize order-by-order, introducing an extra (artificial) mass scale μ. This leads to a coupling which runs with energy and vanishes in the high-energy limit (a property known as asymptotic freedom). In addition, all our perturbative predictions depend upon the scale μ, which we are free to choose as we see fit – although there are a number of common prescriptions.

In the following chapter we will see how we may implement this theory in practice, to match our theoretical model with the experimental reality.

Chapter 2

Hadrons, Partons and Next-to-Leading Order

2.1 Introduction

We have seen in the previous chapter how a proper formulation of QCD leads, via the concept of renormalization, to the idea of asymptotic freedom. The experimental consequences of this result – and the theoretical predictions we may make based on it – will be the subject of this chapter. Reconciling this picture of the real world with our theoretical predictions involving bare states of just partons – quarks and gluons – is our first goal in section 2.2.

A key concept in analysing hadronic final states is that of a jet, the properties of which we can only fully expose by working in higher orders of perturbation theory. The connection between jets and partons beyond lowest order will be the outlined with the simplest example in section 2.3. This basic calculation reveals a further source of divergences in QCD – those caused by vanishing momenta, *infrared* behaviour. These need to be regulated in some manner and section 2.4 describes the method that we will use throughout this thesis, namely dimensional regularization.

The infrared properties of matrix elements are intimately linked to the products of colour factors to which they are proportional. In section 2.5 we describe a convenient method

of decomposing amplitudes according to their colour factors and illustrate their singular behaviour. The numerical combination of terms once the singular pieces have been isolated is the topic of section 2.6, where we describe a variety of methods in common use.

We conclude the chapter with a discussion of further reasons for making predictions beyond lowest order (section 2.7) and give an example of a precision measurement that benefits from a NLO 4-jet analysis, the determination of the QCD colour factors (section 2.8).

2.2 Hadrons and Jets

In an experiment where we observe, for instance, an electron-positron pair annihilating to form hadrons, we might imagine that the final state would be difficult - perhaps impossible - to characterize. Classifying events containing of the order of 30 hadrons and making comparisons with parton level perturbative QCD would then be problematic.

However, examining a typical event such as that shown in Figure 2.1 shows that this is not the case. This end-on view taken from the SLAC-SLD experiment clearly shows that the individual hadron tracks are highly collimated, with three areas of the detector unpopulated by hadrons. Each cluster of hadrons contains one highly energetic particle, with many low energy, soft hadrons radiated very close to it. Thus hadronic events may be classfied according to the number of such clusters of energetic particles, which are referred to as *jets*.

2.2.1 Jet Algorithms

In order to quantify exactly the meaning of a jet, it is necessary to introduce a jet finding measure d_{ij} which represents the distance between the two hadrons i and j in an event. It is typically scaled by the square of the total energy visible in the final state, producing the dimensionless variable $y_{ij} = d_{ij}/E_{\text{vis}}^2$. Then the outline of a typical algorithm to assign hadrons to jets might be:

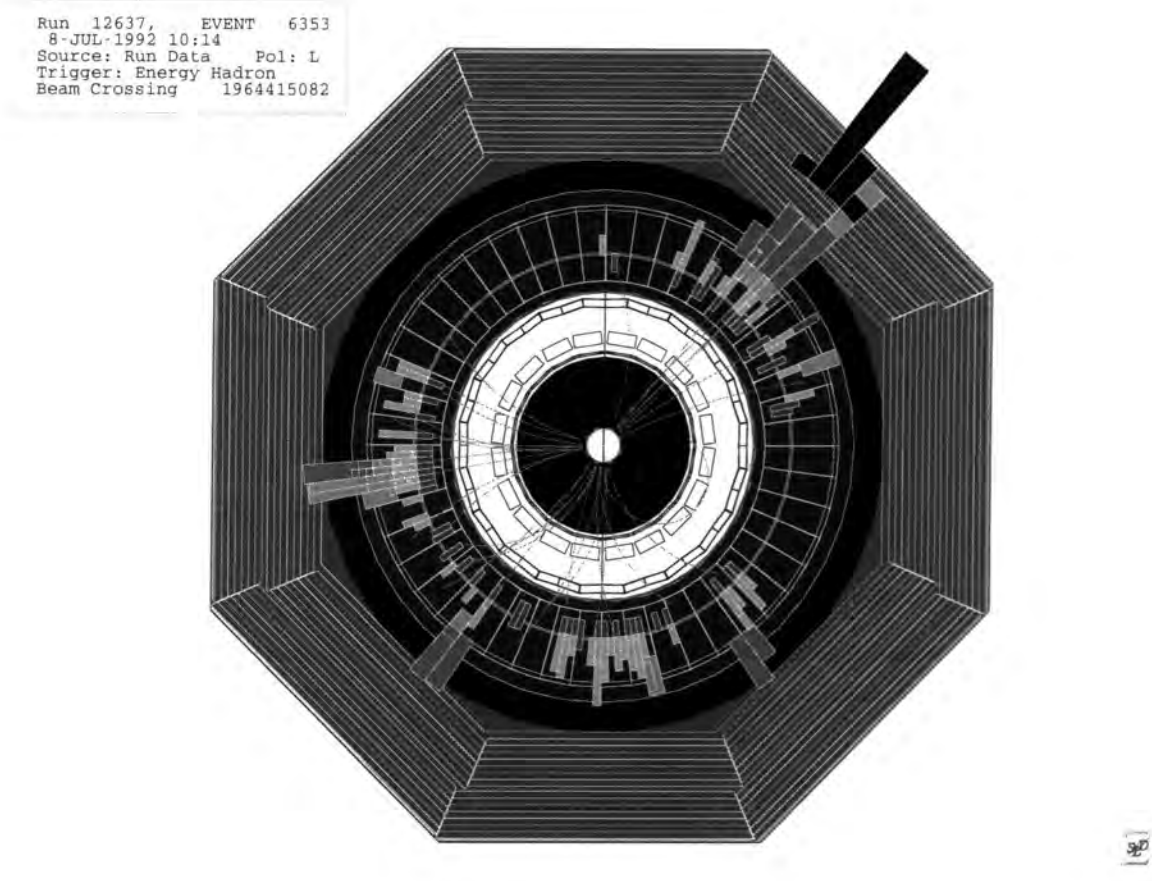

Figure 2.1: A typical 3-jet event observed by the SLD experiment at SLAC. This end-on view of the detector shows the hadron tracks curved in the magnetic field as they travel from the centre to the rings of calorimeters arranged concentrically around the beam.

1. Initially label each hadron as a separate jet.
2. Calculate the quantity y_{ij} for each pair of jets i and j.
3. If y_{ij} is sufficiently small, $y_{ij} < y_{\text{cut}}$ for at least one pair then jets i and j should be combined into one.
4. Repeat from step 2 until all jets have $y_{ij} \geq y_{\text{cut}}$.

This skeleton clearly leaves much scope for variation. The choice of the jet-defining measure y_{ij} and the method of recombination used in step 3 will be discussed shortly. In addition to this our picture of an event changes according to how broad we allow a single jet to be – the choice of the parameter y_{cut}. As y_{cut} approaches zero, we allow very narrow jets, until eventually all hadrons are identified as separate jets. Conversely, increasing the value of y_{cut} produces broader jets with far fewer multi-jet events.

We now detail some of the most common variants of this clustering algorithm and discuss some of the features and merits of each.

JADE [8]

This method chooses the measure to be simply,

$$y_{ij} = \frac{2E_iE_j(1-\cos\theta_{ij})}{E_{\text{vis}}^2},$$

in the centre-of-mass frame of the event. Here the hadrons have energies E_i and E_j and θ_{ij} is the opening angle between their directions. If the particles were massless then the energies and momenta could be related so that $y_{ij} = (p_i + p_j)^2/E_{\text{vis}}^2$, the invariant mass of the pair. Although particularly simple, we shall see that theoretical predictions based on this algorithm suffer from spurious clusterings.

Durham [9]

An attempt to improve the theoretical properties of the JADE algorithm led to the introduction of the Durham, or $k_\perp$-algorithm. In this variant, the measure is replaced by something which more closely resembles the relative transverse momenta of the pair of hadrons, at least at small angles,

$$y_{ij} = \frac{2\min(E_i^2, E_j^2)(1-\cos\theta_{ij})}{E_{\text{vis}}^2}.$$

Geneva [10]

Another possibility to avoid the problems of mis-clustering the hadrons is to use the measure,

$$y_{ij} = \frac{8}{9}\frac{E_i E_j(1-\cos\theta_{ij})}{(E_i+E_j)^2}.$$

Since this depends upon the energies of the partons i and j in both the numerator and denominator, this can be more prone to measurement error than the two alternatives above (which rely on the total energy, which can be more precisely measured). However, it is expected that this algorithm is particularly sensitive to the number of light fermion flavours and could thus prove an efficient tool to search for new physics effects beyond the Standard Model.

2.2.2 Local Parton-Hadron Duality

The crucial observation in connecting theory and experiment is the hypothesis of local parton-hadron duality [11]. We have seen that experimentally events tend to be composed of a small number of jets of hadrons, with the majority of the energy and momentum being carried by a single hadron within each jet. The concept of LPHD extends this further by postulating that in fact the quantum numbers and momentum flow of the produced hadrons closely follow those of the partons that initiated the jets. If one further supposes that the effects of hadronization – the process whereby the quarks and gluons cluster to form hadrons

– are small, one should obtain a reasonable agreement between theory and experiment by associating one jet with each parton.

With this assumption, one can now apply the jet algorithms given above both at the hadron level and in the theoretical parton calculation (where now $E^2_{\rm vis} = s$, the total available energy squared). Typically one uses matrix elements where the partons are massless, so the measures simplify, but lead also to a further ambiguity in how the partons should be combined into jets.

Recombination - E, E0 and P

Even having chosen a measure, there is still further variation possible in the way in which the hadrons are combined into a jet. To examine the differences we shall consider the clustering of partons i and j to form a jet k, $i + j \to k$.

The simplest choice – the *E-scheme* – assigns the momentum and energy of the jet k to the sum of those of i and j. So $E_k = E_i + E_j$ and $\vec{p}_k = \vec{p}_i + \vec{p}_j$. Although this is manifestly Lorentz invariant, we see that $p_k^2 = (p_i + p_j)^2 = 2p_i \cdot p_j \neq 0$. This creates a mis-match when comparing with matrix elements calculated using massless partons.

In order to solve this problem, two alternatives have been proposed. The *P-scheme* simply re-assigns the energy of the cluster in order to retain a zero mass, $\vec{p}_k = \vec{p}_i + \vec{p}_j$ and $E_k = |\vec{p}_k|$. However, we see that now we have maintained Lorentz invariance at the cost of violating energy conservation. The final choice, the *E0-scheme* chooses instead to break momentum conservation, $E_k = E_i + E_j$ with $\vec{p}_k = E_k(\vec{p}_i + \vec{p}_j)/|\vec{p}_i + \vec{p}_j|$.

Experimental results are commonly presented in all these schemes and we must be sure to match our theoretical procedure with the hadron level clustering.

2.3 Jets and Partons

In the preceeding section we have argued that, to first approximation, we can identify the partons of a matrix element calculation with the observed jets of an experiment, provided that we also match the jet definitions used in both analyses. This means that to compute an n-jet cross-section at lowest order we must calculate all the tree-level Feynman diagrams involving n partons in the final state and then integrate over the region of phase space which has $y_{ij} > y_{\text{cut}}$ for all pairs of partons i and j. We now wish to examine how this situation alters in higher orders of perturbation theory.

2.3.1 Jets at Next-to-Leading Order

It is instructive to consider the case of 2-jet production (in e^+e^- annihilation) as a simple example to illustrate the generic features of jet calculations beyond leading order. The tree-

Figure 2.2: The lowest order (left) and next-to-leading order (right) Feynman diagrams for the production of 2 partons in e^+e^- annihilation. The momenta of the particles are incoming and outgoing for initial and final state particles respectively, whilst the arrows on the electron and quark lines represent the direction of fermion flow.

level and 1-loop diagrams for the production of 2 partons – a quark-antiquark pair – via a virtual photon are shown in Figure 2.2, where for simplicity we have taken the intermediate particle as a virtual photon (whereas in fact a Z^0-boson also couples to both electrons and quarks). The loop diagram is simple to evaluate, yet we find that the result is not finite but contains infrared divergences. The solution to this problem lies in the transition from partons

to jets. We know that if two partons have a small invariant mass then (in the JADE scheme) they will cluster to form a jet, with one of them appearing to be *unresolved.* So our 2-jet NLO result should also contain an infrared singular piece representing a 3 parton configuration with one unresolved particle. The two diagrams for 3 parton production, $e^+e^- \to q\bar{q}g$ are shown in Figure 2.3 and are easily evaluated to give the kinematic dependence,

$$|\mathcal{M}|^2_{3 \text{ parton}} \sim \left(\frac{s_{qg}}{s_{\bar{q}g}} + \frac{s_{\bar{q}g}}{s_{qg}} + \frac{2s_{q\bar{q}}s_{q\bar{q}g}}{s_{qg}s_{\bar{q}g}} \right),$$

in terms of the Mandelstam invariants $s_{ij} = (p_i + p_j)^2$. From this explicit form, we can see

Figure 2.3: The two lowest order Feynman diagrams for three parton production, $e^+e^- \to q\bar{q}g$. The gluon simply couples to the quark-antiquark line either side of the photon.

that there is clearly a divergence in the limit where one parton is unresolved, say $s_{qg} \to 0$. In fact, there are two types of unresolved infrared singularity:

- either $s_{qg} \to 0$ or $s_{\bar{q}g} \to 0$, in which case the gluon is *collinear* with the quark (anti-quark);
- or, both of these invariants vanish simultaneously and the gluon is *soft*, $E_g \sim 0$.

If we can find a suitable way of isolating the singularities in the 2 parton (virtual) and 3 parton (real emission) contributions, we will find that the divergences exactly cancel, yielding a finite result. This is a specific case of the cancellation theorems of Bloch and Nordsieck [12] and Kinoshita, Lee and Nauenberg [13], which guarantee that this situation is extended to all orders in perturbation theory and for any number of final state particles.

2.4 Dimensional Regularization

We first consider how we may isolate the singularities in the matrix elements. The crucial point to note is that in the virtual (loop) terms, the divergences are only present because we are working in exactly four dimensions.

Dimensional regularization [14] is the name given to any scheme used to regulate divergences by continuing away from 4 and into D dimensions. This should be an intermediate device only and at the end of our calculation we will want to take the limit $D \to 4$. As opposed to alternative regularization prescriptions (such as imbuing particles with a fictitious mass), this procedure respects unitarity and preserves gauge invariance.

Originally this idea was proposed in order to handle the ultraviolet behaviour of loop integrals, with the loop momenta being continued to $D < 4$ dimensions. In fact by simply continuing to $D = 4 - 2\epsilon$ dimensions without the constraint of $\epsilon \geq 0$ we can also regulate infrared divergences.

However, in fact we may choose a number of schemes since, in addition to continuing the loop momenta into D dimensions, we may specify the dimensionality of both the external particle momenta and the polarizations (external and internal). The original method of t'Hooft and Veltman was to leave all quantities in four dimensions apart from the internal gluon polarizations which were taken as D dimensional.

In practice other choices may be more useful. Although the quark helicities are insensitive to the choice of dimensions, the dimensionality can have important consequences for the gluon polarization. For supersymmetric calculations it is imperative to use the same dimension for the polarizations of both quarks and gluons, in order to preserve the Ward identities of the theory. So-called 'dimensional reduction' was introduced in order to fulfil this condition. Four common schemes are illustrated in Figure 2.4. In this thesis, we shall most often use conventional dimensional regularization, the popular variant of t'Hooft and Veltman's original scheme.

The practical difference between the schemes rests in distinguishing the origin of metric tensors $g^{\mu\nu}$ that appear in one-loop amplitudes. Such tensors arising directly from loop integrals with two or more tensor numerators are D dimensional, whilst those resulting from spin indices in the Feynman rules depend upon the corresponding polarization dimensions.

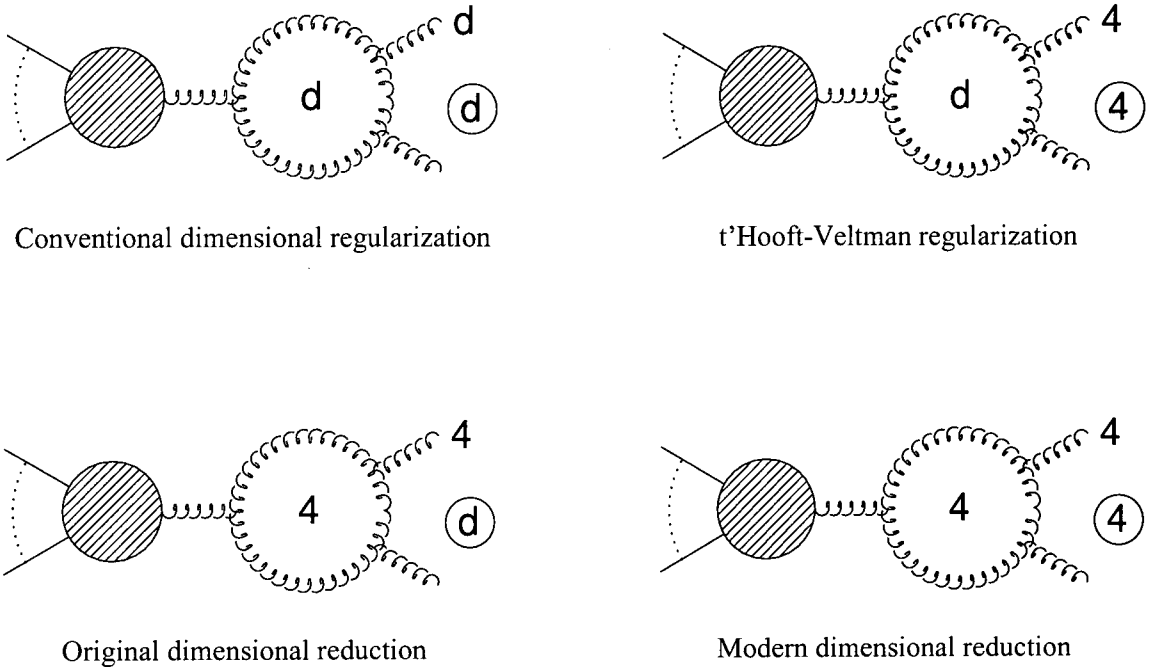

Figure 2.4: A diagrammatic representation of four common variants of dimensional regularization. The number of dimensions used for the polarization of gluons is shown within the gluon loop (internal gluons) and adjacent to the emitted gluon (external gluons). The circled number shows the dimensionality of the momenta of external particles. Internal particle momenta are continued into D dimensions, whilst all quark polarizations are in 4 dimensions.

2.5 Colour Structure of QCD Amplitudes

So far we have demonstrated the types of infrared divergences that may occur in next-to-leading order jet calculations and the means by which they may be exposed. In this section we will discuss a decomposition of the matrix elements – according to their colour factors

– which makes the singularities simple to isolate. To this end, we make a division of the diagrams involved in a given QCD process into a piece representing the colour structure and a purely kinematical factor. Having done this, it is possible to group together diagrams which have the same colour structure, which has several advantages. The remaining *colourless subamplitudes* represent, for example, colour ordered gluon emission off a quark line. Such amplitudes have nice factorization properties when two partons become collinear or a gluon soft.

As an example, consider the matrix elements for the tree-level process $q\bar{q} \to gg$. Labelling the colours of the quark (antiquark) by i (j) and gluons a, b, the relevant diagrams and their associated colour factors are shown in Figure 2.5. The total amplitude $\mathcal{M}$ is simply the sum of these three diagrams.

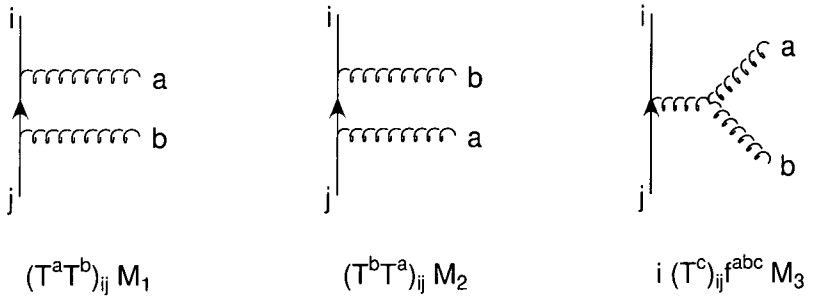

Figure 2.5: The tree-level diagrams for the process $q\bar{q} \to gg$, each divided into a colour factor multiplying a purely kinematical piece $\mathcal{M}_i$, $i = 1$, 2 or 3.

By using the identity $[T^a, T^b] = if^{abc}T^c$ we see that the diagram involving the triple-gluon vertex can be written as a combination of terms with the colour structure of the first two. In this way we find,

$$\mathcal{M} = (T^aT^b)_{ij}(\mathcal{M}_1 + \mathcal{M}_3) + (T^bT^a)_{ij}(\mathcal{M}_2 - \mathcal{M}_3). \tag{2.1}$$

In fact, this colour structure is true for any process where these are the only coloured particles. We may add initial or final state colour neutral particles, or switch these partons between the initial and final states, whilst still retaining the same decomposition. If we do

so, the kinematical pieces $\mathcal{M}_i$ simply contain more diagrams corresponding to the addition of the colourless particle(s) in all possible positions in Figure 2.5.

2.5.1 Colour Algebra

Having made a decomposition of an amplitude into kinematical pieces multiplying factors of generators and structure constants, we wish to construct squared matrix elements. By this we mean either forming the product $\mathcal{M}\mathcal{M}^\dagger$ (all that is necessary at tree-level) or an interference $\mathcal{M}_a\mathcal{M}_b^\dagger$. In this case we need a set of rules for evaluating products of colour factors. As well as employing the identities for the eigenvalues of the Casimirs of the gauge group, we shall also need the *Fierz identity*. This identity also provides a useful pictorial rule which can often be quickly applied in simple cases or as a cross-check, eliminating the need to resort to tedious algebra.

2.5.2 Casimir Colour Charges

Fundamental properties of any gauge group are the eigenvalues of the Casimir operators. At this point, we shall simply introduce the eigenvalue equations and defer a discussion of their experimental determination and relevance until section 2.8.

The three quadratic Casimirs of $SU(N)$ are given in Figure 2.6, together with the colour diagrams by which they can be represented. These diagrams lead to the interpretation of the Casimir factors as *colour charges*, by analogy with the electric charge. For the gauge group $SU(N)$ we find the following values for the colour factors C_A and C_F,

$$C_A = N, \qquad C_F = \frac{N^2 - 1}{2N},$$

whilst T_R is simply a normalization factor which we choose to be $T_R = 1/2$.

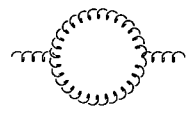

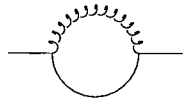

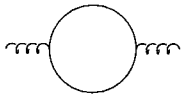

Figure 2.6: The definitions of the Casimir factors (colour charges) in the gauge group $SU(N)$. Repeated indices are summed over the $N^2 - 1$ (N) values of a, c, d (i, j, k) of the adjoint (fundamental) representation.

2.5.3 The Fierz Identity

Let us consider an element of $SU(N)$ in the adjoint representation,

$$M_{ij} = \alpha\delta_{ij} + \sum_a \beta^a T^a_{ij}, \tag{2.2}$$

where a runs over the N generators of $SU(N)$. Since the generators are traceless, we may determine α by taking the trace of this equation, yielding $\mathrm{tr}M = \alpha N$. Similarly, we fix the coefficients β^a by first multiplying by T^b and then taking the trace,

$$\mathrm{tr}(MT^b) = \sum_a \beta^a \mathrm{tr}(T^a T^b) = \sum_a \beta^a T_R \delta^{ab} = T_R \beta^b,$$

where we have used the Casimir definitions of section 2.5.2 to introduce T_R. So the decomposition in equation 2.2 above becomes,

$$M_{ij} = \frac{1}{N}(\mathrm{tr}M)\delta_{ij} + \sum_a \frac{1}{T_R}\mathrm{tr}(MT^a)T^a_{ij}.$$

Alternatively, writing out the contracted indices explicitly we obtain,

$$M_{ij} = \frac{1}{N} M_{kk}\delta_{ij} + \frac{1}{T_R}\sum_a M_{lk} T^a_{kl} T^a_{ij}.$$

Since this equality is true for arbitrary M_{ij} we now choose to write it in the form,

$$M_{lk}\left(\delta_{il}\delta_{kj} - \frac{1}{N}\delta_{kl}\delta_{ij} - \frac{1}{T_R}\sum_a T^a_{ij} T^a_{kl}\right) = 0,$$

so that it is clear that we must have,

$$\sum_a T^a_{ij} T^a_{kl} = T_R\left(\delta_{il}\delta_{jk} - \frac{1}{N}\delta_{ij}\delta_{kl}\right). \tag{2.3}$$

This equality is known as the Fierz identity and can be used to express the colour flow along a gluon between two quark lines ($T^a_{ij}T^a_{kl}$) as simpler quark colour flows ($\delta_{il}, \ldots$). This is illustrated in Figure 2.7.

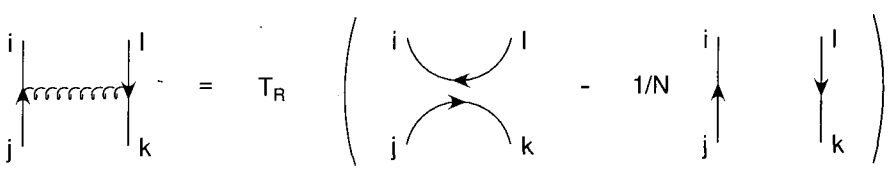

Figure 2.7: The pictorial version of the Fierz identity of equation 2.3.

2.5.4 Factorization of Matrix Elements

Returning to our example of two gluon production from a quark-antiquark pair, we now wish to illustrate the singular behaviour of the matrix elements. To do so, it is easy to use the Fierz identity described above to calculate the squared matrix elements from equation 2.1,

$$|\mathcal{M}|^2 = \frac{C_F N^2}{2}\left(|\mathcal{M}_1 + \mathcal{M}_3|^2 + |\mathcal{M}_2 - \mathcal{M}_3|^2 + \mathcal{O}\left(\frac{1}{N^2}\right)\right). \tag{2.4}$$

Here we have written only the leading colour contribution and dropped the sub-leading term of order $1/N^2$. Since each of the two terms in equation 2.4 represents a colourless

subamplitude where the gluons a and b are emitted in an ordered way from the quarks, it is often convenient to write these as,

$$|\mathcal{M}_1 + \mathcal{M}_3|^2 \equiv \left|\mathcal{S}(Q; a, b; \overline{Q})\right|^2, \qquad |\mathcal{M}_2 - \mathcal{M}_3|^2 \equiv \left|\mathcal{S}(Q; b, a; \overline{Q})\right|^2.$$

This notation then easily extends to multiple gluon production, where the ordered sub-amplitudes have particularly simple singular limits. For example, in the limit where gluon u is soft, we have the QED-like factorisation into an eikonal factor multiplied by the colour ordered amplitude with gluon u removed, but the ordering of the hard gluons preserved. So for an amplitude involving gluons $1 \ldots n$,

$$\left|\mathcal{S}(Q; 1, \ldots, a, u, b, \ldots, n; \overline{Q})\right|^2 \to S_{aub}(s_{ab}, s_{au}, s_{ub}) \left|\mathcal{S}(Q; 1, \ldots, a, b, \ldots, n; \overline{Q})\right|^2, \tag{2.5}$$

with the eikonal factor given by,

$$S_{aub}(s_{ab}, s_{au}, s_{ub}) = \frac{4 s_{ab}}{s_{au} s_{ub}}. \tag{2.6}$$

Similarly, in the limit where two particles become collinear, the sub-amplitudes factorise. For example, if gluons a and b become collinear and form gluon c, then only colour connected gluons give a singular contribution. We shall give a full discussion of colour connectedness in chapter 7, but for now it suffices to observe that in our simple example of $\left|\mathcal{S}(Q; a, b; \overline{Q})\right|^2$, gluon a is colour connected to Q and gluon b because the contributing diagrams contain propagators of s_{Qa} and s_{ab}, whilst Q is not connected to b. For example,

$$\left|\mathcal{S}(Q; 1, \ldots, a, b, \ldots, n; \overline{Q})\right|^2 \to P_{gg\to g}(z, s_{ab}) \left|\mathcal{S}(Q; 1, \ldots, c, \ldots, n; \overline{Q})\right|^2. \tag{2.7}$$

For particles that are not colour connected, there is no singular contribution as $s_{ab} \to 0$, and, when integrated over the small region of phase space where the collinear approximation is valid, give a negligible contribution to the cross section. Here z is the fraction of the momentum carried by one of the gluons and, after integrating over the azimuthal angle of the plane containing the collinear particles with respect to the rest of the hard process, the collinear splitting function $P_{gg\to g}$ is given by,

$$P_{gg\to g}(z, s) = \frac{2}{s} P_{gg\to g}(z). \tag{2.8}$$

The function $P_{gg\to g}(z)$ is one of the *Altarelli-Parisi* splitting kernels [15] (with colour factors removed), which are given by,

$$\begin{aligned} P_{qg\to q}(z) &= \left(\frac{1+z^2-\epsilon(1-z)^2}{1-z}\right), \\ P_{q\bar{q}\to g}(z) &= \left(\frac{z^2+(1-z)^2-\epsilon}{1-\epsilon}\right), \\ P_{gg\to g}(z) &= \left(\frac{1+z^4+(1-z)^4}{z(1-z)}\right), \end{aligned} \tag{2.9}$$

with the symmetry relation, $P_{gq\to q}(z) = P_{qg\to q}(1-z)$. This factorization of the matrix elements is universal and process independent and occurs when any single particle is unresolved.

2.6 Cancellation of Singularities

By using the technique of dimensional regularization as discussed in a section 2.4, infrared divergences appear as poles in ϵ. For the calculation of an n-jet cross-section at next-to-leading order, the phase space integration of the $n+1$ parton terms leads to $1/\epsilon$ poles corresponding to collinear singularities and double $1/\epsilon^2$ divergences from soft gluon emission. These must be cancelled against the poles that are extracted from the D-dimensional one-loop integrations in the virtual contribution.

The differences between the most widely-used methods for cancellation of infrared divergences are best illustrated by a simple one-dimensional example. The original formulation of Kunszt and Soper [16] considers the toy integral,

$$\mathcal{I} = \lim_{\epsilon\to 0}\left\{\int_0^1 \frac{dx}{x}\, x^\epsilon \mathcal{M}(x) - \frac{1}{\epsilon}\mathcal{M}(0)\right\}. \tag{2.10}$$

In this equation, $\mathcal{M}(x)$ represents the $n+1$ parton matrix elements, which are integrated over the extra phase space relative to the n-parton contribution $\mathcal{M}(0)$. x is an invariant controlling the collapsing of the $n+1$ parton configuration into an n jet state: as $x \to 0$ two partons become collinear or a single gluon soft. The explicit $1/\epsilon$ singularity in the virtual term is typical of that found in dimensional regularization, as is the regularizing (as $x \to 0$)

x^ϵ term under the integral. Note that in this example we have neglected any additional weight corresponding to the n jet observable being measured.

We now consider in turn how each of the common methods applies to our test integral $\mathcal{I}$.

- **Subtraction.**

  This is the method originally used by Ellis, Ross and Terrano (ERT) to calculate NLO corrections to 3-jet like quantities in e^+e^- annihilation [17]. The technique is to explicitly add and subtract a divergent term such that the new $n+1$ parton integral is manifestly finite,

$$\begin{aligned} \mathcal{I} &= \lim_{\epsilon\to 0}\left\{\int_0^1 \frac{dx}{x}\,x^\epsilon\Big(\mathcal{M}(x)-\mathcal{M}(0)\Big)+\mathcal{M}(0)\int_0^1\frac{dx}{x}\,x^\epsilon-\frac{1}{\epsilon}\mathcal{M}(0)\right\} \\ &= \int_0^1\frac{dx}{x}\Big(\mathcal{M}(x)-\mathcal{M}(0)\Big). \end{aligned} \tag{2.11}$$

  Here we have used the dimensional regularization convention of $0^\epsilon \to 0$ as $\epsilon \to 0$ in evaluating the integral $\int_0^1 \frac{dx}{x}\,x^\epsilon = [x^\epsilon]_0^1/\epsilon = 1/\epsilon$. Although this procedure appears to be straightforward, the difficulty lies in extracting the singularity from the analogue of $\int_0^1 \frac{dx}{x}\,x^\epsilon$. Indeed, this integration must be carried out separately for every process under consideration. However, in contrast to some of the alternative techniques, the subtraction method introduces only one extra theoretical cutoff[1] and requires approximation of neither the matrix elements nor the phase-space.

  Recently various implementations of the subtraction method have been introduced in order to describe general processes in a more universal manner [18, 19].

- **Slicing.**

  The severe process-dependence of the original cancellation procedure developed by ERT led to the proposal of the universal phase-space slicing method [20, 21]. The price to be paid for this extra portability is the introduction of an artificial theoretical

[1] In practice, we cannot integrate numerically from the lower limit of zero and instead we replace this with a small cut-off parameter δ.

parameter(δ) which controls the approximations made in this approach. In terms of our example integral, the goal is to choose $\delta \ll 1$ such that $\mathcal{M}(x) \approx \mathcal{M}(0)$ is a good approximation for $x < \delta$. Then we can isolate the singularity of the integral by making a division into two regions,

$$\begin{aligned}\mathcal{I} &\sim \lim_{\epsilon\to 0}\left\{\int_\delta^1 \frac{dx}{x}x^\epsilon\mathcal{M}(x) + \mathcal{M}(0)\int_0^\delta \frac{dx}{x}x^\epsilon - \frac{1}{\epsilon}\mathcal{M}(0)\right\} \\ &\sim \lim_{\epsilon\to 0}\left\{\int_\delta^1 \frac{dx}{x}x^\epsilon\mathcal{M}(x) + \mathcal{M}(0)\frac{\delta^\epsilon}{\epsilon} - \frac{1}{\epsilon}\mathcal{M}(0)\right\} \\ &\sim \int_\delta^1 \frac{dx}{x}\mathcal{M}(x) + \mathcal{M}(0)\log\delta. \end{aligned} \tag{2.12}$$

To arrive at the final line we employ the expansion $\delta^\epsilon = e^{\epsilon\log\delta} = 1 + \epsilon\log\delta + \ldots$. The universal approximations of the phase-space and matrix elements in soft and collinear limits lend this method its process-independence. The arbitrary parameter δ should clearly not affect the final result, but the implicit cancellation of (possibly large) logarithms of δ in 2.12 can lead to numerical instabilities. Although we would like to minimize this problem by taking δ as large as possible, we are constrained by the goodness of approximation condition $\delta \ll 1$.

- **Hybrid subtraction.**

The final method draws elements from each of the above techniques, where again the driving inspiration is the universality of the approach. Instead of the single scale(δ) used so far, we introduce two scales, δ and Δ. In the region $0 < x < \delta$, we adopt the slicing procedure, while in the range $\delta < x < \Delta$ we add and subtract an analytically integrable set of universal terms, $E(x)$, to eq. (2.12),

$$\mathcal{I} \sim \int_\delta^1 \frac{dx}{x}\mathcal{M}(x) + \mathcal{M}(0)\log(\delta) - \int_\delta^\Delta \frac{dx}{x}E(x) + \int_\delta^\Delta \frac{dx}{x}E(x), \tag{2.13}$$

which on rearrangement yields,

$$\mathcal{I} \sim \int_\delta^1 \frac{dx}{x}\left(\mathcal{M}(x) - E(x)\Theta(\Delta - x)\right) + \int_\delta^\Delta \frac{dx}{x}E(x) + \mathcal{M}(0)\log(\delta). \tag{2.14}$$

Because we explicitly add and subtract the same quantity, there can be no dependence on Δ which can therefore be taken to be large. However, the slicing approximation

requires $\delta \to 0$. For this approach to be useful, two conditions must be satisfied. First, the second term in eq. (2.14) must be evaluated analytically without making any approximation in the phase space and should produce a term $-\mathcal{M}(0)\log(\delta)$ from the lower boundary that explicitly cancels the third (slicing) term. This allows the limit $\delta \to 0$ to be taken (inasmuch as that can be achieved numerically). Second, $\mathcal{M}(x) \sim E(x)$ as $x \to 0$ and more usefully $E(x)$ is smooth and as close to $\mathcal{M}(x)$ as possible over the whole range of $x < \Delta$, so that the first term in eq. (2.14) can be safely evaluated numerically. This is the technique that we shall adopt later in the thesis, when we return to this discussion in the context of the process $e^+e^- \to 4$ jets.

2.7 Motivation for NLO and Beyond

Having discussed the various techniques that we may employ to calculate next-to-leading order cross-sections (and related observables) we now turn to the benefits that performing such a task may bring. We also consider the further advantages of investigating even higher order terms in the perturbative expansion.

Much of our understanding of strong interaction physics can be gleaned from comparison of experimental data with a lowest order perturbative calculation. Qualitatively, this can be understood by considering a simple perturbative expansion for an observable R in powers of α_S,

$$R(\alpha_S(Q)) = A\alpha_S(Q) + B\alpha_S^2(Q) + \ldots.$$

Typically we might choose the physical scale $Q \sim M_Z$ at LEP, where we have $\alpha_S \sim 0.1$. With the naïve supposition of roughly equal coefficents A, B, ..., a simple geometrical series sum shows that the true answer differs from the lowest order calculation by a mere 10%. Of course, in reality there is no reason to suggest that the coefficients truly behave in this way. Even if this were so, there are a number of reasons why we may still be interested in a higher order prediction:

- Although the shape of a distribution may be successfully described, the normalization

is uncertain. We are free to choose the scale for α_S in any fashion (see chapter 1), typically so as to best fit the experimental data. Apart from the 'physical scale' argument, any other choice relies on a NLO calculation.

- In QCD, higher orders include more quantum mechanical modelling of soft gluon radiation within the event. Therefore they give a more accurate picture of such qualities as jet shape and structure.

- Increased theoretical precision means that we can match experimental errors and thus together improve our understanding of and trust in QCD as the correct theory for the strong interaction. For instance, measurement of the colour factors (group weights) comfirms that the relevant symmetry group is SU(3) (see section 2.8).

- We need a good knowledge of the expectations of perturbative QCD, not only to search for new physics beyond the SM, but also to observe new non-perturbative effects. Expected features such as power corrections, which are invisible in perturbation theory, may be hard to distinguish from genuine possible higher-order contributions. A better knowledge of the perturbative expansion can only help to solve this ambiguity.

In practice, computations beyond NLO are unavailable for many observables. For processes involving more than 5 partons or 4 partons and a vector boson, even the NLO contribution is currently unknown. In this thesis we shall predominantly concentrate on the NLO corrections to processes involving 4 partons and a vector boson – in particular as applied to $e^+e^- \to 4$ jets – with some attention paid to extending the methods that have been developed at NLO to next-to-next-to-leading order (NNLO).

2.8 Determination of the QCD Colour Factors

A measurement of the colour factors of QCD truly tests the dynamics of the strong interaction. As the eigenvalues of the Casimir operators of the underlying gauge group of the theory, they can test the $SU(3)$ symmetry proposed for QCD. We may thus distinguish

between different gauge groups and we are sensitive to new particles that may be present in more exotic theories.

Four-jet observables are particularly well suited to a study of the colour factors. Although both 2- and 3-jet studies have been made (see for example Ref. [22]), the essential non-Abelian nature of QCD only manifests itself at tree-level for the first time when considering 4 jet production. Despite the greater fraction of 2- and 3-jet events, here the triple gluon vertex does not appear at all in the theoretical calculation, or only appears at next-to-leading order and is thus suppressed by an extra factor of α_S. In addition we also become sensitive to particles such as light gluinos (supersymmetric fermionic partners of the gluons, with a mass $\sim$ 1 GeV), favoured by some theorists (for a discussion of some of the implications of such particles see Ref. [23]). The tree-level diagrams representing 4 jet production with gluinos simply mimic extra quark flavours – with the gluinos coupling to a gluon emitted from a quark-antiquark pair – and correspond to the shift $n_F \to n_F + 3$.

In this application, it is convenient to include a factor of C_F for each occurence of the strong coupling α_S in the expression for the 4-jet observable being studied. We can then arrange the remainder of the expression as a collection of kinematic factors multiplying ratios of the group Casimirs. Thus at leading order we have,

$$\frac{1}{\sigma_0}\mathrm{d}\sigma_{4\text{ jet}}^{\mathrm{LO}} = \left(\frac{\alpha_S C_F}{2\pi}\right)^2 \left(A(O) + \frac{C_A}{C_F}B(O) + \frac{T_R}{C_F}C(O)\right)\mathrm{dO}, \tag{2.15}$$

where σ_0 is the 2-jet cross-section and A, B and C are the kinematic weights from the Feynman diagrams for the two contributing processes $e^+e^- \to q\bar{q}gg$ and $e^+e^- \to q\bar{q}Q\overline{Q}$. O represents any 4-jet observable, typically chosen so as to maximize differences between A, B and C. Having chosen a selection of suitable observables, it is simple to fit the experimental data to the theoretical prediction in the form (2.15) and thus extract the colour ratios C_A/C_F and T_R/C_F. A fit of this fashion is performed in [24], yielding the result,

$$\frac{C_A}{C_F} = 2.11 \pm 0.32 \quad , \quad \frac{T_F}{C_F} = 0.40 \pm 0.17,$$

to be compared with the SU(3) prediction of $C_A/C_F = 9/4$ and $T_R/C_F = 3/8$. This determination and the predicted values of the ratios for a selection of symmetry groups are shown in Figure 2.8.

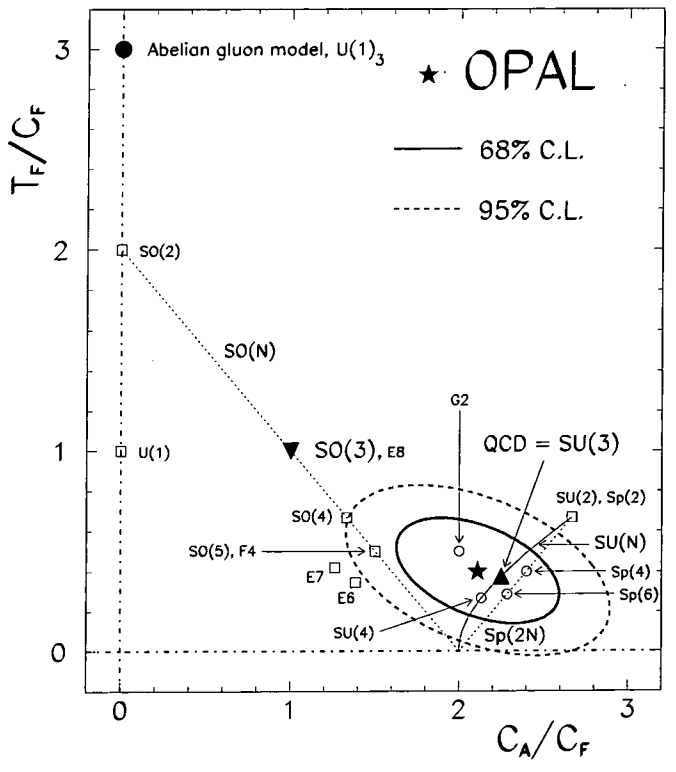

Figure 2.8: A determination of the QCD colour factors by the OPAL collaboration, together with the actual values corresponding to some common gauge groups. The figure is taken from reference [24].

It can be seen that this measurement rules out some of the (more exotic) possible gauge groups, but clearly $SU(3)$ is not singled out by this analysis alone. By performing a next-to-leading order analysis of the same data, the confidence-level contours corresponding to those of Figure 2.8 would be dramatically shrunk [25].

2.9 Summary

In this chapter we have seen how the concept of local parton-hadron duality (LPHD) may be employed to make hadron level predictions from parton level theoretical calculations.

We have demonstrated that to make sense of the definition of a jet beyond the lowest order in perturbation theory, we must combine matrix elements from a number of different sources in order to render the cross-section finite. At next-to-leading order, this involves calculating the real and virtual matrix elements (sections 2.3 and 2.5) in a suitable renormalization scheme (section 2.4) and then combining them suitably during phase-space integration (section 2.6). A next-to-leading order prediction can then be a very useful tool for improving our understanding of QCD (sections 2.7 and 2.8).

In the following chapters, we shall demonstrate how all these techniques may be applied to the calculation of the process $e^+e^- \to 4$ jets at next-to-leading order.

Chapter 3

One-Loop Integrals

3.1 Introduction

As has been outlined in previous chapters, the calculation of higher orders in perturbation theory is a necessary ingredient in our search for a more complete description of the physical world. At next-to-leading order, one of the hurdles which we must overcome is the evaluation of one-loop integrals which arise directly from a Feynman diagram approach. The matrix elements for a given process at one-loop order will in general contain many of these integrals, in different configurations corresponding to the diagrams involved.

Often these integrals need to be performed in an arbitrary dimension in order to isolate any infrared and ultraviolet divergences that may be present [14]. The basic one-loop tensor integral in D dimensions for n external particles scattering with outgoing momenta p_i, n internal propagators with masses M_i and m loop momenta in the numerator can be written,

$$\mathrm{I}_n^D[\ell^{\mu_1}\dots\ell^{\mu_m}] = \int \frac{d^D\ell}{i\pi^{D/2}} \frac{\ell^{\mu_1}\dots\ell^{\mu_m}}{(\ell^2-M_1^2)((\ell+q_1)^2-M_2^2)\cdots((\ell+q_{n-1})^2-M_n^2)},$$

where $m = 1,\dots,n$ and,

$$q_i^\mu = \sum_{j=1}^{i} p_j^\mu, \qquad q_0^\mu = q_n^\mu = 0. \tag{3.1}$$

This is represented diagrammatically in Fig. 3.1.

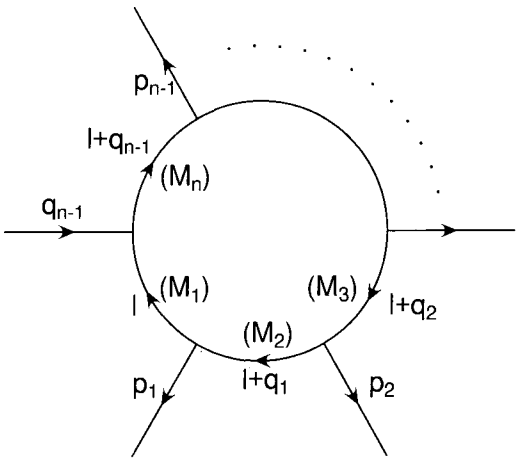

Figure 3.1: The generic n-point one-loop integral. The arrows indicate the direction of the flow of momentum, which is conserved at each vertex on using the relations (3.1). The mass of each internal propagator is shown in parentheses.

The scalar integral is denoted $\mathrm{I}_n^D[1]$, with the tensor integrals $\mathrm{I}_n^D[\ell^{\mu_1}\ldots\ell^{\mu_m}]$ arising from both traces over spin lines involving vertex factors γ^μ and propagators $\not{\ell}$ in the Feynman rules. In the standard approach to such integrals [26] one utilises the fact that the tensor structure must be carried by the external momenta or the metric tensor $g^{\mu\nu}$. For example, the simplest non-trivial tensor integral in D dimensions has a single loop momentum ℓ^μ. It reads,

$$\mathrm{I}_n^D[\ell^\mu] \equiv \sum_{j=1}^{n-1} c_j p_j^\mu, \tag{3.2}$$

using momentum conservation to eliminate one of the momenta. It is the calculation of the formfactors c_j that embodies the difficulty of these integrals. The more traditional methods, together with subsequent improvements and innovations will be outlined briefly in section 3.2. It will be argued there that all these methods suffer from the presence of 'fake' singularities. That is, the integrals will appear to have poles in certain kinematical variables, whose residues are in fact zero. Apart from reducing the chances of numerical instability, elimination of these apparent singularities provides a natural and compact method of evaluating the tensor integrals and reduces the size of the final matrix element expressions.

Although the derived functions will ultimately be used for the specific calulation of the process $\gamma^* \to 4$ jets, this chapter addresses the question of how such finite functions might be generated for arbitrary processes. Closely following the notation and approach of Bern, Kosower and Dixon relationships will be derived between integrals with polynomials of Feynman parameters in the numerators as well as between integrals with fewer parameters but in higher dimensions. The basic definitions and notations are introduced in section 3.3 and the recursive relations for integrals with up to four Feynman parameters in the numerator are presented along with the dimension shifting relation of [27, 28]. These expressions are valid for arbitrary internal and external masses and for general kinematics. However, making sense of these relations with respect to the singular limit depends on the actual integral itself; i.e. on n and the specific values of the kinematic variables. The remaining sections describe a series of explicit realisations of the three, four and five point integrals relevant for the one-loop corrections for the decay of a virtual gauge boson into four massless partons, which will be the topic of chapter 4.

3.2 Tensor Integral Reduction

Recall the formfactor decomposition of the simplest tensor integral (3.2),

$$\mathrm{I}_n^D[\ell^\mu] \equiv \sum_{j=1}^{n-1} c_j p_j^\mu. \tag{3.3}$$

In the original form of Passarino-Veltman reduction, the formfactors c_j are determined by multiplying both sides by all possible momenta $p_{i\mu}$ and rewriting $\ell.p_i$ as a difference of propagator factors. In other words,

$$\ell.p_i = \frac{1}{2}\left[((\ell+q_i)^2 - M_{i+1}^2) - ((\ell+q_{i-1})^2 - M_i^2) + (M_{i+1}^2 - M_i^2 + q_{i-1}^2 - q_i^2)\right],$$

which thus reduces the tensor integral to a sum of scalar integrals,

$$\sum_{j=1}^{n-1} c_j p_j.p_i = \frac{1}{2}\left[\mathrm{I}_{n-1}^{D,(i+1)}[1] - \mathrm{I}_{n-1}^{D,(i)}[1] + (M_{i+1}^2 - M_i^2 + q_{i-1}^2 - q_i^2)\mathrm{I}_n^D[1]\right].$$

Here, $\mathrm{I}^{D,(i)}_{n-1}[1]$ represents the "pinched" loop integral with the $(n-1)$ propagators remaining after the ith propagator factor has cancelled.

The formfactors are then obtained by algebraically solving the system of $(n-1)$ equations. This introduces the $(n-1)\times(n-1)$ Gram determinant,

$$\Delta_n = \det(2p_i \cdot p_j),$$

(where i and j run over the $(n-1)$ independent momenta), into the denominator. Each formfactor is a sum over the scalar integrals present in the problem multiplied by a kinematic coefficient that may be singular at the boundary of phase space where the Gram determinant vanishes. Typically,

$$c_j \sim \alpha \frac{\mathrm{I}^D_n[1]}{\Delta_n} + \sum_{m=1}^{n} \beta_m \frac{\mathrm{I}^{D,(m)}_{n-1}[1]}{\Delta_n}, \tag{3.4}$$

where the sum runs over the n possible pinchings and where α and β_m are coefficients which are functions of the kinematic variables. Since, in many cases, the formfactors c_j are actually finite in the limit $\Delta_n \to 0$, there are large cancellations and there may be problems of numerical stability.

The basic approach has been modified in a variety of ways, including the introduction of a system of $(n-1)$ reciprocal vectors v_i^μ (and the associated second rank tensor $w^{\mu\nu}$ playing the role of $g^{\mu\nu}$) to carry the tensor structure [29, 30, 31] where,

$$v_i^\mu = \epsilon^{p_1 \ldots p_{i-1} \mu p_{i+1} \ldots p_n} \epsilon_{p_1 \ldots\ldots p_n} / \Delta_n,$$

so that,

$$v_i . p_j = \delta_{ij}.$$

This simplifies the identification of the formfactor coefficients, but does not eliminate the Gram determinants. In fact, in both approaches, the number of Gram determinants generated is equal to the number of loop momenta in the numerator of the original integral.

A different approach has been suggested by Davydychev [32], who has identified the formfactors directly as loop integrals in differing numbers of dimensions and with the loop propagator factors raised to different powers. Tarasov [33] has obtained recursion relations for

one-loop integrals of this type, so that a complete reduction is possible. However, in relating the formfactor loop integrals to ordinary scalar loop integrals in 4 (or close to 4) dimensions, the Gram determinant once again appears in the denominator as in equation (3.4).

Finally, Bern, Kosower and Dixon have used the Feynman parameter space formulation for loop integrals to derive explicit results for the scalar integrals including the scalar pentagon [27, 28]. The formfactors of the momentum space decomposition are directly related to Feynman parameter integrals with one or more Feynman parameters in the numerator. One can see this by introducing the auxiliary momentum $\mathcal{P}^\mu$,

$$\mathcal{P}^\mu = -\sum_{i=1}^{n-1} x_{i+1} q_i^\mu, \tag{3.5}$$

so that after integrating out the loop momentum, the tensor integral for a single loop momentum in the numerator can be expressed in terms of the external momenta q_i^μ (see also Appendix A),

$$\mathrm{I}_n^D[\ell^\mu] \to \mathrm{I}_n^D[\mathcal{P}^\mu] \equiv -\sum_{i=1}^{n-1} \mathrm{I}_n^D[x_{i+1}] q_i^\mu.$$

Here, $\mathrm{I}_n^D[x_i]$ represents the scalar integral with a single factor of x_i in the numerator. By comparing with equation (3.2), we see that,

$$c_j = -\sum_{i=j+1}^{n} \mathrm{I}_n^D[x_i].$$

Differentiating with respect to the external kinematic variables, yields relations between integrals with polynomials of Feynman parameters in the numerator and the usual scalar integrals. Once again, the Gram determinant appears in the denominator, and the final result for the formfactor c_j combines n-point integrals with the pinched $(n-1)$-point integrals as in equation (3.4).

The presence of the Gram determinant is, in some ways, no great surprise. In the limit $\Delta_n \to 0$, the $(n-1)$ momenta no longer span an $(n-1)$-dimensional space, the $(n-1)$ equations of the Passarino-Veltman approach are no longer independent and the decomposition is invalid. Stuart [34] has made modifications to the basic approach to account for this, the main observation being that for $\Delta_n = 0$, the scalar n-point integral can be written

as a sum of scalar $(n-1)$-point integrals. As a consequence, there are large cancellations between scalar integrals with differing numbers of external legs in the kinematic limit of vanishing Gram determinants. For loop corrections to processes such as quarkonium decay, where the two heavy quarks are considered to travel collinearly and share the quarkonium momentum, one can eliminate the Gram determinant singularities completely using the method of Stuart [34].

However, for more general scattering processes where the collinear limit may be approached, but is not exact, numerical problems as $\Delta_n \to 0$ may remain. Furthermore, we might imagine a method which clearly retains the simple structure of the $\Delta_n = 0$ case as this limit is smoothly approached.

Therefore, in this chapter the scalar integrals will be combined into functions that are well behaved in the $\Delta_n \to 0$ limit. The formfactors will be written as,

$$c_j \sim \alpha \frac{1}{\Delta_n} \left(\mathrm{I}_n^D[1] + \sum_{m=1}^{n} \beta'_m \mathrm{I}_{n-1}^{D,(m)}[1] \right) + \text{finite},$$

where "finite" represents terms that are manifestly well behaved as $\Delta_n \to 0$, and the grouping $(\cdots)$ vanishes with Δ_n. Such groupings combine a variety of dilogarithms, logarithms and constants together in a non-trivial way. In fact, for higher rank tensor integrals, with higher powers of Gram determinants in the denominator, it becomes even more desirable to organise the scalar integrals in this way. It is possible to construct these well behaved groupings by brute force, making a Taylor expansion of the scalar integrals in the appropriate limit. However, the functions presented in this chapter are generated systematically and naturally arise by considering the scalar integral in $D+2$ or higher dimensions[1] and/or by differentiating the scalar integrals with respect to the external kinematic variables. The approach taken here is therefore to re-express the formfactor coefficients in terms of functions that are finite as $\Delta_n \to 0$, explicitly cancelling off factors of the determinant where possible. The one-loop matrix elements for physical processes will then depend on these finite combinations, which can themselves be expanded as a Taylor series to obtain the required

[1]It will not prove necessary to explicitly compute the scalar integrals in higher dimensions, since they will be obtained recursively from the known scalar integrals in $D = 4 - 2\epsilon$ dimensions.

numerical precision. An additional improvement is that the physical size of the resulting expression is significantly reduced because the scalar integrals have been combined to form new, more natural functions.

Of course, one-loop amplitudes may also contain spurious singularities other than those directly arising from Gram determinants. Such singularities may occur as one or more of the external legs becomes lightlike or as two external momenta become collinear. However, since the new finite functions are obtained by differentiating the scalar integrals, they cannot contain additional kinematic singularities beyond those already present in the scalar integral. This helps to ensure that only genuine poles - those allowed at tree level - are explicitly present in the one-loop matrix elements. Once again, this helps to reduce the size of the expressions for the amplitudes.

3.3 General Notation

The basic integral is the rescaled one-loop integral in D dimensions[2],

$$\mathrm{I}_n^D[1] = (-1)^n\Gamma(n - D/2)\int_0^1 d^n x_i \delta(1 - \sum_i x_i)\left[\sum_{i,j=1}^{n} S_{ij}x_i x_j\right]^{D/2-n}. \tag{3.6}$$

Here, the Feynman parameters x_i have been introduced and the loop momentum has been integrated out (see Appendix A). The symmetric matrix S_{ij} contains all the process specific kinematics and reads,

$$S_{ij} = \frac{(M_i^2 + M_j^2 - (q_{i-1} - q_{j-1})^2)}{2}.$$

It is now beneficial to perform the projective transformation of t'Hooft and Veltman [35],

$$x_i = \alpha_i a_i = \frac{\alpha_i u_i}{\sum_{j=1}^n \alpha_j u_j}, \qquad \sum_{i=1}^{n} u_i = 1,$$

and further to introduce the constant matrix ρ_{ij} such that,

$$S_{ij} = \frac{\rho_{ij}}{\alpha_i \alpha_j}.$$

[2]Note the definition of I here differs from that of [27, 28] by a factor of $(-1)^n$.

The parameters α_i can be related to the kinematic variables present in the problem, while ρ_{ij} is considered independent of the α_i. Provided that all α_i are real and positive the scalar integral is now given by,

$$\mathrm{I}_n^D[1] = (-1)^n\Gamma(n - D/2)\int_0^1 d^n u_i \delta(1 - \sum_i u_i)\left(\prod_{j=1}^n \alpha_j\right)\left(\sum_{j=1}^n \alpha_j u_j\right)^{n-D}\left[\sum_{i,j=1}^n \rho_{ij}u_i u_j\right]^{D/2-n}. \tag{3.7}$$

In the approach which we shall introduce, the most useful quantity will be the rescaled integral $\hat{\mathrm{I}}$, which is related to the basic integral I by,

$$\mathrm{I}_n^D = \left(\prod_{j=1}^n \alpha_j\right)\hat{\mathrm{I}}_n^D. \tag{3.8}$$

Crucially, in $\hat{\mathrm{I}}$ the only dependence on the parameters α_i lies in the factor $\sum_{j=1}^n \alpha_j u_j$.

3.3.1 Basic Results

From the above equations (3.7) and (3.8) it is clear that differentiating with respect to α_i brings down a factor of the rescaled Feynman parameter a_i under the integral,

$$\hat{\mathrm{I}}_n^D[a_i] = \frac{1}{(n-D)}\frac{\partial \hat{\mathrm{I}}_n^D[1]}{\partial \alpha_i}, \tag{3.9}$$

where the notation is obvious. With repeated differentiation, it is possible to generate all integrals with Feynman parameters in the numerator.

The second step of Bern, Kosower and Dixon's work [27, 28] is to relate the n-point integral with one Feynman parameter in the numerator to a collection of scalar n and $(n-1)$-point integrals,

$$\hat{\mathrm{I}}_n^D[a_i] = \frac{1}{2N_n}\sum_{m=1}^n\left(\frac{\hat{\gamma}_i\hat{\gamma}_m}{\hat{\Delta}_n} - \eta_{im}\right)\hat{\mathrm{I}}_{n-1}^{D\,(m)}[1] + \frac{\hat{\gamma}_i}{\hat{\Delta}_n}\hat{\mathrm{I}}_n^D[1], \tag{3.10}$$

where $\hat{\Delta}_n$, $\hat{\gamma}_i$ and η_{ij} are defined by[3],

$$\hat{\Delta}_n = \left(\prod_{i=1}^n \alpha_i\right)^2 \Delta_n = \sum_{i,j=1}^n \eta_{ij}\alpha_i\alpha_j \equiv \sum_{j=1}^n \alpha_j\hat{\gamma}_j \equiv \sum_{j=1}^n \gamma_j,$$

[3]Note that the definition of $\hat{\gamma}$ coincides with γ of [27, 28].

and,

$$N_n = \frac{1}{2}(\det \eta)^{\frac{1}{n-1}}.$$

In later sections, explicit examples using this notation will be worked through. Equation (3.10) is the analogue of the formfactor reduction in momentum space of [26] and is easily obtained by integration by parts. The summation over m represents all possible pinchings of the n-point graph to form $(n-1)$-point integrals. As expected from other reduction methods, the Gram determinant appears in the denominator. However, equations (3.9) and (3.10) are equivalent and since, with a few notable exceptions, the scalar integrals have a Taylor expansion around $\hat{\Delta}_n = 0$, the act of differentiation will not usually introduce a singular behaviour. Therefore, we might expect that the n-point and $(n-1)$-point integrals combine in such a way that the $\hat{\Delta}_n \to 0$ limit is well behaved.

3.3.2 Finite Functions

This conspiracy can best be seen by considering the n-point integral in $D+2$ dimensions [27, 28, 33],

$$\begin{aligned} \hat{\mathrm{I}}_n^{D+2}[1] &= \frac{1}{(n-1-D/2)(n-D)(n-D-1)} \rho_{ij} \frac{\partial^2 \hat{\mathrm{I}}_n^D[1]}{\partial\alpha_j \partial\alpha_i} \\ &= \frac{1}{(n-D-1)} \frac{2N_n}{\hat{\Delta}_n} \left(\hat{\mathrm{I}}_n^D[1] + \frac{1}{2N_n} \sum_{m=1}^{n} \hat{\gamma}_m \hat{\mathrm{I}}_{n-1}^{D\,(m)}[1] \right). \end{aligned} \tag{3.11}$$

By comparison with (3.10), this earlier equation can now be recast in a more useful form,

$$\hat{\mathrm{I}}_n^D[a_i] = \frac{1}{2N_n} \left((n-D-1)\hat{\gamma}_i \hat{\mathrm{I}}_n^{D+2}[1] - \sum_{m=1}^{n} \eta_{im} \hat{\mathrm{I}}_{n-1}^{D\,(m)}[1] \right). \tag{3.12}$$

It is important to note that there are no Gram determinants visible in this equation. They have all been collected into the higher dimensional n-point integral. It is clear that if $\hat{\mathrm{I}}_n^D[1]$ is finite as $\hat{\Delta}_n \to 0$, then so is $\hat{\mathrm{I}}_n^{D+2}[1]$ and therefore so is $\hat{\mathrm{I}}_n^D[a_i]$. This confirms that the apparent divergence as $\hat{\Delta}_n \to 0$ is fake. Furthermore, $\hat{\mathrm{I}}_n^{D+2}[1]$ is an excellent candidate for a finite function - it is well behaved as the Gram determinant vanishes and is easily related to the Feynman parameter integrals via equation (3.11). Of course, it may still be divergent as $\epsilon \to 0$ and the dimensionally regulated poles remain to be isolated.

By applying the derivative approach, this can easily be extended to two or more Feynman parameters in the numerator,

$$\begin{aligned}\hat{\mathrm{I}}_n^D[a_i a_j] &= \frac{1}{(n-D-1)}\frac{\partial \hat{\mathrm{I}}_n^D[a_i]}{\partial \alpha_j} \\ &= \frac{1}{2N_n}\left(\hat{\gamma}_i \frac{\partial \hat{\mathrm{I}}_n^{D+2}[1]}{\partial \alpha_j} + \frac{\partial \hat{\gamma}_i}{\partial \alpha_j}\hat{\mathrm{I}}_n^{D+2}[1] - \frac{1}{(n-D-1)}\sum_{m=1}^{n}\eta_{im}\frac{\partial \hat{\mathrm{I}}_{n-1}^{D\,(m)}[1]}{\partial \alpha_j}\right).\end{aligned}$$

Using equation (3.9) and the identity,

$$\frac{\partial \hat{\gamma}_i}{\partial \alpha_j} \equiv \eta_{ij},$$

yields,

$$\hat{\mathrm{I}}_n^D[a_i a_j] = \frac{1}{2N_n}\left((n-D-2)\hat{\gamma}_i \hat{\mathrm{I}}_n^{D+2}[a_j] + \eta_{ij}\hat{\mathrm{I}}_n^{D+2}[1] - \sum_{m=1}^{n}\eta_{im}\hat{\mathrm{I}}_{n-1}^{D\,(m)}[a_j]\right). \tag{3.13}$$

Note that $\hat{\mathrm{I}}_{n-1}^{D\,(m)}[1]$ does not depend on α_m, and therefore,

$$\hat{\mathrm{I}}_{n-1}^{D\,(j)}[a_j] \sim \frac{\partial \hat{\mathrm{I}}_{n-1}^{D\,(j)}[1]}{\partial \alpha_j} \equiv 0.$$

Consequently, the $m = j$ term in the summation vanishes.

Differentiation has not produced any new Gram determinants and we can treat these integrals as new well behaved building blocks, or substitute for them using equation (3.12) with D replaced by $D+2$,

$$\begin{aligned}\hat{\mathrm{I}}_n^D[a_i a_j] &= \frac{1}{4N_n^2}\Big((n-D-2)(n-D-3)\hat{\gamma}_i\hat{\gamma}_j\hat{\mathrm{I}}_n^{D+4}[1] + 2N_n\eta_{ij}\hat{\mathrm{I}}_n^{D+2}[1] \\ &\quad -(n-D-2)\sum_{m=1}^{n}\hat{\gamma}_i\eta_{jm}\hat{\mathrm{I}}_{n-1}^{D+2\,(m)}[1] - 2N_n\sum_{m=1}^{n}\eta_{im}\hat{\mathrm{I}}_{n-1}^{D\,(m)}[a_j]\Big).\end{aligned}$$

The scalar integrals for $D+4$ dimensions can be obtained recursively from equation (3.11).

Replacing the factors of α_i in equations (3.12) and (3.13) and the analogous equations for three and four Feynman parameters in the numerator, gives,

$$\mathrm{I}_n^D[x_i] = \frac{1}{2N_n}\left((n-D-1)\gamma_i \mathrm{I}_n^{D+2}[1] - \sum_{m=1}^{n}\eta_{im}\alpha_i\alpha_m \mathrm{I}_{n-1}^{D\,(m)}[1]\right), \tag{3.14}$$

$$\mathrm{I}_n^D[x_i x_j] = \frac{1}{2N_n}\Big((n-D-2)\gamma_i \mathrm{I}_n^{D+2}[x_j] + \eta_{ij}\alpha_i\alpha_j \mathrm{I}_n^{D+2}[1] - \sum_{m=1}^{n} \eta_{im}\alpha_i\alpha_m \mathrm{I}_{n-1}^{D\,(m)}[x_j]\Big), \tag{3.15}$$

$$\mathrm{I}_n^D[x_i x_j x_k] = \frac{1}{2N_n}\Big((n-D-3)\gamma_i \mathrm{I}_n^{D+2}[x_j x_k] + \eta_{ij}\alpha_i\alpha_j \mathrm{I}_n^{D+2}[x_k] + \eta_{ik}\alpha_i\alpha_k \mathrm{I}_n^{D+2}[x_j] - \sum_{m=1}^{n} \eta_{im}\alpha_i\alpha_m \mathrm{I}_{n-1}^{D\,(m)}[x_j x_k]\Big), \tag{3.16}$$

$$\mathrm{I}_n^D[x_i x_j x_k x_l] = \frac{1}{2N_n}\Big((n-D-4)\gamma_i \mathrm{I}_n^{D+2}[x_j x_k x_l] + \eta_{ij}\alpha_i\alpha_j \mathrm{I}_n^{D+2}[x_k x_l] + \eta_{ik}\alpha_i\alpha_k \mathrm{I}_n^{D+2}[x_j x_l] + \eta_{il}\alpha_i\alpha_l \mathrm{I}_n^{D+2}[x_j x_k] - \sum_{m=1}^{n} \eta_{im}\alpha_i\alpha_m \mathrm{I}_{n-1}^{D\,(m)}[x_j x_k x_l]\Big). \tag{3.17}$$

Once again, no Gram determinants are apparent and these equations may be solved by recursive iteration. These are our main results and their use will be made clear with the explicit examples in the following sections.

Before proceeding to the explicit examples, we note that the full tensor structure in momentum space is simply obtained from the Feynman parameter integrals by introducing the auxiliary momentum $\mathcal{P}^\mu$ defined in equation (3.5). With an obvious notation (and after integration of the loop momentum) the tensor integrals can be written,

$$\begin{aligned}
\mathrm{I}_n^D[\ell^\mu] &\to \mathrm{I}_n^D[\mathcal{P}^\mu], \\
\mathrm{I}_n^D[\ell^\mu \ell^\nu] &\to \mathrm{I}_n^D[\mathcal{P}^\mu \mathcal{P}^\nu] - \frac{1}{2}\mathrm{I}_n^{D+2}[g^{\mu\nu}], \\
\mathrm{I}_n^D[\ell^\mu \ell^\nu \ell^\rho] &\to \mathrm{I}_n^D[\mathcal{P}^\mu \mathcal{P}^\nu \mathcal{P}^\rho] - \frac{1}{2}\mathrm{I}_n^{D+2}[\{g\mathcal{P}\}^{\mu\nu\rho}], \\
\mathrm{I}_n^D[\ell^\mu \ell^\nu \ell^\rho \ell^\sigma] &\to \mathrm{I}_n^D[\mathcal{P}^\mu \mathcal{P}^\nu \mathcal{P}^\rho \mathcal{P}^\sigma] - \frac{1}{2}\mathrm{I}_n^{D+2}[\{g\mathcal{P}\mathcal{P}\}^{\mu\nu\rho\sigma}] + \frac{1}{4}\mathrm{I}_n^{D+4}[\{gg\}^{\mu\nu\rho\sigma}],
\end{aligned}$$

where $\{a \ldots b\}^{\mu_1 \cdots \mu_n}$ is the usual Passarino-Veltman notation [26], and indicates a sum over all possible permutations of Lorentz indices carried by $a \ldots b$. For example,

$$\{g\mathcal{P}\}^{\mu\nu\rho} = g^{\mu\nu}\mathcal{P}^\rho + g^{\nu\rho}\mathcal{P}^\mu + g^{\rho\mu}\mathcal{P}^\nu.$$

Throughout the next sections, the simplifying choice $M_i = 0$ is made. Such integrals are relevant for a wide range of QCD processes involving loops of gluons or massless quarks. In

particular, all the results presented will be applicable to the process $\gamma^* \to 4$ jets at next-to-leading order, as described in chapter 4. The approach can be straightforwardly extended to include non-zero internal masses [28].

The strategy is to isolate the ultraviolet and infrared poles from the tensor integrals, leaving the finite remainder in the form of groups of terms that are well behaved in all of the kinematic limits. In real calculations where groups of tensor integrals are combined, this grouping will often cancel as a whole. Alternatively, if the kinematic coefficient allows, the determinant can be cancelled off for all of the terms in the function. This approach is well suited to treatment by an algebraic manipulation program, once the raw integrals have been massaged to isolate the poles in ϵ and to group the terms. As will be shown in the explicit examples, this is usually straightforward.

3.4 Three Point Integrals

In processes where the internal lines are massless, there are only three types of triangle graph described by the number of massive external legs. For the one-loop corrections to five parton scattering [36, 37, 38], only the graphs with one and two massless legs occur. For processes involving a gauge boson such as $Z \to 4$ partons, graphs with all external legs massive or off-shell contribute.

First, consider triangle integrals with exiting momenta p_1, p_2 and p_3 as shown in fig. 3.2 and all internal masses equal to zero, $M_i = 0$. Throughout, p_3 (and the Feynman parameter x_2) are systematically eliminated using momentum conservation so that $p_3 = -(p_1 + p_2)$, $p_3^2 = (p_1 + p_2)^2 = s_{12}$ and,

$$\mathcal{P}^\mu = -(1 - x_1)p_1^\mu - x_3 p_2^\mu.$$

The full tensor structure with up to three loop momenta in the numerator can therefore be derived from loop integrals with up to three powers of x_1 or x_3 in the numerator.

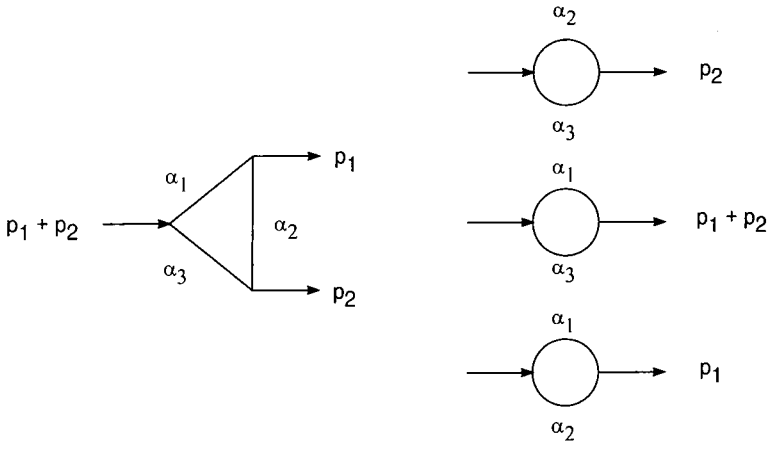

Figure 3.2: The triangle graph and each of the three pinchings obtained by omitting the internal line associated with α_m for $m = 1, 2$ and 3. In each case, the internal line is shrunk to a point and the momenta at either end are combined. The relation between the external momenta and the α_i can be seen by cutting the loop; $\alpha_i\alpha_j = -1/p^2$ where p is the momentum on one side of the cut and α_i, α_j are associated with the cut lines.

3.4.1 Three Massive Legs

As a first step, consider the general case, p_1^2, p_2^2, $s_{12} \neq 0$, where the scalar integral in four dimensions is known to be finite. Here the α_i parameters can be determined by,

$$\alpha_1\alpha_2 p_1^2 = -1, \qquad \alpha_2\alpha_3 p_2^2 = -1, \qquad \alpha_1\alpha_3 s_{12} = -1,$$

while,

$$\begin{aligned} \Delta_3 &= -p_1^4 - p_2^4 - s_{12}^2 + 2p_1^2p_2^2 + 2p_1^2 s_{12} + 2p_2^2 s_{12}, \\ \hat{\Delta}_3 &= -\alpha_1^2 - \alpha_2^2 - \alpha_3^2 + 2\alpha_1\alpha_2 + 2\alpha_1\alpha_3 + 2\alpha_2\alpha_3. \end{aligned}$$

From the definition of the matrix η, we see that,

$$\eta_{ij} = \begin{pmatrix} -1 & 1 & 1 \\ 1 & -1 & 1 \\ 1 & 1 & -1 \end{pmatrix}, \qquad N_3 = 1.$$

The variables γ always appear in the following combinations,

$$\frac{\gamma_i}{\prod_{j=1}^{3}\alpha_j^2} = \begin{cases} p_2^2(p_1^2 + s_{12} - p_2^2) & i = 1 \\ s_{12}(p_2^2 + p_1^2 - s_{12}) & i = 2 \\ p_1^2(p_2^2 + s_{12} - p_1^2) & i = 3 \end{cases} .$$

Scalar Integral

The scalar triangle integral for all external masses non-zero is finite in four dimensions [39, 27, 30] ,[4]

$$\mathrm{I}_3[1] = \frac{1}{\sqrt{-\Delta_3}}\left(\log(a^+a^-)\log\left(\frac{1-a^+}{1-a^-}\right) + 2\mathrm{Li}_2(a^+) - 2\mathrm{Li}_2(a^-)\right), \tag{3.18}$$

where Li_2 is the usual dilogarithm function and $a^\pm$ are two roots of a quadratic equation,

$$a^\pm = \frac{s_{12} + p_2^2 - p_1^2 \pm \sqrt{-\Delta_3}}{2s_{12}}.$$

Although $\mathrm{I}_3[1]$ appears to diverge as $\Delta_3 \to 0$, this is not the case. As noted by Stuart [34], in this limit, the triangle graph reduces to a sum of bubble graphs,

$$\lim_{\Delta_3 \to 0} \mathrm{I}_3[1] = \frac{2}{s_{12} + p_1^2 - p_2^2}\log\left(\frac{s_{12}}{p_2^2}\right) + \frac{2}{s_{12} + p_2^2 - p_1^2}\log\left(\frac{s_{12}}{p_1^2}\right),$$

and there is a well behaved Taylor series in Δ_3.

Tensor Integrals in $D = 4$

The tensor integral can be easily written in terms of higher dimensional scalar integrals and bubble scalar integrals using eqs. (3.14–3.16). For one Feynman parameter in the numerator, this gives,

$$\mathrm{I}_3^{D=4-2\epsilon}[x_i] = -(1-\epsilon)\gamma_i \mathrm{I}_3^{D=6-2\epsilon}[1] - \frac{1}{2}\sum_{m=1}^{3}\eta_{im}\alpha_i\alpha_m \mathrm{I}_2^{D=4-2\epsilon(m)}[1].$$

[4] For scalar integrals in $D = 4 - 2\epsilon$ or $D = 4$ dimensions, we omit the superscript D.

Immediately a problem is apparent – the coefficient of the scalar integral in $(6-2\epsilon)$ dimensions, γ_i, is singular as one or more of the external momenta become lightlike. Although the divergence as the Gram determinant vanishes has been removed, it appears to have been replaced by a divergence as the invariants vanish[5]. However, these divergences cancel between the triangle and bubble contributions and the tensor integral itself is well behaved and finite in all kinematic limits and is therefore a better choice for a finite function.

In fact, since the triangle scalar integral is finite in 4 dimensions, it is convenient to generate the tensor structure directly from derivatives of the scalar integral. However, in order to use equation (3.10), the two point integral for external momentum p (and internal masses $M_i = 0$) is also needed. This is given by,

$$\mathrm{I}_2^D[1] = \frac{\Gamma(2-D/2)\Gamma^2(D/2-1)}{\Gamma(D-2)}(-p^2)^{D/2-2}, \tag{3.19}$$

For pinching $m = 1, 2$ or 3 of fig. 3.2 and $D = 4-2\epsilon$,

$$\hat{\mathrm{I}}_2^{(m)}[1] = \left(\frac{\alpha_m}{\prod_{i=1}^3 \alpha_i}\right)\mathrm{I}_2^{(m)}[1] = \frac{c_\Gamma}{\epsilon(1-2\epsilon)}\left(\frac{\alpha_m}{\prod_{i=1}^3 \alpha_i}\right)^{1-\epsilon},$$

where the usual product of Gamma functions obtained in one-loop integrals c_Γ is given by,

$$c_\Gamma = \frac{\Gamma^2(1-\epsilon)\Gamma(1+\epsilon)}{\Gamma(1-2\epsilon)}.$$

Rewriting equation (3.10) for the case $D = 4$, $n = 3$ and $i = 3$ and adding,

$$\frac{1}{2}\sum_{m=1}^{3}\left(\eta_{3m} - \frac{\hat{\gamma}_3\hat{\gamma}_m}{\hat{\Delta}_3}\right)\frac{\alpha_m}{\alpha_2}\hat{\mathrm{I}}_2^{(2)}[1] = 0,$$

gives,

$$\begin{aligned}\hat{\mathrm{I}}_3[a_3] &= \frac{1}{\hat{\Delta}_3}\left(\hat{\gamma}_3\hat{\mathrm{I}}_3[1] + \frac{1}{2}\sum_{m=1}^{3}\left(\hat{\gamma}_3\hat{\gamma}_m - \eta_{3m}\hat{\Delta}_3\right)\frac{\alpha_m}{\prod\alpha}\left(\mathrm{I}_2^{(m)}[1] - \mathrm{I}_2^{(2)}[1]\right)\right) \\ &= \frac{1}{\hat{\Delta}_3}\left(\hat{\gamma}_3\hat{\mathrm{I}}_3[1] - \frac{\hat{\gamma}_2}{\alpha_3}\log\left(\frac{\alpha_2}{\alpha_1}\right) + 2\log\left(\frac{\alpha_2}{\alpha_3}\right)\right) + \mathcal{O}(\epsilon).\end{aligned} \tag{3.20}$$

Alternatively, this could be obtained by differentiation of equation (3.18). By trivial replacement of factors of α, we find,

$$\mathrm{I}_3[x_3] = \frac{1}{\Delta_3}\left(p_1^2(s_{12}+p_2^2-p_1^2)\mathrm{I}_3[1] + (p_1^2+p_2^2-s_{12})\log\left(\frac{s_{12}}{p_2^2}\right) - 2p_1^2\log\left(\frac{s_{12}}{p_1^2}\right)\right) \tag{3.21}$$

[5]Problems in this limit are to be expected since even the scalar integral itself is not finite as $p_i^2 \to 0$.

Integrals with higher powers of Feynman parameters can now be generated by direct differentiation of $\hat{\mathrm{I}}_3[a_3]$,

$$\mathrm{I}_3[x_i x_3^n] = -\frac{1}{(n+1)}\left(\prod\alpha\right)\alpha_i\alpha_3^n\frac{\partial}{\partial\alpha_i}\hat{\mathrm{I}}_3[a_3^n].$$

All of these functions will be finite in the $\epsilon \to 0$ limit, and can be considered as building blocks in constructing the tensor structures for box and pentagon integrals. In fact, because they are obtained by differentiating a function well behaved as $\Delta_3 \to 0$, they are also finite in this limit. Therefore, they tie together the dilogarithms from the triangle integrals and the logarithms from bubble integrals in an economical and numerically very stable way.

These functions are also directly generated in tensor structures for box graphs (equations (3.14–3.17) with $n = 4$) and will naturally cancel in Feynman diagram calculations involving both triangle and box graphs.

Finite Functions

For general calculations with $p_1^2 \neq 0$ and $p_2^2 \neq 0$, we introduce the notation,

$$\mathrm{Lc}_0(p_1,p_2) = \mathrm{I}_3[1], \qquad \mathrm{Lc}_{2n-1}(p_1,p_2) = \mathrm{I}_3[x_3^n], \qquad \mathrm{Lc}_{2n}(p_1,p_2) = \mathrm{I}_3[x_1 x_3^n], \tag{3.22}$$

for $\mathrm{Lc}_{0\ldots5}$. The symmetry properties of the triangle function imply that the analogous functions for $x_1 \leftrightarrow x_3$ (or $\alpha_1 \leftrightarrow \alpha_3$) are just obtained by exchanging p_1 and p_2. In dealing with box graphs, integrals with x_2 in the numerator will naturally arise. In these cases, we systematically eliminate them using $\sum_i x_i = 1$. Explicitly, we find,

$$\begin{aligned}
\mathrm{I}_3[x_1x_3] &= \frac{1}{2\Delta_3}\Big(2p_2^2(s_{12}+p_1^2-p_2^2)\mathrm{I}_3[x_3] + p_1^2(s_{12}+p_2^2-p_1^2)\mathrm{I}_3[x_1] \\
&\qquad -p_1^2p_2^2\mathrm{I}_3[1] - p_2^2\log\left(\frac{s_{12}}{p_2^2}\right) + p_1^2 + p_2^2 - s_{12}\Big), \qquad (3.23)\\
\mathrm{I}_3[x_3^2] &= \frac{1}{2\Delta_3}\left(3p_1^2(s_{12}+p_2^2-p_1^2)\mathrm{I}_3[x_3] + p_1^4\mathrm{I}_3[1] - (s_{12}-p_2^2)\log\left(\frac{s_{12}}{p_2^2}\right) - 2p_1^2\right), \qquad (3.24)\\
\mathrm{I}_3[x_1x_3^2] &= \frac{1}{6\Delta_3}\Big(4p_2^2(s_{12}+p_1^2-p_2^2)\mathrm{I}_3[x_3^2] + 6p_1^2(s_{12}+p_2^2-p_1^2)\mathrm{I}_3[x_1x_3] \\
&\qquad -3p_1^2p_2^2\mathrm{I}_3[x_3] + p_1^4\mathrm{I}_3[x_1] - p_2^2\log\left(\frac{s_{12}}{p_2^2}\right) + p_2^2 - s_{12}\Big), \qquad (3.25)
\end{aligned}$$

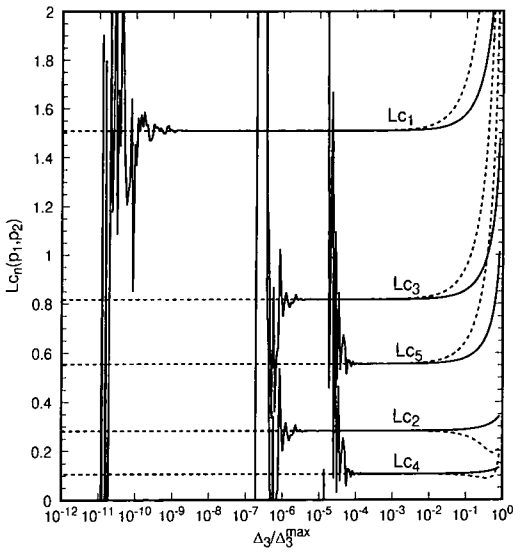

Figure 3.3: The finite functions for the triply massive triangle graph with $s_{12} = 1$, $p_1^2 = 0.2$ as a function of $\Delta_3/\Delta_3^{\max}$ where $\Delta_3^{\max} = -(s_{12} - p_1^2)^2$. The functions have been evaluated using double precision Fortran. The dashed lines show the approximate form for the function in the limit $\Delta_3 \to 0$, retaining only the first term of the Taylor expansion.

$$\mathrm{I}_3[x_3^3] = \frac{1}{3\Delta_3}\left(5p_1^2(s_{12}+p_2^2-p_1^2)\mathrm{I}_3[x_3^2] + 2p_1^4\mathrm{I}_3[x_3] - (s_{12}-p_2^2)\log\left(\frac{s_{12}}{p_2^2}\right) - p_1^2\right) \quad (3.26)$$

By expanding as a series in Δ_3, these functions can be evaluated near the singularity with arbitrary precision. For example,

$$\lim_{\Delta_3\to 0}\mathrm{I}_3[x_3^2] = \frac{(s_{12}+p_1^2-p_2^2)}{3s_{12}(s_{12}-p_1^2-p_2^2)} - \frac{2p_1^4}{3s_{12}(s_{12}-p_1^2-p_2^2)^2}\log\left(\frac{s_{12}}{p_1^2}\right) + \frac{(3s_{12}-3p_1^2+p_2^2)}{6s_{12}(s_{12}-p_1^2-p_2^2)}\log\left(\frac{s_{12}}{p_2^2}\right).$$

To illustrate this, fig. 3.3 shows the various functions at a specific phase space point, $s_{12} = 1$, $p_1^2 = 0.2$ and letting p_2^2 vary in such a way that $\Delta_3 \to 0$. This corresponds to $p_2^2 \to 0.135$. We see that as this limit is approached, the numerical evaluation of the function using double precision (an intrinsic numerical precision, *acc*, of roughly 10^{-14}) becomes uncertain. For this particular phase space point, functions with a single Gram determinant in the denominator (Lc_1) remain stable until $\Delta_3/\Delta_3^{\max} \sim 10^{-9}$ while those with more powers of

the Gram determinant break down correspondingly sooner - at $\Delta_3/\Delta_3^{max} \sim 10^{-6}$ for Lc_2 and Lc_3 and $\Delta_3/\Delta_3^{max} \sim 10^{-4}$ for Lc_4 and Lc_5. In general, numerical problems typically occur when $\Delta_3/\Delta_3^{max} \sim (acc)^{1/N}$ where N is the number of Gram determinants in the denominator of the function. Other phase space points yield a similar behaviour.

The unstable points represent a rather small proportion of the allowed phase space. However, problems may arise using adaptive Monte Carlo methods such as VEGAS [40] where the phase space is preferentially sampled where the matrix elements are large. Finding an anomalously high value for the matrix elements in a region of instability would cause the Monte Carlo integration to focus on that region giving unpredictable results.

Of course, these instabilities could be handled by a brute force increase in numerical precision. While possible, this has the disadvantage of producing significantly slower code, and, since in all cases, the approximate form obtained by making a Taylor expansion about $\Delta_3 = 0$ and keeping only the constant term works well where the numerical instabilities begin, this is not an attractive solution. In fact, the approximation is reliable for $\Delta_3 < 10^{-3}\Delta_3^{max}$. Explicit forms for the approximations are collected in Appendix C.

Scalar Integrals in Higher Dimensions

We now turn to the scalar triangle integrals in higher dimensions. They appear in the $g_{\mu\nu}$ part of the general Lorentz structure and recursively in the determination of $I_4^{D=4-2\epsilon}[x_i...x_l]$. Unlike the triangle in four dimensions, these integrals are ultraviolet divergent due to the presence of the various pinchings - bubble integrals. A function that can usefully be used as a building block of matrix element calculations, must be finite as both $\Delta_3 \to 0$ *and* $\epsilon \to 0$ and we must first isolate the poles in ϵ. Although equation (3.11) suggests that the ultraviolet pole structure involves Δ_3, this is easily shown not to be the case. Adding terms proportional to,

$$\frac{1}{2}\left(\hat{\Delta}_3 - \sum_{m=1}^{3} \hat{\gamma}_m \alpha_m\right) \frac{1}{\alpha_2} \hat{I}_2^{(2)}[1] = 0,$$

to equation (3.11) for $n = 3$, $D = 4 - 2\epsilon$ we see,

$$\hat{\mathrm{I}}_3^{D=6-2\epsilon}[1] = -\frac{1}{(1-\epsilon)}\frac{1}{\hat{\Delta}_3}\left(\hat{\mathrm{I}}_3[1] + \frac{1}{2}\sum_{m=1}^{3}\frac{\gamma_m}{\prod\alpha}\left(\mathrm{I}_2^{(m)}[1] - \mathrm{I}_2^{(2)}[1]\right) + \frac{\hat{\Delta}_3}{2\prod\alpha}\mathrm{I}_2^{(2)}[1]\right),$$

where the divergence as $\epsilon \to 0$ lies exclusively in the last term. Reinserting the factors of α and the definition of $\mathrm{I}_2[1]$ in $D = 4 - 2\epsilon$ dimensions we find,

$$\mathrm{I}_3^{D=6-2\epsilon}[1] = \mathrm{Lc}_{1S}(p_1, p_2) - \frac{1}{2}\left(\frac{(-s_{12})^{-\epsilon}}{\epsilon} + 3\right)c_\Gamma, \tag{3.27}$$

where,

$$\begin{aligned}\mathrm{Lc}_{1S}(p_1, p_2) &= \frac{1}{2\Delta_3}\Bigg(2p_1^2p_2^2s_{12}\mathrm{I}_3[1] - p_1^2(s_{12} + p_2^2 - p_1^2)\log\left(\frac{s_{12}}{p_1^2}\right) \\ &\qquad -p_2^2(s_{12} + p_1^2 - p_2^2)\log\left(\frac{s_{12}}{p_2^2}\right)\Bigg) \\ &= \frac{1}{2}\left(p_1^2\mathrm{I}_3[x_1] + p_2^2\mathrm{I}_3[x_3]\right).\end{aligned} \tag{3.28}$$

In a similar fashion, the ϵ pole structure can be removed from the triangle scalar integral in $D = 8 - 2\epsilon$ and $D = 10 - 2\epsilon$ dimensions yielding two more functions that are finite as both $\Delta_3 \to 0$ and $\epsilon \to 0$. Explicitly we find,

$$\mathrm{I}_3^{D=8-2\epsilon}[1] = \mathrm{Lc}_{2S}(p_1, p_2) - \frac{(p_1^2 + p_2^2 + s_{12})}{24}\left(\frac{(-s_{12})^{-\epsilon}}{\epsilon} + \frac{19}{6}\right)c_\Gamma, \tag{3.29}$$

$$\mathrm{I}_3^{D=10-2\epsilon}[1] = \mathrm{Lc}_{3S}(p_1, p_2) - \frac{(p_1^4 + p_2^4 + s_{12}^2 + p_1^2p_2^2 + p_1^2s_{12} + p_2^2s_{12})}{360}\left(\frac{(-s_{12})^{-\epsilon}}{\epsilon} + \frac{17}{5}\right)c_\Gamma, \tag{3.30}$$

where the finite functions are defined by,

$$\begin{aligned}\mathrm{Lc}_{2S}(p_1, p_2) &= \frac{1}{4\Delta_3}\Bigg(2p_1^2p_2^2s_{12}\mathrm{Lc}_{1S}(p_1, p_2) - \frac{1}{6}\Bigg(p_1^4(s_{12} + p_2^2 - p_1^2)\log\left(\frac{s_{12}}{p_1^2}\right) \\ &\qquad +p_2^4(s_{12} + p_1^2 - p_2^2)\log\left(\frac{s_{12}}{p_2^2}\right) + 2p_1^2p_2^2s_{12}\Bigg)\Bigg),\end{aligned} \tag{3.31}$$

$$\begin{aligned}\mathrm{Lc}_{3S}(p_1, p_2) &= \frac{1}{6\Delta_3}\Bigg(2p_1^2p_2^2s_{12}\mathrm{Lc}_{2S}(p_1, p_2) - \frac{1}{60}\Bigg(p_1^6(s_{12} + p_2^2 - p_1^2)\log\left(\frac{s_{12}}{p_1^2}\right) \\ &\qquad +p_2^6(s_{12} + p_1^2 - p_2^2)\log\left(\frac{s_{12}}{p_2^2}\right) + \frac{p_1^2p_2^2s_{12}}{2}(p_1^2 + p_2^2 + s_{12})\Bigg)\Bigg).\end{aligned} \tag{3.32}$$

Although these functions have been obtained via equation (3.11), they are still related to derivatives of the basic scalar integral in $D = 4 - 2\epsilon$, and are therefore finite in the $\Delta_3 \to 0$ limit. We can see this by examining the same phase space point as before, $s_{12} = 1$, $p_1^2 = 0.2$ and varying Δ_3. As expected, the Lc_{nS} show a similar behaviour to the Lc_n functions - numerically breaking down at larger and larger values of Δ_3 as the number of Gram determinants increases, and being well described by the first term in the Taylor expansion as this happens. For completeness, we collect the limiting approximations in Appendix C.

Tensor Integrals in Higher Dimensions

For triangle loop integrals with three loop momenta in the numerator, it is also necessary to know the $D = 6 - 2\epsilon$ integral with a single Feynman parameter in the numerator. Rather than differentiating the ultraviolet divergent $\mathrm{I}_3^{D=6-2\epsilon}[1]$, we can evaluate it in terms of the $D = 4 - 2\epsilon$ tensor integrals of section 3.1.1. Using (3.13) for $D = 4 - 2\epsilon$, we see that,

$$\begin{aligned}\hat{\mathrm{I}}_3[a_1 a_j] + \hat{\mathrm{I}}_3[a_3 a_j] &= \frac{1}{2}\Bigg(-(3-2\epsilon)(\hat{\gamma}_1+\hat{\gamma}_3)\hat{\mathrm{I}}_3^{D=6-2\epsilon}[a_j] + (\eta_{1j}+\eta_{3j})\hat{\mathrm{I}}_3^{D=6-2\epsilon}[1] \\ &\qquad - \sum_{m=1}^{3}(\eta_{1m}+\eta_{3m})\hat{\mathrm{I}}_2^{(m)}[a_j]\Bigg),\end{aligned}$$

which, for $j = 1, 3$,[6] simplifies using,

$$\eta_{1j} + \eta_{3j} = 0.$$

The same equation simplifies the sum over bubble pinchings so that only $m = 2$ contributes, while $\hat{\gamma}_1 + \hat{\gamma}_3 = 2\alpha_2$. Restoring the factors of α and using,

$$\mathrm{I}_2^{(2)}[x_1] = \mathrm{I}_2^{(2)}[x_3] = \frac{1}{2}\left(\frac{(-s_{12})^{-\epsilon}}{\epsilon} + 2\right) c_\Gamma,$$

yields,

$$\mathrm{I}_3^{6-2\epsilon}[x_j] = \frac{1}{3}\Big(p_1^2 \mathrm{I}_3[x_1 x_j] + p_2^2 \mathrm{I}_3[x_3 x_j]\Big) - \frac{1}{6}\left(\frac{(-s_{12})^{-\epsilon}}{\epsilon} + \frac{8}{3}\right) c_\Gamma. \tag{3.33}$$

Later, we will see that constructing the tensor integrals for box graphs can also generate $\mathrm{I}_3^{6-2\epsilon}[x_j]$ and higher dimensional triangle integrals with more parameters in the numerator.

[6] Since the Feynman parameters add to one, the case $j = 2$ is of little interest.

In each case, we use similar tricks with equations (3.14–3.17) to rewrite them in terms of the four dimensional integrals with the ultraviolet pole made explicit.

3.4.2 The Two-Mass Triangle

We will also be interested in triangle graphs where one or more of the external momenta is lightlike. Here, we first focus on the case, $p_2^2 \to 0$. In $D = 4 - 2\epsilon$ dimensions, we have the well known result,

$$\mathrm{I}_3^{2m}[1] = \frac{c_\Gamma}{\epsilon^2}\left(\frac{(-s_{12})^{-\epsilon} - (-p_1^2)^{-\epsilon}}{s_{12} - p_1^2}\right), \tag{3.34}$$

where the superscript indicates that only two of the three legs are massive. For this choice of kinematics the rescaled integral can be written,

$$\hat{\mathrm{I}}_3^{2m}[1] = \frac{c_\Gamma}{\epsilon^2}\left(\frac{(\alpha_1\alpha_3)^{\epsilon} - (\alpha_1\alpha_2)^{\epsilon}}{\alpha_3 - \alpha_2}\right), \tag{3.35}$$

with,

$$\alpha_1\alpha_2 p_1^2 = -1, \qquad \alpha_1\alpha_3 s_{12} = -1,$$

and

$$\hat{\Delta}_3 = -(\alpha_3 - \alpha_2)^2,$$

so that the singular limit is $\alpha_3 \to \alpha_2$. Because $\hat{\Delta}_3$ makes no reference to α_1, η_{ij} contains a row of zeroes,

$$\eta_{ij} = \begin{pmatrix} 0 & 0 & 0 \\ 0 & -1 & 1 \\ 0 & 1 & -1 \end{pmatrix},$$

and therefore $N_3 = 0$. Consequently, care is needed in applying the equations of section 2. In addition, since the scalar integral for three massive legs is finite (and the results in the preceding subsections have been explicitly derived in $D = 4$), one cannot just set $p_2^2 \to 0$.

In fact, it is easiest just to bypass the problem and generate the whole tensor structure by direct differentiation of the scalar integral with respect to α_3 and α_1. It is easy to see

that,

$$\hat{\mathrm{I}}_3^{2m}[a_3^n] \sim A\hat{\mathrm{I}}_3^{2m}[1] + B\frac{(\alpha_1\alpha_3)^\epsilon}{\epsilon} + C\log\left(\frac{\alpha_3}{\alpha_2}\right) + D,$$

where A, B, C and D are polynomials in $1/\alpha_3$ and $1/(\alpha_3 - \alpha_2)$. Unlike the all massive case discussed before, the scalar integral is singular as $\epsilon \to 0$. As a general rule it is not necessary to be particularly careful with double poles in ϵ, since they must either cancel or form the infrared poles of real matrix elements. However, it is possible for the integrals to be multiplied by factors of ϵ - from expanding factors of dimension - and the resulting logarithms should occur in combinations that are finite as $\alpha_3 \to \alpha_2$. It is easy to see that,

$$\epsilon \times \hat{\mathrm{I}}_3^{2m}[1] = \frac{\log\left(\frac{\alpha_3}{\alpha_2}\right)}{\alpha_3 - \alpha_2} + \mathcal{O}(\epsilon),$$

is finite. So, to tie the logarithms and constants together in combinations that are well behaved in the $\alpha_3 \to \alpha_2$ limit, we use the fact that derivatives of this function are also well behaved, and introduce the functions,

$$\mathrm{Lc}_n^{2m}(p_1, p_2) = -\lim_{\epsilon\to 0}\left(\epsilon \times \mathrm{I}_3^{2m}[x_3^{n-1}]\right), \tag{3.36}$$

for $n = 1, \ldots, 4$. In terms of invariants,

$$\mathrm{Lc}_n^{2m}(p_1, p_2) = -\left(\frac{p_1^2\mathrm{Lc}_{n-1}^{2m}(p_1, p_2) - \frac{1}{n-1}}{s_{12} - p_1^2}\right), \qquad n \geq 2 \tag{3.37}$$

with,

$$\mathrm{Lc}_1^{2m}(p_1, p_2) = \frac{\log\left(\frac{s_{12}}{p_1^2}\right)}{s_{12} - p_1^2}. \tag{3.38}$$

These functions, or functions closely related to them, have appeared in next-to-leading order matrix element calculations [36, 37, 38, 31]. The explicit forms for $\mathrm{I}_3^{2m}[x_i x_j]$ appearing in the momentum expansion are well known and are collected in Appendix B.

Although these functions are rather simple, they still contain numerical instabilities as $p_1^2 \to s_{12}$. This can be seen in Fig. 3.4 where we show Lc_n^{2m} for the specific phase space point $s_{12} = 1$ and let p_1^2 approach s_{12}. While a single inverse powers of $(s_{12} - p_1^2)$ is handled correctly, higher powers cause problems. As can be seen from the figure, a suitable approximation is obtained by the first term in the Taylor expansion,

$$\lim_{p_1^2 \to s_{12}} \mathrm{Lc}_n^{2m}(p_1, p_2) = \frac{1}{np_1^2},$$

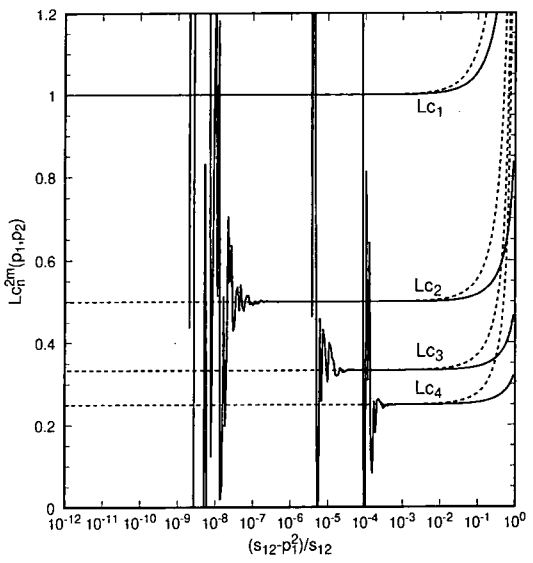

Figure 3.4: The finite functions for the triangle graph with two external masses with $s_{12} = 1$ evaluated in double precision Fortran as a function of $(s_{12} - p_1^2)/s_{12}$. The dashed lines show the approximate form for the function in the limit $p_1^2 \to s_{12}$, retaining only the first term of the Taylor expansion.

for $n \geq 1$.

The other configuration of triangle graph that appears is where two of the momenta are lightlike, $p_1^2 = p_2^2 = 0$. Once again, the tensor structure can be generated by differentiation or canonical Passarino-Veltman reduction. Here, there is only one scale in the problem so there can be no logarithms and it is neither possible nor necessary to introduce well behaved functions. The explicit forms for the Feynman parameter integrals appearing in the momentum expansion are well known and for the sake of completeness are given in Appendix B.

This concludes our discussion of triangle graphs. For the case of three massive external legs (and internal masses set equal to zero) the four dimensional tensor integrals are finite as $\epsilon \to 0$ and are given by the functions $\mathrm{Lc}_{0\ldots5}(p_1, p_2)$ defined in (3.18,3.21,3.23–3.26), while the ultraviolet divergent part $g_{\mu\nu}$ part, $\mathrm{I}_3^{D=6-2\epsilon}[1]$ is expressed in terms of a similar function (Lc_{1S}) with the pole isolated (3.28). For the tensor structure in the simpler case with one lightlike

leg, it is useful to group the logarithms and constants using the functions $\mathrm{Lc}^{2m}_{1\ldots4}(p_1, p_2)$ (3.38, 3.37).

For the more general case where the internal masses are non-zero, the same procedure can be utilised. The matrix η has slightly more entries and there are more scales in the problem. However, the grouping together of triangle graphs and bubble integrals into functions well behaved in the $\Delta_3 \to 0$ limit and the isolation of the ultraviolet singularities can be made explicit in the same way.

3.5 Four Point Integrals

For one-loop corrections to five parton scattering, box graphs with at most one massive external leg occur. However, for processes involving a massive vector boson and four massless partons, we can obtain box graphs with a second massive external leg by pinching together two of the partons. There are two distinct configurations according to the positions of the massive legs; the adjacent box graph and the opposite box graph. The box graph is shown in fig. 3.5 for outgoing momenta p_1, p_2 and p_3. Throughout this section, we will assume that $(p_1 + p_2 + p_3)^2 = s_{123} \neq 0$. In the adjacent two mass case, $p_2^2 = p_3^2 = 0$ and $p_1^2 \neq 0$, while for the opposite box, $p_1^2 = p_3^2 = 0$ and $p_2^2 \neq 0$. Unfortunately, the raw scalar integrals for these two cases behave rather differently. The adjacent box is finite in the limit that $\Delta_4 \to 0$, while the opposite box diverges as $\Delta_4 \to 0$. In this section, we work through these two configurations and rewrite the tensor integrals in terms of well behaved functions and explicit poles in ϵ.

3.5.1 The Adjacent Two-Mass Box

We first consider the adjacent box with $p_2^2 = p_3^2 = 0$ and all internal masses equal to zero. As in the triangle case, we systematically eliminate one of the momenta, $p_4 = -(p_1 + p_2 + p_3)$,

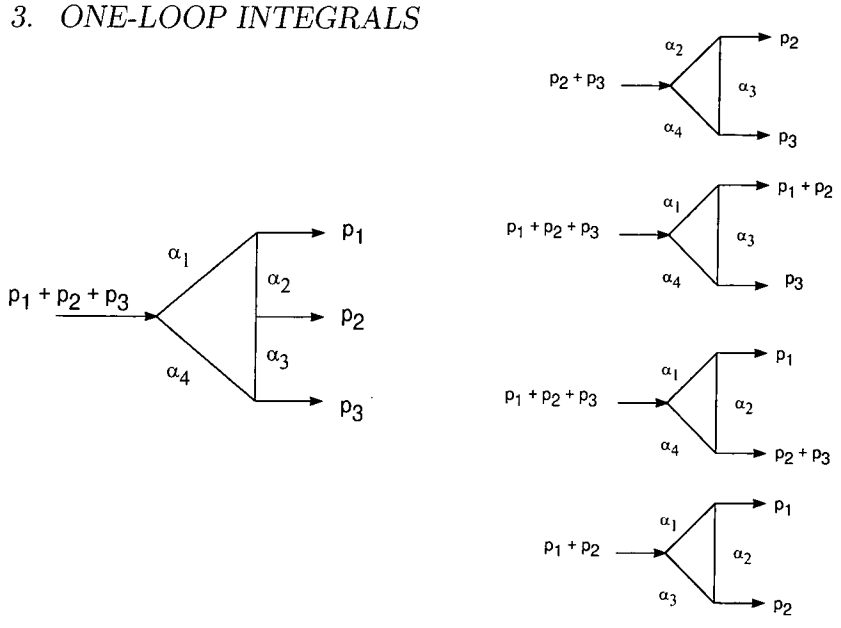

Figure 3.5: The box graph and each of the four pinchings obtained by omitting the internal line associated with α_m for $m = 1, 2, 3$ and 4.

and one of the Feynman parameters, $x_3 = 1 - x_1 - x_2 - x_4$, so that,

$$\mathcal{P}^\mu = -(1 - x_1)p_{12}^\mu + x_2 p_2^\mu - x_4 p_3^\mu.$$

The related integrals with $p_3^2 \neq 0$ and $p_1^2 = 0$ are obtained by $p_1 \leftrightarrow p_3$ (and the indices i and j in α_i and η_{ij} transform as $1 \leftrightarrow 4$ and $2 \leftrightarrow 3$).

For this kinematic configuration, the α parameters are defined by,

$$\alpha_1\alpha_4\, s_{123} = -1, \quad \alpha_1\alpha_2\, p_1^2 = -1$$
$$\alpha_1\alpha_3\, s_{12} = -1, \quad \alpha_2\alpha_4\, s_{23} = -1,$$

while,

$$\eta_{ij} = \begin{pmatrix} 0 & 0 & 1 & 0 \\ 0 & 0 & -1 & 1 \\ 1 & -1 & 2 & -1 \\ 0 & 1 & -1 & 0 \end{pmatrix}, \quad N_4 = \tfrac{1}{2},$$

and,

$$\Delta_4 = 2s_{23}\left((s_{123} - s_{12})(s_{12} - p_1^2) - s_{12}s_{23}\right).$$

The coefficients γ_i always appear in the following combinations which are directly related to the conventional variables,

$$\frac{\gamma_i}{\prod_{j=1}^{4}\alpha_j} = \begin{cases} -s_{23} & i=1 \\ s_{123}-s_{12} & i=2 \\ s_{123}+p_1^2-s_{23}-\frac{2p_1^2 s_{123}}{s_{12}} & i=3 \\ p_1^2-s_{12} & i=4 \end{cases}.$$

The scalar integral in $D=4-2\epsilon$ can be written [30, 27],

$$\hat{\mathrm{I}}_4[1] = \frac{c_\Gamma}{\epsilon^2}\left((\alpha_2\alpha_4)^\epsilon + 2(\alpha_1\alpha_3)^\epsilon - (\alpha_1\alpha_2)^\epsilon - (\alpha_1\alpha_4)^\epsilon\right) + 2\mathrm{Ld}_0(p_1,p_2,p_3) + \mathcal{O}(\epsilon), \tag{3.39}$$

where,

$$\mathrm{Ld}_0(p_1,p_2,p_3) = \mathrm{Li}_2\left(1-\frac{\alpha_4}{\alpha_3}\right) - \mathrm{Li}_2\left(1-\frac{\alpha_3}{\alpha_2}\right) + \frac{1}{2}\log\left(\frac{\alpha_2\alpha_4}{\alpha_3^2}\right)\log\left(\frac{\alpha_1}{\alpha_2}\right). \tag{3.40}$$

In constructing the tensor integrals in $D=4-2\epsilon$, we see from equations (3.14–3.17) that the box integral in higher dimensions is needed. In fact, in $D=6-2\epsilon$, the box integral is infrared and ultraviolet finite. This can be seen by inspection of equation (3.11) and noting that the pinchings with $m=1,2$ and 4 in the expression,

$$\hat{\mathrm{I}}_4[1] + \sum_{m=1}^{4}\hat{\gamma}_m\hat{\mathrm{I}}_3^{(m)}[1],$$

are proportional to $1/\epsilon^2$ and, when combined with the appropriate $\hat{\gamma}$ factor, precisely cancel with the pole structure of the box integral. The final pinching ($m=3$) corresponds to the triangle graph with three massive external legs which is itself finite. Altogether, we find that the adjacent box integral in $D=6$ is,

$$\begin{aligned} \mathrm{I}_4^{D=6}[1] &= -\frac{2s_{12}s_{23}}{\Delta_4}\left(\mathrm{Ld}_0(p_1,p_2,p_3) + \frac{1}{2}\left(s_{123}+p_1^2-s_{23}-\frac{2p_1^2 s_{123}}{s_{12}}\right)\mathrm{Lc}_0(p_1,p_{23})\right) \\ &\equiv \mathrm{Ld}_{1S}(p_1,p_2,p_3), \end{aligned} \tag{3.41}$$

where $\mathrm{Lc}_0(p_1,p_{23}) = \mathrm{I}_3[1]$ is defined in equation (3.18). Because of the finiteness properties of the three mass triangle, we will find repeatedly that the $m=3$ pinching should be treated differently from the other three.

Scalar Integrals in Higher Dimensions

For higher dimensions, we just reuse equation (3.11), noting that the triangle pinchings in $D = 6 - 2\epsilon$ reintroduce ultraviolet poles. These can easily be isolated by adding and subtracting combinations of scalar integrals as in section 3.1.2. Explicitly,

$$\mathrm{I}_4^{D=8-2\epsilon}[1] = \mathrm{Ld}_{2S}(p_1,p_2,p_3) + \frac{c_\Gamma}{6}\left(\frac{(-s_{123})^{-\epsilon}}{\epsilon} + \frac{11}{3}\right), \tag{3.42}$$

$$\mathrm{I}_4^{D=10-2\epsilon}[1] = \mathrm{Ld}_{3S}(p_1,p_2,p_3) + \frac{c_\Gamma(s_{123}+s_{12}+s_{23}+p_1^2)}{120}\left(\frac{(-s_{123})^{-\epsilon}}{\epsilon} + \frac{107}{30}\right), \tag{3.43}$$

$$\mathrm{I}_4^{D=12-2\epsilon}[1] = \mathrm{Ld}_{4S}(p_1,p_2,p_3) + \frac{c_\Gamma P}{2520}\left(\frac{(-s_{123})^{-\epsilon}}{\epsilon} + \frac{129}{35}\right), \tag{3.44}$$

where,

$$P = s_{123}^2 + s_{12}^2 + s_{23}^2 + p_1^4 + s_{123}s_{12} + s_{123}s_{23} + s_{123}p_1^2 + s_{12}p_1^2 + s_{23}p_1^2 + \frac{s_{12}s_{23}}{2}.$$

The finite parts of the higher dimension boxes are given by,

$$\begin{aligned}\mathrm{Ld}_{2S}(p_1,p_2,p_3) = &-\frac{s_{12}s_{23}}{3\Delta_4}\Bigg(s_{12}s_{23}\mathrm{Ld}_{1S}(p_1,p_2,p_3)\\ &+\left(s_{123}+p_1^2-s_{23}-\frac{2p_1^2s_{123}}{s_{12}}\right)\mathrm{Lc}_{1S}(p_1,p_{23})\\ &+\frac{s_{23}}{2}\log\left(\frac{s_{123}}{s_{23}}\right)+s_{12}\log\left(\frac{s_{123}}{s_{12}}\right)-\frac{p_1^2}{2}\log\left(\frac{s_{123}}{p_1^2}\right)\Bigg),\end{aligned} \tag{3.45}$$

$$\begin{aligned}\mathrm{Ld}_{3S}(p_1,p_2,p_3) = &-\frac{s_{12}s_{23}}{5\Delta_4}\Bigg(s_{12}s_{23}\mathrm{Ld}_{2S}(p_1,p_2,p_3)\\ &+\left(s_{123}+p_1^2-s_{23}-\frac{2p_1^2s_{123}}{s_{12}}\right)\mathrm{Lc}_{2S}(p_1,p_{23})\\ &+\frac{s_{23}^2}{24}\log\left(\frac{s_{123}}{s_{23}}\right)+\frac{s_{12}^2}{12}\log\left(\frac{s_{123}}{s_{12}}\right)-\frac{p_1^4}{24}\log\left(\frac{s_{123}}{p_1^2}\right)+\frac{s_{12}s_{23}}{12}\Bigg),\end{aligned} \tag{3.46}$$

$$\begin{aligned}\mathrm{Ld}_{4S}(p_1,p_2,p_3) = &-\frac{s_{12}s_{23}}{7\Delta_4}\Bigg(s_{12}s_{23}\mathrm{Ld}_{3S}(p_1,p_2,p_3)\\ &+\left(s_{123}+p_1^2-s_{23}-\frac{2p_1^2s_{123}}{s_{12}}\right)\mathrm{Lc}_{3S}(p_1,p_{23})\\ &+\frac{s_{23}^3}{360}\log\left(\frac{s_{123}}{s_{23}}\right)+\frac{s_{12}^3}{180}\log\left(\frac{s_{123}}{s_{12}}\right)-\frac{p_1^6}{360}\log\left(\frac{s_{123}}{p_1^2}\right)\end{aligned}$$

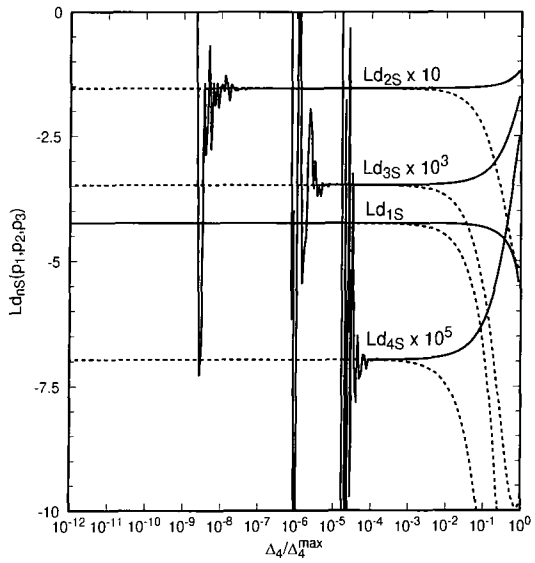

Figure 3.6: The finite functions for the box graph with two adjacent massive legs as a function of $\Delta_4/\Delta_4^{\max}$ where $\Delta_4^{\max} = 2s_{12}s_{23}(s_{123} - s_{12} - s_{23})$. The phase space point is $s_{123} = 1$, $s_{12} = 0.4$, $s_{23} = 0.08$ and p_1^2 altered so the limit is approached and the functions have been evaluated in double precision Fortran. The dashed lines show the approximate form for the function in the limit $\Delta_4 \to 0$, retaining only the first term of the Taylor expansion as given in Appendix C.

$$+\frac{s_{12}s_{23}(s_{123}+s_{12}+s_{23}+p_1^2)}{720}\Bigg). \tag{3.47}$$

The $D = 6 - 2\epsilon$ and $D = 8 - 2\epsilon$ box integrals explicitly appear in the momentum space tensor structure with one and two factors of $g_{\mu\nu}$ respectively. All of these integrals appear either directly or indirectly in the tensor box integrals of equations (3.14–3.17).

Once again, all of these functions are well behaved as $\Delta_4 \to 0$ and group a variety of dilogarithms, logarithms and constants together in a non-trivial way. This is shown in Fig. 3.6 for a particular point in phase space; $s_{123} = 1$, $s_{12} = 0.4$, $s_{23} = 0.08$ with p_1^2 varying so the $\Delta_4 \to 0$ limit is approached. We see that although Ld_{1S}, with a single inverse power of the Gram determinant, is numerically stable, the functions with more powers of Gram determinant in the denominator break down at much larger values of Δ_4. In all cases, the function is well approximated by the first term of the Taylor expansion provided $\Delta_4 < 10^{-4}\Delta_4^{\max}$. These approximations are collected in Appendix C.

Tensor Integrals

Armed with the integrals in $D > 4$, we return to the tensor integrals and use equations (3.14–3.17) as the starting point. Rewriting equation (3.14) for $n = 4$, $D = 4 - 2\epsilon$ and noting that we have eliminated x_3 so that $i = 1, 2$ and 4 only, we have,

$$\mathrm{I}_4[x_i] = -\gamma_i \mathrm{I}_4^{D=6}[1] - \sum_{m=1}^{4} \eta_{im}\alpha_i\alpha_m \mathrm{I}_3^{(m)}[1].$$

The factor $\alpha_i\alpha_m$ multiplying the triangle pinchings will always produce a factor of $1/s$. For triangle graphs with at least one massless leg (pinchings $m = 1, 2$ and 4), the contribution is $\sim 1/\epsilon^2$ and will combine with similar poles from other Feynman diagrams. On the other hand, the $m = 3$ pinching (corresponding to the triangle graph with momenta p_1 and p_{23} flowing outwards) is finite and, provided the value of s is related kinematically to that triangle pinching, there may be a possibility of cancellation with other triangle Feynman graphs. However, for the case $i = 1$ and $m = 3$, the associated invariant mass is s_{12}. This term cannot combine with any other naturally generated triangle graph with the same kinematics. Therefore, we group this term with the box integral, by adding and subtracting,

$$\sum_{m=1}^{4} \eta_{im}\alpha_i\alpha_m \mathrm{I}_3^{(3)}[1] = \gamma_i \mathrm{I}_3^{(3)}[1],$$

so that,

$$\mathrm{I}_4[x_i] = \gamma_i \mathrm{Ld}_1(p_1, p_2, p_3) - \sum_{m=1}^{4} \eta_{im}\alpha_i\alpha_m \left(\mathrm{I}_3^{(m)}[1] - \mathrm{I}_3^{(3)}[1]\right), \tag{3.48}$$

with,

$$\mathrm{Ld}_1(p_1, p_2, p_3) = -\left(\mathrm{I}_4^{D=6}[1] + \mathrm{I}_3^{(3)}[1]\right). \tag{3.49}$$

The only non-zero entries in η_{im} for $i \neq 3$ and $m \neq 3$ are $i = 2$, $m = 4$ or $i = 4$, $m = 2$ corresponding to $\alpha_i\alpha_m = -1/s_{23}$ which *is* appropriate for $\mathrm{I}_3^{(3)}[1]$.

For integrals with more Feynman parameters it is convenient to introduce the following functions,

$$\mathrm{Ld}_{ni_1\ldots i_{n-1}}(p_1, p_2, p_3) = -\left\{n\mathrm{I}_4^{D=6}[x_{i_1}\ldots x_{i_{n-1}}] + \mathrm{I}_3^{(3)}[x_{i_1}\ldots x_{i_{n-1}}]\right\}, \tag{3.50}$$

for $n = 2, 3$ and 4. Suppressing the arguments of Ld_n, and using equations (3.15-3.17), we find,

$$\mathrm{I}_4[x_i x_j] = \gamma_i \mathrm{Ld}_{2j} - \eta_{ij}\alpha_i\alpha_j\Big\{\mathrm{Ld}_1 + \mathrm{I}_3^{(3)}[1]\Big\} - \sum_{m=1}^{4}\eta_{im}\alpha_i\alpha_m\Big\{\mathrm{I}_3^{(m)}[x_j] - \mathrm{I}_3^{(3)}[x_j]\Big\}, \quad (3.51)$$

$$\begin{aligned}\mathrm{I}_4[x_i x_j x_k] = {} & \gamma_i \mathrm{Ld}_{3jk} - \frac{1}{2}\eta_{ij}\alpha_i\alpha_j\Big\{\mathrm{Ld}_{2k} + \mathrm{I}_3^{(3)}[x_k]\Big\} - \frac{1}{2}\eta_{ik}\alpha_i\alpha_k\Big\{\mathrm{Ld}_{2j} + \mathrm{I}_3^{(3)}[x_j]\Big\} \\ & - \sum_{m=1}^{4}\eta_{im}\alpha_i\alpha_m\Big\{\mathrm{I}_3^{(m)}[x_j x_k] - \mathrm{I}_3^{(3)}[x_j x_k]\Big\}, \end{aligned} \quad (3.52)$$

$$\begin{aligned}\mathrm{I}_4[x_i x_j x_k x_l] = {} & \gamma_i \mathrm{Ld}_{4jkl} - \frac{1}{3}\eta_{ij}\alpha_i\alpha_j\Big\{\mathrm{Ld}_{3kl} + \mathrm{I}_3^{(3)}[x_k x_l]\Big\} - \frac{1}{3}\eta_{ik}\alpha_i\alpha_k\Big\{\mathrm{Ld}_{3jl} + \mathrm{I}_3^{(3)}[x_j x_l]\Big\} \\ & - \frac{1}{3}\eta_{il}\alpha_i\alpha_l\Big\{\mathrm{Ld}_{3jk} + \mathrm{I}_3^{(3)}[x_j x_k]\Big\} - \sum_{m=1}^{4}\eta_{im}\alpha_i\alpha_m\Big\{\mathrm{I}_3^{(m)}[x_j x_k x_l] - \mathrm{I}_3^{(3)}[x_j x_k x_l]\Big\}. \end{aligned} \quad (3.53)$$

Since we have systematically eliminated x_3 using the delta function, i, j, k and l run over 1, 2 and 4. This guarantees that the coefficients of the form $\eta_{ij}\alpha_i\alpha_j$ are only non-zero for $i = 2$ and $j = 4$ (or vice-versa). In these cases, $\eta_{24}\alpha_2\alpha_4 = -1/s_{23}$, which is again appropriate for the $m = 3$ pinching to form a completely massive triangle, $\mathrm{I}_3^{(3)}[1]$. Altogether, equations (3.48,3.51–3.53) are sufficient to completely describe the tensor structure of the adjacent box.

However, in order to determine the $\mathrm{Ld}_{ni_1\ldots i_{n-1}}$ combinations, we need tensor integrals for $D = 6 - 2\epsilon$ dimensional box graphs with two or more Feynman parameters. These can be obtained from equation (3.15) once the $D = 6 - 2\epsilon$ box integral with a single Feynman parameter, $\mathrm{I}_4^{D=6-2\epsilon}[x_i]$ is known. This can be derived by differentiating (3.9) which indicates that $\mathrm{I}_4^{D=6-2\epsilon}[x_i]$ is also finite as $\epsilon \to 0$. To see this, we reuse equation (3.14) and our usual trick of adding and subtracting combinations of the $m = 3$ pinching in $D = 6 - 2\epsilon$,

$$\begin{aligned}\mathrm{I}_4^{D=6-2\epsilon}[x_i] = {} & \gamma_i\left(-(3-2\epsilon)\mathrm{I}_4^{D=8-2\epsilon}[1] - \mathrm{I}_3^{D=6-2\epsilon(3)}[1]\right) \\ & - \sum_{m=1}^{4}\eta_{im}\alpha_i\alpha_m\left(\mathrm{I}_3^{D=6-2\epsilon(m)}[1] - \mathrm{I}_3^{D=6-2\epsilon(3)}[1]\right).\end{aligned}$$

Both brackets are separately finite. First, the divergent part of $\mathrm{I}_4^{D=8-2\epsilon}[1]$ precisely cancels against that of $\mathrm{I}_3^{D=6-2\epsilon(3)}[1]$. Second, all triangles in $D = 6 - 2\epsilon$ dimensions have $1/\epsilon$ poles

and the difference of any two, is either zero or a log. Further differentiation does not change the finiteness properties of the $I_4^{D=6-2\epsilon}$ tensor integrals.

The $\mathrm{Ld}_{ni_1\ldots i_{n-1}}$ combinations are also well behaved in certain kinematic limits. For example, $I_4^{D=6}[1]$ and $I_3^{(3)}[1]$ are finite as $s_{12} \to 0$ or $s_{23} \to 0$. Just as differentiating functions which are finite as $\epsilon \to 0$ does not introduce poles in ϵ, neither can it introduce poles in the kinematic invariants s_{12} or s_{23}. As an example, consider the function Ld_{24} given by,

$$\begin{aligned}\mathrm{Ld}_{24}(p_1,p_2,p_3) &= \frac{2(p_1^2-s_{12})}{s_{12}s_{23}}\left(3\mathrm{Ld}_{2S}(p_1,p_2,p_3)+\mathrm{Lc}_{1S}(p_1,p_{23})\right)-\frac{s_{12}}{s_{23}}\mathrm{Lc}_1(p_3,p_{12}) \\ &\quad +\frac{p_1^2}{s_{23}}\mathrm{Lc}_1(p_{23},p_1),\end{aligned}$$

which appears to contain a pole in s_{12}. In the $s_{12} \to 0$ limit, $\Delta_4 \to -2s_{23}s_{123}p_1^2$ and

$$\mathrm{Ld}_{2S} \to \frac{2s_{23}s_{123}p_1^2}{3\Delta_4}\mathrm{Lc}_{1S}(p_1,p_{23}) \to -\frac{1}{3}\mathrm{Lc}_{1S}(p_1,p_{23}),$$

so that,

$$\lim_{s_{12}\to 0}\left(3\mathrm{Ld}_{2S}(p_1,p_2,p_3)+\mathrm{Lc}_{1S}(p_1,p_{23})\right) \to 0,$$

and therefore,

$$\lim_{s_{12}\to 0} s_{12} \times \mathrm{Ld}_{24}(p_1,p_2,p_3) \to 0.$$

Similarly, Ld_{24} contains no power-like divergences[7] in the $s_{23} \to 0$ limit and, with a little more work, it can be shown that,

$$\lim_{s_{23}\to 0} s_{23} \times \mathrm{Ld}_{24}(p_1,p_2,p_3) \to 0.$$

Once again, these functions combine dilogarithms, logarithms and constants in a highly non-trivial way to form well behaved building blocks. Explicit forms for the $\mathrm{Ld}_{ni_1\ldots i_{n-1}}$ functions for $n = 1, 2$ and 3 are given in Appendix B.

[7] Although these functions do not behave as inverse powers of the vanishing kinematic variables, they do contain logarithms of s_{12} and s_{23}. This is because the $\epsilon \to 0$ limit has already been taken, and the order of taking the two limits does not commute. For next-to-leading order calculations, we only approach the limit $s_{ij} \to 0$ and ϵ can safely be taken to zero first.

3.5.2 The One-Mass Box

The higher dimension and Feynman parameter integrals for the one-mass box integral obtained by taking $p_1^2 \to 0$ can also be constructed in a similar way. For this kinematic configuration, the α parameters are defined by,

$$\alpha_1\alpha_4\, s_{123} = -1, \quad \alpha_1\alpha_3\, s_{12} = -1, \quad \alpha_2\alpha_4\, s_{23} = -1,$$

while,

$$\eta_{ij} = \begin{pmatrix} 0 & 0 & 1 & 0 \\ 0 & 0 & -1 & 1 \\ 1 & -1 & 0 & 0 \\ 0 & 1 & 0 & 0 \end{pmatrix}, \quad N_4 = \tfrac{1}{2},$$

and,

$$\Delta_4^{1m} = 2s_{12}s_{23}\left(s_{123} - s_{12} - s_{23}\right).$$

In terms of invariants,

$$\frac{\gamma_i}{\prod_{j=1}^4 \alpha_j} = \begin{cases} -s_{23} & i = 1 \\ s_{123} - s_{12} & i = 2 \\ s_{123} - s_{23} & i = 3 \\ -s_{12} & i = 4 \end{cases}.$$

The scalar integral can be written,

$$\hat{\mathrm{I}}_4^{1m}[1] = \frac{c_\Gamma}{\epsilon^2}\left(2(\alpha_1\alpha_3)^\epsilon + 2(\alpha_2\alpha_4)^\epsilon - 2(\alpha_1\alpha_4)^\epsilon\right) + 2\mathrm{Ld}_0^{1m}(p_1,p_2,p_3) + \mathcal{O}(\epsilon), \tag{3.54}$$

where,

$$\mathrm{Ld}_0^{1m}(p_1,p_2,p_3) = \mathrm{Li}_2\left(1 - \frac{\alpha_4}{\alpha_3}\right) + \mathrm{Li}_2\left(1 - \frac{\alpha_1}{\alpha_2}\right) + \log\left(\frac{\alpha_4}{\alpha_3}\right)\log\left(\frac{\alpha_1}{\alpha_2}\right) - \frac{\pi^2}{6}. \tag{3.55}$$

As expected, in $D = 6 - 2\epsilon$ dimensions, the scalar integral is finite,

$$\mathrm{I}_4^{1m,D=6}[1] = -\frac{2s_{12}s_{23}}{\Delta_4^{1m}}\mathrm{Ld}_0^{1m}(p_1,p_2,p_3) \equiv \mathrm{Ld}_{1S}^{1m}(p_1,p_2,p_3). \tag{3.56}$$

In higher dimensions, the scalar integrals satisfy analagous equations to (3.42–3.44) with $p_1^2 \to 0$, and finite parts given by,

$$\mathrm{Ld}^{1m}_{2S}(p_1,p_2,p_3) = -\frac{s_{12}s_{23}}{3\Delta_4^{1m}}\left(s_{12}s_{23}\mathrm{Ld}^{1m}_{1S}(p_1,p_2,p_3) + s_{23}\log\left(\frac{s_{123}}{s_{23}}\right) + s_{12}\log\left(\frac{s_{123}}{s_{12}}\right)\right), \tag{3.57}$$

$$\mathrm{Ld}^{1m}_{3S}(p_1,p_2,p_3) = -\frac{s_{12}s_{23}}{5\Delta_4^{1m}}\left(s_{12}s_{23}\mathrm{Ld}^{1m}_{2S}(p_1,p_2,p_3) + \frac{s_{23}^2}{12}\log\left(\frac{s_{123}}{s_{23}}\right) + \frac{s_{12}^2}{12}\log\left(\frac{s_{123}}{s_{12}}\right) + \frac{s_{12}s_{23}}{12}\right), \tag{3.58}$$

$$\mathrm{Ld}^{1m}_{4S}(p_1,p_2,p_3) = -\frac{s_{12}s_{23}}{7\Delta_4^{1m}}\left(s_{12}s_{23}\mathrm{Ld}^{1m}_{3S}(p_1,p_2,p_3) + \frac{s_{23}^3}{180}\log\left(\frac{s_{123}}{s_{23}}\right) + \frac{s_{12}^3}{180}\log\left(\frac{s_{123}}{s_{12}}\right) + \frac{s_{12}s_{23}(s_{123}+s_{12}+s_{23})}{720}\right). \tag{3.59}$$

The stability of these functions as $\Delta_4^{1m} \to 0$ is illustrated in fig. 3.7 for a particular point in phase space; $s_{123} = 1$, $s_{12} = 0.3$, with s_{23} varying so the limit is approached. The maximum possible value of Δ_4^{1m} occurs when $s_{23} = (s_{123} - s_{12})/2$; i.e. $\Delta_4^{1m\ \max} = s_{12}(s_{123} - s_{12})^2/2$. As before, Ld^{1m}_{1S}, with a single inverse power of the Gram determinant, is numerically stable. However there are numerical instabilities for the other functions with more powers of Gram determinant in the denominator. In all cases, the function is well approximated by the first term of the Taylor expansion provided $\Delta_4^{1m} < 10^{-3}\Delta_4^{1m\ \max}$.

Tensor Integrals

Unlike the $p_1^2 \neq 0$ case, the scalar triangle pinchings all contain infrared poles and there is no benefit in absorbing the $m = 3$ piece in the tensor integrals. Therefore we introduce,

$$\mathrm{Ld}^{1m}_{ni_1\ldots i_{n-1}}(p_1,p_2,p_3) = -n\mathrm{I}_4^{1m,D=6}[x_{i_1}\ldots x_{i_{n-1}}], \tag{3.60}$$

for $n = 1,\ 2,\ 3$ and 4. Using equations (3.14–3.17) with $n = 4$ and $D = 4 - 2\epsilon$ we find,

$$\mathrm{I}_4^{1m}[x_i] = \gamma_i\mathrm{Ld}_1^{1m} - \sum_{m=1}^{4}\eta_{im}\alpha_i\alpha_m\mathrm{I}_3^{(m)}[1], \tag{3.61}$$

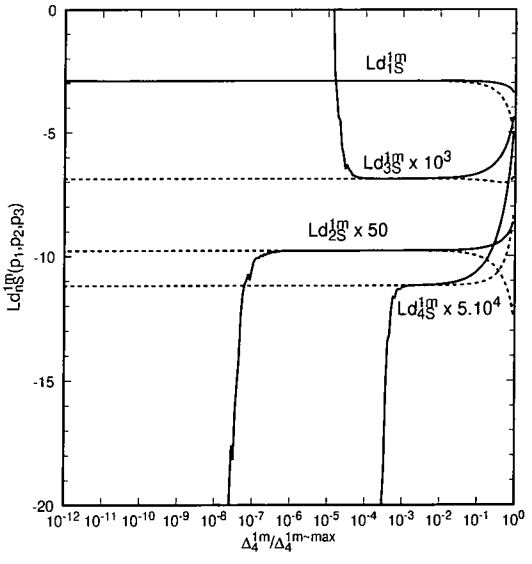

Figure 3.7: The finite functions for the box graph with one massive leg as a function of $\Delta_4^{1m}/\Delta_4^{1m\ \max}$. The functions have been evaluated in double precision Fortran. The dashed lines show the approximate form for the function in the limit $\Delta_4^{1m} \to 0$, retaining only the first term of the Taylor expansion as given in Appendix C.

$$\mathrm{I}_4^{1m}[x_i x_j] = \gamma_i \mathrm{Ld}_{2j}^{1m} - \eta_{ij}\alpha_i\alpha_j \mathrm{Ld}_1^{1m} - \sum_{m=1}^{4} \eta_{im}\alpha_i\alpha_m \mathrm{I}_3^{(m)}[x_j], \tag{3.62}$$

$$\mathrm{I}_4^{1m}[x_i x_j x_k] = \gamma_i \mathrm{Ld}_{3jk}^{1m} - \frac{1}{2}\eta_{ij}\alpha_i\alpha_j \mathrm{Ld}_{2k}^{1m} - \frac{1}{2}\eta_{ik}\alpha_i\alpha_k \mathrm{Ld}_{2j}^{1m} - \sum_{m=1}^{4} \eta_{im}\alpha_i\alpha_m \mathrm{I}_3^{(m)}[x_j x_k], \tag{3.63}$$

$$\mathrm{I}_4^{1m}[x_i x_j x_k x_l] = \gamma_i \mathrm{Ld}_{4jkl}^{1m} - \frac{1}{3}\eta_{ij}\alpha_i\alpha_j \mathrm{Ld}_{3kl}^{1m} - \frac{1}{3}\eta_{ik}\alpha_i\alpha_k \mathrm{Ld}_{3jl}^{1m} - \frac{1}{3}\eta_{il}\alpha_i\alpha_l \mathrm{Ld}_{3jk}^{1m} - \sum_{m=1}^{4} \eta_{im}\alpha_i\alpha_m \mathrm{I}_3^{(m)}[x_j x_k x_l]. \tag{3.64}$$

As in the previous section, the $\mathrm{Ld}^{1m}_{ni_1\ldots i_{n-1}}$ functions are finite as $\epsilon \to 0$ and contain no power-like divergences in the $s_{12} \to 0$, $s_{23} \to 0$ and $\Delta_4^{1m} \to 0$ limits. For convenience, explicit forms are given in Appendix B.

3.5.3 The Opposite Two-Mass Box

The two mass box graph where the massive legs sit on opposite sides is a special case because the scalar integral itself is not finite as $\Delta_4^{opp} \to 0$. We must therefore proceed with care. To make best use of the symmetry under $p_1 \leftrightarrow p_3$, it is convenient to write,

$$\mathcal{P}^\mu = -(1-x_1)p_1^\mu - (x_3+x_4)p_2^\mu - x_4 p_3^\mu.$$

Under this flip symmetry, $x_1 \leftrightarrow x_4$, $x_2 \leftrightarrow x_3$ and

$$\mathcal{P}^\mu \to -\mathcal{P}^\mu - p_1^\mu - p_2^\mu - p_3^\mu.$$

In this kinematic configuration, the α parameters can be defined by,

$$\alpha_1\alpha_4\, s_{123} = -\lambda, \quad \alpha_2\alpha_3\, p_2^2 = -1$$
$$\alpha_1\alpha_3\, s_{12} = -1, \quad \alpha_2\alpha_4\, s_{23} = -1,$$

where λ is an extra kinematic variable that ensures that the α_i are independent,

$$\lambda = \frac{s_{123}p_2^2}{s_{12}s_{23}}.$$

With this choice of α_i,

$$\eta_{ij} = (1-\lambda)\begin{pmatrix} 0 & 0 & 1 & -1 \\ 0 & 0 & -\lambda & 1 \\ 1 & -\lambda & 0 & 0 \\ -1 & 1 & 0 & 0 \end{pmatrix}, \qquad N_4 = \frac{1}{2}(1-\lambda)^2.$$

Each row of η naturally couples together two of the pinchings (triangles) of this box, so we might expect such structure to dominate the integrals. The associated Gram determinant is given by,

$$\Delta_4^{opp} = 2(s_{12}s_{23} - p_2^2 s_{123})s_{13} = \frac{2(1-\lambda)s_{13}}{\prod_{i=1}^4 \alpha_i},$$

where,

$$s_{13} = s_{123} - s_{12} - s_{23} + p_2^2,$$

and,

$$\frac{\gamma_i}{\prod_{j=1}^{4}\alpha_j} = (1-\lambda)\begin{cases} p_2^2 - s_{23} & i=1 \\ s_{123} - s_{12} & i=2 \\ s_{123} - s_{23} & i=3 \\ p_2^2 - s_{12} & i=4 \end{cases}.$$

We note that the presence of the Gram determinant is synonymous both with a factor of $(1-\lambda)$ and s_{13}.

The scalar integral for the opposite box in $D = 4-2\epsilon$ is given by,

$$\hat{\mathrm{I}}_4^{opp}[1] = \frac{2}{(1-\lambda)}\left(\frac{c_\Gamma}{\epsilon^2}\left((\alpha_1\alpha_3)^\epsilon + (\alpha_2\alpha_4)^\epsilon - (\alpha_2\alpha_3)^\epsilon - (\alpha_1\alpha_4)^\epsilon\lambda^{-\epsilon}\right) + \mathrm{Ld}_0^{opp}(p_1,p_2,p_3)\right) + \mathcal{O}(\epsilon), \tag{3.65}$$

where the finite part Ld_0 can be written,

$$\begin{aligned}\mathrm{Ld}_0^{opp}(p_1,p_2,p_3) &= \mathrm{Li}_2(1-\lambda) + \mathrm{Li}_2\left(1-\frac{\alpha_4}{\lambda\alpha_3}\right) + \mathrm{Li}_2\left(1-\frac{\alpha_1}{\lambda\alpha_2}\right) \\ &\quad -\mathrm{Li}_2\left(1-\frac{\alpha_4}{\alpha_3}\right) - \mathrm{Li}_2\left(1-\frac{\alpha_1}{\alpha_2}\right) + \log\left(\frac{\alpha_4}{\lambda\alpha_3}\right)\log\left(\frac{\alpha_1}{\lambda\alpha_2}\right).\end{aligned} \tag{3.66}$$

As $\lambda \to 1$, there is a manifest singularity in $\hat{\mathrm{I}}_4^{opp}[1]$ since,

$$\mathrm{Ld}_0^{opp}(p_1,p_2,p_3) \to -\log\left(\frac{\alpha_1}{\alpha_2}\right)\log\left(\frac{\alpha_3}{\alpha_4}\right).$$

This double logarithm can never combine with lower point scalar integrals to form a combination well behaved as $\Delta_4^{opp} \to 0$. In fact, it is easy to see from fig. 3.5 that the only scalar integrals which are available by pinching are the triangle integrals with one and two massive legs. These are pure poles in ϵ and cannot be combined with the finite parts of the opposite box integral. There is no appropriate function which can generate the double logarithm as $\lambda \to 1$ and consequently no finite function can be formed. Since the matrix elements are in general finite in the limit of vanishing Gram determinants, all occurences of Ld_0^{opp} divided by the determinant must vanish.

On the other hand, in $D = 6-2\epsilon$, the opposite box is not only finite as $\epsilon \to 0$ as expected, but also as $\lambda \to 1$. This is because N_4 is effectively $(\Delta_4^{opp})^2$ and its presence in the numerator

of equation (3.11) removes the Gram determinant from the denominator. Consequently, we see that,

$$\mathrm{I}_4^{opp\ D=6-2\epsilon}[1] = -\frac{1}{s_{13}}\mathrm{Ld}_0^{opp}(p_1,p_2,p_3), \tag{3.67}$$

which, since,

$$\begin{aligned}\lim_{s_{13}\to 0}\mathrm{Ld}_0(p_1,p_2,p_3) &= \frac{s_{13}}{s_{12}s_{23}-p_2^2 s_{123}}\left(s_{12}\log\left(\frac{s_{123}}{s_{12}}\right)+s_{23}\log\left(\frac{s_{123}}{s_{23}}\right)-p_2^2\log\left(\frac{s_{123}}{p_2^2}\right)\right)\\ &\quad +\mathcal{O}(s_{13}^2),\end{aligned} \tag{3.68}$$

is also finite as $s_{13}\to 0$.

So in dealing with the tensor decomposition of the opposite-mass box we are faced with poles in s_{13}, which we must protect, but also denominators of $(1-\lambda)$ which may or may not be protected. However, we know that for physical processes that are finite as $\Delta_4^{opp}\to 0$, there must be cancellations amongst the various tensor integrals so that no terms containing $\mathrm{Ld}_0/\Delta_4^{opp}$ remain. Therefore we always choose to leave one factor of $(1-\lambda)$ exposed when multiplied by box functions, so as to facilitate the cancellation of these terms. We therefore introduce a set of functions in the same way as for the one-mass box, eq. (3.60),

$$\mathrm{Ld}^{opp}_{ni_1\ldots i_{n-1}}(p_1,p_2,p_3) = -n\mathrm{I}_4^{opp,D=6}[x_{i_1}\ldots x_{i_{n-1}}], \tag{3.69}$$

for $n=1$, 2, 3 and 4. This leads to equations for the integrals with additional Feynman parameters also very similar to the one-mass case. In fact, the only difference from equations (3.61)-(3.64) is an extra factor of $(1-\lambda)^{-2}$ throughout the r.h.s., due to the difference in N_4. So, for example, we find,

$$\mathrm{I}_4^{opp}[x_i] = \frac{1}{(1-\lambda)^2}\left(\gamma_i\mathrm{Ld}_1^{opp}-\sum_{m=1}^{4}\eta_{im}\alpha_i\alpha_m\mathrm{I}_3^{(m)}[1]\right). \tag{3.70}$$

Notice here that the function Ld_1^{opp} is multiplied by the factor $1/(1-\lambda)$ (one power is cancelled by γ_i), as claimed above. Again, the functions $\mathrm{Ld}^{opp}_{ni_1\ldots i_{n-1}}$ are finite as $\epsilon\to 0$ and contain no power-like divergences as $s_{13}\to 0$. Explicit forms of the functions relevant for up to three tensor numerators are given in Appendix B.

There still appear to be problematic terms (divergent as $\lambda\to 1$) in the tensor reductions which correspond to the remaining triangle-like pinchings of the opposite box. However,

these terms are the only ones that would survive in the $\epsilon \to 0$ limit of the tensor integral multiplied by ϵ. Since these terms will naturally be produced in the calculation of a physical process, we expect that the resulting single logarithms occur in groups that are finite as $\lambda \to 1$. We therefore introduce the auxiliary functions,

$$\begin{aligned}
\mathrm{Lcd}_n(p_1,p_2,p_3) &= -\lim_{\epsilon\to 0}\left(\epsilon \times \mathrm{I}_4^{opp}[x_4^n]\right) \\
&= -\frac{1}{(1-\lambda)}\lim_{\epsilon\to 0}\left(\alpha_4\alpha_1\mathrm{I}_3^{(1)}[x_4^{n-1}] - \alpha_4\alpha_2\mathrm{I}_3^{(2)}[x_4^{n-1}]\right) \\
&= \frac{2s_{13}}{\Delta_4^{opp}}\left(s_{12}\mathrm{Lc}_n^{2m}(p_{12},p_3) - p_2^2\mathrm{Lc}_n^{2m}(p_2,p_3)\right), \qquad (3.71)
\end{aligned}$$

for $n = 1,\ldots,4$ and,

$$\mathrm{Lcd}_0(p_1,p_2,p_3) = \frac{2s_{13}}{\Delta_4^{opp}}\log\left(\frac{s_{12}s_{23}}{p_2^2 s_{123}}\right). \qquad (3.72)$$

Because these functions contain only a single power of the Gram determinant, they are not difficult to evaluate numerically.

In summary, the situation for box integrals is very similar to that for triangle graphs. When the scalar integral is finite as $\Delta_4 \to 0$, differentiating - or equivalently adding factors of Feynman parameters - does not introduce kinematic singularities. Hence natural groupings of box and triangle integrals arise that are finite as $\Delta_4 \to 0$. Furthermore, the infrared and ultraviolet singularities can be isolated easily. Although we have explicitly worked through a subset of kinematic configurations relevant to certain QCD processes, this method is systematic and can be applied to processes with more general kinematics (and particularly non-zero internal masses).

3.6 Five Point Integrals

In this section we consider five point integrals with only one external mass. The outflowing lightlike momenta are denoted p_i, $i = 1,\ldots,4$ while the fifth $p_5 = -p_{1234}$ is massive, $p_5^2 \neq 0$ as shown in fig. 3.8. The auxiliary momentum is then,

$$\mathcal{P}^\mu = -(1-x_1)p_1^\mu - (1-x_1-x_2)p_2^\mu - (x_4+x_5)p_3^\mu - x_5 p_4^\mu.$$

We can make the choice,

$$\begin{aligned} \alpha_1\alpha_5\, s_{1234} &= -\lambda, \quad \alpha_2\alpha_4\, s_{23} = -1 \\ \alpha_1\alpha_3\, s_{12} &= -1, \quad \alpha_2\alpha_5\, s_{234} = -1 \\ \alpha_1\alpha_4\, s_{123} &= -1, \quad \alpha_3\alpha_5\, s_{34} = -1, \end{aligned}$$

with,

$$(1-\lambda) = \frac{1}{\alpha_3}\prod_{i=1}^{5}\alpha_i(s_{123}s_{234} - s_{23}s_{1234}).$$

As in the opposite box integral, λ is an extra kinematic variable that ensures the α_i are independent. It is the same variable that occurs in the third pinching which forms an opposite box configuration. The matrix η_{ij} is given by,

$$\eta_{ij} = \begin{pmatrix} 1 & -1 & 1-\lambda & 1 & -1 \\ -1 & 1 & \lambda-1 & 1-2\lambda & 1 \\ 1-\lambda & \lambda-1 & (1-\lambda)^2 & \lambda-1 & 1-\lambda \\ 1 & 1-2\lambda & \lambda-1 & 1 & -1 \\ -1 & 1 & 1-\lambda & -1 & 1 \end{pmatrix},$$

and the normalisation factor is,

$$N_5 = 1-\lambda.$$

The γ_i are rather lengthy, but can be read off from η_{ij}. The scalar pentagon integral is by now well-known in $D = 4$ [41, 35, 29] and in $D = 4-2\epsilon$ [30, 27, 28] and can be written in terms of these variables as,

$$\hat{\mathrm{I}}_5[1] = -\frac{1}{2N_5}\sum_{m=1}^{5}\hat{\gamma}_m\hat{\mathrm{I}}_4^{(m)}[1] + \mathcal{O}(\epsilon). \tag{3.73}$$

The five pinchings and the momenta associated with each is illustrated in fig. 3.8. The limit $N_5 \to 0$ corresponds to the vanishing of the Gram determinant associated with the $m = 3$ pinching. The scalar integral for this pinching is not well behaved in this limit and so should not be expected to combine with the other pinchings. Therefore, we separate $\hat{\mathrm{I}}_5[1]$ according to the pole structure in ϵ and N_5. We identify the function Le_1 which is finite as both $N_5 \to 0$

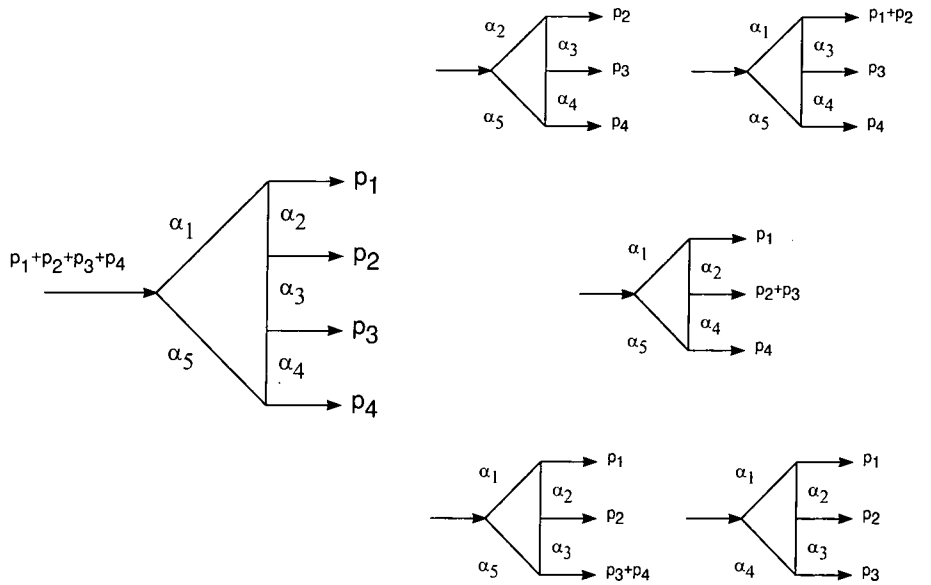

Figure 3.8: The pentagon graph and each of the five pinchings obtained by omitting the internal line associated with α_m for $m = 1, 2, 3, 4$ and 5. For box pinchings, the entering momentum is fixed by momentum conservation.

and $\epsilon \to 0$ and does not depend on the opposite-box pinching, $m = 3$, plus a combination of scalar box integrals containing all the infrared poles and the remaining $N_5 \to 0$ singularities,

$$\begin{aligned} \mathrm{I}_5[1] &= \left(\sum_{i=1}^{5} \alpha_3\alpha_i\kappa_i\right) \mathrm{Le}_1 - \frac{1}{2N_5}\gamma_3 \mathrm{I}_4^{(3)}[1] - \alpha_2\alpha_4 \left(\mathrm{I}_4^{(2)}[1] + \mathrm{I}_4^{(4)}[1]\right) \\ &\quad -\frac{1}{2}\alpha_3 \left(\alpha_1 \mathrm{I}_4^{(1)}[1] - \alpha_2 \mathrm{I}_4^{(2)}[1] - \alpha_4 \mathrm{I}_4^{(4)}[1] + \alpha_5 \mathrm{I}_4^{(5)}[1]\right), \end{aligned} \tag{3.74}$$

where $\kappa_i = (1, -1, 0, 1, -1)$ and,

$$\mathrm{Le}_1 = -\frac{\alpha_1\alpha_2\alpha_4\alpha_5}{2N_5} \sum_{m=1}^{5} \kappa_m \hat{\mathrm{I}}_4^{(m)}[1]. \tag{3.75}$$

Applying equation (3.14) and noting that $\mathrm{I}_5^{D=6}$ is both infrared and ultraviolet finite, the integrals with one insertion are also determined in terms of box integrals in $D = 4 - 2\epsilon$ dimensions,

$$\hat{\mathrm{I}}_5[a_i] = -\frac{1}{2N_5} \sum_{m=1}^{5} \eta_{im} \hat{\mathrm{I}}_4^{(m)}[1] + \mathcal{O}(\epsilon). \tag{3.76}$$

Making the same separation as before,

$$\mathrm{I}_5[x_i] = (\alpha_3\alpha_i\kappa_i)\,\mathrm{Le}_1 - \frac{1}{2N_5}\sum_{m=1}^{5}\alpha_i\alpha_m\,(\eta_{im} - \kappa_i\kappa_m)\,\mathrm{I}_4^{(m)}[1] + \mathcal{O}(\epsilon), \tag{3.77}$$

where the bracket multiplying the scalar box integral is always proportional to N_5.

Similarly, using the usual formula for two Feynman parameters (3.15) and concentrating all of the Δ_5 dependence into $\hat{c}_{i,j}$, where,

$$c_{i,j} = \alpha_i\alpha_j\hat{c}_{i,j} = \frac{\alpha_i\alpha_j}{2N_5}\left(\eta_{ij} - \frac{\hat{\gamma}_i\hat{\gamma}_j}{\hat{\Delta}_5}\right), \tag{3.78}$$

we find,

$$\begin{aligned}
\hat{\mathrm{I}}_5[a_ia_j] &= \hat{c}_{i,j}\left(\hat{\mathrm{I}}_5^{D=6}[1] + \frac{1}{2N_5}\sum_{m=1}^{5}\hat{\gamma}_m\hat{\mathrm{I}}_4^{D=6,(m)}[1]\right) \\
&\quad + \frac{1}{4N_5^2}\sum_{m=1}^{5}(\eta_{im}\hat{\gamma}_j - \eta_{ij}\hat{\gamma}_m)\hat{\mathrm{I}}_4^{D=6,(m)}[1] - \frac{1}{2N_5}\sum_{m=1}^{5}\eta_{jm}\hat{\mathrm{I}}_4^{(m)}[a_i] \\
&= -\hat{c}_{i,j}\frac{\hat{\Delta}_5\hat{\mathrm{I}}_5^{D=8}[1]}{N_5} \\
&\quad + \frac{1}{2N_5}\sum_{m=1}^{5}\left(\left(\frac{\hat{\gamma}_j^{(m)}\eta_{im} - \hat{\gamma}_m\eta_{ij}^{(m)}}{\eta_{mm}}\right)\hat{\mathrm{I}}_4^{D=6,(m)}[1] - \eta_{jm}\hat{\mathrm{I}}_4^{(m)}[a_i]\right).
\end{aligned} \tag{3.79}$$

To simplify the non-$\hat{c}_{i,j}$ terms (and eliminate one power of N_5), we have rewritten some of the variables appropriate to the pentagon integral in terms of those appropriate to the box pinchings, $\eta_{ij}^{(m)}$ and $\hat{\gamma}_i^{(m)}$, using the relations [28],

$$\gamma_i^{(m)} = \frac{\eta_{mm}\gamma_i - \eta_{im}\gamma_m}{2N_5}, \qquad \eta_{ij}^{(m)} = \frac{\eta_{mm}\eta_{ij} - \eta_{im}\eta_{jm}}{2N_5}.$$

Bern, Dixon and Kosower have shown [27, 28] that I_5^6 drops out of the calculation of any gauge theory amplitudes by using the identity [30],

$$\sum_{i,j=1}^{4} q_i^{\mu_i}q_j^{\mu_j}c_{i+1,j+1} = \frac{1}{2}g_{[4]}^{\mu_i\mu_j}, \tag{3.80}$$

where $g_{[4]}^{\mu_i\mu_j}$ represents the metric tensor in $D = 4$. Since,

$$\begin{aligned}
\mathrm{I}_5[\ell^{\mu_i}\ell^{\mu_j}] &= \mathrm{I}_5[\mathcal{P}^{\mu_i}\mathcal{P}^{\mu_j}] - \frac{1}{2}\mathrm{I}_5^{D=6}[1]g^{\mu_i\mu_j} \\
&= \sum_{i,j=1}^{5}\mathrm{I}_5[x_{i+1}x_{j+1}]q_i^{\mu_i}q_j^{\mu_j} - \frac{1}{2}\mathrm{I}_5^{D=6}[g^{\mu_i\mu_j}],
\end{aligned} \tag{3.81}$$

all terms proportional to $\hat{c}_{i,j}$ in $\hat{\mathrm{I}}_5[a_i a_j]$ can be moved into the existing $g^{\mu_i\mu_j}$ piece. Inspection of equation (3.79) indicates that the correct term to reshuffle is $-\Delta_5\hat{\mathrm{I}}_5^{\hat{8}}[1]/N_5$ rather than merely $\hat{\mathrm{I}}_5^{D=6}[1]$. Retaining only the $c_{i,j}$ terms,

$$\begin{aligned} g^{\mu_i\mu_j} \text{ terms} &= -\frac{1}{2}\mathrm{I}_5^{D=6}[1]g^{\mu_i\mu_j} - \frac{\hat{\Delta}_5\mathrm{I}_5^{D=8}[1]}{N_5}\sum_{i,j=1}^{4} q_i^{\mu_i}q_j^{\mu_j}c_{i+1,j+1} \\ &= -\frac{1}{2}\mathrm{I}_5^{D=6}[1]g^{\mu_i\mu_j} + \frac{1}{2}\left(\mathrm{I}_5^{D=6}[1] + \frac{1}{2N_5}\sum_{m=1}^{5}\gamma_m\mathrm{I}_4^{D=6,(m)}[1]\right)g_{[4]}^{\mu_i\mu_j} \\ &= \frac{1}{4N_5}\sum_{m=1}^{5}\gamma_m\mathrm{I}_4^{D=6,(m)}[1]g^{\mu_i\mu_j} + \mathcal{O}(\epsilon). \end{aligned} \tag{3.82}$$

As expected the $\mathrm{I}_5^{D=6}[1]$ terms precisely cancel. Here the finiteness of $\mathrm{I}_5^{D=6}[1]$ and $\mathrm{I}_5^{D=8}[1]$ has been used to ensure that this term generates only $\mathcal{O}(\epsilon)$ corrections when replacing $g_{[4]}^{\mu_i\mu_j}$ with the dimensionally regularised $g^{\mu_i\mu_j}$. The remaining piece should not contain any kinematic singularities associated with lower-point Gram determinants, in particular N_5, as it originates from the well-behaved $\mathrm{I}_5^{D=8}$. This is indeed the case and we write,

$$\mathrm{Le}_2 = \frac{1}{2N_5}\sum_{m=1}^{5}\gamma_m\mathrm{I}_4^{D=6,(m)}[1]. \tag{3.83}$$

The pentagon integrals with three insertions can be obtained by direct differentiation of equation (3.79). We find,

$$\begin{aligned} \hat{\mathrm{I}}_5[a_i a_j a_k] &= \hat{c}_{i,j}\left(\hat{\mathrm{I}}_5^{D=6}[a_k] + \frac{1}{6N_5}\sum_{m=1}^{5}\left(\eta_{km}\hat{\mathrm{I}}_4^{D=6,(m)}[1] + 2\hat{\gamma}_m\hat{\mathrm{I}}_4^{D=6,(m)}[a_k]\right)\right) \\ &+\frac{1}{6N_5}\sum_{m=1}^{5}\left(2\left(\frac{\hat{\gamma}_j^{(m)}\eta_{im} - \hat{\gamma}_m\eta_{ij}^{(m)}}{\eta_{mm}}\right)\hat{\mathrm{I}}_4^{D=6,(m)}[a_k]\right. \\ &\left. -\left(\frac{\eta_{im}\eta_{jk}^{(m)} - \eta_{ij}^{(m)}\eta_{km}}{\eta_{mm}}\right)\hat{\mathrm{I}}_4^{D=6,(m)}[1] - \eta_{jm}\hat{\mathrm{I}}_4^{(m)}[a_i a_k]\right) + \text{cyclic i,j,k.} \end{aligned} \tag{3.84}$$

Since the $\hat{c}_{i,j}$ term is obtained by differentiating $c_{i,j}\mathrm{I}_5^{D=8}[1]$, it must be finite as both $N_5 \to 0$ and $\epsilon \to 0$ and we introduce the finite function,

$$\mathrm{Le}_{3k} = \frac{1}{6N_5}\sum_{m=1}^{5}\left(\alpha_k\alpha_m\eta_{km}\mathrm{I}_4^{D=6,(m)}[1] + 2\gamma_m\mathrm{I}_4^{D=6,(m)}[x_k]\right). \tag{3.85}$$

Recalling that,

$$\begin{aligned}
\mathrm{I}_5[\ell^{\mu_i}\ell^{\mu_j}\ell^{\mu_k}] &= \mathrm{I}_5[\mathcal{P}^{\mu_i}\mathcal{P}^{\mu_j}\mathcal{P}^{\mu_k}] - \frac{1}{2}\mathrm{I}_5^{D=6}[\{g\mathcal{P}\}^{\mu_i\mu_j\mu_k}] \\
&= -\sum_{i,j,k=1}^{5} \mathrm{I}_5[x_{i+1}x_{j+1}x_{k+1}]q_i^{\mu_i}q_j^{\mu_j}q_k^{\mu_k} \\
&\quad +\frac{1}{2}\left\{\sum_{k=1}^{5}\mathrm{I}_5^{D=6}[x_{k+1}]g^{\mu_i\mu_j}q_k^{\mu_k} + \text{cyclic i,j,k}\right\},
\end{aligned} \tag{3.86}$$

and keeping only the $c_{i,j}$ terms in equation (3.84) we find,

$$\begin{aligned}
g^{\mu_i\mu_j}q_k^{\mu_k}\text{ terms} &= \frac{1}{2}\mathrm{I}_5^{D=6}[x_{k+1}]g^{\mu_i\mu_j}q_k^{\mu_k} - \left(\mathrm{I}_5^{D=6}[x_{k+1}] + \mathrm{Le}_{3k}\right)\sum_{i,j=1}^{4} c_{i+1,j+1}q_i^{\mu_i}q_j^{\mu_j}q_k^{\mu_k} \\
&= \frac{1}{2}\mathrm{I}_5^{D=6}[x_{k+1}]g^{\mu_i\mu_j}q_k^{\mu_k} - \frac{1}{2}\left(\mathrm{I}_5^{D=6}[x_{k+1}] + \mathrm{Le}_{3k}\right)g_{[4]}^{\mu_i\mu_j}q_k^{\mu_k} \\
&= -\frac{1}{2}\mathrm{Le}_{3k}g^{\mu_i\mu_j}q_k^{\mu_k} + \mathcal{O}(\epsilon).
\end{aligned} \tag{3.87}$$

As in the previous case, the finiteness of the coefficient of $g_{[4]}^{\mu_i\mu_j}$ has been used to promote it to the full $D = 4 - 2\epsilon$ metric tensor.

The tensor integrals with four and five insertions may be obtained by further differentiation, and the same trick used to rewrite the $c_{i,j}$ terms as a contribution to the metric tensor structure. In this way, all vestiges of the pentagon in $D = 6 - 2\epsilon$ and higher dimensions can be removed, along with the inverse powers of Δ_5.

The functions introduced in this section, Le_1, Le_2 and Le_{3i}, only contain a single power of the Gram determinant. Consequently, they can be evaluated without numerical problems. To illustrate this, we choose a representative phase space point, $s_{1234} = 1$, $s_{123} = 0.4$, $s_{234} = 0.3$, $s_{13} = 0.1$ and use the variable s_{23} to control λ. The sixth variable s_{24} is chosen to lie within the physical region defined by the pentagon Gram determinant, $\Delta_5 < 0$. Fig. 3.9 shows the functions Le_1 and Le_2 together with Le_{35}. In each case, we see that the $\lambda \to 1$ limit is smoothly approached indicating that the function is intrinsically well behaved in that limit.

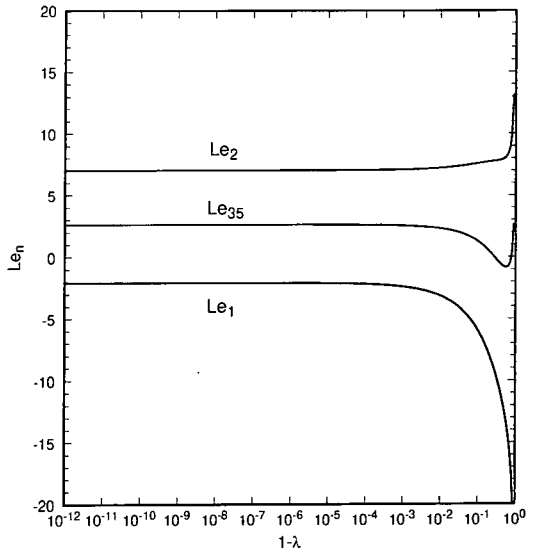

Figure 3.9: The finite functions for the pentagon graph with one external mass and evaluated in double precision Fortran as a function of $1 - \lambda$. Because the functions only contain single inverse powers of $(1 - \lambda)$, no numerical problems are evident.

3.7 Summary

In this chapter we have developed a new strategy for evaluating one-loop tensor integrals. It avoids the usual problems associated with the presence of Gram determinants. Such Gram determinants arise when the tensor integrals are expressed in terms of the physical momenta and generate false singularities at the edges of phase space. In addition to creating numerical instabilities, they tend to increase the size of the one-loop matrix elements. Our approach is to construct groups of scalar integrals which are well behaved in the limit of vanishing Gram determinant ($\Delta_n \to 0$), and which can be evaluated with arbitrary precision by making a Taylor series expansion in Δ_n. In fact such combinations arise naturally by either differentiating with respect to the external parameters - essentially yielding scalar integrals with Feynman parameters in the numerator - or by developing the scalar integral in $D = 6 - 2\epsilon$ or higher dimensions. Evaluating these new integrals is straightforward - they are just linear combinations of the known scalar integrals in $D = 4$ or $D = 4 - 2\epsilon$. As such, they combine the dilogarithms, logarithms and constants from different scalar integrals in

an extremely non-trivial way. As a bonus other spurious kinematic singularities are also controlled - they appear in the denominator of the finite functions, which are well behaved in the singular limit. Although the number of basic functions has increased, the number of dilogarithm evaluations has not, since the functions are generated recursively. Furthermore, because the Gram determinant singularities are not genuine, by grouping integrals in this way, the expressions for one loop integrals are compactified.

To illustrate the approach for specific integrals, we have applied the method to 3-, 4- and 5-point integrals where the internal masses have been set equal to zero. These tensor integrals are relevant for a range of QCD processes where the quark and gluon masses are negligible. For more general processes with arbitrary internal masses and external kinematics, the relevant combinations of scalar integrals can be obtained using equations (3.11,3.14–3.17). As a by-product we have shown how all the Gram determinants associated with pentagon graphs can be eliminated.

In chapter 4 we will make use of the basic 1-loop functions defined here to calculate the matrix elements for the next-to-leading order corrections to $e^+e^- \to 4$ jets. The relevant partonic processes contain all the mass configurations of the integrals (up to the pentagon level) described in this chapter. The sheer number of diagrams involved in the calculation will make the grouping of terms described in this chapter highly desirable, in order to compactify both the intermediate algebra and the final result.

Chapter 4

Partonic Matrix Elements

4.1 Introduction

As has been discussed in chapter 2, multi-jet events in electron-positron annihilation have long been a source of vital information about the physics of the strong interaction. In particular, the study of four-jet production can give us both a firmer test of QCD (through determination of the colour factors of the gauge group) and a window on possible new physics (for instance, the signature of a 'light' gluino).

To progress beyond the simplest Born level identification of each jet with a single parton, we must compute the next-to-leading order corrections. Such a calculation naturally divides into the 3 distinct areas which have already been briefly outlined in chapter 2. In particular, for the case of 4 jet production in e^+e^- annihilation, these are:

- **Virtual contributions**
  The 4 jet rate receives next-to-leading order virtual contributions from the two subprocesses $e^+e^- \to q\bar{q}gg$ and $e^+e^- \to q\bar{q}Q\overline{Q}$. The $\mathcal{O}(\alpha_S^3)$ terms arise from the interference of one-loop with Born level amplitudes.

- **Real contributions**
  The soft and collinear divergences of the virtual corrections, manifest as poles in ϵ

in dimensional regularization, cancel with the phase space singularities from the real contributions. These are the 5-parton Born level processes which contain an extra radiated gluon, namely $e^+e^- \to q\bar{q}ggg$ and $e^+e^- \to q\bar{q}Q\overline{Q}g$.

- **Numerical combination**
  For the above mentioned cancellation to take place, the four and five parton matrix elements must be suitably combined. Isolating the infrared divergences and cancelling them in an efficient manner by Monte Carlo methods is the final step in the 4 jet calculation.

In this chapter we shall concentrate on the explicit calculation of the matrix elements for the partonic processes relevant for both the virtual and the real contributions. The virtual matrix elements have long proved a 'bottle-neck' for QCD calculations, partly due to the large number of contributing diagrams and also because of the appearance of one-loop diagrams with five external legs. In particular, we will describe a suitable colour decomposition of the contributing Feynman diagrams and the resulting squared matrix elements. The virtual matrix elements will consist of a finite piece (composed of the special functions of the previous chapter) and infrared and ultraviolet poles. Discussion of the implementation of the cancellation of the infrared poles between real and virtual terms is deferred until chapter 5.

In discussing the calculation of the matrix elements, we shall focus on the QCD current, namely the sub-process $\gamma^* \to$ partons. In other words, the leptonic current $e^+e^- \to \gamma^*$ is factored out of the amplitudes. Such a factor is elementary to restore and in fact will often be a common factor, such as when normalizing the result of a calculation to the lowest order $e^+e^- \to q\bar{q}$ results. Moreover, the matrix elements may then also be directly implemented in general purpose next-to-leading order Monte Carlo programs for the processes $e^\pm p \to e^\pm + 3$ jets and $p\bar{p} \to V + 2$ jets.

Note that due to the difficulty involved in defining γ_5 away from four dimensions, we have restricted ourselves to the channel $e^+e^- \to \gamma^* \to 4$ jets, rather than including an intermediate Z boson. The mixed vector-axial coupling of the Z presents problems in conventional dimensional regularization, which is the scheme used throughout our calculation here. We

also choose to neglect contributions where the boson couples to a closed fermion loop. Both of these contributions are in fact very small, because of cancellations between up- and down-type quarks and kinematical constraints.

The first stage in the calculation of the virtual corrections is to make a systematic organization of the contributing diagrams into groups which have the same colour factor. Having made this division at the amplitude level in lowest and one-loop order, we calculate the relevant squared interference. This procedure is very similar for both sub-processes and we present the calculation of the colour structure for each in turn in sections 4.2 and 4.3. A subtlety involved in 'squaring' the amplitudes involving more than one gluon is described in section 4.4. The implementation of the loop integral formulae of chapter 3 is outlined in sections 4.5 and 4.7, whilst the isolation of the infrared and ultraviolet poles is detailed in section 4.6. Comparison of the results presented here with those obtained from a very different approach [42, 43, 44] follow in 4.8. Finally, the structure of the 5 parton tree level matrix elements is given in sections 4.9 and 4.10.

4.2 The 2-Quark, 2-Gluon Sub-Process: $\gamma^* \to q\bar{q}gg$

We first consider the process, $\gamma^* \to q\bar{q}gg$ in some detail. Momenta are labelled as,

$$\gamma^*(p_{1234}) \to q(p_1) + \bar{q}(p_2) + g(p_3) + g(p_4), \tag{4.1}$$

and the photon momentum is systematically eliminated in favour of the four massless parton momenta.

The colour structure of the matrix element at tree-level ($n = 0$) and one-loop ($n = 1$) is rather simple and we have,

$$\begin{aligned}\mathcal{M}^{(n)} &= \epsilon^{\mu}\epsilon^{\nu_3}\epsilon^{\nu_4}\mathcal{M}^{(n)}_{\mu\nu_3\nu_4} = e g_s^2 \left(\frac{g_s}{4\pi}\right)^{2n} \\ &\times \left\{(T^{a_3}T^{a_4})_{c_1c_2}\mathcal{A}_1^{(n)}(3,4) + (T^{a_4}T^{a_3})_{c_1c_2}\mathcal{A}_1^{(n)}(4,3) + \frac{1}{2}\delta_{c_1c_2}\delta_{a_3a_4}\mathcal{A}_2^{(n)}(3,4)\right\},\end{aligned} \tag{4.2}$$

where c_1, c_2 are the colours of the quarks and a_3, a_4 the colours of the gluons. The arguments

of $\mathcal{A}_i$ indicate a permutation of the momenta of the external gluons. At lowest order,

$$\mathcal{A}_2^{(0)}(3,4) = 0, \tag{4.3}$$

while at one-loop we find,

$$\mathcal{A}_1^{(1)}(3,4) = N\mathcal{A}_A^{(1)}(3,4) - \frac{1}{N}\mathcal{A}_B^{(1)}(3,4), \tag{4.4}$$

$$\mathcal{A}_2^{(1)}(3,4) \equiv \mathcal{A}_C^{(1)}(3,4) \equiv \mathcal{A}_C^{(1)}(4,3). \tag{4.5}$$

The functions $A_\alpha^{(1)}(i,j)$, $\alpha = A, B, C$ represent the contributions of the three gauge invariant sets of Feynman diagrams shown in Figs. 4.1, 4.2 and 4.3 respectively. The derivation of this decomposition is simple application of the colour algebra rules given in chapter 2.

At leading order, the squared matrix elements were first obtained in [17]. The colour structure is,

$$\sum_{\text{spins}} |\mathcal{M}^{(0)}|^2 = \frac{e^2 g_s^4}{4}(N^2-1)N\left\{\mathcal{T}(3,4) + \mathcal{T}(4,3) - \frac{1}{N^2}\mathcal{T}\right\}, \tag{4.6}$$

where,

$$\mathcal{T}(3,4) = \sum_{\text{spins}} \left|\mathcal{A}_1^{(0)\dagger}(3,4)\mathcal{A}_1^{(0)}(3,4)\right|, \tag{4.7}$$

and,

$$\mathcal{T} = \sum_{\text{spins}} \left| \left(\mathcal{A}_1^{(0)\dagger}(3,4) + \mathcal{A}_1^{(0)\dagger}(4,3)\right)\left(\mathcal{A}_1^{(0)}(3,4) + \mathcal{A}_1^{(0)}(4,3)\right)\right|. \tag{4.8}$$

The 3-gluon vertex contributions to $\mathcal{A}_1^{(0)}(3,4)$ and $\mathcal{A}_1^{(0)}(4,3)$ enter with opposite sign, so $\mathcal{T}$ (with no arguments) is the contribution from the pure QED-like diagrams.

The relevant squared matrix elements are the interference between the tree-level and one-loop amplitudes,

$$\sum_{\text{spins}} 2|\mathcal{M}^{(0)\dagger}\mathcal{M}^{(1)}| = \frac{e^2 g_s^4}{4}\left(\frac{\alpha_S N}{2\pi}\right)(N^2-1)N$$
$$\times \left\{\mathcal{L}_A(3,4) + \mathcal{L}_A(4,3) - \frac{1}{N^2}\Big(\mathcal{L}_A + \mathcal{L}_B(3,4) + \mathcal{L}_B(4,3) - \mathcal{L}_C\Big) + \frac{1}{N^4}\mathcal{L}_B\right\}, \tag{4.9}$$

with,

$$\mathcal{L}_\alpha(3,4) = \sum_{\text{spins}} \Re\, \mathcal{A}_\alpha^{(1)\dagger}(3,4)\mathcal{A}_1^{(0)}(3,4), \tag{4.10}$$

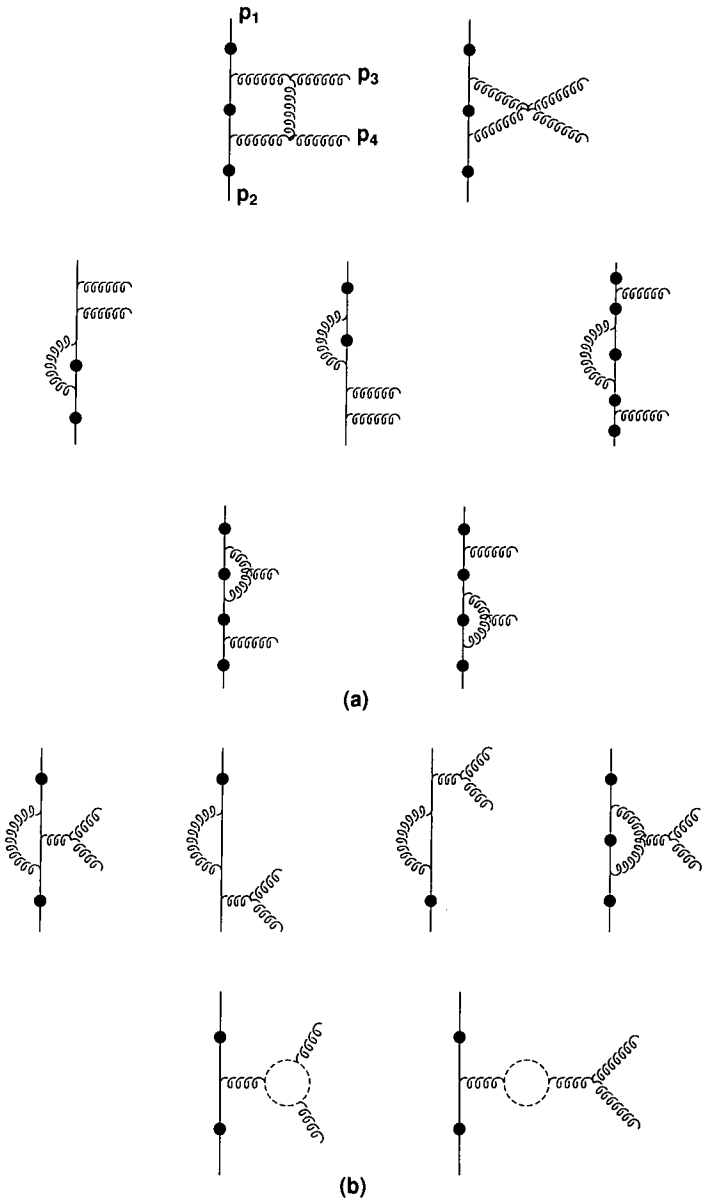

Figure 4.1: The classes of Feynman diagrams relevant for the function $\mathcal{A}_A^{(1)}(3,4)$. Reading clockwise round the diagram and starting from the quark (p_1) at the top, we encounter gluon (p_3) before gluon (p_4) and end at antiquark (p_2). The solid circle indicates the possible positions for attaching the off-shell photon to the quark-antiquark pair. Diagrams (a), taken with both permutations of gluons 3 and 4, contribute to the piece $\mathcal{L}_A$ while the permutation shown in (a)+(b) gives the contribution to $\mathcal{L}_A(3,4)$. Diagrams with self-energy corrections on the external lines are zero in dimensional regularisation and have been omitted.

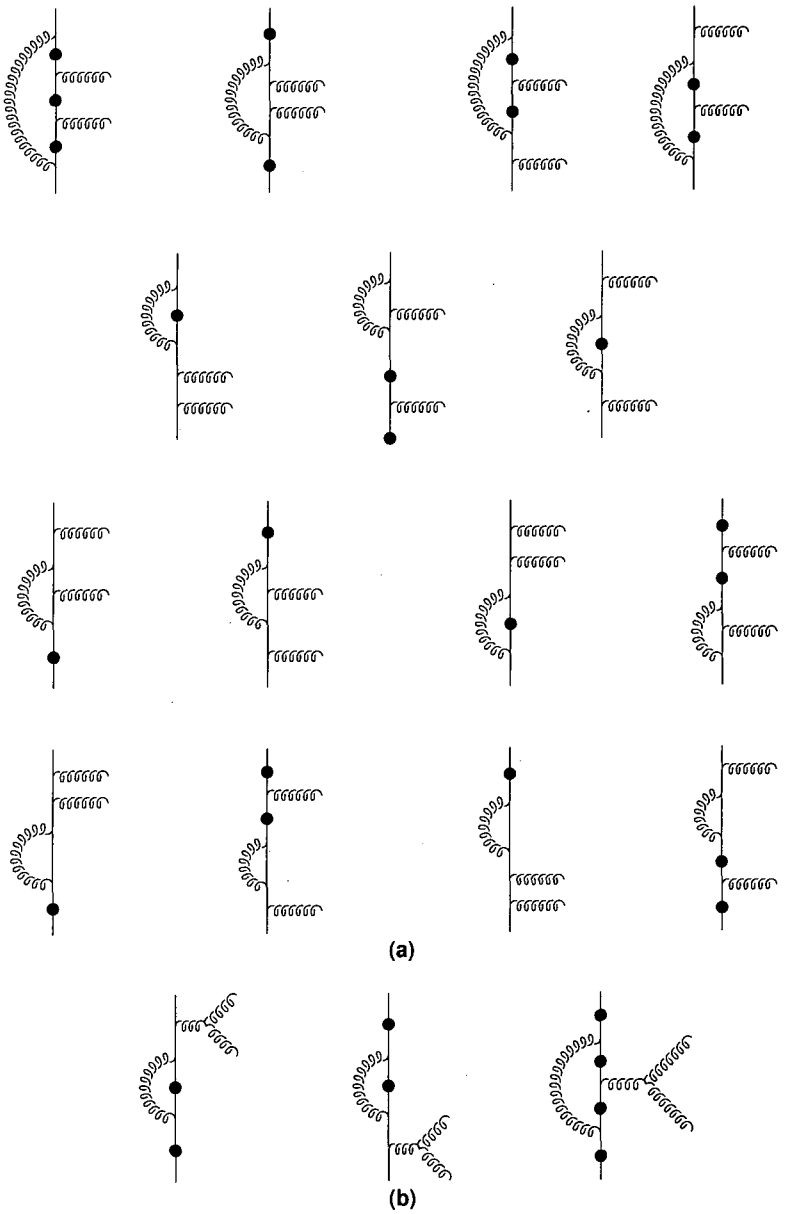

Figure 4.2: The classes of Feynman diagrams relevant for the function $\mathcal{A}_B^{(1)}(3,4)$ Reading clockwise round the diagram and starting from the quark (p_1) at the top, we encounter gluon (p_3) before gluon (p_4) and end at antiquark (p_2). The solid circle indicates the possible positions for attaching the off-shell photon to the quark-antiquark pair. Diagrams (a), taken with both permutations of gluons 3 and 4, contribute to the piece $\mathcal{L}_B$ while the permutation shown in (a)+(b) gives the contribution to $\mathcal{L}_B(3,4)$.

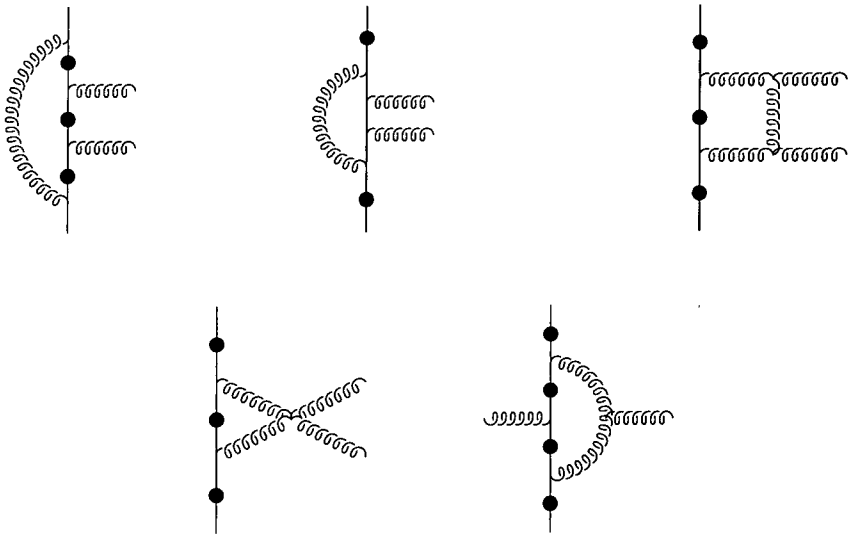

Figure 4.3: The classes of Feynman diagrams relevant for the function $\mathcal{A}_C^{(1)}$ when taken with both permutations of the gluons. Reading clockwise round the diagram and starting from the quark (p_1) at the top, we encounter gluon (p_3) before gluon (p_4) and end at antiquark (p_2). The solid circle indicates the possible positions for attaching the off-shell photon to the quark-antiquark pair.

for $\alpha = A,\ B$ and the QED-like structures,

$$\mathcal{L}_\alpha = \sum_{\text{spins}} \Re\left(\mathcal{A}_\alpha^{(1)\dagger}(3,4) + \mathcal{A}_\alpha^{(1)\dagger}(4,3)\right)\left(\mathcal{A}_1^{(0)}(3,4) + \mathcal{A}_1^{(0)}(4,3)\right). \tag{4.11}$$

Note that the function $\mathcal{L}_A(3,4)$ contains some finite terms proportional to n_F/N due to the fermionic vertex and self-energy corrections in Fig. 4.1. Hence the squared matrix elements are described by 5 independent $\mathcal{L}_\alpha$. The $\mathcal{L}_\alpha(3,4)$ are symmetric under the exchange $p_1 \leftrightarrow p_2$ *and* $p_3 \leftrightarrow p_4$ while the $\mathcal{L}_\alpha$ are symmetric under either $p_1 \leftrightarrow p_2$ *or* $p_3 \leftrightarrow p_4$.

4.3 The 4-Quark Sub-Process: $\gamma^* \to q\bar{q}Q\overline{Q}$

The calculation described in this section was first carried out by the authors of [45]. In repeating the computation, some simplification of the final results was found and the method is presented here for completeness.

In the four quark final state we produce two pairs of (possibly non-identical) quarks, $q\bar{q}$ and $Q\bar{Q}$, with corresponding quark charges e_q and e_Q. Again the momentum of the virtual photon is eliminated in favour of the massless quark momenta, which are labelled as,

$$\gamma^*(p_{1234}) \to q(p_1) + \bar{q}(p_2) + Q(p_3) + \overline{Q}(p_4). \tag{4.12}$$

The colour decomposition of the tree-level ($n = 0$) and one-loop ($n = 1$) amplitudes analogous to equation (4.2) is,

$$\begin{aligned}\mathcal{M}^{(n)} = \epsilon^\mu \mathcal{M}^{(n)}_\mu = \frac{e g_s^2}{2}\left(\frac{g_s}{4\pi}\right)^{2n} \\ \times \left\{\delta_{c_1 c_4}\delta_{c_3 c_2}\left(\mathcal{A}_1^{(n)}(1,2) + \mathcal{A}_1^{(n)}(3,4) + \frac{\delta_{qQ}}{N}\left(\mathcal{A}_2^{(n)}(1,4) + \mathcal{A}_2^{(n)}(3,2)\right)\right)\right. \\ \left. - \delta_{c_1 c_2}\delta_{c_3 c_4}\left(\frac{1}{N}\left(\mathcal{A}_2^{(n)}(1,2) + \mathcal{A}_2^{(n)}(3,4)\right) + \delta_{qQ}\left(\mathcal{A}_1^{(n)}(1,4) + \mathcal{A}_1^{(n)}(3,2)\right)\right)\right\},\end{aligned} \tag{4.13}$$

where the colours of the quarks are labelled by c_i, $i = 1, \ldots, 4$. Here there are many diagrams which appear similar, but in which the vector boson couples to different quark lines. For identical quarks, the vector boson may couple to the pairs $q\bar{q}$, $Q\bar{Q}$, $q\bar{Q}$ and $Q\bar{q}$, whilst in the non-identical case only the first two pairs are allowed. This is represented by the delta function, $\delta_{qQ} = 1$ for identical quarks and zero otherwise. The arguments of $\mathcal{A}_i$ indicate which quark line is attached to the vector boson (by specifying the momenta labels of the quark-antiquark pair) and hence which quark charge that function is proportional to. The generic structure given above simplifies at tree level,

$$\mathcal{A}_1^{(0)}(i,j) = \mathcal{A}_2^{(0)}(i,j), \tag{4.14}$$

while at one-loop we find the more complicated expressions,

$$\mathcal{A}_1^{(1)}(i,j) = N A_C^{(1)}(i,j) - \frac{1}{N}\left(2A_A^{(1)}(i,j) + A_B^{(1)}(i,j)\right), \tag{4.15}$$

$$\mathcal{A}_2^{(1)}(i,j) = N\left(A_C^{(1)}(i,j) - A_A^{(1)}(i,j)\right) - \frac{1}{N}\left(A_A^{(1)}(i,j) + A_B^{(1)}(i,j)\right). \tag{4.16}$$

All the contributing Feynman diagrams have again been divided into three gauge invariant sets, represented by the functions $A_\alpha^{(1)}(i,j)$, $\alpha = A, B, C$. These diagrams are illustrated in Fig. 4.4. The contribution from the fermion loop in the fourth diagram of Fig. 4.4(c),

which is proportional to the number of flavours n_F, is included in the leading colour part $\mathcal{A}_C$. There is a set of diagrams which is not included here, namely that which includes diagrams containing closed fermion triangles. However, this contribution must vanish by Furry's theorem. Although this amplitude is not itself zero, the symmetric phase space integration over the final state ensures that this QED result extends to the gluonic case when calculating the contribution to a 4 jet cross-section.

At lowest order the squared matrix elements are [17],

$$\begin{aligned}\sum_{\text{spins}} |\mathcal{M}^{(0)}|^2 &= \frac{e^2 g_s^4}{4}(N^2-1) \\ &\times \left\{\Big(\mathcal{T}(1,2;1,2)+\mathcal{T}(1,2;3,4)\Big)+\frac{\delta_{qQ}}{N}\Big(\mathcal{T}(1,2;1,4)+\mathcal{T}(1,2;3,2)\Big)\right\} \\ &+(1\leftrightarrow 3, 2\leftrightarrow 4)+\delta_{qQ}(2\leftrightarrow 4)+\delta_{qQ}(1\leftrightarrow 3),\end{aligned} \tag{4.17}$$

where,

$$\mathcal{T}(i,j;k,l) = \sum_{\text{spins}} |A^{(0)\dagger}(i,j)\mathcal{A}^{(0)}(k,l)|. \tag{4.18}$$

The relevant next-to-leading order squared matrix elements are the interference between the tree-level and one-loop amplitudes,

$$\begin{aligned}\sum_{\text{spins}} 2|\mathcal{M}^{(0)\dagger}\mathcal{M}^{(1)}| &= \frac{e^2 g_s^4}{4}\left(\frac{\alpha_S N}{2\pi}\right)(N^2-1) \\ &\times \left\{\left[\Big(\mathcal{L}_C(1,2;1,2)+\mathcal{L}_C(1,2;3,4)\Big)\right.\right. \\ &\qquad \left.-\frac{1}{N^2}\Big(2\mathcal{L}_A(1,2;1,2)+2\mathcal{L}_A(1,2;3,4)+\mathcal{L}_B(1,2;1,2)+\mathcal{L}_B(1,2;3,4)\Big)\right] \\ &+\delta_{qQ}\left[\frac{1}{N}\Big(\mathcal{L}_C(1,2;1,4)+\mathcal{L}_C(1,2;3,2)-\mathcal{L}_A(1,2;1,4)-\mathcal{L}_A(1,2;3,2)\Big)\right. \\ &\qquad \left.\left.-\frac{1}{N^3}\Big(\mathcal{L}_A(1,2;1,4)+\mathcal{L}_A(1,2;3,2)+\mathcal{L}_B(1,2;1,4)+\mathcal{L}_B(1,2;3,2)\Big)\right]\right\} \\ &+(1\leftrightarrow 3, 2\leftrightarrow 4)+\delta_{qQ}(2\leftrightarrow 4)+\delta_{qQ}(1\leftrightarrow 3),\end{aligned} \tag{4.19}$$

with,

$$\mathcal{L}_\alpha(i,j;k,l) = \sum_{\text{spins}} |A_\alpha^{(1)\dagger}(i,j)\mathcal{A}^{(0)}(k,l)|. \tag{4.20}$$

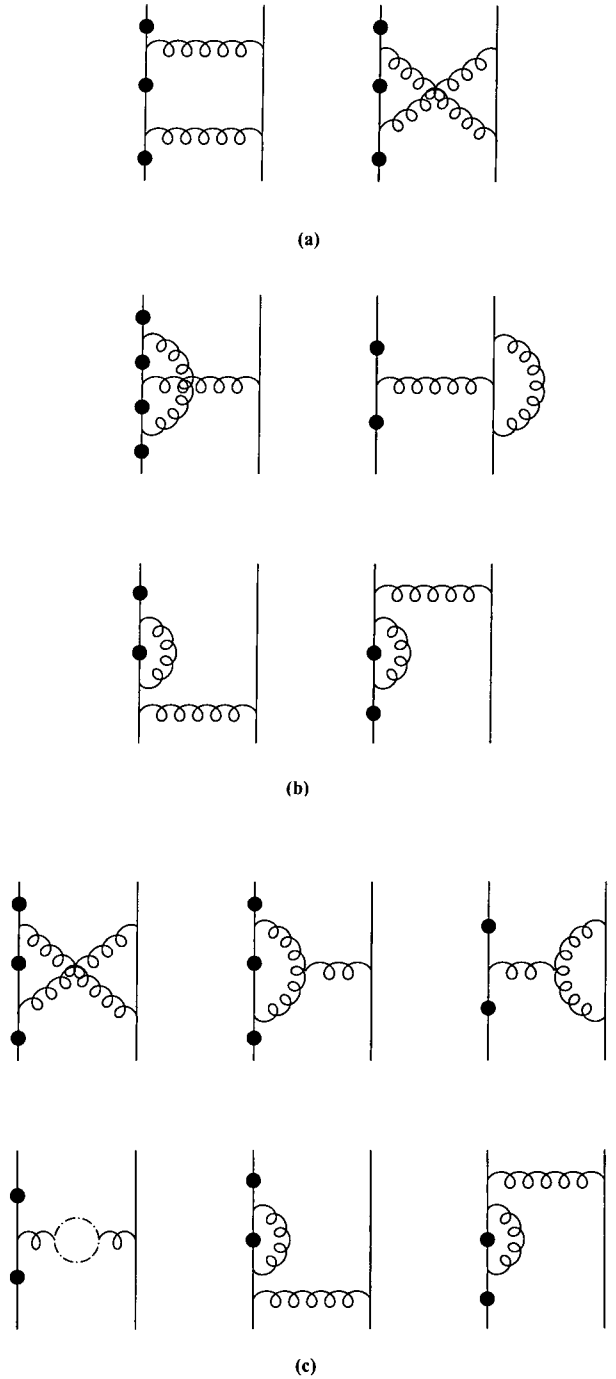

Figure 4.4: The classes of Feynman diagrams relevant for the different colour structures. The solid circle indicates the possible positions for attaching the off-shell photon to the quark-antiquark pair i, j. Group (a) contributes to $A_A^{(1)}(i,j)$, (b) to $A_B^{(1)}(i,j)$ and group (c) to the leading colour amplitude $A_C^{(1)}(i,j)$. Diagrams with self-energy corrections on the external lines are zero in dimensional regularisation and have been omitted.

Using the symmetry properties of the Feynman diagrams, we find that,

$$\mathcal{L}_\alpha(1,2;3,2) = \mathcal{L}_\alpha(1,2;1,4)(p_1 \leftrightarrow p_2, p_3 \leftrightarrow p_4), \tag{4.21}$$

so that for this sub-process the squared matrix elements are described by 9 independent $\mathcal{L}_\alpha$.

4.4 Gluon Polarization Sums

In QED, the sum over photon polarization states is straightforward to perform. A direct consequence of the Ward identity is that, in the Feynman gauge,

$$\sum_{\text{spins}} \epsilon^\mu \epsilon^{*\nu} \to -g^{\mu\nu}, \tag{4.22}$$

is a valid replacement. This may be used for any number of initial or final state photons.

When working within QCD this is only true for processes involving a single gluon. With more than one gluon, the presence of the triple-gluon vertex allows non-physical, longitudinal degrees of freedom to propagate, which can be compensated for by additional diagrams involving loops of ghost particles. To illustrate an alternative resolution (first used in [46]), consider a process involving two gluons of momenta p_1 and p_2, with corresponding polarization vectors ϵ_1^μ and ϵ_2^ν. The amplitude for such a process may be written as,

$$\mathcal{M} = \epsilon_1^\mu \epsilon_2^\nu \mathcal{M}_{\mu\nu}, \tag{4.23}$$

where the uncontracted form of the matrix elements, $\mathcal{M}_{\mu\nu}$ satisfies the Ward identities,

$$p_1^\mu \epsilon_2^\nu \mathcal{M}_{\mu\nu} = \epsilon_1^\mu p_2^\nu \mathcal{M}_{\mu\nu} = 0. \tag{4.24}$$

So at the amplitude level, we must obtain zero when replacing one or other of the gluon polarization vectors by the corresponding momentum. However, to legitimately make the replacement in equation (4.22), we need the more stringent conditions,

$$p_1^\mu \mathcal{M}_{\mu\nu} = p_2^\nu \mathcal{M}_{\mu\nu} = 0. \tag{4.25}$$

Inspecting the form of the triple-gluon vertex for two external gluons (Fig. 4.5) and the Feynman rules from chapter 1,

$$(2p_1 + p_2)^\nu g^{\mu\rho} - (p_1 + 2p_2)^\mu g^{\nu\rho} + (p_2 - p_1)^\rho g^{\mu\nu}, \tag{4.26}$$

we find two terms that will vanish only by transversality, $\epsilon(p) \cdot p = 0$, namely $p_2^\nu g^{\mu\rho} - p_1^\mu g^{\nu\rho}$. These terms are therefore admitted by equation (4.24) but not by (4.25).

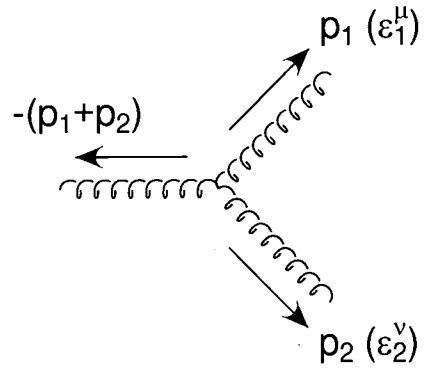

Figure 4.5: The triple gluon vertex for two external gluons p_1 and p_2.

Thus use of the sum (4.22), without the addition of ghost diagrams, is allowed providing we use a modified form of the three-gluon vertex for two external gluons,

$$2p_1^\nu g^{\mu\rho} - 2p_2^\mu g^{\nu\rho} + (p_2 - p_1)^\rho g^{\mu\nu}. \tag{4.27}$$

So, having replaced the relevant three-gluon vertices in our diagrams with the modified form (4.27), all the boson polarization sums (ie. for the off-shell photon and the two gluons in our particular case) may be performed with the simple replacement (4.22).

4.5 Loop Integrals

It is now an arduous but well-defined task to calculate the 14 required functions relevant for the next-to-leading order corrections to $\gamma^* \to 4$ jets. After adding up the relevant diagrams

prescribed by the colour structure and 'squaring' with the polarization sums and external triple gluon vertices as above, it remains to perform the usual algebra. FORM [47] is used repeatedly to perform D-dimensional traces and to handle the lengthy expressions that are generated.

As discussed in the previous chapter, the loop integrals which are generated in this way may contain tensor numerators, deriving from terms such as ℓ^2 and $\ell \cdot p$. The simplest form of reduction possible involves a re-writing of numerator factors thus,

$$\frac{\ell \cdot p}{\ell^2(\ell+p)^2} = \frac{(\ell+p)^2 - \ell^2 - p^2}{2\ell^2(\ell+p)^2}. \tag{4.28}$$

The tensor numerator is removed and replaced by a combination of scalar integrals with either none or one of the propagators cancelled through. Such a trick may clearly only be used when the momentum p in the numerator can be related to those in the propagators. In the case of pentagon diagrams, where all momenta are present in the propagators, this type of reduction results in no pentagon tensor integrals.

Thus these simple cancellations lead to an instant reduction of the number of loop configurations that need to be calculated. In particular, we require only the scalar pentagon integral and box (triangle) tensor integrals with at most three (two) loop momenta in the numerator. This is a primary motivation for calculating the squared matrix elements rather than the individual amplitudes. We have seen in the previous chapter how these tensor reductions can be carried out and the special functions that need to be introduced in order to describe all these integrals (collected in Appendix B).

4.6 Pole Structure

Working in dimensional regularisation with $4-2\epsilon$ spacetime dimensions, it is straightforward to remove the infrared and ultraviolet poles from the functions $\mathcal{L}_\alpha$. These are the singularities which are expected to cancel with those from the corresponding 5-parton configurations containing an extra gluon and those generated by ultraviolet renormalisation. This can-

cellation relies upon the factorization into pole terms $1/\epsilon$, $1/\epsilon^2$ multiplying the tree-level amplitudes.

In particular, for the sub-process $\gamma^* \to q\bar{q}gg$ we find,

$$\mathcal{L}_A(3,4) = \left(-\frac{\mathcal{P}_{13}}{\epsilon^2} - \frac{\mathcal{P}_{24}}{\epsilon^2} - \frac{\mathcal{P}_{34}}{\epsilon^2} - \frac{3}{2}\frac{\mathcal{P}_{1234}}{\epsilon}\right)\mathcal{T}(3,4) + \hat{\mathcal{L}}_A(3,4), \tag{4.29}$$

$$\begin{aligned}\mathcal{L}_A = &+\frac{1}{2}\left(-\frac{\mathcal{P}_{13}}{\epsilon^2} - \frac{\mathcal{P}_{24}}{\epsilon^2} - \frac{\mathcal{P}_{34}}{\epsilon^2} - \frac{3}{2}\frac{\mathcal{P}_{1234}}{\epsilon}\right)(\mathcal{T} + \mathcal{T}(3,4) - \mathcal{T}(4,3)) \\ &+\frac{1}{2}\left(-\frac{\mathcal{P}_{14}}{\epsilon^2} - \frac{\mathcal{P}_{23}}{\epsilon^2} - \frac{\mathcal{P}_{34}}{\epsilon^2} - \frac{3}{2}\frac{\mathcal{P}_{1234}}{\epsilon}\right)(\mathcal{T} + \mathcal{T}(4,3) - \mathcal{T}(3,4)) + \hat{\mathcal{L}}_A,\end{aligned} \tag{4.30}$$

$$\mathcal{L}_B(3,4) = \left(-\frac{\mathcal{P}_{12}}{\epsilon^2} - \frac{3}{2}\frac{\mathcal{P}_{1234}}{\epsilon}\right)\mathcal{T}(3,4) + \hat{\mathcal{L}}_B(3,4), \tag{4.31}$$

$$\mathcal{L}_B = \left(-\frac{\mathcal{P}_{12}}{\epsilon^2} - \frac{3}{2}\frac{\mathcal{P}_{1234}}{\epsilon}\right)\mathcal{T} + \hat{\mathcal{L}}_B, \tag{4.32}$$

$$\begin{aligned}\mathcal{L}_C = &+\frac{1}{2}\left(-\frac{\mathcal{P}_{12}}{\epsilon^2} - \frac{\mathcal{P}_{34}}{\epsilon^2} + \frac{\mathcal{P}_{14}}{\epsilon^2} + \frac{\mathcal{P}_{23}}{\epsilon^2}\right)(\mathcal{T} + \mathcal{T}(3,4) - \mathcal{T}(4,3)) \\ &+\frac{1}{2}\left(-\frac{\mathcal{P}_{12}}{\epsilon^2} - \frac{\mathcal{P}_{34}}{\epsilon^2} + \frac{\mathcal{P}_{13}}{\epsilon^2} + \frac{\mathcal{P}_{24}}{\epsilon^2}\right)(\mathcal{T} + \mathcal{T}(4,3) - \mathcal{T}(3,4)) + \hat{\mathcal{L}}_C.\end{aligned} \tag{4.33}$$

where we have introduced the notation,

$$\mathcal{P}_x = \left(\frac{4\pi\mu^2}{-s_x}\right)^{\epsilon} \frac{\Gamma^2(1-\epsilon)\Gamma(1+\epsilon)}{\Gamma(1-2\epsilon)}. \tag{4.34}$$

Similarly, the poles isolated from the sub-process $\gamma^* \to q\bar{q}Q\bar{Q}$ are,

$$\mathcal{L}_A(1,2;i,j) = \left(+\frac{\mathcal{P}_{13}}{\epsilon^2} - \frac{\mathcal{P}_{14}}{\epsilon^2} - \frac{\mathcal{P}_{23}}{\epsilon^2} + \frac{\mathcal{P}_{24}}{\epsilon^2}\right)\mathcal{T}(1,2;i,j) + \hat{\mathcal{L}}_A(1,2;i,j), \tag{4.35}$$

$$\mathcal{L}_B(1,2;i,j) = \left(-\frac{\mathcal{P}_{12}}{\epsilon^2} - \frac{\mathcal{P}_{34}}{\epsilon^2} - \frac{3\mathcal{P}_{34}}{\epsilon}\right)\mathcal{T}(1,2;i,j) + \hat{\mathcal{L}}_B(1,2;i,j), \tag{4.36}$$

$$\mathcal{L}_C(1,2;i,j) = \left(-\frac{\mathcal{P}_{14}}{\epsilon^2} - \frac{\mathcal{P}_{23}}{\epsilon^2} + \frac{2}{3}\frac{\mathcal{P}_{34}}{\epsilon} - \frac{2n_F}{3N}\frac{\mathcal{P}_{34}}{\epsilon}\right)\mathcal{T}(1,2;i,j) + \hat{\mathcal{L}}_C(1,2;i,j). \tag{4.37}$$

This pole structure is in agreement with the expectations of ref. [21] and reproduces that given in [31, 48].

4.7 Reduction Relations

In determining the finite pieces, $\hat{\mathcal{L}}$, we are concerned to ensure that the singularity structure matches that of the tree-level functions. Upon examining the tree-level matrix elements for the $q\bar{q}gg$ sub-process and in terms of the generalised Mandelstam invariants,

$$s_{ij} = (p_i + p_j)^2, \qquad s_{ijk} = (p_i + p_j + p_k)^2, \qquad s_{ijkl} = (p_i + p_j + p_k + p_l)^2, \tag{4.38}$$

$\mathcal{T}$ contains single poles in s_{13}, s_{23}, s_{14} and s_{24} while $\mathcal{T}(3,4)$ has poles in s_{13}, s_{34} and s_{24}. In addition, both $\mathcal{T}$ and $\mathcal{T}(3,4)$ contain double poles in the triple invariants s_{134} and s_{234}. As discussed in the previous chapter, the tensor reduction employed automatically protects possible singularities due to Gram determinants. However, it is possible to generate apparent singularities in double or triple invariants such as s_{12} or s_{123}. These poles do not correspond to any of the allowed infrared singularities and the matrix elements are finite as, for example, $s_{12} \to 0$ or $s_{123} \to 0$. In fact, it is straightforward to explicitly remove such poles using identities amongst the combinations of scalar integrals. For example, the identity,

$$\frac{(s_{123} - s_{12})}{s_{123}} \mathrm{Ld}_{22}(p_{12}, p_3, p_4) = -\mathrm{Ld}_{21}(p_{12}, p_3, p_4) + \mathrm{Ld}_1(p_{12}, p_3, p_4) + \mathrm{Lc}_1(p_{12}, p_{34}), \tag{4.39}$$

relating the functions for box integral functions with two adjacent masses is useful to eliminate poles in s_{123}. A complete list of such identities for all the loop integral functions is given in Appendix D. The finite pieces can then be written symbolically as,

$$\hat{\mathcal{L}} = \sum_i P_i(s) \mathrm{L}_i, \tag{4.40}$$

where the coefficients $P_i(s)$ are rational polynomials of invariants multiplying the finite functions L_i, which are well-behaved in all kinematic limits. Any denominators of the corresponding tree-level matrix element are allowed in the coefficient $P_i(s)$, with any additional fake singularities protected by L_i.

Typically the coefficient of a given function contains $\mathcal{O}(100)$ terms for the $q\bar{q}gg$ sub-process (and $\mathcal{O}(30)$ for $q\bar{q}Q\bar{Q}$), comparable with the size of the tree-level matrix elements. The number of functions is rather large, of $\mathcal{O}(100)$, but is a minimal set which protects

all the kinematic limits and is therefore numerically stable. Although the expressions for the individual $\hat{\mathcal{L}}_\alpha$ are in closed form, they are still rather lengthy and may contain many hundreds of terms in total. Therefore, rather than explicitly list each of these functions, it is more useful to provide FORTRAN code which can return the value of any of these functions at a specific phase-space point. However, to stress the analytic nature of these results, one of the smaller four-quark functions, $\mathcal{L}_C(1,2;1,2)$ is presented in full in Appendix E.

4.8 Comparison of Matrix Elements

The above calculations were also performed (contemporaneously) by another group, consisting of Bern, Dixon, Kosower and Weinzierl (BDKW) [42, 43, 44]. However, their choice of method was clearly different to the one presented here. In particular, the main differences were:

- **'Squaring' of amplitudes.**
  We chose to compute the interference of the tree-level with the one-loop amplitudes in order to simplify considerably the tensor integrals involved. BDKW instead worked directly in the helicity amplitude approach, where in particular the helicities of the initial electron and positron are specified.

- **Dimensional regularization.**
  Treating all particles in D dimensions as we have done is the conventional scheme. This is not suitable for a helicity calculation, where the external particles should be kept in 4 dimensions. BDKW therefore used the dimensional reduction scheme, as described in chapter 2.

- **Loop integrals.**
  Rather than using a conventional Feynman diagram approach and reducing the integrals as we have done, BDKW appealed to the analytic structure of the amplitudes and general results such as unitarity. These tools allowed them to completely reconstruct the amplitudes directly from certain specific collinear limits.

Given these major differences, direct comparison of the final spin-summed matrix elements at specific points in physical phase space is a highly non-trivial check of both approaches. By averaging over the initial electron and positron directions, summing over helicity combinations and numerically squaring the amplitudes, the BDKW results can be compared with the matrix elements presented here. For the two specific points in phase space given in Table 4.1, the comparison is shown in Table 4.2 [49].

Invariant	Point 1	Point 2
s_{12}	0.0140351646	0.406021454
s_{13}	0.0648812165	0.0621334973
s_{14}	0.144051806	0.0709877341
s_{23}	0.119662557	0.211110091
s_{24}	0.0284402186	0.247534016
s_{34}	0.628929035	0.00221319515

Table 4.1: The phase space points used for the comparison in Table 4.2.

The results obtained from each calculation for both of the sub-processes are clearly in very good agreement.

4.9 The 2-Quark, 3-Gluon Current

Since we shall later be interested in the behaviour of the five parton matrix elements in soft and collinear limits, we shall present the colour decomposition in rather more detail than the four parton ones above. In particular we will endeavour to always write the matrix elements in terms of colourless subamplitudes where the colour quantum number flows are clear.

The two quark-three gluon current $\widehat{\mathcal{S}}^5_\mu$ may be decomposed according to the colour struc-

Colour factor	Source	Point 1	Point 2
N	$q\bar{q}Q\overline{Q}$	10.1502095	11.718672
		10.1502120	11.718774
$\frac{1}{N}$	$q\bar{q}Q\overline{Q}$	-13.869213	-51.3942815
		-13.869226	-51.3947206
$N \times n_F$	$q\bar{q}Q\overline{Q}$	6.46323291	0.0812643912
		6.46323267	0.0812645416
$\frac{n_F}{N}$	$q\bar{q}Q\overline{Q}$	4.2077780	2.05627511
	(fermion loop)	4.2077794	2.05627466
1	$q\bar{q}Q\overline{Q}$	-1.47205477	1.96450861
	(identical)	-1.47205426	1.96450796
$\frac{1}{N^2}$	$q\bar{q}Q\overline{Q}$	1.47454064	5.74016623
	(identical)	1.47454122	5.74016476
1	$q\bar{q}gg$	-4.84091715	-13.4359536
		-4.84091714	-13.4359535
$\frac{n_F}{N}$	$q\bar{q}gg$	-0.00111172722	-0.0170968872
	(fermion loop)	-0.00111172717	-0.0170968799
$\frac{1}{N^2}$	$q\bar{q}gg$	21.5573194	7.24466256
		21.5573192	7.24466266
$\frac{1}{N^4}$	$q\bar{q}gg$	-15.1560743	-0.432338074
		-15.1560739	-0.432338183

Table 4.2: Numerical comparison of the matrix elements presented in this thesis with those obtained by the BDKW group. The matrix elements are divided according to the sub-process from which they originate and their colour weight. In each row, the uppermost number is that obtained using the squared matrix elements of this chapter, whilst the lower is the one produced by the helicity amplitudes for $e^+e^- \to q\bar{q}Q\overline{Q}$ [42, 43] and $e^+e^- \to q\bar{q}gg$ [44, 43]. The comparison is made for the two four-parton phase space points characterized by the invariants in Table 4.1.

ture [50],

$$\widehat{\mathcal{S}}^5_\mu(Q_1;1,2,3;\overline{Q}_2) = ieg^3 \sum_{P(1,2,3)} (T^{a_1}T^{a_2}T^{a_3})_{c_1c_2} S_\mu(Q_1;1,2,3;\overline{Q}_2), \tag{4.41}$$

where $\mathcal{S}_\mu(Q_1;1,2,3;\overline{Q}_2)$ represents the colourless subamplitude where the gluons are emitted in an ordered way from the quark line. By summing over all permutations of gluon emission, all Feynman diagrams and colour structures are accounted for.

The squared matrix elements (again using the polarization sums and triple-gluon vertex of section 4.4) are simply,

$$\begin{aligned}\left|\widehat{\mathcal{S}}^5_\mu V^\mu\right|^2 &= e^2 \left(\frac{g^2N}{2}\right)^3 \left(\frac{N^2-1}{N}\right) \\ &\times \left[\sum_{P(1,2,3)} \left(\left|\mathcal{S}_\mu(Q_1;1,2,3;\overline{Q}_2)V^\mu\right|^2 - \frac{1}{N^2}\left|\mathcal{S}_\mu(Q_1;1,2,\tilde{3};\overline{Q}_2)V^\mu\right|^2\right)\right. \\ &\left. + \left(\frac{N^2+1}{N^4}\right)\left|\mathcal{S}_\mu(Q_1;\tilde{1},\tilde{2},\tilde{3};\overline{Q}_2)V^\mu\right|^2\right],\end{aligned} \tag{4.42}$$

with V^μ representing the lepton current $e^+e^- \to \gamma^*$. In the last two terms, the tilde indicates that that gluon should be inserted in all positions in the amplitude. In other words,

$$\mathcal{S}_\mu(Q_1;1,2,\tilde{3};\overline{Q}_2) = \mathcal{S}_\mu(Q_1;1,2,3;\overline{Q}_2) + \mathcal{S}_\mu(Q_1;1,3,2;\overline{Q}_2) + \mathcal{S}_\mu(Q_1;3,1,2;\overline{Q}_2). \tag{4.43}$$

In this case, gluon 3 is effectively photon-like and the contribution from the triple and quartic gluon vertices drops out.

4.10 The 4-Quark, 1-Gluon Current

The four quark-one gluon current may be decomposed according to its colour structure in a similar fashion,

$$\begin{aligned}\widehat{\mathcal{T}}^5_\mu(Q_1,\overline{Q}_2;Q_3,\overline{Q}_4;1) &= i\frac{eg^3}{2} \\ &\times \left[T^{a_1}_{c_1c_4}\delta_{c_3c_2}\mathcal{T}_\mu(Q_1,\overline{Q}_2;Q_3,\overline{Q}_4;1) + (Q_1 \leftrightarrow Q_3, \overline{Q}_2 \leftrightarrow \overline{Q}_4) - (Q_1 \leftrightarrow Q_3) - (\overline{Q}_2 \leftrightarrow \overline{Q}_4)\right],\end{aligned} \tag{4.44}$$

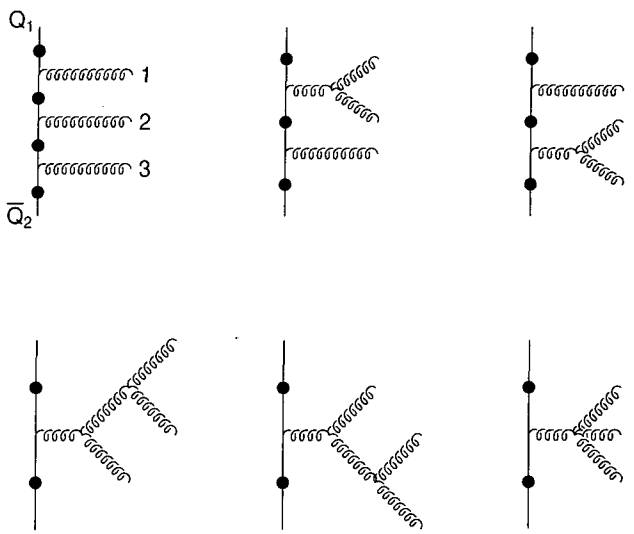

Figure 4.6: The diagrams included in the colourless subamplitude $\mathcal{S}_\mu(Q_1; 1, 2, 3; \overline{Q}_2)$. In each diagram, the gluons are emitted in an ordered fashion, such that reading clockwise from the quark at the top (Q_1) we encounter gluons 1, 2 and 3 in that order before reaching the antiquark ($\overline{Q}_2$). The off-shell photon can be attached to the quark line in the positions indicated by the solid circle.

where the exchanges are understood to apply to the colour labels as well. The colour ordered sub-current can be written,

$$\begin{aligned}\mathcal{T}_\mu(Q_1,\overline{Q}_2;Q_3,\overline{Q}_4;1) &= \delta_{Q_1Q_2}\delta_{Q_3Q_4}\mathcal{T}_\mu^A(Q_1,\overline{Q}_2;Q_3,\overline{Q}_4;1)\\ &+ \frac{1}{N}\delta_{Q_3Q_2}\delta_{Q_1Q_4}\mathcal{T}_\mu^B(Q_1,\overline{Q}_2;Q_3,\overline{Q}_4;1),\end{aligned} \tag{4.45}$$

where,

$$\begin{aligned}\mathcal{T}_\mu^A(Q_1,\overline{Q}_2;Q_3,\overline{Q}_4;1) &= \mathcal{A}_\mu^{Q_1Q_2}(Q_1;1;\overline{Q}_4|Q_3;\overline{Q}_2)+\mathcal{A}_\mu^{Q_3Q_4}(Q_3;\overline{Q}_2|Q_1;1;\overline{Q}_4)\\ \mathcal{T}_\mu^B(Q_1,\overline{Q}_2;Q_3,\overline{Q}_4;1) &= \mathcal{B}_\mu^{Q_1Q_4}(Q_1;1;\overline{Q}_4|Q_3;\overline{Q}_2)+\mathcal{B}_\mu^{Q_3Q_2}(Q_3;\overline{Q}_2|Q_1;1;\overline{Q}_4).\end{aligned} \tag{4.46}$$

Here, $\delta_{Q_iQ_j}=1$ if quarks i and j have the same flavour. The functions $\mathcal{A}_\mu^{Q_1Q_2}$ and $\mathcal{B}_\mu^{Q_1Q_2}$ describe Feynman diagrams where the gauge boson couples to the Q_1Q_2 pair. However, in $\mathcal{A}_\mu^{Q_1Q_2}$, the colour flows along the gluon connecting the two quark pairs, so that Q_1 and $\overline{Q}_4$ are the endpoints of a colour line (and similarly Q_3 and $\overline{Q}_2$) while in $\mathcal{B}_\mu^{Q_1Q_2}$, no colour is transmitted between the quark pairs and now Q_1 and $\overline{Q}_2$ form the endpoints of a colour line (and similarly Q_3 and $\overline{Q}_4$). In each case, the gluon may be emitted from any position on the colour line.

Squaring the four quark-one gluon amplitude and summing over colours yields,

$$\begin{aligned}\left|\widehat{\mathcal{T}}_\mu^5 V^\mu\right|^2 &= e^2\left(\frac{g^2N}{2}\right)^3\left(\frac{N^2-1}{N^2}\right)\\ &\times\left[\left|\mathcal{T}_\mu(Q_1,\overline{Q}_2;Q_3,\overline{Q}_4;1)V^\mu\right|^2+\left|\mathcal{T}_\mu(Q_1,\overline{Q}_4;Q_3,\overline{Q}_2;1)V^\mu\right|^2\right.\\ &-\left.\frac{2}{N}\Re\left(\mathcal{T}_\mu(Q_1,\overline{Q}_2;Q_3,\overline{Q}_4;1)V^\mu+\mathcal{T}_\mu(Q_3,\overline{Q}_4;Q_1,\overline{Q}_2;1)V^\mu\right)\left(\mathcal{T}_\mu(Q_1,\overline{Q}_4;Q_3,\overline{Q}_2;1)V^\mu\right)^\dagger\right]\\ &+(Q_1\leftrightarrow Q_3,\overline{Q}_2\leftrightarrow\overline{Q}_4),\end{aligned} \tag{4.47}$$

or equivalently,

$$\begin{aligned}\left|\widehat{\mathcal{T}}_\mu^5 V^\mu\right|^2 &= e^2\left(\frac{g^2N}{2}\right)^3\left(\frac{N^2-1}{N^2}\right)\\ &\times\left[\left|\mathcal{T}_\mu^A(Q_1,\overline{Q}_2;Q_3,\overline{Q}_4;1)V^\mu\right|^2\right.\end{aligned}$$

$$+\frac{1}{N^2}\left(\left|\mathcal{T}_\mu^B(Q_1,\overline{Q}_4;Q_3,\overline{Q}_2;1)V^\mu\right|^2-\left|\overline{\mathcal{T}}_\mu(Q_1,\overline{Q}_2;Q_3,\overline{Q}_4;1)V^\mu\right|^2\right)$$
$$+\frac{2\delta_{Q_1Q_3}}{N}\Re\left(\mathcal{T}_\mu^A(Q_1,\overline{Q}_2;Q_3,\overline{Q}_4;1)V^\mu\right)\left(\mathcal{T}_\mu^B(Q_1,\overline{Q}_2;Q_3,\overline{Q}_4;1)V^\mu\right)^\dagger$$
$$-\frac{(N^2+1)}{2N^3}\delta_{Q_2Q_4}\Re\left(\overline{\mathcal{T}}_\mu(Q_1,\overline{Q}_2;Q_3,\overline{Q}_4;1)V^\mu\right)\left(\overline{\mathcal{T}}_\mu(Q_1,\overline{Q}_4;Q_3,\overline{Q}_2;1)V^\mu\right)^\dagger$$
$$+(Q_1\leftrightarrow Q_3,\overline{Q}_2\leftrightarrow\overline{Q}_4)+\delta_{Q_1Q_3}(Q_1\leftrightarrow Q_3)+\delta_{Q_2Q_4}(\overline{Q}_2\leftrightarrow\overline{Q}_4)\Big]. \qquad (4.48)$$

Here we have introduced the shorthand notation,

$$\begin{aligned}\overline{\mathcal{T}}_\mu(Q_1,\overline{Q}_2;Q_3,\overline{Q}_4;1) &= \mathcal{T}_\mu^A(Q_1,\overline{Q}_2;Q_3,\overline{Q}_4;1)+\mathcal{T}_\mu^A(Q_3,\overline{Q}_4;Q_1,\overline{Q}_2;1)\\ &= \mathcal{T}_\mu^B(Q_1,\overline{Q}_4;Q_3,\overline{Q}_2;1)+\mathcal{T}_\mu^B(Q_3,\overline{Q}_2;Q_1,\overline{Q}_4;1). \qquad (4.49)\end{aligned}$$

Note that in the case of identical quarks, there is an extra symmetry factor of 1/4 multiplying the matrix elements.

4.11 Summary

In this chapter we have presented the calculation of the squared matrix elements for the partonic sub-processes relevant for the next-to-leading order corrections for $\gamma^* \to 4$ jets. The lowest order matrix elements for both $q\bar{q}gg$ and $q\bar{q}Q\overline{Q}$ are both simple to obtain, whilst the one-loop virtual corrections are considerably more complicated. The colour structure of the 5 parton processes $\gamma^* \to q\bar{q}ggg$ and $\gamma^* \to q\bar{q}Q\overline{Q}g$ is more involved and there are many diagrams, but evaluation of the matrix elements is straightforward.

By grouping the Feynman diagrams according to their colour structure, we find that the one-loop matrix elements can be described by 14 independent functions. Working in conventional dimensional regularization in $D = 4 - 2\epsilon$ dimensions, we have isolated the single and double poles in ϵ which are proportional to the lowest order matrix elements. The remaining finite pieces are algebraically lengthy but do not contain any spurious singularities. By this we mean that the finite terms contain only the kinematic denominators present in the corresponding tree-level terms and that we have used the functions of chapter 3 to protect the Gram determinant $\Delta \to 0$ limits. The full results are not presented here, although an

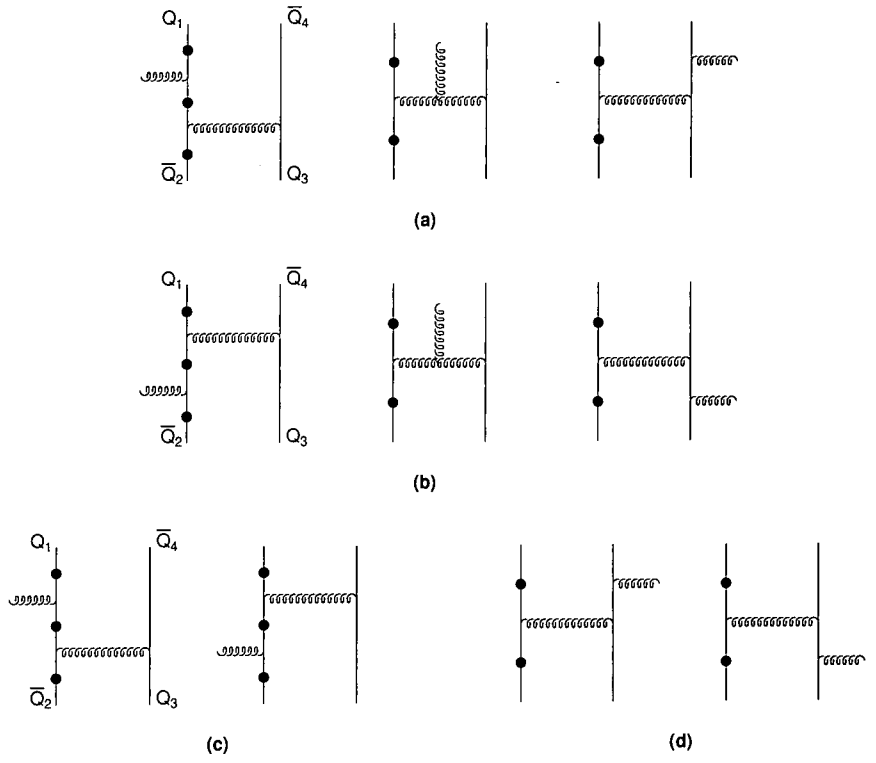

Figure 4.7: The Feynman diagrams contributing to the colour ordered sub-currents (a) $\mathcal{A}_\mu^{Q_1Q_2}(Q_1;1;\overline{Q}_2|Q_3;\overline{Q}_4)$, (b) $\mathcal{A}_\mu^{Q_1Q_2}(Q_1;\overline{Q}_2|Q_3;1;\overline{Q}_4)$, (c) $\mathcal{B}_\mu^{Q_1Q_2}(Q_1;1;\overline{Q}_2|Q_3;\overline{Q}_4)$ and (d) $\mathcal{B}_\mu^{Q_1Q_2}(Q_1;\overline{Q}_2|Q_3;1;\overline{Q}_4)$. In each diagram, the off-shell photon couples to the quark-antiquark pair $Q_1\overline{Q}_2$ in one of the positions represented by a solid circle. The second quark line is oriented in the opposite direction, so that in each case the quark Q_3 is located towards the bottom-right of the diagram.

example function is presented in Appendix E. The numerical implementation of these results will be presented in chapter 5.

In order to make a proper study of $e^+e^- \to 4$ jets at next-to-leading order accuracy, we must now show how these matrix elements may be implemented with an efficient Monte Carlo phase space integration. This, together with discussion of the cancellation of infrared divergences between the real and virtual terms, will be the subject of chapter 5.

Chapter 5

Implementation of the Matrix Elements

5.1 Introduction

We have now assembled all the matrix elements that are necessary for the calculation of the process $e^+e^- \to 4$ jets at next-to-leading order. In this chapter we will see how these may be implemented to yield predictions for physical observables. Essentially this means combining the four and five parton contributions in a sensible way whilst integrating over the relevant phase space in a Monte Carlo fashion.

In the first instance we re-examine the matrix elements in the light of the phase space integration. Partial cancellations between some of the terms mean that some of the matrix elements may be dropped in a numerical implementation. Moreover, many of the additional terms of chapter 4 that are generated by symmetry operations can be simply included merely by counting the numbers of permutations. The use of arguments such as these to massage the partonic matrix elements into a more amenable form is the subject of sections 5.2 – 5.5.

The remainder of the chapter is devoted to the cancellation of the infrared singularities between the real and the virtual contributions to the cross-section. Elaborating on the basic outline of chapter 2, we follow the hybrid subtraction scheme and illustrate its application in

our case. In particular, we identify the relevant *antenna* subtraction terms and slicing contributions and show that the exposed singularities cancel. We then present (finite) formulae for the four and five parton contributions which may be directly implemented in a Monte Carlo integration.

5.2 Four Quarks

We first study the implementation of the four-quark matrix elements of section 4.3. This is best illustrated by the example of the tree level matrix elements, with the more complicated loop corrections following this discussion.

5.2.1 Tree Level

In the calculation of the matrix elements in chapter 4 we provided a complete set of functions $\mathcal{T}(i,j;k,l)$, where the off-shell photon couples to the quark lines $Q_i, \overline{Q}_j$ and $Q_k, \overline{Q}_l$. However, in a numerical implementation of these matrix elements we can reduce the number of evaluations that need to be made by appealing to the phase space integration to restore some of the symmetries. In addition we find that some of the contributions will vanish by application of Furry's theorem.

Neglected Contributions

The class of squared diagrams that we will neglect is that corresponding to $\mathcal{T}(1,2;3,4)$ and its symmetries, where the photon couples to a different quark line in each amplitude. Two of the squared diagrams that contribute to this piece are shown in Figure 5.1. It can be seen that one term is obtained from the other by simply reversing the direction of the fermion loop involving Q_3 and $\overline{Q}_4$. Since this loop is cut, these diagrams do not cancel, as would be the case by Furry's theorem for an uncut loop. Instead, the cancellation only takes place after phase space integration.

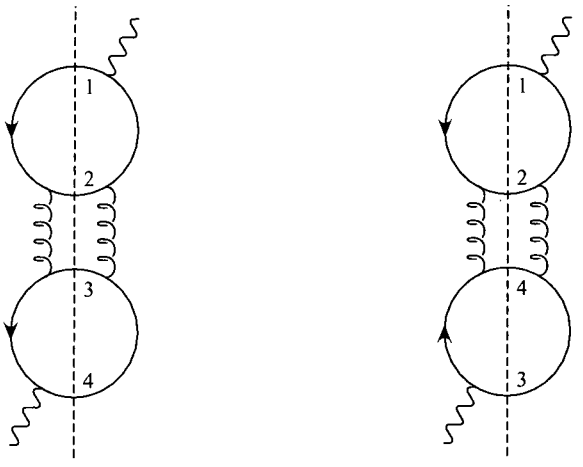

Figure 5.1: Two of the total of four squared diagrams that contribute to the function $\mathcal{T}(1,2;3,4)$. The dotted lines cut the on-shell quark lines to indicate the corresponding Feynman diagrams, with the labels indicating the (anti-)quarks at each cut.

Symmetries

In equation 4.17 of chapter 4 we only explicitly wrote down a small number of the functions that contribute to the matrix elements at lowest order, with the remainder being generated by symmetry. Here we appeal to that same symmetry and phase space integration to simply replace all the extra terms generated by the symmetry by copies of the original. In doing so, we also note that the term $\mathcal{T}(1,2;3,2)$ is generated by the symmetry $p_1 \leftrightarrow p_2$, $p_3 \leftrightarrow p_4$ acting on $\mathcal{T}(1,2;1,4)$.

At this point it is useful to consider the different factors that will apply to terms in the matrix element which are relevant for identical and non-identical quarks. We shall always sum over all n_F flavours of quark for each quark line, in addition noting that terms involving identical quarks will acquire an identical particle factor of $1/4$.

For terms in the matrix elements which are only present when dealing with identical quarks it is then clear that we must attribute a factor of $n_F/4$. Those terms which appear in both cases, $\delta_{qQ} = 0$ and $\delta_{qQ} = 1$, are slightly more complex. We can choose a pair of

non-identical quarks in $n_F(n_F-1)/2$ ways. In addition, the identical quark contribution enters twice for every single occurence of the non-identical term – once for $\delta_{qQ}=0$ and again (with a symmetry) for $\delta_{qQ}=1$. Hence the total factor is $n_F(n_F-1)/2+2\times n_F\times 1/4 = n_F^2/2$.

In particular, we have,

$$\begin{aligned} \mathcal{T}(1,2;1,2) + (1 \text{ symmetry}) &\longrightarrow 2\times n_F^2/2 = n_F^2, \\ \mathcal{T}(1,2;3,4) &\longrightarrow 0, \\ \mathcal{T}(1,2;1,4) + (3 \text{ symmetries}) & \\ + (4 \text{ symmetries from } \mathcal{T}(1,2;3,2)) &\longrightarrow 8\times n_F/4 = 2n_F. \end{aligned} \tag{5.1}$$

5.2.2 One-Loop

The one-loop matrix elements are very similar in structure to the lowest order result. We will again appeal to the same types of symmetry argument to reduce the number of function evaluations and also neglect contributions similar to those dropped above.

Neglected Contributions

We will again neglect the squared diagrams where the photon couples to a different quark line in each amplitude, namely functions of the form $\mathcal{L}_\alpha(1,2;3,4)$. Although the corresponding tree-level function $T(1,2;3,4)$ vanished after phase space integration, according to Furry's theorem, the one-loop functions do not. However, the sum over the quark couplings together with some phase space cancellation related to that at tree-level, means that this neglected piece is small [51].

Symmetries

Using the symmetry of the diagrams and the appropriate factors for sums over quark flavours, we find that the extra symmetries can be replaced by factors as follows,

$$\begin{aligned} \mathcal{L}_\alpha(1,2;1,2) + (1 \text{ symmetry}) &\longrightarrow 2 \times n_F^2/2 = n_F^2, \\ \mathcal{L}_\alpha(1,2;1,4) + (3 \text{ symmetries}) & \\ + (4 \text{ symmetries from } \mathcal{L}_\alpha(1,2;3,2)) &\longrightarrow 8 \times n_F/4 = 2n_F. \end{aligned} \tag{5.2}$$

5.3 2 Quarks, 2 Gluons

The implementation of the matrix elements for the production of a quark-antiquark pair together with two gluons given in section 4.2 is more straightforward. There are no neglected contributions and it only remains to utilize the symmetries of the matrix element functions.

5.3.1 Tree Level

The tree level squared matrix elements are described by the two functions $\mathcal{T}(3,4)$ and $\mathcal{T}$ (with no arguments). The function $\mathcal{T}(4,3)$ is related by the symmetry operation interchanging the two gluons and will be restored by phase space integration. The sum over quark flavours generates a factor of n_F and the gluons provide an identical particle factor of $1/2$. Hence we find,

$$\begin{aligned} \mathcal{T}(3,4) + (1 \text{ symmetry}) &\longrightarrow 2 \times n_F/2 = n_F, \\ \mathcal{T} &\longrightarrow n_F/2. \end{aligned} \tag{5.3}$$

5.3.2 One-Loop

The situation at the one-loop level is very similar. The functions $\mathcal{L}_\alpha(3,4)$ and $\mathcal{L}_\alpha$ behave in the same way as the tree-level functions $\mathcal{T}(3,4)$ and $\mathcal{T}$,

$$\begin{aligned} \mathcal{L}_\alpha(3,4) + (1 \text{ symmetry}) &\longrightarrow 2 \times n_F/2 = n_F, \\ \mathcal{L}_\alpha &\longrightarrow n_F/2. \end{aligned} \tag{5.4}$$

5.4 Combined 4 Parton Cross-Sections

By putting together the factors in the 4 parton matrix elements given in equations (5.1) and (5.3) we can write the implemented form for the lowest order matrix elements for four jet production. In doing so, it is convenient to normalize the result by the lowest order result for $\gamma^* \to q\bar{q}$. This is simply calculated, yielding,

$$\sigma_0 = e^2 N n_F \frac{s}{2\pi}, \tag{5.5}$$

where s is the centre-of-mass energy squared. In this equation the factor $N \times n_F$ results from the sum over quark colours and flavours, with the electromagnetic coupling supplying a further e^2. Hence we have,

$$\frac{\sigma_4^{\mathrm{LO}}}{\sigma_0} = \frac{(2\pi)^5}{s}\left(\frac{\alpha_S N}{2\pi}\right)^2\left(\frac{N^2-1}{N^2}\right)\left(\mathcal{T}(3,4) - \frac{1}{2N^2}\mathcal{T} + \frac{n_F}{N}\mathcal{T}(1,2;1,2) + \frac{2}{N^2}\mathcal{T}(1,2;1,4)\right). \tag{5.6}$$

Similarly the next-to-leading order 4-parton contribution to the cross-section can be obtained by examining equations (5.2) and (5.4) together with the form for the matrix elements given in chapter 4. The result is,

$$\begin{aligned} \frac{\sigma_4^{\mathrm{NLO}}}{\sigma_0} = \frac{(2\pi)^5}{s}\left(\frac{\alpha_S N}{2\pi}\right)^3\left(\frac{N^2-1}{N^2}\right)\Bigg(&\mathcal{L}_A(3,4) - \frac{1}{2N^2}\big(\mathcal{L}_A + 2\mathcal{L}_B(3,4) - \mathcal{L}_C\big) + \frac{1}{2N^4}\mathcal{L}_B \\ &+ \frac{n_F}{N}\mathcal{L}_C(1,2;1,2) - \frac{n_F}{N^3}\big(2\mathcal{L}_A(1,2;1,2) + \mathcal{L}_B(1,2;1,2)\big) \\ &+ \frac{2}{N^2}\big(\mathcal{L}_C(1,2;1,4) - \mathcal{L}_A(1,2;1,4)\big) - \frac{2}{N^4}\big(\mathcal{L}_A(1,2;1,4) + \mathcal{L}_B(1,2;1,4)\big)\Bigg). \end{aligned} \tag{5.7}$$

5.5 5 Parton Expressions

In this section we summarize the symmetries of the five parton matrix elements for the two sub-processes and combine them in a form which is more suitable for numerical implementation.

5.5.1 The 2 quark, 3 gluon Sub-Process

The style of decomposition used for the matrix elements given in chapter 4 is again implemented in a straightforward manner when only one quark-antiquark pair is produced. After integration, all the permutations of the gluons are equivalent and it remains to include the quark sum (n_F) and the identical particle factor 1/3!. This results in,

$$\begin{aligned}
\left|\mathcal{S}_\mu(Q_1;1,2,3;\overline{Q}_2)\right|^2 &\rightarrow 6\times n_F\times 1/3! = n_F,\\
\left|\mathcal{S}_\mu(Q_1;1,2,\tilde{3};\overline{Q}_2)\right|^2 &\rightarrow 6\times n_F\times 1/3! = n_F,\\
\left|\mathcal{S}_\mu(Q_1;\tilde{1},\tilde{2},\tilde{3};\overline{Q}_2)\right|^2 &\rightarrow n_F\times 1/3! = n_F/6.
\end{aligned} \tag{5.8}$$

5.5.2 The 4 quark, 1 gluon Sub-Process

The structure of the matrix elements in this case is very similar to that obtained for four quark production without the additional gluon. In particular, there is again the division of terms into those that are relevant only for identical flavour quarks, and those applicable to all flavours. In addition, the diagrams are characterized by the quark charges that the photon couples to in each half of the interference. As explained in the preceeding discussion of the virtual corrections to the four quark process, we neglect the functions which are interferences of diagrams where the photon couples to different quark charges. The discussion of the factors attached to each term in the matrix elements also carries through from section 5.2.1. Straightforward application of these rules yields the following factors,

$$\left|\mathcal{A}_\mu^{Q_1Q_2}(Q_1;1;\overline{Q}_4|Q_3;\overline{Q}_2)\right|^2 + (1\text{ symmetry}) \longrightarrow 2\times n_F^2/2 = n_F^2,$$

$$
\begin{aligned}
\left|\mathcal{A}_\mu^{Q_1Q_2}(Q_1;\overline{Q}_4|Q_3;1;\overline{Q}_2)\right|^2 + (1\text{ symmetry}) &\longrightarrow 2\times n_F^2/2 = n_F^2,\\
\left|\mathcal{B}_\mu^{Q_1Q_2}(Q_1;1;\overline{Q}_2|Q_3;\overline{Q}_4)\right|^2 + (1\text{ symmetry}) &\longrightarrow 2\times n_F^2/2 = n_F^2,\\
\left|\mathcal{B}_\mu^{Q_1Q_2}(Q_1;\overline{Q}_2|Q_3;1;\overline{Q}_4)\right|^2 + (1\text{ symmetry}) &\longrightarrow 2\times n_F^2/2 = n_F^2,\\
\left|\mathcal{A}_\mu^{Q_1Q_2}(Q_1;1;\overline{Q}_4|Q_3;\overline{Q}_2) + \mathcal{A}_\mu^{Q_1Q_2}(Q_1;\overline{Q}_4|Q_3;1;\overline{Q}_2)\right|^2 & \\
+ (3\text{ symmetries}) &\longrightarrow 4\times n_F^2/2 = 2n_F^2,\\
\Re(\mathcal{A}_\mu^{Q_1Q_2}(Q_1;1;\overline{Q}_4|Q_3;\overline{Q}_2))(\mathcal{B}_\nu^{Q_1Q_4}(Q_1;1;\overline{Q}_4|Q_3;\overline{Q}_2))^\dagger & \\
+ (3\text{ symmetries}) &\longrightarrow 4\times n_F/4 = n_F,\\
\Re\Big(\mathcal{A}_\mu^{Q_1Q_2}(Q_1;1;\overline{Q}_4|Q_3;\overline{Q}_2) + \mathcal{A}_\mu^{Q_1Q_2}(Q_1;\overline{Q}_4|Q_3;1;\overline{Q}_2)\Big) & \\
\times\Big(\mathcal{A}_\mu^{Q_1Q_4}(Q_1;1;\overline{Q}_2|Q_3;\overline{Q}_4) + \mathcal{A}_\mu^{Q_1Q_4}(Q_1;\overline{Q}_2|Q_3;1;\overline{Q}_4)^2\Big)^\dagger & \qquad (5.9)\\
+ (15\text{ symmetries}) &\longrightarrow 16\times n_F/4 = 4n_F.
\end{aligned}
$$

5.5.3 Combined 5 Parton Cross-Section

It is now easy to combine the expressions for the matrix elements with the combinatorial factors to produce the form convenient for numerical evaluation. The final result is,

$$
\begin{aligned}
\frac{\sigma_5^{\rm LO}}{\sigma_0} = \frac{(2\pi)^7}{s}\left(\frac{\alpha_S N}{2\pi}\right)^3\left(\frac{N^2-1}{N}\right)\Bigg(&\left|\mathcal{S}_\mu(Q_1;1,2,3;\overline{Q}_2)\right|^2\\
&-\frac{1}{N^2}\left|\mathcal{S}_\mu(Q_1;1,2,\tilde{3};\overline{Q}_2)\right|^2+\frac{1}{6}\left(\frac{N^2+1}{N^4}\right)\left|\mathcal{S}_\mu(Q_1;\tilde{1},\tilde{2},\tilde{3};\overline{Q}_2)\right|^2\\
&+\frac{n_F}{N}\left(\left|\mathcal{A}_\mu^{Q_1Q_2}(Q_1;1;\overline{Q}_4|Q_3;\overline{Q}_2)\right|^2+\left|\mathcal{A}_\mu^{Q_1Q_2}(Q_1;\overline{Q}_4|Q_3;1;\overline{Q}_2)\right|^2\right)\\
&+\frac{n_F}{N^3}\Bigg(\left|\mathcal{B}_\mu^{Q_1Q_2}(Q_1;1;\overline{Q}_2|Q_3;\overline{Q}_4)\right|^2+\left|\mathcal{B}_\mu^{Q_1Q_2}(Q_1;\overline{Q}_2|Q_3;1;\overline{Q}_4)\right|^2\\
&\qquad-\frac{2}{N^2}\left|\mathcal{A}_\mu^{Q_1Q_2}(Q_1;1;\overline{Q}_4|Q_3;\overline{Q}_2)+\mathcal{A}_\mu^{Q_1Q_2}(Q_1;\overline{Q}_4|Q_3;1;\overline{Q}_2)\right|^2\Bigg)\\
&+2\Big(\Re(\mathcal{A}_\mu^{Q_1Q_2}(Q_1;1;\overline{Q}_4|Q_3;\overline{Q}_2))(\mathcal{B}_\nu^{Q_1Q_4}(Q_1;1;\overline{Q}_4|Q_3;\overline{Q}_2))^\dagger\\
&\quad+\Re(\mathcal{A}_\mu^{Q_1Q_4}(Q_1;1;\overline{Q}_2|Q_3;\overline{Q}_4))(\mathcal{B}_\nu^{Q_1Q_2}(Q_1;1;\overline{Q}_2|Q_3;\overline{Q}_4))^\dagger\\
&\quad+\Re(\mathcal{A}_\mu^{Q_1Q_2}(Q_1;\overline{Q}_4|Q_3;1;\overline{Q}_2))(\mathcal{B}_\nu^{Q_1Q_4}(Q_1;\overline{Q}_4|Q_3;1;\overline{Q}_2))^\dagger\\
&\quad+\Re(\mathcal{A}_\mu^{Q_1Q_4}(Q_1;\overline{Q}_2|Q_3;1;\overline{Q}_4))(\mathcal{B}_\nu^{Q_1Q_2}(Q_1;\overline{Q}_2|Q_3;1;\overline{Q}_4))^\dagger\Big)
\end{aligned}
$$

$$- 2\left(\frac{N^2+1}{N^4}\right)\Big(\Re\Big(\mathcal{A}_\mu^{Q_1Q_2}(Q_1;1;\overline{Q}_4|Q_3;\overline{Q}_2)+\mathcal{A}_\mu^{Q_1Q_2}(Q_1;\overline{Q}_4|Q_3;1;\overline{Q}_2)\Big) \quad (5.10)$$
$$\times\Big(\mathcal{A}_\mu^{Q_1Q_4}(Q_1;1;\overline{Q}_2|Q_3;\overline{Q}_4)+\mathcal{A}_\mu^{Q_1Q_4}(Q_1;\overline{Q}_2|Q_3;1;\overline{Q}_4)^2\Big)^\dagger\Big)\Big).$$

5.6 Cancellation of Infrared Singularities

As we have seen in chapter 2, in both the soft and collinear limits, the colour ordered squared amplitudes factorise into a squared amplitude containing one less parton multiplied by a factor that depends on the the unresolved particle and the two adjacent 'hard' particles. We view the two 'hard' particles as an *antenna* from which the unresolved parton is radiated. It therefore makes sense to divide the phase space in a similar way and to treat the subtraction term as the singular factor for the whole antenna integrated over the unresolved phase space. Clearly the choice of the subtraction function $E(x)$ in equation 2.14 requires some care, as does the integration over the phase space variables x.

5.6.1 Phase Space Factorisation

Let us consider an $(n+1)$ particle phase space described by momenta p_i with $p_i^2 = 0$ for $i = 1,\ldots,n$. If the total centre of mass energy is Q, then let us denote the phase space by, $\mathrm{d}PS(Q^2;p_1,\ldots,p_n)$. As discussed above, we wish to relate the full $(n+1)$ particle phase space to an n particle phase space whenever one of the original $(n+1)$ particles is unresolved. Let the unresolved particle be labelled by u and the two adjacent hard particles by a and b, then the phase space can be factorised as,

$$\mathrm{d}PS(Q^2;p_1,\ldots,p_n) = \mathrm{d}PS(Q^2;p_1,\ldots,p_{aub},\ldots,p_n)\,\frac{\mathrm{d}s_{aub}}{2\pi}\,\mathrm{d}PS(s_{aub};p_a,p_u,p_b), \quad (5.11)$$

where $p_{aub} = p_a + p_u + p_b$ and $p_{aub}^2 = s_{aub}$. To factorise the phase space into an n particle phase space multiplied by a factor containing integrals over the unresolved invariants s_{au} and s_{ub} that appear in the singular limits of the matrix elements, we multiply the r.h.s. of

eq. (5.11) by,

$$\mathrm{d}PS(s_{AB};p_A,p_B) \,/\, \int \mathrm{d}PS(s_{AB};p_A,p_B), \tag{5.12}$$

where particles A and B have momenta p_A and p_B such that, $p_{aub} = p_{AB} = p_A + p_B$, $p_A^2 = p_B^2 = 0$ and $s_{aub} = s_{AB}$. In other words,

$$\begin{aligned}\mathrm{d}PS(Q^2;p_1,\ldots,p_n) &= \mathrm{d}PS(Q^2;p_1,\ldots,p_{AB},\ldots,p_n)\,\frac{\mathrm{d}s_{AB}}{2\pi}\,\mathrm{d}PS(s_{AB};p_A,p_B)\times \mathrm{d}PS^{\mathrm{sing}} \\ &= \mathrm{d}PS(Q^2;p_1,\ldots,p_A,p_B,\ldots,p_n)\times \mathrm{d}PS^{\mathrm{sing}}.\end{aligned} \tag{5.13}$$

As desired, we have the phase space for an final state containing n lightlike particles multiplied by $\mathrm{d}PS^{\mathrm{sing}}$. Working in four-dimensions and after integration over the Euler angles,

$$\begin{aligned}\mathrm{d}PS^{\mathrm{sing}} &= \frac{\mathrm{d}PS(s_{aub};p_a,p_u,p_b)}{\int \mathrm{d}PS(s_{AB};p_A,p_B)} \\ &= \frac{1}{16\pi^2}s_{aub}\mathrm{d}x_{au}\mathrm{d}x_{ub}\mathrm{d}x_{ab}\delta(1-x_{au}-x_{ub}-x_{ab}),\end{aligned} \tag{5.14}$$

where $x_{ij} = s_{ij}/s_{aub}$. For this to work, a mapping must exist that determines p_A and p_B for a given set of momenta p_a, p_b and p_u. Many choices are possible [19, 52] and we choose the symmetric mapping of [52],

$$\begin{aligned}p_A &= \frac{1}{2}\left[1+\rho+\frac{s_{ub}(1+\rho-2r_1)}{s_{ab}+s_{au}}\right]p_a + r_1 p_u + \frac{1}{2}\left[1-\rho+\frac{s_{au}(1-\rho-2r_1)}{s_{ab}+s_{ub}}\right]p_b, \\ p_B &= \frac{1}{2}\left[1-\rho-\frac{s_{ub}(1+\rho-2r_1)}{s_{ab}+s_{au}}\right]p_a + (1-r_1)p_u + \frac{1}{2}\left[1+\rho-\frac{s_{au}(1-\rho-2r_1)}{s_{ab}+s_{ub}}\right]p_b,\end{aligned} \tag{5.15}$$

where,

$$r_1 = \frac{s_{ub}}{s_{au}+s_{ub}}, \tag{5.16}$$

and,

$$\rho = \sqrt{\frac{s_{ab}^2+(s_{au}+s_{ub})s_{ab}+4r_1(1-r_1)s_{au}s_{ub}}{s_{ab}s_{aub}}}. \tag{5.17}$$

Note that this transformation approaches the singular limits smoothly. For example, as $s_{au} \to 0$, then $r_1 \to 1$, $\rho \to 1$ and $p_A \to p_a + p_u$, $p_B \to p_b$.

5.6.2 Antenna Factorisation of the Matrix Elements

Having factorised the phase space, we now wish to find the analogues of the subtraction functions $E(x)$ discussed in chapter 2. These functions should ideally be valid over the whole of the antenna phase space $\mathrm{d}PS^{\mathrm{sing}}$ and, in the soft and collinear regions must match onto the relevant singular limits. In other words, for a given $(n+1)$ particle amplitude, in the limit where particle u is unresolved,

$$\left|\mathcal{S}_\mu(\ldots,a,u,b,\ldots)V^\mu\right|^2 \to \mathcal{A}_{aub}\left|\mathcal{S}_\mu(\ldots,A,B,\ldots)V^\mu\right|^2, \tag{5.18}$$

where we have replaced the antenna comprising a,u,b by the hard partons A and B to obtain an n particle amplitude. The antenna function $\mathcal{A}_{aub}$ depends on the momenta of the radiated particles a, b and u, but the n particle amplitude $|\mathcal{S}_\mu V^\mu|^2$ does not.

The leading colour contribution to an observable cross section from an $(n+1)$ particle final state with a particular colour ordering is proportional to,

$$\left(\frac{N^2-1}{N^2}\right)\left(\frac{g^2N}{2}\right)^{n+1}\left|\mathcal{S}_\mu(\ldots,a,u,b,\ldots)V^\mu\right|^2\mathcal{J}_{(n+1)}\,\mathrm{d}PS(Q^2;\ldots,p_a,p_u,p_b,\ldots), \tag{5.19}$$

where the observable function $\mathcal{J}_{(n+1)}$ represents the cuts applied to the $(n+1)$ particle phase space to define the observable. Using the factorisation of the matrix elements defined in eq. (5.18), when particle u is unresolved we should subtract,

$$\left(\frac{g^2N}{2}\right)^{n+1}\mathcal{A}_{aub}\left|\mathcal{S}_\mu(\ldots,A,B,\ldots)V^\mu\right|^2\mathcal{J}_{(n)}\,\mathrm{d}PS(Q^2;\ldots,p_a,p_u,p_b,\ldots), \tag{5.20}$$

from the $(n+1)$ particle contribution and, using the phase space factorisation of eq. (5.13), add,

$$\left(\frac{g^2N}{2}\right)^{n+1}\mathcal{A}_{aub}\,\mathrm{d}PS^{\mathrm{sing}}\left|\mathcal{S}_\mu(\ldots,A,B,\ldots)V^\mu\right|^2\mathcal{J}_{(n)}\,\mathrm{d}PS(Q^2;\ldots,p_A,p_B,\ldots), \tag{5.21}$$

to the n particle contribution where both the observable function $\mathcal{J}$ and matrix elements $|\mathcal{S}_\mu V^\mu|^2$ depend only on the momenta of the n remaining hard partons. Note that for any infrared safe observable, in the limit that one particle is unresolved, $\mathcal{J}_{(n+1)} \to \mathcal{J}_{(n)}$. In the subtraction term eq. (5.20), we use the transformations of eq. (5.15) to map the momenta

p_a, p_u and p_b defined in the $(n+1)$ particle phase space onto the momenta p_A and p_B used in the n-particle matrix elements and observable functions. In eq. (5.21), all dependence on the momenta of particles a, b and u may be integrated out to give the antenna factor, $\mathcal{F}$,

$$\mathcal{F}_{AB}(s_{AB}) = \left(\frac{g^2 N}{2}\right) \int \mathcal{A}_{aub} \, \mathrm{d}PS^{\mathrm{sing}}, \tag{5.22}$$

multiplying the n particle cross section (for a given colour ordered amplitude),

$$\left(\frac{g^2 N}{2}\right)^n \left|\mathcal{S}_\mu(\ldots, A, B, \ldots) V^\mu\right|^2 \mathcal{J}_{(n)} \, \mathrm{d}PS(Q^2; \ldots, p_A, p_B, \ldots). \tag{5.23}$$

The full set of subtraction terms is obtained by summing over all possible antennae.

The Dalitz plot for the $(AB) \to aub$ phase space is shown in Fig. 5.2. In the hybrid scheme we are implementing, we use the slicing method of [21] in the region $\min(s_{au}, s_{ub}) < \delta$, and the subtraction scheme in the region, $\delta < \min(s_{au}, s_{ub}) < \Delta$. In the slicing region, the phase space and soft and collinear approximations to the matrix elements are kept in $D = 4 - 2\epsilon$ dimensions to regularise the singularities present when either invariant vanishes. Using the approach of [21], there are three separate contributions (a) soft gluon when $\max(s_{au}, s_{ub}) < \delta$, (b) a and u collinear when $s_{au} < \delta$ but $s_{ub} > \delta$ and (c) b and u collinear when $s_{ub} < \delta$ but $s_{au} > \delta$.

Before turning to the explicit forms for the antenna subtraction terms, we note that while quarks are only directly colour connected to one particle - a gluon or antiquark, gluons are directly connected to two particle - the gluon (or quark) on either side. Therefore,while the quark (or antiquark) appear in a single antenna, gluons appear in two. This gives an ambiguity in how to assign the collinear singularities of a pair of gluons to each antenna. Later we will exploit this ambiguity to make the antenna functions $\mathcal{A}_{aub}$ for different pairs of hard partons finite simpler.

Quark-Antiquark Antenna

Let us first consider a system containing a quark, antiquark and a gluon. This is produced by an antenna comprising of a hard quark and antiquark pair that decays by radiating a

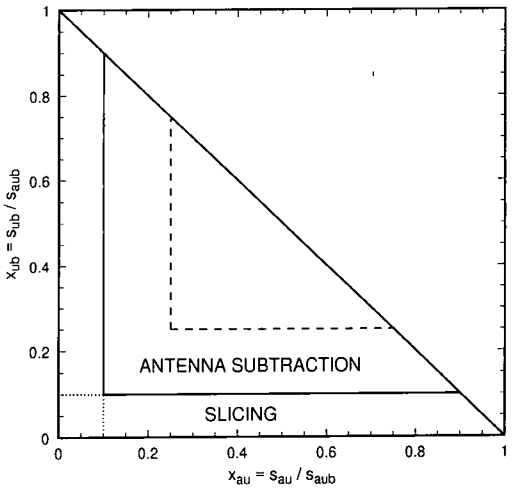

Figure 5.2: The phase space for the decay $(AB) \to aub$. The cut $\min(s_{au}, s_{ub}) = \delta$ with $\delta = 0.1$ s_{aub} is shown as a solid line while $\min(s_{au}, s_{ub}) = \Delta$ is shown as a dashed line for $\Delta = 0.25$ s_{aub}. The region $\min(s_{au}, s_{ub}) < \delta$ defines where the slicing approach is utilised, with the soft and collinear regions demarked by dotted lines. Antenna subtraction is applied when $\delta < \min(s_{au}, s_{ub}) < \Delta$.

gluon. Any function that has the correct soft gluon and collinear quark/gluon singularities in the appropriate limit is satisfactory. Here the hard particles in the antenna are Q and $\overline{Q}$ which radiate to form q, $\bar{q}$ and the gluon g. A suitable choice for the antenna function is,

$$\begin{aligned} \mathcal{A}_{qg\bar{q}} &= \frac{|\mathcal{S}_\mu(q;g;\bar{q})V^\mu|^2}{|\mathcal{S}_\mu(Q;\overline{Q})V^\mu|^2} \\ &= \frac{2}{s_{aub}}\left(\frac{x_{au}}{x_{ub}} + \frac{x_{ub}}{x_{au}} + \frac{2x_{ab}x_{aub}}{x_{au}x_{ub}}\right). \end{aligned} \tag{5.24}$$

Because this is proportional to the three parton matrix elements, $|\mathcal{S}_\mu(q;g;\bar{q})V^\mu|^2$, it automatically contains the correct soft and collinear limits. Furthermore, it is smooth over the whole three particle phase space and singularities only appear in the $s_{au} \to 0$ and $s_{ub} \to 0$ limits.

Explicitly integrating over the antenna phase space for $\delta < \min(s_{au}, s_{ub}) < \Delta$ we find,

$$\mathcal{F}_{Q\overline{Q}}(s_{Q\overline{Q}}) = \left(\frac{g^2 N}{2}\right) \int \mathcal{A}_{qg\bar{q}} \, \mathrm{d}PS^{\mathrm{sing}}$$

$$= \left(\frac{\alpha_S N}{2\pi}\right)\left(\ln^2\left(\frac{\delta}{s_{Q\overline{Q}}}\right) + \frac{3}{2}\ln\left(\frac{\delta}{s_{Q\overline{Q}}}\right)\right) + \mathcal{F}^{\Delta}_{Q\overline{Q}}\left(\frac{\Delta}{s_{Q\overline{Q}}}\right) + \mathcal{O}(\delta). \quad (5.25)$$

The δ independent function $\mathcal{F}^{\Delta}_{Q\overline{Q}}$ is given by,

$$\mathcal{F}^{\Delta}_{Q\overline{Q}}(x) = \left(\frac{\alpha_S N}{2\pi}\right)\left(-\ln^2(x) + \frac{5x}{2} - 2\mathrm{Li}_2(x) + \left(\frac{3}{2} - 2x + \frac{x^2}{2}\right)\ln\left(\frac{1-x}{x}\right)\right). \quad (5.26)$$

Quark-Gluon Antenna

For antenna made of a quark Q and gluon G, there are two possible ways of radiating. Either a gluon can be radiated so that a quark-gluon-gluon system is formed, or the gluon may split into a antiquark-quark pair. This latter possibility is subleading in the number of colours and the discussion of situations like this is deferred to sec. 5.6.2.

For a quark-gluon-gluon system, produced by a quark-gluon antenna there is a less obvious choice of antenna function, particularly since the singularity that is produced when the gluon splits sits in more than one antenna. If, in the collinear limit, the gluon splits into an unresolved gluon u which carries momentum fraction z and a hard gluon b with momentum fraction $1-z$, the antenna function should naively be proportional to $P_{gg\to g}$ which is singular as $z \to 0$ and $z \to 1$. This corresponds to singularities as both $s_{ub} \to 0$ and $s_{ab} \to 0$. However, because the collinear singularity sits in more than one antenna – the two gluons also occur in a second antenna where the role of the two gluons is reversed – we can make use of the $N = 1$ supersymmetric identity to rewrite $P_{gg\to g}$ as,

$$P_{gg\to g} = P_{qg\to q} + P_{gq\to q} - P_{q\bar{q}\to g}. \quad (5.27)$$

The soft singularities as $z \to 0$ are contained in $P_{gq\to q}$ while those as $z \to 1$ are in $P_{qg\to q}$. We therefore divide $P_{gg\to g}$ amongst the two antennae such that $P_{gq\to q}$ sits in the antenna where gluon u is unresolved. The $z \to 1$ singularities are placed in the antenna where the role of the two gluons is reversed. The remaining $P_{q\bar{q}\to g}$ may be divided between the two antennae according to choice. With a slight modification due to the $P_{q\bar{q}\to g}$ term, the antenna function used for the $Q\overline{Q}$ antenna has the correct limits, so that,

$$\mathcal{A}_{qgg} = \mathcal{A}_{qg\bar{q}} - \frac{2}{s_{aub}}\left(\frac{x^2_{au}}{x_{ub}x_{aub}}\right). \quad (5.28)$$

This is again smooth over the whole three particle phase space with singularities only appearing in the $s_{au} \to 0$ and $s_{ub} \to 0$ limits. In particular, as $z \to 0$, the collinear limit matches onto the soft limit which would not have been the case if we had divided the soft/collinear singularities equally between the two antenna.

After integrating over the antenna phase space for $\delta < \min(s_{au}, s_{ub}) < \Delta$ we find,

$$\begin{aligned} \mathcal{F}_{QG}(s_{QG}) &= \left(\frac{g^2 N}{2}\right) \int \mathcal{A}_{qgg} \, \mathrm{d}PS^{\mathrm{sing}} \\ &= \left(\frac{\alpha_S N}{2\pi}\right) \left(\ln^2\left(\frac{\delta}{s_{QG}}\right) + \frac{10}{6} \ln\left(\frac{\delta}{s_{QG}}\right)\right) + \mathcal{F}^{\Delta}_{QG}\left(\frac{\Delta}{s_{QG}}\right) \end{aligned} \tag{5.29}$$

with the δ independent function $\mathcal{F}^{\Delta}_{QG}$ is given by,

$$\begin{aligned} \mathcal{F}^{\Delta}_{QG}(x) &= \left(\frac{\alpha_S N}{2\pi}\right) \left(-\ln^2(x) + \frac{19x}{6} - \frac{x^2}{6} + \frac{x^3}{9} - 2\mathrm{Li}_2(x) \right. \\ &\quad \left. + \left(\frac{10}{6} - 2x + \frac{x^2}{2} - \frac{x^3}{6}\right) \ln\left(\frac{1-x}{x}\right)\right). \end{aligned} \tag{5.30}$$

Antennae containing a gluon and an antiquark are described by,

$$\mathcal{A}_{gg\bar{q}} = \mathcal{A}_{qgg}(a \leftrightarrow b), \tag{5.31}$$

and,

$$\mathcal{F}_{G\overline{Q}}(s_{G\overline{Q}}) = \mathcal{F}_{QG}(s_{G\overline{Q}}). \tag{5.32}$$

Gluon-Gluon Antenna

For antenna comprising only gluons, we repeat this SUSY inspired trick for each of the resolved gluons so that,

$$\mathcal{A}_{ggg} = \mathcal{A}_{gg\bar{q}} - \frac{2}{s_{aub}} \left(\frac{x^2_{au}}{x_{ub}x_{aub}} + \frac{x^2_{ub}}{x_{au}x_{aub}}\right). \tag{5.33}$$

Note that Kosower [52] has proposed an antenna factorisation for gluonic processes,

$$\mathcal{A}^{\mathrm{Kosower}}_{ggg} = \frac{4}{s_{aub}} \left(\frac{(x_{aub}(x_{aub} - x_{ab}) + x^2_{ab})^2}{x_{au}x_{ub}x_{ab}x_{sub}}\right), \tag{5.34}$$

which, in the u/b collinear limit regenerates the full $P_{gg\to g}$ splitting function, as well as the soft limits.

Integration of the antenna function $\mathcal{A}_{ggg}$ over the whole of the subtraction region yields,

$$\begin{aligned}\mathcal{F}_{GG}(s_{GG}) &= \left(\frac{g^2N}{2}\right)\int \mathcal{A}_{ggg}\,\mathrm{d}PS^{\mathrm{sing}} \\ &= \left(\frac{\alpha_S N}{2\pi}\right)\left(\ln^2\left(\frac{\delta}{s_{GG}}\right)+\frac{11}{6}\ln\left(\frac{\delta}{s_{GG}}\right)\right)+\mathcal{F}^{\Delta}_{GG}\left(\frac{\Delta}{s_{GG}}\right) \qquad (5.35)\end{aligned}$$

with the δ independent function $\mathcal{F}^{\Delta}_{GG}$ is given by,

$$\begin{aligned}\mathcal{F}^{\Delta}_{GG}(x) &= \left(\frac{\alpha_S N}{2\pi}\right)\left(-\ln^2(x)+\frac{23x}{6}-\frac{2x^2}{6}+\frac{2x^3}{9}-2\mathrm{Li}_2(x)\right. \\ &\qquad \left.+\left(\frac{11}{6}-2x+\frac{x^2}{2}-\frac{x^3}{3}\right)\ln\left(\frac{1-x}{x}\right)\right). \qquad (5.36)\end{aligned}$$

Antenna where a Quark-Antiquark Pair Merge

There are also configurations when two (or more) colour lines are present, one ending in an antiquark the other starting with a quark of the same flavour. Here the matrix elements have the form,

$$\left|\mathcal{S}_\mu(\ldots,a,\bar{q}|q,b,\ldots)V^\mu\right|^2. \qquad (5.37)$$

In the collinear limit, the quark-antiquark pinch the two colour lines together to form a single colour line,

$$\left|\mathcal{S}_\mu(\ldots,a,\bar{q}|q,b,\ldots)V^\mu\right|^2 \to P_{\bar{q}q\to g}(z,s_{\bar{q}q})\left|\mathcal{S}_\mu(\ldots,a,G,b,\ldots)V^\mu\right|^2, \qquad (5.38)$$

with $P_{\bar{q}q\to G}(z,s)$ given by eqs. (2.8) and (2.9). There is no soft singularity, nor is there any dependence on the type of adjacent parton, a or b. Clearly, the quark-antiquark pair can sit in two antennae, $(a,\bar{q},q)$ and $(\bar{q},q,b)$ and we have some freedom of how to assign the singularities to the antennae. There are two obvious choices. Either we divide the singular contribution equally over the two antennae, or, we place the z^2 part of $P_{\bar{q}q\to g}(z)$ in one antenna and the $(1-z)^2$ part in the other (as we did with the three gluon antenna before).

While there appears to be no preference, we follow this latter route so that the antenna function vanishes as the unresolved particle becomes soft,

$$\mathcal{A}_{a\bar{q}q} = \frac{2}{s_{a\bar{q}q}}\left(\frac{x_{a\bar{q}}^2}{x_{\bar{q}q}x_{a\bar{q}q}}\right), \tag{5.39}$$

and,

$$\mathcal{A}_{\bar{q}qb} = \mathcal{A}_{a\bar{q}q}(x_{a\bar{q}} \to x_{qb}, x_{a\bar{q}q} \leftrightarrow x_{\bar{q}qb}). \tag{5.40}$$

Following this procedure and integrating over the whole of the subtraction region yields,

$$\begin{aligned}\mathcal{F}_{aG}^{n_F}(s_{aG}) &= \left(\frac{g^2 n_F}{2}\right)\int \mathcal{A}_{a\bar{q}q}\, \mathrm{d}PS^{\text{sing}} \\ &= \left(\frac{\alpha_S n_F}{2\pi}\right)\left(-\frac{1}{6}\ln\left(\frac{\delta}{s_{aG}}\right)\right) + \mathcal{F}_{aG}^{n_F\Delta}\left(\frac{\Delta}{s_{aG}}\right),\end{aligned} \tag{5.41}$$

and,

$$\mathcal{F}_{Gb}^{n_F}(s_{Gb}) = \mathcal{F}_{aG}^{n_F}(s_{Gb}). \tag{5.42}$$

The factor of n_F arises because each of the n_F quark flavours may contribute. The δ independent function is,

$$\begin{aligned}\mathcal{F}_{aG}^{n_F\Delta}(x) &= \mathcal{F}_{Gb}^{n_F\Delta}(x) \\ &= \left(\frac{\alpha_S n_F}{2\pi}\right)\left(-\frac{2x}{3} + \frac{x^2}{6} - \frac{x^3}{9} - \left(\frac{1}{6} - \frac{x^3}{6}\right)\ln\left(\frac{1-x}{x}\right)\right).\end{aligned} \tag{5.43}$$

5.6.3 Leading Colour Contribution to $e^+e^- \to 4$ jets.

As a pedagogical example, we consider the leading colour contribution relevant for $e^+e^- \to 4$ jets. At leading order in the number of colours, only the two quark and two gluon process contributes and, at lowest order, we can read off the cross section from equation 5.6,

$$\begin{aligned}\frac{\mathrm{d}\sigma_4^{\text{LO}}}{\sigma_0} &= \frac{(2\pi)^5}{s}\left(\frac{N^2-1}{N^2}\right)\left(\frac{\alpha_S N}{2\pi}\right)^2 \\ &\times \left|\mathcal{S}_\mu(Q_1; G_1, G_2; \overline{Q}_2)V^\mu\right|^2 \mathcal{J}_{(4)}\, \mathrm{d}PS(Q^2; Q_1 G_1, G_2, \overline{Q}_2),\end{aligned} \tag{5.44}$$

where we have switched notation from that of chapter 4 by writing,

$$\mathcal{T}(3,4) \equiv \left|\mathcal{S}_\mu(Q_1;G_1,G_2;\overline{Q}_2)V^\mu\right|^2. \tag{5.45}$$

Similarly, the leading colour contribution from the five parton bremstrahlung process can be read from equation 5.10,

$$\frac{\mathrm{d}\sigma_5}{\sigma_0} = \frac{(2\pi)^7}{s}\left(\frac{N^2-1}{N^2}\right)\left(\frac{\alpha_S N}{2\pi}\right)^3 \left|\mathcal{S}_\mu(q_1;g_1,g_2,g_3;\bar{q}_2)V^\mu\right|^2 \mathcal{J}_{(5)}\ \mathrm{d}PS(Q^2;q_1,g_1,g_2,g_3,\bar{q}_2). \tag{5.46}$$

Note that $\mathcal{J}_5$ projects the five parton momenta onto the four jet like observable.

For this colour ordering, there will be three contributing antennae, (q_1,g_1,g_2), (g_1,g_2,g_3) and $(g_2,g_3,\bar{q}_2)$ where in each case the parton in the middle is unresolved. In the first antenna, $\{p_{q_1},p_{g_1},p_{g_2}\} \to \{p_{Q_1},p_{G_1}\}$ according to eq. (5.15), the slicing cuts are $\min(s_{q_1g_1},s_{g_1g_2}) < \delta$ and the subtraction occurs over the range $\delta < \min(s_{q_1g_1},s_{g_1g_2}) < \Delta$. Similar transformations and cuts act over the other two antenna.

Slicing Contribution

For the five parton matrix elements of eq. (5.46), the sum of infrared singularities from the three antennae in the slicing approach gives a contribution to the four particle final state which can be read directly from eq. (3.79) of ref. [21],

$$\mathrm{d}\sigma_4^{\mathrm{slice}} = R(Q_1;G_1,G_2;\overline{Q}_2)\mathrm{d}\sigma_4^{\mathrm{LO}}. \tag{5.47}$$

Retaining only the leading colour contribution (i.e. dropping the contributions from the four quark process proportional to the number of quark flavours),

$$\begin{aligned} R(Q_1;G_1,G_2;\overline{Q}_2) &= \left(\frac{\alpha_S N}{2\pi}\right)\frac{1}{\Gamma(1-\epsilon)}\left[\sum_{ij}\left\{\frac{1}{\epsilon^2}\left(\frac{4\pi\mu^2}{s_{ij}}\right)^\epsilon - \log^2\left(\frac{s_{ij}}{\delta}\right)\right\}\right. \\ &\quad \left. + \frac{3}{2\epsilon}\left(\frac{4\pi\mu^2}{\delta}\right)^\epsilon + \frac{197}{18} - \pi^2\right] \\ &\quad + \left(\frac{\alpha_S}{2\pi}\right)\frac{2b_0}{\epsilon}\frac{1}{\Gamma(1-\epsilon)}\left(\frac{4\pi\mu^2}{\delta}\right)^\epsilon + \mathcal{O}(\epsilon) + \mathcal{O}(\delta), \end{aligned}$$

with (at leading order in the number of colours) $b_0 = 11N/6$ and where the sum runs over the pairs of adjacent (colour connected) hard partons, $ij = Q_1G_1$, G_1G_2 and $G_2\overline{Q}_2$.

Subtraction Term

Since there are three antennae, we subtract three antennae factors, such that the total subtraction term is,

$$\begin{aligned}\frac{\mathrm{d}\sigma_5^{\mathrm{sub}}}{\sigma_0} &= \frac{(2\pi)^7}{s}\left(\frac{N^2-1}{N^2}\right)\left(\frac{\alpha_S N}{2\pi}\right)^3 \mathrm{d}PS(Q^2; q_1, g_1, g_2, g_3, \bar{q}_2) \\ &\times \Big(\mathcal{A}_{q_1g_1g_2}\left|\mathcal{S}_\mu(Q_1; G_1, g_3; \bar{q}_2)V^\mu\right|^2 \mathcal{J}_{(4)} \\ &+ \mathcal{A}_{g_1g_2g_3}\left|\mathcal{S}_\mu(q_1; G_1, G_2; \bar{q}_2)V^\mu\right|^2 \mathcal{J}_{(4)} \\ &+ \mathcal{A}_{g_2g_2\bar{q}_2}\left|\mathcal{S}_\mu(q_1; g_1, G_2; \overline{Q}_2)V^\mu\right|^2 \mathcal{J}_{(4)} \Big). \end{aligned} \tag{5.48}$$

Here, we have used the mappings $\{p_{q_1}, p_{g_1}, p_{g_2}\} \to \{p_{Q_1}, p_{G_1}\}$ according to eq. (5.15) for the first antenna. We recall that the subtraction occurs over the range $\delta < \min(s_{q_1g_1}, s_{g_1g_2}) < \Delta$ and that the observable function $\mathcal{J}_4$ is applied to the momenta for Q_1, G_1, g_3 and $\bar{q}_2$. Similar procedures are applied to the other antennae.

However, we must add these terms back to the four parton contribution. Here it is simplest to re-identify each of the four particle momenta with the momenta relevant for tree level. In other words, for the first antenna, $\{p_{q_1}, p_{g_1}, p_{g_2}\} \to \{p_{Q_1}, p_{G_1}\}$ as before and $p_{g_3} \to p_{G_2}$, $p_{\bar{q}_2} \to p_{\overline{Q}_2}$. This is safe to do since we integrate over the whole four particle phase space. Altogether, we have,

$$\mathrm{d}\sigma_4^{\mathrm{sub}} = \left(\mathcal{F}_{Q_1G_1} + \mathcal{F}_{G_1G_2} + \mathcal{F}_{G_2\overline{Q}_2}\right)\mathrm{d}\sigma_4^{\mathrm{LO}}. \tag{5.49}$$

Virtual Contribution

The leading colour virtual matrix elements can simply be read from equation 5.7. In terms of cross sections we have,

$$\mathrm{d}\sigma_4^{\mathrm{V}} = V(Q_1; G_1, G_2; \overline{Q}_2)\mathrm{d}\sigma_4^{\mathrm{LO}} + \mathrm{d}\sigma_4^{\mathrm{V,finite}}, \tag{5.50}$$

with,

$$\frac{\mathrm{d}\sigma_4^{\mathrm{V,finite}}}{\sigma_0} = \frac{(2\pi)^5}{s}\left(\frac{N^2-1}{N^2}\right)\left(\frac{\alpha_S N}{2\pi}\right)^3 \hat{\mathcal{L}}_A(G_1,G_2)\ \mathcal{J}_{(4)}\ \mathrm{d}PS(Q^2;p_{Q_1},p_{G_1},p_{G_2},p_{\overline{Q}_2}), \quad (5.51)$$

and the divergent factor V given by,

$$V(Q_1;G_1,G_2;\overline{Q}_2) = \left(\frac{\alpha_S N}{2\pi}\right)\left(-\frac{\mathcal{P}(s_{Q_1G_1})}{\epsilon^2} - \frac{\mathcal{P}(s_{G_2\overline{Q}_2})}{\epsilon^2} - \frac{\mathcal{P}(s_{G_1G_2})}{\epsilon^2} - \frac{3}{2}\frac{\mathcal{P}(Q^2)}{\epsilon}\right). \quad (5.52)$$

Next-to-Leading Order Cross Section

Assembling the various pieces, and applying coupling constant renormalisation,

$$\left(\frac{\alpha_S}{2\pi}\right) \to \left(\frac{\alpha_S(\mu)}{2\pi}\right)\left(1 - b_0\left(\frac{\alpha_S(\mu)}{2\pi}\right)\frac{(4\pi)^\epsilon}{\epsilon\Gamma(1-\epsilon)}\right), \quad (5.53)$$

the NLO four parton contribution is,

$$\begin{aligned}\mathrm{d}\sigma_4^{\mathrm{NLO}} &= \mathrm{d}\sigma_4^{\mathrm{V}} + \mathrm{d}\sigma_4^{\mathrm{sub}} + \mathrm{d}\sigma_4^{\mathrm{slice}} \\ &= K(Q_1;G_1,G_2;\overline{Q}_2)\mathrm{d}\sigma_4^{\mathrm{LO}} + \mathrm{d}\sigma_4^{\mathrm{V,finite}}, \end{aligned} \quad (5.54)$$

where $\mathrm{d}\sigma_4^{\mathrm{LO}}$ and $\mathrm{d}\sigma_4^{\mathrm{V,finite}}$ are given by eqs. (5.44) and (5.51) respectively with the replacement $\alpha_S \to \alpha_S(\mu)$. The factor K is the sum of the divergent one-loop factor (eq. (5.52)), the slicing factor (eq. (5.48)) and the subtraction term (eq. (5.49)),

$$\begin{aligned} K(Q_1;G_1,G_2;\overline{Q}_2) &= V(Q_1;G_1,G_2;\overline{Q}_2) + R(Q_1;G_1,G_2;\overline{Q}_2) \\ &\quad + \mathcal{F}_{Q_1G_1}(s_{Q_1G_1}) + \mathcal{F}_{G_1G_2}(s_{G_1G_2}) + \mathcal{F}_{G_2\overline{Q}_2}(s_{G_2\overline{Q}_2}) \\ &= \left(\frac{\alpha_S(\mu)N}{2\pi}\right)\left(\frac{197}{18} + \frac{\pi^2}{2}\right. \\ &\quad + \mathcal{F}^{\Delta}_{Q_1G_1}\left(\frac{\Delta}{s_{Q_1G_1}}\right) + \mathcal{F}^{\Delta}_{G_1G_2}\left(\frac{\Delta}{s_{G_1G_2}}\right) + \mathcal{F}^{\Delta}_{G_2\overline{Q}_2}\left(\frac{\Delta}{s_{G_2\overline{Q}_2}}\right) \\ &\quad \left. - \frac{10}{6}\log\left(\frac{s_{Q_1G_1}}{Q^2}\right) - \frac{11}{6}\log\left(\frac{s_{G_1G_2}}{Q^2}\right) - \frac{10}{6}\log\left(\frac{s_{G_2\overline{Q}_2}}{Q^2}\right)\right) \\ &\quad + \left(\frac{\alpha_S(\mu)}{2\pi}\right) 2b_0 \log\left(\frac{\mu^2}{Q^2}\right). \end{aligned} \quad (5.55)$$

Similarly, the five parton leading colour contribution to four jet-like observables is obtained from eqs. (5.46) and (5.48),

$$\mathrm{d}\sigma_5^{\mathrm{NLO}} = \mathrm{d}\sigma_5 - \mathrm{d}\sigma_5^{\mathrm{sub}}, \tag{5.56}$$

evaluated with the running $\alpha_S(\mu)$. By construction this is finite as any one particle becomes unresolved. In the slicing regions, $\mathrm{d}\sigma_5^{\mathrm{NLO}} = 0$, while the phase space regions over which the subtraction terms are applied are implicit in the definition of the antenna functions.

Note that the four-dimensional limit of all cross sections may be taken with impunity now that the singularities have cancelled. Furthermore, there is no dependence in K on the slicing parameter δ which may also be taken as small as desired. The subtraction parameter Δ remains, and both $\mathrm{d}\sigma_4^{\mathrm{NLO}}$ and $\mathrm{d}\sigma_5^{\mathrm{NLO}}$ individually depend on it. However, the sum of both contributions is independent of the choice of Δ. The precise value of Δ can be made bearing in mind the numerical stability and speed of the final computer code. For small Δ, there may be sizeable cancellations between the four and five parton contributions, while for large Δ more CPU time is required to evaluate the subtraction terms.

5.6.4 Sub-Leading Contribution to the Cross-Section

It is straightforward to extend this approach to deal with all the sub-leading contributions to the cross-section. Here we detail all the necessary subtraction and slicing terms to render the full four and five parton contributions finite.

Five Parton Contribution

It is simplest to first identify the antennae that will contribute to each colourless subamplitude. The form of the five parton matrix elements is such that these are easily read off from equation 5.10. The subtraction terms are divided into pieces corresponding to the four parton matrix elements that are subtracted,

$$\frac{\mathrm{d}\sigma_5^{\mathrm{sub}}}{\sigma_0} = \frac{(2\pi)^7}{s}\left(\frac{N^2-1}{N^2}\right)\left(\frac{\alpha_S N}{2\pi}\right)^3 \mathrm{d}PS(Q^2;\ldots)\,\mathcal{J}_{(4)}$$

$$\times \left(\mathcal{A}^a - \frac{1}{2N^2}\,\mathcal{A}^b + \frac{n_F}{N}\,\mathcal{A}^c + \frac{2}{N^2}\,\mathcal{A}^d\right), \tag{5.57}$$

with the antenna terms given by,

$$\begin{aligned}
\mathcal{A}^a &= \mathcal{A}_{q_1g_1g_2}\left|\mathcal{S}_\mu(Q_1;G_1,g_3;\bar{q}_2)V^\mu\right|^2 + \mathcal{A}_{g_1g_2g_3}\left|\mathcal{S}_\mu(q_1;G_1,G_2;\bar{q}_2)V^\mu\right|^2 \\
&\quad + \mathcal{A}_{g_2g_3\bar{q}_2}\left|\mathcal{S}_\mu(q_1;g_1,G_2;\overline{Q}_2)V^\mu\right|^2 + \frac{n_F}{N}\Big(\mathcal{A}_{q_1\bar{q}_4q_3}\left|\mathcal{S}_\mu(Q_1;G_1,g_2;\bar{q}_2)V^\mu\right|^2 \\
&\quad + \mathcal{A}_{\bar{q}_4q_3g}\left|\mathcal{S}_\mu(q_1;G_1,G_2;\bar{q}_2)V^\mu\right|^2 + \mathcal{A}_{q_3\bar{q}_4\bar{q}_2}\left|\mathcal{S}_\mu(q_1;g_1,G_2;\overline{Q}_2)V^\mu\right|^2 \\
&\quad + \mathcal{A}_{g\bar{q}_4q_3}\left|\mathcal{S}_\mu(q_1;G_1,G_2;\bar{q}_2)V^\mu\right|^2\Big) - \frac{1}{N^2}\mathcal{A}_{q_1g_3\bar{q}_2}\left|\mathcal{S}_\mu(q_1;G_1,G_2;\bar{q}_2)V^\mu\right|^2, \\
\mathcal{A}^b &= \mathcal{A}_{q_1g_1g_2}\left|\mathcal{S}_\mu(Q_1;\tilde{G}_1,\tilde{g}_3;\bar{q}_2)V^\mu\right|^2 + \mathcal{A}_{q_1g_1g_2}\left|\mathcal{S}_\mu(Q_1;\tilde{g}_3,\tilde{G}_1;\bar{q}_2)V^\mu\right|^2 \\
&\quad + \mathcal{A}_{g_1g_2\bar{q}_2}\left|\mathcal{S}_\mu(q_1;\tilde{G}_1,\tilde{g}_3;\overline{Q}_2)V^\mu\right|^2 + \mathcal{A}_{g_1g_2\bar{q}_2}\left|\mathcal{S}_\mu(q_1;\tilde{g}_3,\tilde{G}_1;\overline{Q}_2)V^\mu\right|^2 \\
&\quad + \frac{2n_F}{N}\left(\mathcal{A}_{q_3\bar{q}_4\bar{q}_2}\left|\mathcal{S}_\mu(q_1;\tilde{g}_1,\tilde{G}_2;\overline{Q}_2)V^\mu\right|^2 + \mathcal{A}_{q_1q_3\bar{q}_4}\left|\mathcal{S}_\mu(Q_1;\tilde{g}_1,\tilde{G}_2;\bar{q}_2)V^\mu\right|^2\right) \\
&\quad - \frac{1}{3}\left(1+\frac{1}{N^2}\right)\Big(\mathcal{A}_{q_1g_1\bar{q}_2}\left|\mathcal{S}_\mu(Q_1;\tilde{g}_2,\tilde{g}_3;\overline{Q}_2)V^\mu\right|^2 \\
&\qquad + \mathcal{A}_{q_1g_2\bar{q}_2}\left|\mathcal{S}_\mu(Q_1;\tilde{g}_1,\tilde{g}_3;\overline{Q}_2)V^\mu\right|^2 + \mathcal{A}_{q_1g_3\bar{q}_2}\left|\mathcal{S}_\mu(Q_1;\tilde{g}_1,\tilde{g}_2;\overline{Q}_2)V^\mu\right|^2\Big), \\
\mathcal{A}^c &= \Big(\mathcal{A}_{q_1g\bar{q}_4} + \mathcal{A}_{q_3g\bar{q}_2} - \frac{1}{N^2}(2\mathcal{A}_{q_1g\bar{q}_4} + 2\mathcal{A}_{q_3g\bar{q}_2} \\
&\quad - 2\mathcal{A}_{q_1gq_3} - 2\mathcal{A}_{\bar{q}_4g\bar{q}_2} + \mathcal{A}_{q_1g\bar{q}_2} + \mathcal{A}_{q_3g\bar{q}_4})\Big)\mathcal{T}(1,2;1,2), \\
\mathcal{A}^d &= \Big(\mathcal{A}_{q_1gq_3} + \mathcal{A}_{\bar{q}_4g\bar{q}_2} - \frac{1}{N^2}(\mathcal{A}_{q_1g\bar{q}_2} + \mathcal{A}_{q_3g\bar{q}_4} + \mathcal{A}_{q_1g\bar{q}_4} + \mathcal{A}_{q_3g\bar{q}_2} \\
&\quad - \mathcal{A}_{q_1gq_3} - \mathcal{A}_{\bar{q}_4g\bar{q}_2})\Big)\mathcal{T}(1,2;1,4).
\end{aligned} \tag{5.58}$$

Four Parton Contribution

By examining equation 5.6, we see that the lowest order cross section for $e^+e^- \to 4$ jets can similarly be written as,

$$\mathrm{d}\sigma_4^{\mathrm{LO}} = \mathrm{d}\sigma_{4a}^{\mathrm{LO}} - \frac{1}{2N^2}\,\mathrm{d}\sigma_{4b}^{\mathrm{LO}} + \frac{n_F}{N}\,\mathrm{d}\sigma_{4c}^{\mathrm{LO}} + \frac{2}{N^2}\,\mathrm{d}\sigma_{4d}^{\mathrm{LO}}, \tag{5.59}$$

where each term $\mathrm{d}\sigma_{4x}^{\mathrm{LO}}$ contains matrix elements multiplied by the four-parton phase-space factor,

$$\frac{\mathrm{d}\sigma_{4x}^{\mathrm{LO}}}{\sigma_0} = \frac{(2\pi)^5}{s}\left(\frac{N^2-1}{N^2}\right)\left(\frac{\alpha_S N}{2\pi}\right)^2 \mathcal{M}_x\, \mathcal{J}_{(4)}\, \mathrm{d}PS(Q^2;\ldots), \tag{5.60}$$

with the matrix elements given (in the notation of chapter 4) by,

$$\begin{aligned} \mathcal{M}_a = \mathcal{T}(3,4) = \left|\mathcal{S}_\mu(Q_1;G_1,G_2:\overline{Q}_2)V^\mu\right|^2 \quad , \qquad & M_b = \mathcal{T} = \left|\mathcal{S}_\mu(Q_1;\tilde{G}_1,\tilde{G}_2:\overline{Q}_2)V^\mu\right|^2 \\ \mathcal{M}_c = T(1,2;1,2) \quad , \qquad & \mathcal{M}_d = T(1,2;1,4). \end{aligned} \tag{5.61}$$

Following the same steps as we have explicitly demonstrated for the leading colour piece, we can write the full four parton next-to-leading order contribution to the cross-section as,

$$\begin{aligned} \mathrm{d}\sigma_4^{\mathrm{NLO}} &= \mathrm{d}\sigma_4^V + \mathrm{d}\sigma_4^{\mathrm{sub}} + \mathrm{d}\sigma_4^{\mathrm{slice}} \\ &= \left\{(\mathcal{K}(Q_1;G_1,G_2;\overline{Q}_2) - \frac{1}{N^2}\mathcal{K}(Q_1;\overline{Q}_2)\right\}\mathrm{d}\sigma_{4a}^{\mathrm{LO}} \\ &\quad - \frac{1}{2N^2}\left\{\mathcal{K}(Q_1;G_1;\overline{Q}_2) + \mathcal{K}(Q_1;G_2;\overline{Q}_2) - \left(1+\frac{1}{N^2}\right)\mathcal{K}(Q_1;\overline{Q}_2)\right\}\mathrm{d}\sigma_{4b}^{\mathrm{LO}} \\ &\quad + \frac{n_F}{N}\Bigg\{\mathcal{K}(Q_1;\overline{Q}_4) + \mathcal{K}(Q_3;\overline{Q}_2) - \frac{2}{3}\log\left(\frac{s_{Q_3\overline{Q}_4}}{Q^2}\right) + \frac{31}{9} \\ &\qquad - \frac{1}{N^2}\Bigg(2\mathcal{K}(Q_1;\overline{Q}_4) + 2\mathcal{K}(Q_3;\overline{Q}_2) - 2\mathcal{K}(Q_1;Q_3) - 2\mathcal{K}(\overline{Q}_2;\overline{Q}_4) + \mathcal{K}(Q_1;\overline{Q}_2) \\ &\qquad + \mathcal{K}(Q_3;\overline{Q}_4) + 3\log\left(\frac{s_{Q_3\overline{Q}_4}}{Q^2}\right)\Bigg) + \frac{n_F}{N}\left(-\frac{10}{9} + \frac{2}{3}\log\left(\frac{s_{Q_3\overline{Q}_4}}{Q^2}\right)\right)\Bigg\}\mathrm{d}\sigma_{4c}^{\mathrm{LO}} \\ &\quad + \frac{2}{N^2}\Bigg\{\mathcal{K}(Q_1;Q_3) + \mathcal{K}(\overline{Q}_2;\overline{Q}_4) - \frac{2}{3}\log\left(\frac{s_{Q_3\overline{Q}_4}}{Q^2}\right) + \frac{31}{9} \\ &\qquad - \frac{1}{N^2}\Bigg(\mathcal{K}(Q_1;\overline{Q}_2) + \mathcal{K}(Q_3;\overline{Q}_4) + \mathcal{K}(Q_1;\overline{Q}_4) + \mathcal{K}(Q_3;\overline{Q}_2) - \mathcal{K}(Q_1;Q_3) \\ &\qquad - \mathcal{K}(\overline{Q}_2;\overline{Q}_4) + 3\log\left(\frac{s_{Q_3\overline{Q}_4}}{Q^2}\right)\Bigg) + \frac{n_F}{N}\left(-\frac{10}{9} + \frac{2}{3}\log\left(\frac{s_{Q_3\overline{Q}_4}}{Q^2}\right)\right)\Bigg\}\mathrm{d}\sigma_{4d}^{\mathrm{LO}} \\ &\quad + \mathrm{d}\sigma_4^{\mathrm{V,finite}}. \end{aligned} \tag{5.62}$$

The finite term $\mathrm{d}\sigma_4^{\mathrm{V,finite}}$ represents the functions $\hat{\mathcal{L}}$ of chapter 4 and is easily read off from equation 5.7, as are the extra logarithm terms that appear above. The factors of $(31/9 - 10n_F/9N)$ are due to the self-energy insertions which are included in the pieces $\mathcal{L}_C(1,2;i,j)$. By inspecting the form of the 5 parton matrix elements it is straightforward

to deduce the subleading combinations of $\mathcal{K}$ factors needed, which are given by the slicing terms from eq.(3.79) of [21] with $n = 1$ and $n = 0$ respectively, added to the integrated antenna subtraction terms given earlier,

$$\begin{aligned} K(Q;G;\overline{Q}) &= \left(\frac{\alpha_S(\mu)N}{2\pi}\right)\left\{\frac{130}{18}+\frac{\pi^2}{3}+\mathcal{F}^{\Delta}_{QG}\left(\frac{\Delta}{s_{QG}}\right)+\mathcal{F}^{\Delta}_{G\overline{Q}}\left(\frac{\Delta}{s_{G\overline{Q}}}\right)\right. \\ &\quad \left.-\frac{10}{6}\log\left(\frac{s_{QG}}{\Delta}\right)-\frac{10}{6}\log\left(\frac{s_{G\overline{Q}}}{\Delta}\right)\right\} \\ &\quad +\left(\frac{\alpha_S(\mu)}{2\pi}\right)b_0\log\left(\frac{\mu^2}{Q^2}\right), \end{aligned} \tag{5.63}$$

$$K(Q;\overline{Q}) = \left(\frac{\alpha_S(\mu)N}{2\pi}\right)\left\{\frac{63}{18}+\frac{\pi^2}{6}+\mathcal{F}^{\Delta}_{Q\overline{Q}}\left(\frac{\Delta}{s_{Q\overline{Q}}}\right)-\frac{3}{2}\log\left(\frac{s_{Q\overline{Q}}}{\Delta}\right)\right\}. \tag{5.64}$$

In addition, the function for two quarks (or antiquarks) in an antenna is identical to that for a quark-antiquark pair,

$$\mathcal{K}(Q_i;Q_j) = \mathcal{K}(Q = Q_i;\overline{Q} = Q_j). \tag{5.65}$$

5.7 Summary

In this chapter we have bridged the gap between the theoretical matrix element calculations of chapter 4 and a numerical implementation of them suitable for making physical predictions. By appealing to the symmetries of the matrix elements (ultimately, of the Feynman diagrams themselves) we may reduce the number of function evaluations that are necessary and thus decrease the required CPU time. More importantly, we have shown how the matrix element and phase space singularities may be cancelled between the four and five parton contributions.

By using a version of the hybrid subtraction scheme based on the radiation of a soft parton from an antenna of two hard particles, we have identified all the relevant subtraction and slicing terms that are necessary to render both partonic pieces finite. The resulting contributions to the cross-section are summarized in equations 5.58 and 5.62.

The following chapter will now be devoted to the study of a particular program written using this approach, EERAD2. By performing Monte Carlo integrations over the appropriate phase spaces, we can obtain predictions for a variety of four-jet like quantities that are well defined in perturbation theory.

Chapter 6

Four Jet Predictions at NLO

6.1 Introduction

Electron-positron colliders, in particular those at both CERN and SLAC, have provided much precision data with which to probe the structure of QCD. This is particularly valuable data because the strong interactions occur only in the final state and are not entangled with the parton density functions associated with beams of hadrons. In addition to measuring multi-jet production rates, more specific information about the topology of the events can be extracted. To this end, many variables have been introduced which characterize the hadronic structure of an event. For example, we can ask how planar or how collimated an event is. In general, a variable is described as n-jet like if it vanishes for a final state configuration of $n-1$ hadrons. With the precision data from LEP and SLC, experimental distributions for such event shape variables have been studied and have been compared where possible with theoretical calculations. Generally speaking, leading order (LO) predictions successfully predict the general features of distributions, but can be improved by resumming kinematically-dominant logarithms, by including more perturbative information or both. A next-to-leading order (NLO) treatment of three-jet like variables was first performed in [17, 20] and systematically completed in [53]. Armed with such calculations, one can extract a value for the strong coupling α_S either directly from the event shape distributions [54] or from the energy dependence of their average value [55]. Alternatively, one can study the

group parameters of the gauge theory of the strong interactions, as we have already discussed in chapter 2.

Having assembled all the relevant matrix elements in chapter 4 and described a suitable numerical implementation of them in chapter 5, we are now ready to compute next-to-leading order predictions for four-jet like observables. In section 6.2 we give the definitions of a selection of these infrared safe observables that may be safely calculated in perturbation theory. These are all non-zero only for event configurations which contain at least four resolved particles and so may be predicted only by considering the process $e^+e^- \to 4$ jets.

The theory of the preceeding two chapters is used to construct the Monte Carlo program which we refer to as `EERAD2`. Section 6.3 demonstrates the consistency of this program by comparing some results with those produced by two other four jet programs `MENLO PARC` [51, 56] and `DEBRECEN` [57]. In particular, we compare the thrust minor and D parameter distributions as well as the four jet rate as a function of the jet resolution parameter $y_{\rm cut}$.

In the remainder of the chapter we present next-to-leading order coefficients for the differential distributions of the narrow jet broadening and light hemisphere mass and the y_4 distribution for the JADE algorithm. We compare these with experimental data from the DELPHI collaboration.

6.2 Four Jet Shape Variables

The sorts of variables we are interested in are four-jet like, since they can only be non-zero for final states in which there are four or more particles. They rely on the hadronic final state having some volume and, when the event is coplanar, the observables are identically zero. In the following definitions, the sums run over all N final state particles, $k = 1, \ldots, N$. $\vec{p}_k$ is the three-momentum of particle k in the c.m. frame, with components p_k^i, $i = 1, \ldots, 3$.

(a) C and D parameters.

We first construct the linear momentum tensor,

$$\Theta^{ij} = \frac{\sum_k \frac{p_k^i p_k^j}{|\vec{p}_k|}}{\sum_k |\vec{p}_k|}, \tag{6.1}$$

with eigenvalues λ_i for $i = 1, 2, 3$. The normalisation is such that $\sum \lambda_i = 1$. For planar events one of the eigenvalues is zero. The C and D parameters are defined by,

$$D = 27\lambda_1\lambda_2\lambda_3, \tag{6.2}$$

and,

$$C = 3(\lambda_1\lambda_2 + \lambda_2\lambda_3 + \lambda_3\lambda_1). \tag{6.3}$$

D is only non-zero for four parton events, while for $C < 0.75$, three parton events contribute. Only the region $C > 0.75$ should be considered four jet like.

(b) Thrust minor, T_{minor}.

We first define the thrust, major and minor axes $(\vec{n}_1, \vec{n}_2, \vec{n}_3)$ by,

$$T_i = \max_{\vec{n}_i} \frac{\sum_k |\vec{p}_k \cdot \vec{n}_k|}{\sum_k |\vec{p}_k|}, \tag{6.4}$$

where $\vec{n}_2$ is constrained by $\vec{n}_1 \cdot \vec{n}_2 = 0$ and $\vec{n}_3 = \vec{n}_1 \times \vec{n}_2$.

(c) Light hemisphere mass, m_L^2/s.

The event is separated into two hemispheres H_1, H_2 divided by the plane normal to the thrust axis $\vec{n}_1$, as defined above. Particles that satisfy $\vec{p}_i.\vec{n}_1 > 0$ are assigned to hemisphere H_1, while all other particles are in H_2. Then,

$$\frac{m_L^2}{s} = \frac{1}{s} \cdot \min_{i=1,2} \left(\sum_{\vec{p}_k \in H_i} p_k \right)^2. \tag{6.5}$$

(d) Narrow jet broadening, B_{min}.

Using the same division into hemispheres as above, we define,

$$B_{\text{min}} = \min_{i=1,2} \frac{\sum_{\vec{p}_k \in H_i} |\vec{p}_k \times \vec{n}|}{2 \sum_k |\vec{p}_k|}. \tag{6.6}$$

(e) Jet transition variable y_4^S.

The y_4^S variable denotes the value of the jet resolution parameter $y_{\rm cut}$ at which an event changes from a four jet event to a three jet event where the jets are defined according to algorithm S. We consider the three algorithms already previously discussed (see chaoter 2): the JADE-E0 ($S = J$), Durham ($S = D$) and Geneva ($S = G$) algorithms.

Of these variables, the D distribution has been considered in [57, 58] and the C, $T_{\rm minor}$ and y_4^D distributions have been studied in [25].

The differential cross-section for one of these four-jet variables (O_4) at next-to-leading order can then be parametrized by two coefficients (just as for the 3-jet variable 1-Thrust, equation 1.14 of chapter 1),

$$\frac{1}{\sigma_0}\cdot O_4\frac{d\sigma}{dO_4} = \left(\frac{\alpha_S(\mu)}{2\pi}\right)^2 B_{O_4} + \left(\frac{\alpha_S(\mu)}{2\pi}\right)^3 \left(2\beta_0 \log\left(\frac{\mu^2}{Q^2}\right) B_{O_4} + C_{O_4}\right). \qquad (6.7)$$

The parameters B_{O_4} and C_{O_4} represent the leading and next-to-leading scale-independent factors for the observable O_4. The coupling α_S is calculated at renormalization scale μ, extra dependence on which enters through the first coefficient of the beta-function, $\beta_0 = (33 - 2n_F)/6$. σ_0 represents, as in the previous chapter, the lowest order 2-jet cross-section, $e^+e^- \to q\bar{q}$.

6.3 Monte Carlo Comparison

As a check of the numerical results, Table 6.1 shows the predictions for each of the three Monte Carlo programs for the four jet rate for three jet clustering algorithms; the JADE-E0 [8], Durham-E [9] and Geneva-E [10] algorithms. We show results with $\alpha_S(M_Z) = 0.118$ for three values of the jet resolution parameter y_{cut}. There is good agreement with the results from the other two calculations.

As a further comparison with the program DEBRECEN, we also compare the differential distributions for the D parameter and thrust minor. For each observable O_4, the coefficients

Algorithm	y_{cut}	MENLO PARC	DEBRECEN	EERAD2
Durham	0.005	$(1.04 \pm 0.02) \cdot 10^{-1}$	$(1.05 \pm 0.01) \cdot 10^{-1}$	$(1.05 \pm 0.01) \cdot 10^{-1}$
	0.01	$(4.70 \pm 0.06) \cdot 10^{-2}$	$(4.66 \pm 0.02) \cdot 10^{-2}$	$(4.65 \pm 0.02) \cdot 10^{-2}$
	0.03	$(6.82 \pm 0.08) \cdot 10^{-3}$	$(6.87 \pm 0.04) \cdot 10^{-3}$	$(6.86 \pm 0.03) \cdot 10^{-3}$
Geneva	0.02	$(2.56 \pm 0.06) \cdot 10^{-1}$	$(2.63 \pm 0.06) \cdot 10^{-1}$	$(2.61 \pm 0.05) \cdot 10^{-1}$
	0.03	$(1.71 \pm 0.03) \cdot 10^{-1}$	$(1.75 \pm 0.03) \cdot 10^{-1}$	$(1.72 \pm 0.03) \cdot 10^{-1}$
	0.05	$(8.58 \pm 0.15) \cdot 10^{-2}$	$(8.37 \pm 0.12) \cdot 10^{-2}$	$(8.50 \pm 0.06) \cdot 10^{-2}$
JADE-E0	0.005	$(3.79 \pm 0.08) \cdot 10^{-1}$	$(3.88 \pm 0.07) \cdot 10^{-1}$	$(3.87 \pm 0.03) \cdot 10^{-1}$
	0.01	$(1.88 \pm 0.03) \cdot 10^{-1}$	$(1.92 \pm 0.01) \cdot 10^{-1}$	$(1.93 \pm 0.01) \cdot 10^{-1}$
	0.03	$(3.46 \pm 0.05) \cdot 10^{-2}$	$(3.37 \pm 0.01) \cdot 10^{-2}$	$(3.35 \pm 0.01) \cdot 10^{-2}$

Table 6.1: The four-jet fraction as calculated by the program described in this chapter, EERAD2 and the alternatives MENLO PARC and DEBRECEN. Results are shown for the different jet recombination schemes and varying y_{cut}. The rate is normalized by the $\mathcal{O}(\alpha_S)$ total hadronic cross-section, which is related to the 2-jet cross-section by $\sigma_{\text{tot}} = \sigma_0 (1 + \alpha_S/\pi)$.

B_{O_4} and C_{O_4} of equation 6.7 are presented in Tables 6.2 and 6.3. The results are tabulated for the same bins as used in the papers [58] and [25], with each bin labelled by its central value. The errors associated with each bin are those estimated by the Monte Carlo integration.

In Figures 6.1 and 6.2 we show the same results, normalized by the corresponding results from DEBRECEN. Ideally we should obtain a straight line at unity, but in reality the Monte Carlo errors mean that the errors associated with each point should simply encompass this ideal. We see that this is the case for each of the distributions, with the agreement deteriorating slightly towards the tails. This just reflects the fact that each program is biased to place more Monte Carlo weight (and thus smaller errors) where the cross-section is largest, which corresponds to the observable O_4 being small (approaching the 3-jet region).

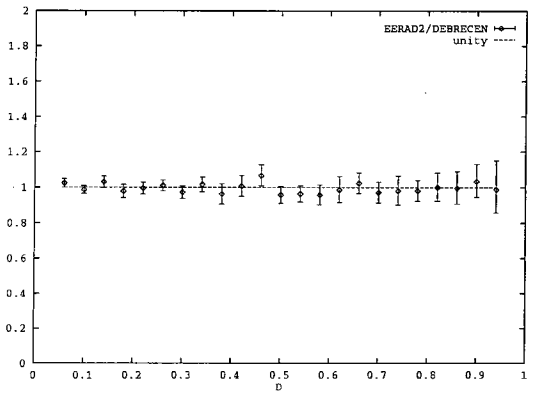

Figure 6.1: Comparison of the differential distribution of the D parameter, as calculated by the programs EERAD2 and DEBRECEN. Each point represents the ratio EERAD2/DEBRECEN, with the dotted line showing perfect agreement.

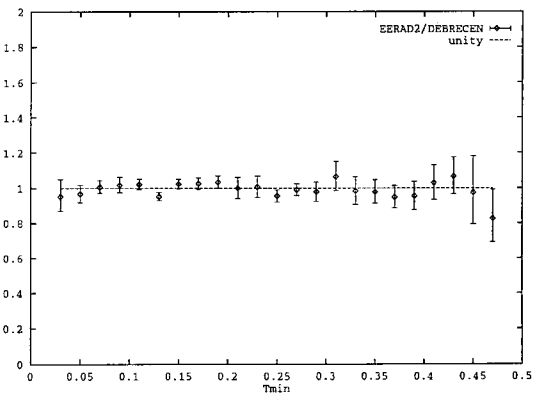

Figure 6.2: As for Figure 6.1, but for the distribution of thrust minor, T_{minor}.

D	B_D	C_D
0.06	$(2.33 \pm 0.01) \cdot 10^2$	$(1.27 \pm 0.01) \cdot 10^4$
0.10	$(1.48 \pm 0.01) \cdot 10^2$	$(8.47 \pm 0.07) \cdot 10^3$
0.14	$(1.03 \pm 0.01) \cdot 10^2$	$(6.43 \pm 0.08) \cdot 10^3$
0.18	$(7.71 \pm 0.07) \cdot 10^1$	$(4.88 \pm 0.08) \cdot 10^3$
0.22	$(5.86 \pm 0.04) \cdot 10^1$	$(3.83 \pm 0.07) \cdot 10^3$
0.26	$(4.70 \pm 0.04) \cdot 10^1$	$(3.01 \pm 0.04) \cdot 10^3$
0.30	$(3.73 \pm 0.03) \cdot 10^1$	$(2.45 \pm 0.04) \cdot 10^3$
0.34	$(2.97 \pm 0.03) \cdot 10^1$	$(1.97 \pm 0.03) \cdot 10^3$
0.38	$(2.44 \pm 0.03) \cdot 10^1$	$(1.53 \pm 0.05) \cdot 10^3$
0.42	$(1.98 \pm 0.02) \cdot 10^1$	$(1.38 \pm 0.05) \cdot 10^3$
0.46	$(1.61 \pm 0.02) \cdot 10^1$	$(1.13 \pm 0.03) \cdot 10^3$
0.50	$(1.32 \pm 0.01) \cdot 10^1$	$(8.35 \pm 0.23) \cdot 10^2$
0.54	$(1.06 \pm 0.01) \cdot 10^1$	$(6.85 \pm 0.16) \cdot 10^2$
0.58	$(8.48 \pm 0.10) \cdot 10^0$	$(5.44 \pm 0.18) \cdot 10^2$
0.62	$(6.88 \pm 0.09) \cdot 10^0$	$(4.40 \pm 0.11) \cdot 10^2$
0.66	$(5.44 \pm 0.08) \cdot 10^0$	$(3.60 \pm 0.09) \cdot 10^2$
0.70	$(3.99 \pm 0.06) \cdot 10^0$	$(2.66 \pm 0.07) \cdot 10^2$
0.74	$(3.04 \pm 0.03) \cdot 10^0$	$(2.04 \pm 0.09) \cdot 10^2$
0.78	$(2.25 \pm 0.03) \cdot 10^0$	$(1.51 \pm 0.03) \cdot 10^2$
0.82	$(1.58 \pm 0.02) \cdot 10^0$	$(1.03 \pm 0.04) \cdot 10^2$
0.86	$(9.99 \pm 0.11) \cdot 10^{-1}$	$(6.63 \pm 0.29) \cdot 10^1$
0.90	$(5.72 \pm 0.07) \cdot 10^{-1}$	$(4.02 \pm 0.15) \cdot 10^1$
0.94	$(2.50 \pm 0.03) \cdot 10^{-1}$	$(1.69 \pm 0.06) \cdot 10^1$
0.98	$(5.29 \pm 0.05) \cdot 10^{-2}$	$(2.95 \pm 0.15) \cdot 10^0$

Table 6.2: The leading and next-to-leading order coefficients for the D parameter.

6.4 Further Results

We now present the results for the differential distributions of the remainder of the four-jet observables, namely the narrow jet broadening $B_{\min}$, the light jet mass m_L^2/s and the four jet resolution parameter in the JADE scheme, y_4^J.

As we have explained in chapter 5, `EERAD2` uses hybrid subtraction to isolate infrared singularities, which involves introducing the two parameters δ and Δ to control the slicing and subtraction cuts. By running the program with different values of these parameters,

it is straightforward to verify that the results are independent of them. For the tables and plots presented here we have used the values,

$$\delta = 10^{-8} \qquad \text{and} \qquad \Delta = 10^{-4}.$$

The next-to-leading order coefficients for the further variables are presented in Tables 6.4 – 6.6. These coefficients may be inserted into equation 6.7 with a suitable choice of scale μ and strong coupling α_S. We may present the canonical comparison by choosing the physical scale $\mu = M_Z$, $\alpha_S(M_Z) = 0.118$ and comparing with data from the DELPHI collaboration [59]. Predictions for the light jet mass, narrow jet broadening and jet resolution y_4^J in this scheme are shown as the solid lines in Figures 6.3 – 6.5. These are to be contrasted with the lowest order predictions which are represented by the dashed lines and which lie substantially lower than the data. In all the distributions, it can be seen that the inclusion of the next-to-leading order terms increases the theoretical prediction by a factor of approximately 100% throughout most of the range.

As we have discussed in chapter 1, although results for jet distributions are typically presented at the physical scale, it may be theoretically advantageous to consider other choices of scale. Since for many of the distributions the physical scale yields NLO corrections which are large but still lie well below the data[1], such considerations seem even more pertinent. Given that at present the evaluation of the NNLO corrections to 4-jet like quantities seems rather infeasible we should attempt to utilize our NLO knowledge in as complete a manner as possible.

At this point it is worthwhile to recall the discussion of chapter 1, where we considered different schemes for choosing the renormalization scale. Where the data lies above our prediction with the physical scale, clearly a smaller scale μ is preferred, where $\alpha_S(\mu)$ would be larger. In the case of the thrust distribution, we found that both the FAC and PMS scales naturally selected such a smaller scale and a similar treatment here may be beneficial.

[1] In fact, this is the case for all the distributions except the jet resolution y_4 in the JADE scheme.

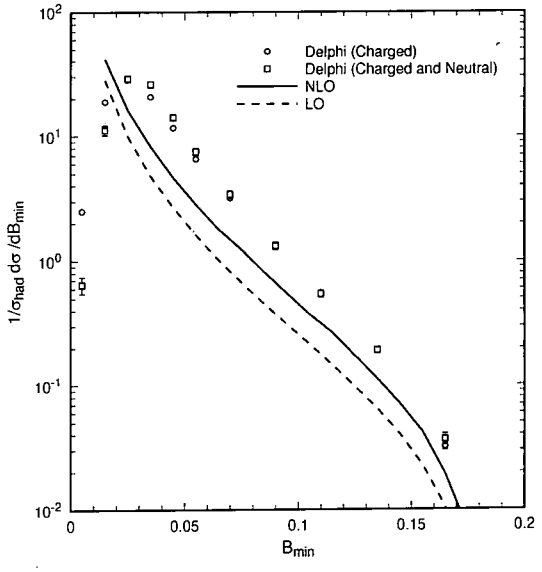

Figure 6.3: The B_{min} distribution at next-to-leading order (solid line), compared with the lowest order result (dotted line). The open circles (boxes) show the charged (charged and neutral) data from the DELPHI collaboration.

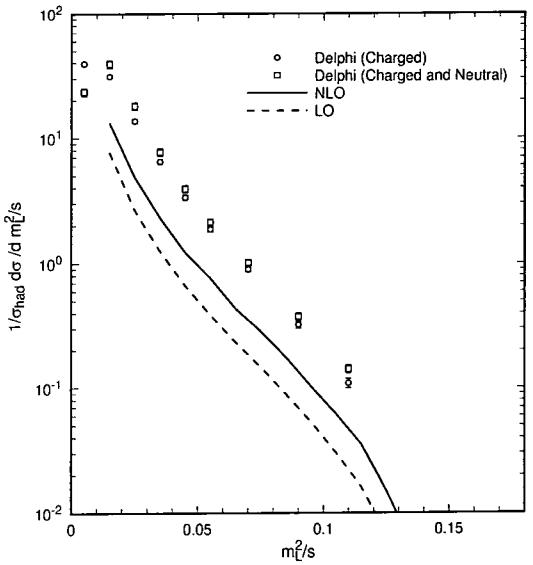

Figure 6.4: As for Figure 6.3, but for the light mass distribution.

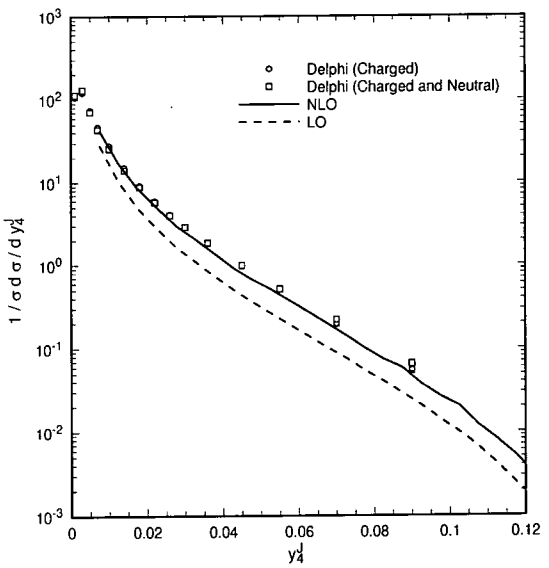

Figure 6.5: As for Figure 6.3, but for the y_4^J distribution.

6.5 Summary

In this chapter we have introduced a selection of four-jet observables and made next-to-leading order predictions for them using the program EERAD2 which is based upon the work of chapters 3-5.

For some of the observables, such as the jet rates, thrust minor and the D parameter, where next-to-leading order results were already available, EERAD2 provides consistent results. The remaining distributions are presented in the form of tables of scale-independent coefficients and plots with the strong coupling α_S evaluated at the physical scale. At this scale, the next-to-leading order corrections are large, but typically leave the perturbative prediction still well below the DELPHI data.

This concludes our discussion of the calculation of this 4 jet process. We now turn our attention briefly to the consideration of infrared singularities and factorization when applied at next-to-next-to-leading order.

T_{minor}	$B_{T_{\text{minor}}}$	$C_{T_{\text{minor}}}$
0.03	$(1.95 \pm 0.02) \cdot 10^{3}$	$(7.48 \pm 0.10) \cdot 10^{4}$
0.05	$(1.06 \pm 0.01) \cdot 10^{3}$	$(5.45 \pm 0.09) \cdot 10^{4}$
0.07	$(6.83 \pm 0.04) \cdot 10^{2}$	$(3.94 \pm 0.04) \cdot 10^{4}$
0.09	$(4.69 \pm 0.03) \cdot 10^{2}$	$(2.82 \pm 0.05) \cdot 10^{4}$
0.11	$(3.32 \pm 0.02) \cdot 10^{2}$	$(2.08 \pm 0.03) \cdot 10^{4}$
0.13	$(2.43 \pm 0.02) \cdot 10^{2}$	$(1.47 \pm 0.01) \cdot 10^{4}$
0.15	$(1.79 \pm 0.01) \cdot 10^{2}$	$(1.14 \pm 0.01) \cdot 10^{4}$
0.17	$(1.37 \pm 0.01) \cdot 10^{2}$	$(8.52 \pm 0.17) \cdot 10^{3}$
0.19	$(1.03 \pm 0.01) \cdot 10^{2}$	$(6.56 \pm 0.13) \cdot 10^{3}$
0.21	$(7.84 \pm 0.07) \cdot 10^{1}$	$(4.77 \pm 0.23) \cdot 10^{3}$
0.23	$(6.01 \pm 0.06) \cdot 10^{1}$	$(3.58 \pm 0.18) \cdot 10^{3}$
0.25	$(4.65 \pm 0.05) \cdot 10^{1}$	$(2.54 \pm 0.08) \cdot 10^{3}$
0.27	$(3.63 \pm 0.04) \cdot 10^{1}$	$(1.94 \pm 0.04) \cdot 10^{3}$
0.29	$(2.76 \pm 0.03) \cdot 10^{1}$	$(1.41 \pm 0.06) \cdot 10^{3}$
0.31	$(2.17 \pm 0.02) \cdot 10^{1}$	$(1.14 \pm 0.04) \cdot 10^{3}$
0.33	$(1.70 \pm 0.02) \cdot 10^{1}$	$(7.05 \pm 0.42) \cdot 10^{2}$
0.35	$(1.28 \pm 0.02) \cdot 10^{1}$	$(5.16 \pm 0.24) \cdot 10^{2}$
0.37	$(9.62 \pm 0.13) \cdot 10^{0}$	$(3.48 \pm 0.12) \cdot 10^{2}$
0.39	$(6.96 \pm 0.11) \cdot 10^{0}$	$(2.50 \pm 0.15) \cdot 10^{2}$
0.41	$(5.17 \pm 0.07) \cdot 10^{0}$	$(1.73 \pm 0.11) \cdot 10^{2}$
0.43	$(3.62 \pm 0.06) \cdot 10^{0}$	$(1.12 \pm 0.06) \cdot 10^{2}$
0.45	$(2.45 \pm 0.04) \cdot 10^{0}$	$(6.19 \pm 0.78) \cdot 10^{1}$
0.47	$(1.60 \pm 0.03) \cdot 10^{0}$	$(2.83 \pm 0.22) \cdot 10^{1}$
0.49	$(9.38 \pm 0.12) \cdot 10^{-1}$	$(1.46 \pm 0.28) \cdot 10^{1}$
0.51	$(5.08 \pm 0.10) \cdot 10^{-1}$	$(7.98 \pm 1.50) \cdot 10^{0}$
0.53	$(2.17 \pm 0.04) \cdot 10^{-1}$	$(1.35 \pm 0.68) \cdot 10^{0}$
0.55	$(6.41 \pm 0.13) \cdot 10^{-2}$	$(-1.44 \pm 0.15) \cdot 10^{0}$
0.57	$(4.90 \pm 0.20) \cdot 10^{-3}$	$(-2.97 \pm 0.28) \cdot 10^{-1}$

Table 6.3: The leading and next-to-leading order coefficients for T_{minor}.

$B_{\min}$	$B_{B_{\min}}$	$C_{B_{\min}}$
0.0150	$(1.19 \pm 0.01) \cdot 10^{3}$	$(3.31 \pm 0.06) \cdot 10^{4}$
0.0250	$(7.07 \pm 0.07) \cdot 10^{2}$	$(2.51 \pm 0.02) \cdot 10^{4}$
0.0350	$(4.75 \pm 0.05) \cdot 10^{2}$	$(1.91 \pm 0.02) \cdot 10^{4}$
0.0450	$(3.42 \pm 0.03) \cdot 10^{2}$	$(1.40 \pm 0.01) \cdot 10^{4}$
0.0550	$(2.51 \pm 0.02) \cdot 10^{2}$	$(1.06 \pm 0.02) \cdot 10^{4}$
0.0650	$(1.86 \pm 0.02) \cdot 10^{2}$	$(7.99 \pm 0.07) \cdot 10^{3}$
0.0750	$(1.42 \pm 0.01) \cdot 10^{2}$	$(6.25 \pm 0.08) \cdot 10^{3}$
0.0850	$(1.09 \pm 0.01) \cdot 10^{2}$	$(4.82 \pm 0.08) \cdot 10^{3}$
0.0950	$(8.33 \pm 0.06) \cdot 10^{1}$	$(3.58 \pm 0.09) \cdot 10^{3}$
0.1050	$(6.37 \pm 0.06) \cdot 10^{1}$	$(2.77 \pm 0.08) \cdot 10^{3}$
0.1150	$(4.72 \pm 0.04) \cdot 10^{1}$	$(2.13 \pm 0.04) \cdot 10^{3}$
0.1250	$(3.42 \pm 0.03) \cdot 10^{1}$	$(1.39 \pm 0.02) \cdot 10^{3}$
0.1350	$(2.45 \pm 0.02) \cdot 10^{1}$	$(1.06 \pm 0.02) \cdot 10^{3}$
0.1450	$(1.64 \pm 0.02) \cdot 10^{1}$	$(6.91 \pm 0.11) \cdot 10^{2}$
0.1550	$(9.90 \pm 0.09) \cdot 10^{0}$	$(4.30 \pm 0.14) \cdot 10^{2}$
0.1650	$(4.85 \pm 0.06) \cdot 10^{0}$	$(2.12 \pm 0.08) \cdot 10^{2}$
0.1750	$(1.71 \pm 0.03) \cdot 10^{0}$	$(7.01 \pm 0.21) \cdot 10^{1}$
0.1850	$(4.29 \pm 0.06) \cdot 10^{-1}$	$(1.62 \pm 0.06) \cdot 10^{1}$
0.1950	$(5.61 \pm 0.13) \cdot 10^{-2}$	$(1.18 \pm 0.14) \cdot 10^{0}$
0.2050	$(4.16 \pm 0.22) \cdot 10^{-4}$	$(9.68 \pm 5.46) \cdot 10^{-3}$

Table 6.4: The leading and next-to-leading order coefficients for the narrow jet broadening $B_{\min}$.

m_L^2/s	$B_{m_L^2/s}$	$C_{m_L^2/s}$
0.0150	$(3.26 \pm 0.07) \cdot 10^2$	$(1.38 \pm 0.02) \cdot 10^4$
0.0250	$(1.88 \pm 0.03) \cdot 10^2$	$(8.71 \pm 0.08) \cdot 10^3$
0.0350	$(1.24 \pm 0.02) \cdot 10^2$	$(5.92 \pm 0.07) \cdot 10^3$
0.0450	$(8.46 \pm 0.11) \cdot 10^1$	$(4.07 \pm 0.06) \cdot 10^3$
0.0550	$(6.01 \pm 0.08) \cdot 10^1$	$(3.08 \pm 0.08) \cdot 10^3$
0.0650	$(4.27 \pm 0.05) \cdot 10^1$	$(2.10 \pm 0.04) \cdot 10^3$
0.0750	$(3.11 \pm 0.05) \cdot 10^1$	$(1.60 \pm 0.03) \cdot 10^3$
0.0850	$(2.14 \pm 0.03) \cdot 10^1$	$(1.09 \pm 0.02) \cdot 10^3$
0.0950	$(1.44 \pm 0.02) \cdot 10^1$	$(7.43 \pm 0.16) \cdot 10^2$
0.1050	$(8.94 \pm 0.11) \cdot 10^0$	$(4.84 \pm 0.15) \cdot 10^2$
0.1150	$(5.26 \pm 0.08) \cdot 10^0$	$(3.19 \pm 0.06) \cdot 10^2$
0.1250	$(2.38 \pm 0.04) \cdot 10^0$	$(1.68 \pm 0.05) \cdot 10^2$
0.1350	$(8.49 \pm 0.24) \cdot 10^{-1}$	$(6.34 \pm 0.24) \cdot 10^1$
0.1450	$(2.45 \pm 0.06) \cdot 10^{-1}$	$(1.78 \pm 0.05) \cdot 10^1$
0.1550	$(4.46 \pm 0.14) \cdot 10^{-2}$	$(3.89 \pm 0.20) \cdot 10^0$
0.1650	$(1.70 \pm 0.13) \cdot 10^{-3}$	$(1.97 \pm 0.20) \cdot 10^{-1}$
0.1750	–	$(8.98 \pm 3.09) \cdot 10^{-6}$

Table 6.5: The leading and next-to-leading order coefficients for the light jet mass m_L^2/s.

y_4^J	$B_{y_4^J}$	$C_{y_4^J}$
0.0075	$(5.97 \pm 0.03) \cdot 10^{2}$	$(1.74 \pm 0.04) \cdot 10^{4}$
0.0125	$(3.65 \pm 0.02) \cdot 10^{2}$	$(1.32 \pm 0.02) \cdot 10^{4}$
0.0175	$(2.45 \pm 0.02) \cdot 10^{2}$	$(9.68 \pm 0.12) \cdot 10^{3}$
0.0225	$(1.80 \pm 0.01) \cdot 10^{2}$	$(7.86 \pm 0.12) \cdot 10^{3}$
0.0275	$(1.30 \pm 0.01) \cdot 10^{2}$	$(5.83 \pm 0.14) \cdot 10^{3}$
0.0325	$(1.03 \pm 0.01) \cdot 10^{2}$	$(4.97 \pm 0.13) \cdot 10^{3}$
0.0375	$(7.96 \pm 0.08) \cdot 10^{1}$	$(3.85 \pm 0.08) \cdot 10^{3}$
0.0425	$(6.19 \pm 0.06) \cdot 10^{1}$	$(2.82 \pm 0.06) \cdot 10^{3}$
0.0475	$(4.91 \pm 0.05) \cdot 10^{1}$	$(2.27 \pm 0.07) \cdot 10^{3}$
0.0525	$(3.93 \pm 0.04) \cdot 10^{1}$	$(1.95 \pm 0.08) \cdot 10^{3}$
0.0575	$(3.12 \pm 0.03) \cdot 10^{1}$	$(1.47 \pm 0.03) \cdot 10^{3}$
0.0625	$(2.48 \pm 0.02) \cdot 10^{1}$	$(1.22 \pm 0.04) \cdot 10^{3}$
0.0675	$(1.94 \pm 0.02) \cdot 10^{1}$	$(9.47 \pm 0.41) \cdot 10^{2}$
0.0725	$(1.57 \pm 0.02) \cdot 10^{1}$	$(7.70 \pm 0.26) \cdot 10^{2}$
0.0775	$(1.19 \pm 0.01) \cdot 10^{1}$	$(5.92 \pm 0.33) \cdot 10^{2}$
0.0825	$(9.40 \pm 0.10) \cdot 10^{0}$	$(4.16 \pm 0.18) \cdot 10^{2}$
0.0875	$(7.08 \pm 0.11) \cdot 10^{0}$	$(3.45 \pm 0.20) \cdot 10^{2}$
0.0925	$(5.39 \pm 0.06) \cdot 10^{0}$	$(2.51 \pm 0.08) \cdot 10^{2}$
0.0975	$(3.87 \pm 0.07) \cdot 10^{0}$	$(1.85 \pm 0.09) \cdot 10^{2}$
0.1025	$(2.85 \pm 0.04) \cdot 10^{0}$	$(1.46 \pm 0.08) \cdot 10^{2}$
0.1075	$(2.00 \pm 0.04) \cdot 10^{0}$	$(1.00 \pm 0.09) \cdot 10^{2}$
0.1125	$(1.31 \pm 0.03) \cdot 10^{0}$	$(5.93 \pm 0.40) \cdot 10^{1}$
0.1175	$(8.14 \pm 0.15) \cdot 10^{-1}$	$(5.19 \pm 0.46) \cdot 10^{1}$
0.1225	$(5.28 \pm 0.12) \cdot 10^{-1}$	$(2.45 \pm 0.16) \cdot 10^{1}$
0.1275	$(3.12 \pm 0.07) \cdot 10^{-1}$	$(1.44 \pm 0.14) \cdot 10^{1}$
0.1325	$(1.63 \pm 0.03) \cdot 10^{-1}$	$(7.68 \pm 0.57) \cdot 10^{0}$
0.1375	$(9.22 \pm 0.18) \cdot 10^{-2}$	$(4.32 \pm 0.37) \cdot 10^{0}$
0.1425	$(4.32 \pm 0.11) \cdot 10^{-2}$	$(2.36 \pm 0.20) \cdot 10^{0}$
0.1475	$(1.62 \pm 0.04) \cdot 10^{-2}$	$(7.92 \pm 1.18) \cdot 10^{-1}$
0.1525	$(5.14 \pm 0.17) \cdot 10^{-3}$	$(2.34 \pm 0.22) \cdot 10^{-1}$
0.1575	$(1.03 \pm 0.03) \cdot 10^{-3}$	$(4.15 \pm 0.77) \cdot 10^{-2}$
0.1625	$(6.42 \pm 0.34) \cdot 10^{-5}$	$(3.73 \pm 0.60) \cdot 10^{-3}$
0.1675	$(8.16 \pm 4.91) \cdot 10^{-8}$	$(-1.07 \pm 0.97) \cdot 10^{-6}$

Table 6.6: The leading and next-to-leading order coefficients for the jet resolution parameter y_4^J, where the superscript denotes that the jets are defined according to the JADE algorithm.

Chapter 7

Double Unresolved Factorization

7.1 Introduction

In this chapter we now return to the calculation of the five parton matrix elements of chapter 4 and consider some other uses of those results. There, and in subsequent chapters, we concentrated on their specific application to 4-jet production. In this chapter we will use these matrix elements to illustrate a more general feature of QCD amplitudes, that of factorization in soft and collinear limits. As a specific example, we will show how we may introduce new factorization functions that would play a role in the NNLO calculation of the process $e^+e^- \to 3$ jets.

The soft gluon and collinear parton limits of multiparton scattering amplitudes are well known. As discussed in chapter 2, colour-ordered n parton sub amplitudes factorize into $(n-1)$ parton amplitudes with the unresolved particle removed, multiplied by eikonal (soft) factors,

$$S_{abc}(s_{ac}, s_{ab}, s_{bc}) = \frac{4s_{ac}}{s_{ab}s_{bc}}, \tag{7.1}$$

or Altarelli-Parisi (collinear) splitting functions (equations 2.9).

In this chapter, we shall extend the factorization of multiparton scattering amplitudes to include all the cases where two particles are considered unresolved (pictured in Figure 7.1).

There are a variety of different configurations, comprising:

(a) two soft particles, **(b)** two pairs of collinear particles,

(c) three collinear particles, **(d)** one soft and two collinear.

Figure 7.1: An illustration of the double unresolved factorization from an $(n+2)$ particle state into one containing only n resolved particles. The hard part of the process remains unchanged while two of the gluons are unresolved by one of (a)-(d) described in the text.

Such configurations are relevant for calculations at next-to-next-to-leading order and beyond, and in particular we will present suitable double-unresolved approximations for the $e^+e^- \to 5$ partons matrix elements, relevant for the calculation of $e^+e^- \to 3$ jets at NNLO. A brief discussion of the calculational structure of this process follows in section 7.2. Sections 7.3 and 7.4 are organised according to whether the two unresolved particles are colour connected or not. The precise meaning of what colour connected means will be given in sect. 7.3. In the unconnected case, the singular limits are obtained by merely multiplying single unresolved factors. However, when the particles are colour connected, the structure is more involved (sect. 7.4) and we give explicit formulae detailing the double unresolved singular factors for all of the configurations (a)-(d) above. In each case we write down expressions for the double unresolved limits of the five parton process.

7.2 Three Jet Production at NNLO

One of the next steps in theoretical perturbative QCD calculations is to evaluate the next-to-next-to-leading order corrections to the three-jet rate. Current analysis of three jet events and other hadronic event shapes gives a global average value of the strong coupling constant

as [54],

$$\alpha_S(M_Z) = 0.121 \pm 0.005.$$

Together with LEP/SLC data and hadronic events from the next linear collider, NNLO input would play a role in reducing this error on $\alpha_S(M_Z)$ to the 2-3% level.

However, to accomplish this, several ingredients are necessary. As has been extensively discussed in preceding chapters, the calculation of any n-jet observable at the one-loop level requires the evaluation of both real $(n+1)$-parton and virtual n-parton matrix elements. At two loops, there is a still greater number of contributing partonic processes. These are illustrated in Figure 7.2 for the case of three jet production, where we consider all the possible cuts of a relevant $\mathcal{O}(\alpha_S^3)$ 3-loop diagram. There are four types of contribution:

- **(a) 2-loop, 3 partons**
  The interference of the 2-loop with tree-level 3-parton diagrams forms the first contribution. Evaluation of these matrix elements appears to be a major hurdle, since even the scalar two loop box integrals with massless internal and external legs are not known analytically. Some progress towards the evaluation of these formidable integrals has been made in [60, 61].

- **(b) 1-loop, 3 partons**
  A second category of matrix elements is formed by the interference of the 1-loop 3 parton matrix elements with themselves. These are known amplitudes and their implementation should not be problematic.

- **(c) 1-loop, 4 partons**
  The matrix elements of chapter 4 form a third contribution, when one of the partons is unresolved. The singularities must be systematically isolated when either a gluon is soft or two partons are collinear. In ref. [62], Bern et al., have developed appropriate splitting functions for one-loop processes where two external particles are collinear.

- **(d) Tree level, 5 partons**
  Finally, two particles may be unresolved, again leading to infrared singularities that

must be analytically isolated and then numerically combined with all the above contributions. In order to extract all the singularities, we must first find suitable approximations to the five parton matrix elements with two particles unresolved. This is the problem which we shall address later in this chapter, extending the earlier study of multiple soft gluon emission by Berends and Giele [63].

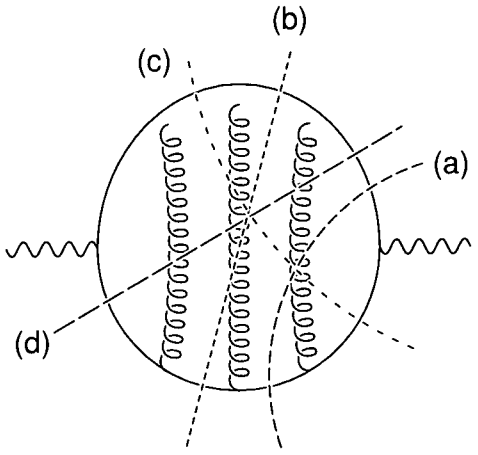

Figure 7.2: A 3-loop diagram which, when cut in all possible ways, shows the partonic contributions that need to be calculated for $e^+e^- \to 3$ jets at next-to-next-to-leading order. Writing the ℓ-loop, n-parton amplitude as $\mathcal{M}_n^{(\ell)}$, the dashed lines represent the cuts that correspond to the following squared interferences of amplitudes: (a) $\mathcal{M}_3^{(0)} \times \mathcal{M}_3^{(2)}$, (b) $\mathcal{M}_3^{(1)} \times \mathcal{M}_3^{(1)}$, (c) $\mathcal{M}_4^{(0)} \times \mathcal{M}_4^{(1)}$ and (d) $\mathcal{M}_5^{(0)} \times \mathcal{M}_5^{(0)}$.

Of course, much work still remains to be carried out before a genuine NNLO prediction may be made. Not least of these is analytically integrating the double unresolved approximations over the appropriate regions of phase space. However, the approximations presented in the remainder of this chapter provide a first step in this direction.

7.3 Colour Unconnected Double Unresolved

In the cases where the two unresolved particles are not colour connected, the factorisation of the amplitudes involves the well-known functions describing single soft and collinear emission.

We first describe what is meant by colour connected and colour unconnected.

7.3.1 Colour Connection

We have seen how tree level matrix elements can be decomposed into colour ordered subamplitudes which have nice factorisation properties in the infrared limits. Therefore it is useful to view the matrix elements in terms of the colour structure associated with the subamplitudes. For example, in chapter 4, we introduce the two quark-three gluon subamplitude $S_\mu(Q_1;1,2,3;\overline{Q}_2)$, which is associated with the colour structure $(T^{a_1}T^{a_2}T^{a_3})_{c_1c_2}$. This is a colour antenna that ends on the quark/antiquark colour charges c_1 and c_2 with ordered emission of gluons with colour $a_1,\ldots,a_3$. Within this colour antenna, gluon 1 is colour connected to the quark Q_1 and gluon 2, but not to the antiquark $\overline{Q}_2$ or to gluon 3. It is easy to re-interpret the colour connection in terms of the singularity structure of the matrix elements: particles a and b are colour connected when the matrix elements have a pole in the invariant s_{ab}. In cases involving more than one quark-antiquark pair there can be many colour antennae. For example, the four quark amplitude $\mathcal{A}_\mu^{Q_1Q_2}(Q_1;1;\overline{Q}_4|Q_3;\overline{Q}_2)$ in chapter 4 describes a process with two separate colour antennae. In general, the particles in one antenna are not colour connected to the particles in one of the other antennae. However, there is one case where particles in adjoining antenna can usefully be thought of as colour connected. This is when there is an antiquark at the end of one antenna and a like flavour quark at the beginning of another,

$$\mathcal{A}(\ldots,\overline{Q}|Q,\ldots).$$

When this quark-antiquark pair are collinear, they combine to form a gluon G, which then connects, or pinches together, the two separate colour antennae, so that,

$$|\mathcal{A}(\ldots,\overline{Q}|Q,\ldots)|^2 \to P_{q\bar{q}\to G}(z,s_{Q\overline{Q}})|\mathcal{A}(\ldots,a,G,b,\ldots)|^2.$$

This is illustrated diagrammatically in Figure 7.3. A useful definition of colour "connected" therefore includes these antennae pinching configurations along with the more straightforward colour connection within a single antenna. All other cases are colour "unconnected".

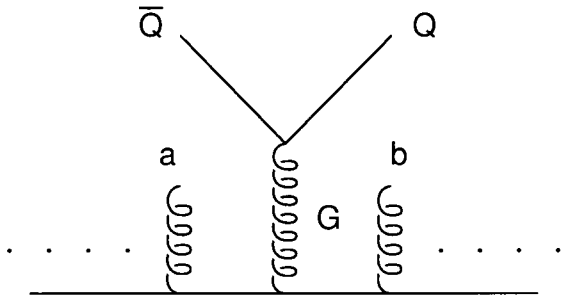

Figure 7.3: The pinching together of two antennae which gives rise to the factorization of equation 7.3.1.

7.3.2 Two Collinear Pairs

Two pairs of particles may become collinear separately, but with the particles in one or both of the pairs themselves not colour "connected". In these cases, there are no singular contributions containing both of the vanishing invariants. For instance, if partons $\{a, d\}$ and $\{b, c\}$ are collinear then,

$$|\mathcal{A}(\ldots, a, \ldots, b, \ldots, c, \ldots, d, \ldots)|^2 \to \text{less singular.} \tag{7.2}$$

By this we mean there is no contribution proportional to $1/s_{ad}s_{bc}$ and once again, when integrated over the small region of phase space relevant for this approximation yields a negligible contribution.

The situation where two pairs of colour "connected" particles are collinear is also rather trivial. If partons a and b form P, while c and d cluster to form Q, so that P and Q are themselves colour unconnected, then,

$$|\mathcal{A}(\ldots, a, b, \ldots, c, d, \ldots)|^2 \to P_{ab\to P}(z_1, s_{ab})\, P_{cd\to Q}(z_2, s_{cd})\, |\mathcal{A}(\ldots, P, \ldots, Q, \ldots)|^2. \tag{7.3}$$

Here, z_1 and z_2 are the momentum fractions carried by a and c respectively. A similar result holds if either of the pairs involves particles in separate antennae, but which are able to undergo antenna pinching. The collinear splitting functions are related to the (colourless)

Altarelli-Parisi splitting kernels by eq. (2.8) which, in the conventional dimensional regularisation scheme [14] with all particles treated in $D = 4 - 2\epsilon$ dimensions, are given by (2.9) of chapter 2. As before, azimuthal averaging of the collinear particle plane is understood.

Double Collinear Limit of $e^+e^- \to 5$ Partons

In this limit where two pairs of partons are simultaneously collinear, the five parton matrix elements factorise into the three parton matrix elements multiplied by a combination of products of collinear splitting functions. Summing over all possible unconnected double collinear limits, for the two-quark currents we find,

$$\begin{aligned}
\left|\mathcal{S}_\mu(Q_1;1,2,3;\overline{Q}_2)V^\mu\right|^2 &\to \left(P_{Q_11\to Q}P_{23\to G} + P_{Q_11\to Q}P_{3\overline{Q}_2\to\overline{Q}} + P_{12\to G}P_{3\overline{Q}_2\to\overline{Q}}\right)\left|\mathcal{S}^3_\mu V^\mu\right|^2, \\
\left|\mathcal{S}_\mu(Q_1;1,2,\tilde{3};\overline{Q}_2)V^\mu\right|^2 &\to \left(P_{Q_11\to Q}P_{2\overline{Q}_2\to\overline{Q}} + P_{Q_13\to Q}P_{2\overline{Q}_2\to\overline{Q}} + P_{Q_11\to Q}P_{3\overline{Q}_2\to\overline{Q}}\right. \\
&\quad \left. + P_{Q_13\to Q}P_{12\to G} + P_{12\to G}P_{3\overline{Q}_2\to\overline{Q}}\right)\left|\mathcal{S}^3_\mu V^\mu\right|^2, \\
\left|\mathcal{S}_\mu(Q_1;\tilde{1},\tilde{2},\tilde{3};\overline{Q}_2)V^\mu\right|^2 &\to \sum_{P(1,2,3)} P_{Q_11\to Q}P_{2\overline{Q}_2\to\overline{Q}}\left|\mathcal{S}^3_\mu V^\mu\right|^2,
\end{aligned} \tag{7.4}$$

whilst the only contributing pieces for the four-quark process are,

$$\begin{aligned}
\left|\mathcal{T}^A_\mu(Q_1,\overline{Q}_2;Q_3,\overline{Q}_4;1)V^\mu\right|^2 &\to \left(P_{Q_11\to Q}P_{\overline{Q}_4Q_3\to G} + P_{1\overline{Q}_4\to\overline{Q}}P_{\overline{Q}_2Q_1\to G}\right)\left|\mathcal{S}^3_\mu V^\mu\right|^2, \\
\left|\mathcal{T}^B_\mu(Q_1,\overline{Q}_4;Q_3,\overline{Q}_2;1)V^\mu\right|^2 &\to \left(P_{Q_11\to Q}P_{\overline{Q}_4Q_3\to G} + P_{1\overline{Q}_2\to\overline{Q}}P_{\overline{Q}_4Q_3\to G}\right)\left|\mathcal{S}^3_\mu V^\mu\right|^2, \\
\left|\overline{\mathcal{T}}_\mu(Q_1,\overline{Q}_2;Q_3,\overline{Q}_4;1)V^\mu\right|^2 &\to \left(P_{Q_11\to Q}P_{\overline{Q}_4Q_3\to G} + P_{1\overline{Q}_2\to\overline{Q}}P_{\overline{Q}_4Q_3\to G}\right. \\
&\quad \left. + P_{Q_31\to Q}P_{\overline{Q}_2Q_1\to G} + P_{1\overline{Q}_4\to\overline{Q}}P_{\overline{Q}_2Q_1\to G}\right)\left|\mathcal{S}^3_\mu V^\mu\right|^2.
\end{aligned} \tag{7.5}$$

For brevity we have dropped the arguments of the splitting functions. Explicitly, for n_F flavours of quark, we find,

$$\begin{aligned}
\frac{1}{3!}\left|\widehat{\mathcal{S}}^5_\mu V^\mu\right|^2 + \left|\widehat{\mathcal{T}}^5_\mu V^\mu\right|^2 &= \left(\frac{g^2N}{2}\right)^2\left(\frac{N^2-1}{N^2}\right)\left|\widehat{\mathcal{S}}^3_\mu V^\mu\right|^2 \\
&\times \left(P_{Q_11\to Q}P_{23\to G} + P_{3\overline{Q}_2\to\overline{Q}}P_{12\to G} + P_{Q_11\to Q}P_{3\overline{Q}_2\to\overline{Q}}\right. \\
&\quad \left. + \frac{2n_F}{N}P_{Q_11\to Q}P_{\overline{Q}_4Q_3\to G} - \frac{1}{2N^2}\left(P_{Q_11\to Q}P_{2\overline{Q}_2\to\overline{Q}} + P_{Q_13\to Q}P_{2\overline{Q}_2\to\overline{Q}}\right)\right).
\end{aligned} \tag{7.6}$$

Note also that the identical gluon factor 1/3! is eliminated since each term in the sum over permutations produces an identical contribution. It is interesting to review the origin of the factor of n_F. There are $n_F(n_F-1)/2$ contributions from two unlike pairs of quarks, each of which generates two sets of singular limits - that indicated plus the symmetric term $(Q_1 \leftrightarrow Q_3, \overline{Q}_2 \leftrightarrow \overline{Q}_4)$. In addition there are n_F like-quark pair contributions, which after the symmetries have been applied yield four singular limits. However, the identical quark contribution is multiplied by the identical particle factor 1/4 so that the net result is,

$$\frac{n_F(n_F-1)}{2} \times 2 + n_F \times 4 \times \frac{1}{4} = n_F^2.$$

One factor of n_F is absorbed into the three parton matrix elements $\left|\widehat{\mathcal{S}}_\mu^3 V^\mu\right|^2$, while the other appears as an explicit factor.

7.3.3 Triple Collinear Factorisation

If three collinear particles are colour "unconnected" then there is no singularity. So if a, b and c all become collinear,

$$|\mathcal{A}(\ldots, a, \ldots, b, \ldots, c, \ldots)|^2 \to \text{finite}, \tag{7.7}$$

and there is no singular contribution involving the invariants s_{ab}, s_{bc} or s_{abc}. As before, because the region of phase space where the triple collinear limit is valid is extremely small, this gives a negligible contribution to the cross section. When two of the three collinear particles are colour "connected" we find a singular result,

$$|\mathcal{A}(\ldots, a, \ldots, b, c, \ldots)|^2 \to 1/s_{bc}. \tag{7.8}$$

However, when integrated over the triple collinear region of phase space that requires s_{ab}, s_{bc} or s_{abc} all to be small, we again obtain a negligible contribution that is proportional to the small parameter defining the extent of the triple collinear phase space. We therefore ignore contributions of this type.

7.3.4 Soft/Collinear Factorisation

Two particles may be unresolved if one of them is a soft gluon and another pair are collinear. When the soft gluon g is not colour connected to either of the colour "connected" collinear particles c and d, factorisation is straightforward,

$$|\mathcal{A}(\ldots,a,g,b,\ldots,c,d,\ldots)|^2 \to S_{agb}(s_{ab},s_{ag},s_{bg})P_{cd\to P}(z,s_{cd})\,|\mathcal{A}(\ldots,a,b,\ldots,P,\ldots)|^2. \tag{7.9}$$

Soft/Collinear Limit of $e^+e^- \to 5$ Partons

In the soft/collinear limit, the five parton matrix elements again factorise into a singular factor multiplying the squared two-quark current relevant for three parton production,

$$\begin{aligned}
\left|\mathcal{S}_\mu(Q_1;1,2,3;\overline{Q}_2)V^\mu\right|^2 &\to \left(S_{Q_112}P_{3\overline{Q}_2\to\overline{Q}} + P_{Q_11\to Q}S_{23\overline{Q}_2}\right)\left|\mathcal{S}^3_\mu V^\mu\right|^2,\\
\left|\mathcal{S}_\mu(Q_1;1,2,\tilde{3};\overline{Q}_2)V^\mu\right|^2 &\to \left(S_{Q_112}P_{3\overline{Q}_2\to\overline{Q}} + P_{Q_13\to Q}S_{12\overline{Q}_2} + P_{12\to G}S_{Q_13\overline{Q}_2}\right)\left|\mathcal{S}^3_\mu V^\mu\right|^2.
\end{aligned} \tag{7.10}$$

Note that for $\left|\mathcal{S}_\mu(Q_1;\tilde{1},\tilde{2},\tilde{3};\overline{Q}_2)V^\mu\right|^2$, the soft and collinear limits are considered to be overlapping and will be dealt with in section 7.4.2.

In the four-quark current case, the soft/collinear limit has only two colour-unconnected contributions. The first is given by,

$$\left|\mathcal{T}^B_\mu(Q_1,\overline{Q}_4;Q_3,\overline{Q}_2;1)V^\mu\right|^2 \to S_{Q_11\overline{Q}_2}P_{Q_3\overline{Q}_4\to G}\left|\mathcal{S}^3_\mu V^\mu\right|^2, \tag{7.11}$$

whilst the limit of, $\left|\overline{\mathcal{T}}_\mu(Q_1,\overline{Q}_2;Q_3,\overline{Q}_4;1)V^\mu\right|^2$, again involves both unconnected and connected factors and therefore discussion of this will also be deferred until section 7.4.2. The other subamplitudes vanish in the unconnected soft/collinear limit.

Applying these limits to the full five parton matrix elements is straightfoward and, after removing identical particle factors where necessary, we find,

$$\frac{1}{3!}\left|\widehat{\mathcal{S}}^5_\mu V^\mu\right|^2 + \left|\widehat{\mathcal{T}}^5_\mu V^\mu\right|^2 = \left(\frac{g^2N}{2}\right)^2\left|\widehat{\mathcal{S}}^3_\mu V^\mu\right|^2$$

$$\times \left[\left(\frac{N^2-1}{N^2}\right)\left(S_{Q_1 12}P_{3\overline{Q}_2\to\overline{Q}} + P_{Q_1 1\to Q}S_{23\overline{Q}_2}\right) - \frac{1}{N^2}P_{12\to G}S_{Q_1 3\overline{Q}_2} + \frac{n_F}{N^3}S_{Q_1 1\overline{Q}_2}P_{Q_3\overline{Q}_4\to G}\right]. \tag{7.12}$$

7.3.5 Two Soft Gluons

When two unconnected gluons are soft, the factorisation is again simple [63]. For gluons g_1 and g_2 soft we find,

$$\begin{aligned}|\mathcal{A}(\ldots,a,g_1,b,\ldots,c,g_2,d,\ldots)|^2 \;\to\; & S_{ag_1b}(s_{ab},s_{ag_1},s_{bg_1})S_{cg_2d}(s_{cd},s_{cg_2},s_{dg_2}) \\ & \times|\mathcal{A}(\ldots,a,b,\ldots,c,d,\ldots)|^2,\end{aligned} \tag{7.13}$$

so that the singular factor is merely the product of two single soft gluon emission factors given by eq. (7.1). Note that $b = c$ is allowed.

Double Soft Limit of $e^+e^- \to 5$ Partons

The sum over the unconnected double soft limits of the colour ordered subamplitudes can be easily read off,

$$\begin{aligned}\left|\mathcal{S}_\mu(Q_1;1,2,3;\overline{Q}_2)V^\mu\right|^2 &\to S_{Q_1 12}S_{23\overline{Q}_2}\left|\mathcal{S}^3_\mu V^\mu\right|^2, \\ \left|\mathcal{S}_\mu(Q_1;1,2,\tilde{3};\overline{Q}_2)V^\mu\right|^2 &\to \left(S_{Q_1 12}S_{Q_1 3\overline{Q}_2} + S_{Q_1 3\overline{Q}_2}S_{12\overline{Q}_2}\right)\left|\mathcal{S}^3_\mu V^\mu\right|^2, \\ \left|\mathcal{S}_\mu(Q_1;\tilde{1},\tilde{2},\tilde{3};\overline{Q}_2)V^\mu\right|^2 &\to \frac{1}{2}\sum_{P(1,2,3)} S_{Q_1 1\overline{Q}_2}S_{Q_1 2\overline{Q}_2}\left|\mathcal{S}^3_\mu V^\mu\right|^2.\end{aligned} \tag{7.14}$$

There is no contribution from the four-quark matrix elements. Inserting these limits into the full five parton matrix elements yields,

$$\begin{aligned}\frac{1}{3!}\left|\widehat{\mathcal{S}}^5_\mu V^\mu\right|^2 + \left|\widehat{\mathcal{T}}^5_\mu V^\mu\right|^2 &= \left(\frac{g^2N}{2}\right)^2\left|\widehat{\mathcal{S}}^3_\mu V^\mu\right|^2 \\ \times &\left[S_{Q_1 12}S_{23\overline{Q}_2} - \frac{1}{N^2}\left(S_{Q_1 12}S_{Q_1 3\overline{Q}_2} + S_{Q_1 3\overline{Q}_2}S_{12\overline{Q}_2}\right)\right. \\ &\left. + \left(\frac{N^2+1}{2N^4}\right)S_{Q_1 1\overline{Q}_2}S_{Q_1 2\overline{Q}_2}\right],\end{aligned} \tag{7.15}$$

where once again the sum over permutations is eliminated by the identical particle factor.

7.4 Colour Connected Double Unresolved

The factorisation that occurs when the two unresolved particles are colour "connected" is necessarily more involved than that in section 7.3. In particular, we will need to intoduce new functions to describe this factorisation.

7.4.1 Triple Collinear Factorisation

When three colour "connected" particles cluster to form a single parent parton there are four basic clusterings,

$$ggg \to G, \qquad qgg \to Q,$$
$$g\bar{q}q \to G, \qquad q\bar{q}q \to Q,$$

and the colour ordered sub-amplitude squared for an n-parton process then factorises in the triple collinear limit,

$$|\mathcal{A}(\ldots, a, b, c, \ldots)|^2 \to P_{abc\to P}|\mathcal{A}(\ldots, P, \ldots)|^2. \tag{7.1}$$

As before, partons able to undergo antenna pinching are considered to be colour connected, so that there may be contributions from amplitudes such as $\mathcal{A}(\ldots, a, b|c, \ldots)$. The triple collinear splitting function for partons a, b and c clustering to form the parent parton P is generically,

$$P_{abc\to P}(w, x, y, s_{ab}, s_{ac}, s_{bc}, s_{abc}), \tag{7.2}$$

where w, x and y are the momentum fractions of the clustered partons,

$$p_a = wp_P, \qquad p_b = xp_P, \qquad p_c = yp_P, \qquad \text{with } w + x + y = 1. \tag{7.3}$$

In addition to depending on the momentum fractions carried by the clustering partons, the splitting function also depends on the invariant masses of parton-parton pairs and the

invariant mass of the whole cluster. In this respect, they are different from the splitting functions derived in the jet-calculus approach [64], and implemented in the shower Monte Carlo NLLJET [65], which depend only on the momentum fractions.

The triple collinear splitting functions $P_{abc\to P}$ are obtained by retaining terms in the full matrix element squared that possess two of the 'small' denominators s_{ab}, s_{ac}, s_{bc} and s_{abc}. As before, we consider the explicit forms of the $\gamma^* \to$ four and five parton squared matrix elements and work in conventional dimensional regularisation, with all external particles in $D = 4 - 2\epsilon$ dimensions. Similar results could be derived using helicity methods or by examining the on-shell limits of the recursive gluonic and quark currents of ref. [66].

Although the splitting functions are universal, and apply to any process involving the same three colour connected particles, for processes involving spin-1 particles, there are additional (non-universal) azimuthal correlations due to rotations of the polarisation vectors. These angular correlations do not contribute to the underlying infrared singularity structure and vanish after all azimuthal integrations have been carried out and we therefore systematically omit them. A discussion of the methods used to obtain the correct azimuthal dependence is contained in Appendix F.

Strong Ordering

A further check on our results is provided by the strong-ordered limit, where the particles become collinear sequentially rather than at the same time. In the limit where one of the double invariants is much smaller than the triple invariant, the triple collinear function should factorize into the product of two (usual) Altarelli-Parisi splitting functions, plus azimuthal terms [67].

As a concrete example, consider the splitting $(123) \to 1\,2\,3$ where $s_{12} \ll s_{123}$, with the particles carrying momentum fractions w, x and y of the parent momentum P. In the strong-ordered picture this corresponds to two consecutive splittings into fractions a and b, as shown in Fig. 7.4.

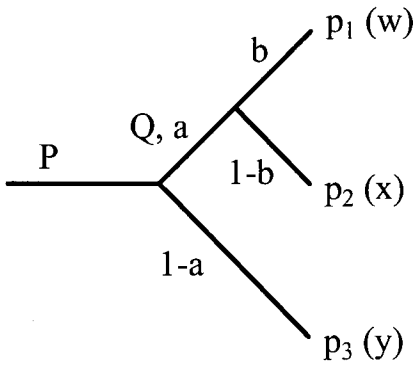

Figure 7.4: Consecutive splittings in the strong-ordered approach. The momentum carried by the intermediate parton (q) is Q.

Thus we expect,

$$P_{(123)\to 1\,2\,3}(w,x,y) = \frac{1}{s_{12}s_{123}}\left(P_{(123)\to q3}(a)P_{q\to 1\,2}(b) + \Phi_{(123)\to 1\,2\,3}(a,b)\right), \tag{7.4}$$

where $\Phi_{1\,2\,3}(a,b)$ represents angular correlations. In fact we know that these angular correlations are only present when the intermediate parton in the strong-ordered picture is a gluon and $\Phi_{1\,2\,3}(a,b) = 0$ otherwise.

From the relations,

$$\begin{aligned} p_1 &= wP = bQ, \\ p_2 &= xP = (1-b)Q, \\ p_3 &= yP = (1-a)P, \\ Q &= aP, \end{aligned}$$

we find that we should set,

$$a = 1-y, \qquad b = \frac{w}{1-y}. \tag{7.5}$$

We also have $s_{23}/s_{13} = (1-b)/b$ so that,

$$s_{13} = bs_{123}, \qquad s_{23} = (1-b)s_{123}.$$

By using these substitutions we can make comparisons with the expectations of the strong-ordered approach and thus provide further checks on the functions describing triple collinear emission which we shall present in the remainder of this section.

Three Collinear Gluons

Firstly, examining the sub-amplitudes for multiple gluon scattering, we find that the colour-ordered function $P_{ggg\to G}$ is given by,

$$\begin{aligned}
P_{abc\to G}(w,x,y,s_{ab},s_{bc},s_{abc}) = 8\times\Bigg\{ & \\
+\ & \frac{(1-\epsilon)}{s_{ab}^2 s_{abc}^2}\frac{(xs_{abc}-(1-y)s_{bc})^2}{(1-y)^2}+\frac{2(1-\epsilon)s_{bc}}{s_{ab}s_{abc}^2}+\frac{3(1-\epsilon)}{2s_{abc}^2} \\
+\ & \frac{1}{s_{ab}s_{abc}}\left(\frac{(1-y(1-y))^2}{yw(1-w)}-2\frac{x^2+xy+y^2}{1-y}+\frac{xw-x^2y-2}{y(1-y)}+2\epsilon\frac{x}{(1-y)}\right) \\
+\ & \frac{1}{2s_{ab}s_{bc}}\left(3x^2-\frac{2(2-w+w^2)(x^2+w(1-w))}{y(1-y)}+\frac{1}{yw}+\frac{1}{(1-y)(1-w)}\right)\Bigg\} \\
+\ & (s_{ab}\leftrightarrow s_{bc}, w\leftrightarrow y)+\text{azimuthal terms.}
\end{aligned} \tag{7.6}$$

This splitting function is symmetric under the exchange of the outer gluons a and c, and contains poles only in s_{ab} and s_{bc}.

Two Gluons with a Collinear Quark or Antiquark

There are two distinct splitting functions representing the clustering of two gluons and a quark which depend on whether or not the gluons are symmetrised over. In the unsymmetrised case, there will be poles in $s_{g_1g_2}$, due to contributions from the triple gluon vertex which are not present in the QED-like case. For the pure QCD splitting we find,

$$\begin{aligned}
P_{qg_1g_2\to Q}(w,x,y,s_{qg_1},s_{qg_2},s_{g_1g_2},s_{qg_1g_2}) = 4\times\Bigg\{ & \\
+\ & \frac{1}{s_{qg_1}s_{g_1g_2}}\left((1-\epsilon)\left(\frac{1+w^2}{y}+\frac{1+(1-y)^2}{(1-w)}\right)+2\epsilon\left(\frac{w}{y}+\frac{1-y}{1-w}\right)\right) \\
+\ & \frac{1}{s_{qg_1}s_{qg_1g_2}}\left((1-\epsilon)\left(\frac{(1-y)^3+w(1-x)-2y}{y(1-w)}\right)-\epsilon\left(\frac{2(1-y)(y-w)}{y(1-w)}-x\right)-\epsilon^2x\right)
\end{aligned}$$

$$+ \frac{1}{s_{g_1g_2}s_{qg_1g_2}}\left((1-\epsilon)\left(\frac{(1-y)^2(2-y)+x^3+2xw-2-y}{y(1-w)}\right)+2\epsilon\frac{(xw-y-2yw)}{y(1-w)}\right)$$
$$+ (1-\epsilon)\left(\frac{2\left(xs_{qg_1g_2}-(1-w)s_{qg_1}\right)^2}{s^2_{g_1g_2}s^2_{qg_1g_2}(1-w)^2}+\frac{1}{s^2_{qg_1g_2}}\left(4\frac{s_{qg_1}}{s_{g_1g_2}}+(1-\epsilon)\frac{s_{g_1g_2}}{s_{qg_1}}+(3-\epsilon)\right)\right)\Bigg\}, \quad (7.7)$$

while for the QED-like splitting where one or other or both gluons in the colour ordered amplitude are symmetrised over,

$$P_{q\tilde{g}_1\tilde{g}_2\to Q}(w,x,y,s_{qg_1},s_{qg_2},s_{qg_1g_2}) = 4\times\Bigg\{$$
$$+ \frac{1}{2s_{qg_1}s_{qg_2}}\frac{w}{xy}\left(1+w^2-\epsilon(x^2+xy+y^2)-\epsilon^2xy\right)$$
$$+ \frac{1}{s_{qg_1}s_{qg_1g_2}}\frac{1}{xy}\left(w(1-x+\epsilon^2xy)+(1-y)^3-\epsilon(1-y)(x^2+xy+y^2)+\epsilon^2xy\right)$$
$$- \frac{(1-\epsilon)}{s^2_{qg_1g_2}}\left((1-\epsilon)\frac{s_{qg_1}}{s_{qg_2}}-\epsilon\right)\Bigg\}+(s_{qg_1}\leftrightarrow s_{qg_2},x\leftrightarrow y). \quad (7.8)$$

The function $P_{q\tilde{g}_1\tilde{g}_2\to Q}$ can be interpreted as the relevant triple collinear splitting function with one or both of the gluons replaced by photons. As such, this result echoes that found in [68] for $P_{qg\gamma\to Q}$. Using charge conjugation, we see that the functions representing clustering of two gluons with an antiquark are simply,

$$\begin{aligned} P_{g_1g_2\bar{q}\to\overline{Q}}(w,x,y,s_{g_1g_2},s_{g_2\bar{q}},s_{g_1\bar{q}},s_{g_1g_2\bar{q}}) &= P_{qg_1g_2\to Q}(y,x,w,s_{\bar{q}g_2},s_{\bar{q}g_1},s_{g_1g_2},s_{g_1g_2\bar{q}}), \\ P_{\tilde{g}_1\tilde{g}_2\bar{q}\to\overline{Q}}(w,x,y,s_{g_2\bar{q}},s_{g_1\bar{q}},s_{g_1g_2\bar{q}}) &= P_{q\tilde{g}_1\tilde{g}_2\to Q}(y,x,w,s_{\bar{q}g_2},s_{\bar{q}g_1},s_{g_1g_2\bar{q}}). \end{aligned} \quad (7.9)$$

A Quark-Antiquark Pair with a Collinear Gluon

Similarly the clustering of a gluon with a quark-antiquark pair into a parent gluon again has two distinct functions. For example, there is a singular contribution from the four quark matrix elements when $\overline{Q}_4$, Q_3 and the gluon cluster,

$$\begin{aligned} \left|\mathcal{T}^A_\mu(Q_1,\overline{Q}_2;Q_3,\overline{Q}_4;1)V^\mu\right|^2 &= \left|\mathcal{A}^{Q_1Q_2}_\mu(Q_1;1;\overline{Q}_4|Q_3;\overline{Q}_2)V^\mu+\mathcal{A}^{Q_3Q_4}_\mu(Q_3;\overline{Q}_2|Q_1;1;\overline{Q}_4)V^\mu\right|^2 \\ &\to P_{1\overline{Q}_4Q_3\to G}\left|\mathcal{S}^3_\mu V^\mu\right|^2. \end{aligned}$$

Here, the singular contribution comes entirely from the first $\mathcal{A}$ term where combining $\overline{Q}_4$, Q_3 pinches the two colour lines together. Explicit evaluation yields,

$$
\begin{aligned}
P_{g\bar{q}q\to G}(w,x,y,s_{g\bar{q}},s_{\bar{q}q},s_{g\bar{q}q}) = 4\times\Bigg\{ & \\
-\ & \frac{1}{s^2_{g\bar{q}q}}\left(4\frac{s_{g\bar{q}}}{s_{\bar{q}q}}+(1-\epsilon)\frac{s_{\bar{q}q}}{s_{g\bar{q}}}+(3-\epsilon)\right)-\frac{2\left(xs_{g\bar{q}q}-(1-w)s_{g\bar{q}}\right)^2}{s^2_{\bar{q}q}s^2_{g\bar{q}q}(1-w)^2} \\
+\ & \frac{1}{s_{g\bar{q}}s_{g\bar{q}q}}\left(\frac{(1-y)}{w(1-w)}-y-2w-\epsilon-\frac{2x(1-y)(y-w)}{(1-\epsilon)w(1-w)}\right) \\
+\ & \frac{y}{s_{g\bar{q}}s_{\bar{q}q}}\left(\frac{x\left((1-w)^3-w^3\right)}{w(1-w)}-\frac{2x^2\left(1-yw-(1-y)(1-w)\right)}{(1-\epsilon)w(1-w)}\right) \\
+\ & \frac{1}{s_{\bar{q}q}s_{g\bar{q}q}}\left(\frac{(1+w^3+4xw)}{w(1-w)}+\frac{2x\left(w(x-y)-y(1+w)\right)}{(1-\epsilon)w(1-w)}\right)\Bigg\}+\text{azimuthal terms}
\end{aligned}
\tag{7.10}
$$

Again applying charge conjugation yields the further relation,

$$
P_{\bar{q}qg\to G}(w,x,y,s_{\bar{q}q},s_{qg},s_{\bar{q}qg}) = P_{g\bar{q}q\to G}(y,x,w,s_{gq},s_{\bar{q}q},s_{\bar{q}qg}), \tag{7.11}
$$

describing instances where the gluon is colour connected to the quark rather than the anti-quark.

There is a further contribution when the quark-antiquark and gluon combine to form a photon-like colour singlet. This occurs when,

$$
\begin{aligned}
\left|\mathcal{T}^B_\mu(Q_3,\overline{Q}_2;Q_1,\overline{Q}_4;1)V^\mu\right|^2 &= \left|\mathcal{B}^{Q_3Q_4}_\mu(Q_3;1;\overline{Q}_4|Q_1;\overline{Q}_2)V^\mu+\mathcal{B}^{Q_1Q_2}_\mu(Q_1;\overline{Q}_2|Q_3;1;\overline{Q}_4)V^\mu\right|^2 \\
&\to P_{Q_3\tilde{1}\overline{Q}_4\to\tilde{G}}\left|\mathcal{S}^3_\mu V^\mu\right|^2.
\end{aligned}
$$

In this case the singular contribution is produced by the second $\mathcal{B}$ term and is due to the entire $Q_3;1;\overline{Q}_4$ antenna pinching to form a gluon which is then inserted in a symmetrised way (i.e. with a tilde) into the remaining colour antenna. This QED-like splitting function is given by,

$$
\begin{aligned}
P_{qg\bar{q}\to\tilde{G}}(w,x,y,s_{qg},s_{g\bar{q}},s_{\bar{q}q},s_{qg\bar{q}}) = 4\times\Bigg\{ & \\
-\ & \frac{1}{s^2_{qg\bar{q}}}\left((1-\epsilon)\frac{s_{q\bar{q}}}{s_{qg}}+1\right)+\frac{1}{s_{g\bar{q}}s_{qg}}\left((1+x^2)-\frac{x+2wy}{1-\epsilon}\right) \\
-\ & \frac{1}{s_{qg}s_{qg\bar{q}}}\left(1+2x+\epsilon-\frac{2(1-y)}{(1-\epsilon)}\right)\Bigg\}+(s_{qg}\leftrightarrow s_{g\bar{q}},w\leftrightarrow y)+\text{azimuthal terms.}
\end{aligned}
\tag{7.12}
$$

A Quark-Antiquark Pair with a Collinear Quark or Antiquark

Lastly, we consider the clustering of a quark-antiquark pair $(Q\overline{Q})$ and a quark (q) to form a parent quark q' with the same flavour as q. The splitting function depends upon whether or not the quarks are identical,

$$P_{q\overline{Q}Q\to q'} = P^{\text{non-ident.}}_{q\overline{Q}Q\to q'} - \frac{\delta_{qQ}}{N} P^{\text{ident.}}_{q\overline{Q}Q\to q'}, \tag{7.13}$$

where $\delta_{qQ} = 1$ for identical quarks. If quarks Q_1, Q_3 and $\overline{Q}_4$ are clustered to form Q, then we find a non-identical quark contribution,

$$\begin{aligned}\left|\mathcal{T}^A_\mu(Q_3,\overline{Q}_4;Q_1,\overline{Q}_2;1)V^\mu\right|^2 &= \left|\mathcal{A}^{Q_3Q_4}_\mu(Q_3;1;\overline{Q}_2|Q_1;\overline{Q}_4)V^\mu + \mathcal{A}^{Q_1Q_2}_\mu(Q_1;\overline{Q}_4|Q_3;1;\overline{Q}_2)V^\mu\right|^2 \\ &\to P^{\text{non-ident.}}_{Q_1\overline{Q}_4Q_3\to Q}\left|\mathcal{S}^3_\mu V^\mu\right|^2,\end{aligned}$$

with,

$$\begin{aligned}P^{\text{non-ident.}}_{q\overline{Q}Q\to q'}(w,x,y,s_{q\overline{Q}},s_{Q\overline{Q}},s_{qQ\overline{Q}}) = 4\times\Bigg\{&-\frac{1}{s^2_{qQ\overline{Q}}}\left((1-\epsilon)+\frac{2s_{q\overline{Q}}}{s_{Q\overline{Q}}}\right) \\ &-\frac{2\left(xs_{qQ\overline{Q}}-(1-w)s_{q\overline{Q}}\right)^2}{s^2_{Q\overline{Q}}s^2_{qQ\overline{Q}}(1-w)^2}+\frac{1}{s_{Q\overline{Q}}s_{qQ\overline{Q}}}\left(\frac{1+x^2+(x+w)^2}{(1-w)}-\epsilon(1-w)\right)\Bigg\}.\end{aligned} \tag{7.14}$$

The singular contribution is now generated by the square of the second $\mathcal{A}$ term; pinching Q_3 and $\overline{Q}_4$ together connects the two colour antennae together and combining with Q_1 ensures that the vector boson couples to a flavour singlet $Q_1\overline{Q}_2$ pair. Precisely the same function describes the triple collinear limit of the $\mathcal{T}^B$ functions. We find that in the same limit,

$$\begin{aligned}\left|\mathcal{T}^B_\mu(Q_1,\overline{Q}_4;Q_3,\overline{Q}_2;1)V^\mu\right|^2 &= \left|\mathcal{B}^{Q_1Q_2}_\mu(Q_1;1;\overline{Q}_2|Q_3;\overline{Q}_4)V^\mu + \mathcal{B}^{Q_3Q_4}_\mu(Q_3;\overline{Q}_4|Q_1;1;\overline{Q}_2)V^\mu\right|^2 \\ &\to P^{\text{non-ident.}}_{Q_1\overline{Q}_4Q_3\to Q}\left|\mathcal{S}^3_\mu V^\mu\right|^2,\end{aligned}$$

where this time the first term alone contributes. Here Q_3 and $\overline{Q}_4$ combine to form a photon which clusters with Q_1. As before, charge conjugation generates the associated function for an antiquark combining with a quark-antiquark pair,

$$P^{\text{non-ident.}}_{\overline{q}Q\overline{Q}\to\overline{q}'}(w,x,y,s_{\overline{q}Q},s_{Q\overline{Q}},s_{\overline{q}Q\overline{Q}}) = P^{\text{non-ident.}}_{q\overline{Q}Q\to q'}(w,x,y,s_{q\overline{Q}},s_{Q\overline{Q}},s_{qQ\overline{Q}}). \tag{7.15}$$

When the flavours of the clustering quarks are the same, there is an additional contribution coming from the interference terms of the four-quark matrix elements. For instance, when Q_1, $\overline{Q}_4$ and Q_3 combine,

$$\begin{aligned}
&\Re\left(\mathcal{T}_\mu^A(Q_3,\overline{Q}_4;Q_1,\overline{Q}_2;1)V^\mu\right)\left(\mathcal{T}_\mu^B(Q_3,\overline{Q}_4;Q_1,\overline{Q}_2;1)V^\mu\right)^\dagger \\
&\quad\sim\ \mathcal{A}_\mu^{Q_3Q_4}(Q_3;1;\overline{Q}_2|Q_1;\overline{Q}_4)V^\mu\left(\mathcal{B}_\mu^{Q_3Q_2}(Q_3;1;\overline{Q}_2|Q_1;\overline{Q}_4)V^\mu\right)^\dagger \\
&\quad\to\ -\frac{1}{2}P^{\text{ident.}}_{Q_1\overline{Q}_4Q_3\to Q}\left|\mathcal{S}^3_\mu V^\mu\right|^2,
\end{aligned}$$

where,

$$\begin{aligned}
&P^{\text{ident.}}_{q\overline{Q}Q\to q'}(w,x,y,s_{q\overline{Q}},s_{Q\overline{Q}},s_{qQ\overline{Q}}) = 4\times\Bigg\{ \\
&-\ \frac{(1-\epsilon)}{s^2_{qQ\overline{Q}}}\left(\frac{2s_{q\overline{Q}}}{s_{Q\overline{Q}}}+2+\epsilon\right)-\frac{1}{2s_{q\overline{Q}}s_{Q\overline{Q}}}\left(\frac{x(1+x^2)}{(1-y)(1-w)}-\epsilon x\left(\frac{2(1-y)}{(1-w)}+1+\epsilon\right)\right) \\
&+\ \frac{1}{s_{Q\overline{Q}}s_{qQ\overline{Q}}}\left(\frac{1+x^2}{(1-y)}+\frac{2x}{(1-w)}-\epsilon\left(\frac{(1-w)^2}{(1-y)}+(1+x)+\frac{2x}{(1-w)}+\epsilon(1-w)\right)\right)\Bigg\} \\
&+\ (s_{q\overline{Q}}\leftrightarrow s_{Q\overline{Q}},y\leftrightarrow w).
\end{aligned}\tag{7.16}$$

Here, there are poles in the matrix elements when $\overline{Q}_4$ clusters with both Q_3 and Q_1 and the triple collinear function is symmetric under $q\leftrightarrow Q$.

The $N=1$ SUSY Identity

These triple-collinear splitting functions, like the ordinary Altarelli-Parisi splitting kernels, can be related by means of an $N=1$ supersymmetry identity. In unbroken supersymmetric theories, the masses of gluon and gluino are identical thereby ensuring that the self-energies of the two particles are equal. By considering all two particle cuts of the one-loop diagrams contributing to these self-energies, we obtain a relation between the colour stripped Altarelli-Parisi kernels,

$$P_{gg\to g}(z)+P_{q\bar{q}\to g}(z)=P_{qg\to q}(z)+P_{gq\to q}(z). \tag{7.17}$$

Here the quark plays the role of the gluino. Note that in conventional dimensional regularisation the number of degrees of freedom for the gluon and gluino are no longer equal and

the supersymmetry is broken. Therefore this result is not true away from four dimensions[1]. Similarly, by considering the three particle cuts of the relevant two-loop contributions to the self energies (as in Figure 7.5), and omitting the invariants in the arguments of the functions, we find,

$$\sum_{P(a,b,c)} \left(P_{ggg\to G}(a,b,c) + 2P_{g\tilde{q}\bar{q}\to G}(a,b,c) + P_{q\tilde{g}\bar{q}\to G}(a,b,c) \right) = \tag{7.18}$$
$$\sum_{P(a,b,c)} \left(2P_{qgg\to Q}(a,b,c) + P_{q\tilde{g}\tilde{g}\to Q}(a,b,c) + 2P^{\text{non-ident.}}_{q\bar{q}q\to Q}(a,b,c) + P^{\text{ident.}}_{q\bar{q}q\to Q}(a,b,c) \right),$$

provided we set $\epsilon = 0$. This non-trivial relation between the splitting functions is a further check on the results presented in this section.

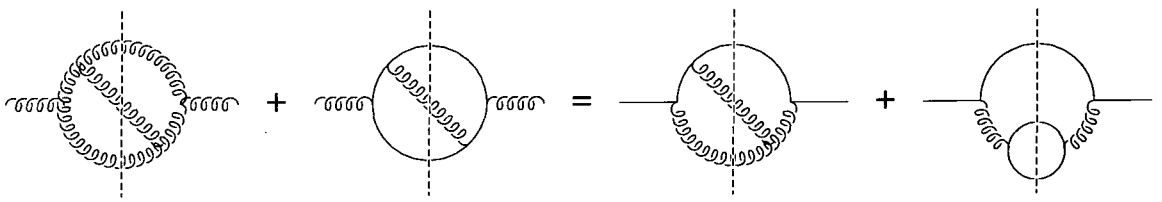

Figure 7.5: A diagrammatic representation of the equality between the gluon and gluino self-energies in $N = 1$ SUSY. The dashed lines represent the three-particle cuts that lead to the relation between the triple collinear splitting functions given in equation 7.18.

Triple Collinear Limit of $e^+e^- \to 5$ Partons

Examining the two-quark currents in the triple collinear limit is now straightforward. Summing over all triple collinear limits, we find,

$$\begin{aligned}
\left|\mathcal{S}_\mu(Q_1;1,2,3;\overline{Q}_2)V^\mu\right|^2 &\to \left(P_{Q_1 12\to Q} + P_{123\to G} + P_{23\overline{Q}_2\to\overline{Q}}\right)\left|\mathcal{S}^3_\mu V^\mu\right|^2, \\
\left|\mathcal{S}_\mu(Q_1;1,2,\tilde{3};\overline{Q}_2)V^\mu\right|^2 &\to \left(P_{Q_1 12\to Q} + P_{12\overline{Q}_2\to\overline{Q}} + P_{Q_1\tilde{1}\tilde{3}\to Q} + P_{\tilde{2}\tilde{3}\overline{Q}_2\to\overline{Q}}\right)\left|\mathcal{S}^3_\mu V^\mu\right|^2, \\
\left|\mathcal{S}_\mu(Q_1;\tilde{1},\tilde{2},\tilde{3};\overline{Q}_2)V^\mu\right|^2 &\to \frac{1}{2}\sum_{P(1,2,3)}\left(P_{Q_1\tilde{1}\tilde{2}\to Q} + P_{\tilde{2}\tilde{3}\overline{Q}_2\to\overline{Q}}\right)\left|\mathcal{S}^3_\mu V^\mu\right|^2.
\end{aligned} \tag{7.19}$$

[1]Other variants of dimensional regularisation where the gluon and gluino degrees of freedom are equal, such as dimensional reduction discussed in chapter 2, preserve the symmetry, and therefore the relation, for $D \neq 4$.

The four-quark current contributions are more complicated, but in each case yield factors multiplying the two-quark current,

$$\begin{aligned}
\left|\mathcal{T}^A_\mu(Q_1,\overline{Q}_2;Q_3,\overline{Q}_4;1)V^\mu\right|^2 &\to \left(P_{1\overline{Q}_4Q_3\to G}+P_{\overline{Q}_2Q_1 1\to G}\right.\\
&\quad \left.+P^{\text{non-ident.}}_{\overline{Q}_2Q_3\overline{Q}_4\to\overline{Q}}+P^{\text{non-ident.}}_{Q_3\overline{Q}_2Q_1\to Q}\right)\left|\mathcal{S}^3_\mu V^\mu\right|^2,\\
\left|\mathcal{T}^B_\mu(Q_1,\overline{Q}_4;Q_3,\overline{Q}_2;1)V^\mu\right|^2 &\to \left(P_{Q_1\tilde{1}\overline{Q}_2\to\tilde{G}}+P^{\text{non-ident.}}_{\overline{Q}_2Q_3\overline{Q}_4\to\overline{Q}}+P^{\text{non-ident.}}_{Q_1\overline{Q}_4Q_3\to Q}\right)\left|\mathcal{S}^3_\mu V^\mu\right|^2,\\
\left|\overline{\mathcal{T}}_\mu(Q_1,\overline{Q}_2;Q_3,\overline{Q}_4;1)V^\mu\right|^2 &\to \left(P_{Q_1\tilde{1}\overline{Q}_2\to\tilde{G}}+P^{\text{non-ident.}}_{\overline{Q}_2Q_3\overline{Q}_4\to\overline{Q}}+P^{\text{non-ident.}}_{Q_1\overline{Q}_4Q_3\to Q}\right.\\
&\quad \left.+P_{Q_3\tilde{1}\overline{Q}_4\to\tilde{G}}+P^{\text{non-ident.}}_{\overline{Q}_4Q_1\overline{Q}_2\to\overline{Q}}+P^{\text{non-ident.}}_{Q_3\overline{Q}_2Q_1\to Q}\right)\left|\mathcal{S}^3_\mu V^\mu\right|^2,\\
\Re\left(\overline{\mathcal{T}}_\mu(Q_1,\overline{Q}_2;Q_3,\overline{Q}_4;1)V^\mu\right)&\left(\overline{\mathcal{T}}_\mu(Q_1,\overline{Q}_4;Q_3,\overline{Q}_2;1)V^\mu\right)^\dagger\\
&\to -\frac{1}{2}\left(P^{\text{ident.}}_{Q_1\overline{Q}_2Q_3\to Q}+P^{\text{ident.}}_{Q_3\overline{Q}_4Q_1\to Q}+P^{\text{ident.}}_{\overline{Q}_2Q_3\overline{Q}_4\to\overline{Q}}+P^{\text{ident.}}_{\overline{Q}_4Q_1\overline{Q}_2\to\overline{Q}}\right)\left|\mathcal{S}^3_\mu V^\mu\right|^2,\\
\Re\left(\mathcal{T}^A_\mu(Q_1,\overline{Q}_2;Q_3,\overline{Q}_4;1)V^\mu\right)&\left(\mathcal{T}^B_\mu(Q_1,\overline{Q}_2;Q_3,\overline{Q}_4;1)V^\mu\right)^\dagger\\
&\to -\frac{1}{2}\left(P^{\text{ident.}}_{Q_1\overline{Q}_2Q_3\to Q}+P^{\text{ident.}}_{\overline{Q}_2Q_3\overline{Q}_4\to\overline{Q}}\right)\left|\mathcal{S}^3_\mu V^\mu\right|^2. \qquad (7.20)
\end{aligned}$$

Combining these limits and eliminating the identical particle factors where appropriate provides the triple collinear singular factor for the five parton squared matrix elements,

$$\begin{aligned}
\frac{1}{3!}\left|\widehat{\mathcal{S}}^5_\mu V^\mu\right|^2+\left|\widehat{\mathcal{T}}^5_\mu V^\mu\right|^2 &= \left(\frac{g^2N}{2}\right)^2\left|\widehat{\mathcal{S}}^3_\mu V^\mu\right|^2\\
\times\ &\left[P_{123\to G}+\left(\frac{N^2-1}{N^2}\right)\left(P_{Q_1 12\to Q}+P_{12\overline{Q}_2\to\overline{Q}}\right)-\left(\frac{N^2-1}{2N^4}\right)\left(P_{Q_1\tilde{1}\tilde{3}\to Q}+P_{\tilde{2}\tilde{3}\overline{Q}_2\to\overline{Q}}\right)\right.\\
&+\frac{n_F}{N}\left(P_{1\overline{Q}_4Q_3\to G}+P_{\overline{Q}_4Q_3 1\to G}-\frac{1}{N^2}P_{Q_3\tilde{1}\overline{Q}_4\to\tilde{G}}\right)\\
&\left.+\frac{n_F}{N}\left(\frac{N^2-1}{N^2}\right)\left(P^{\text{non-ident.}}_{Q_1\overline{Q}_4Q_3\to Q}-\frac{1}{N}P^{\text{ident.}}_{Q_1\overline{Q}_4Q_3\to Q}+P^{\text{non-ident.}}_{\overline{Q}_2Q_3\overline{Q}_4\to\overline{Q}}-\frac{1}{N}P^{\text{ident.}}_{\overline{Q}_2Q_3\overline{Q}_4\to\overline{Q}}\right)\right] \qquad (7.21)
\end{aligned}$$

7.4.2 Soft/Collinear Factorisation

We now examine the configurations where one gluon is soft and two particles are collinear. In this case, the sub-amplitudes factorise as,

$$|\mathcal{A}(\ldots,d,\ldots,a,b,c,\ldots)|^2\to P_{d;abc}|\mathcal{A}(\ldots,d,\ldots,P,\ldots)|^2, \qquad (7.22)$$

where gluon a is soft, partons b and c are collinear and either colour connected or able to undergo antenna pinching. Parton d is the adjacent colour-connected hard parton in the antenna containing the soft gluon. If a is symmetrised over ($\tilde{a}$, so QED-like) then d is the quark in that colour-line; otherwise d is simply the parton adjacent to a. In this limit the collinear partons form parton P and carry momentum fractions,

$$p_b = x p_P, \qquad p_c = (1-x) p_P, \tag{7.23}$$

and we write the soft/collinear factor as,

$$P_{d;abc}(x, s_{ab}, s_{bc}, s_{abc}, s_{ad}, s_{bd}, s_{cd}). \tag{7.24}$$

To determine the limiting behaviour, we again consider the explicit forms of the $\gamma^* \to$ four and five parton squared matrix elements. All terms that possess three of the 'small' denominators s_{ab}, s_{ad}, s_{bc} and s_{abc} contribute in the soft/collinear limit. Similar results could be derived using helicity methods or by examining the on-shell limits of the recursive gluonic and quark currents of ref. [66]. Alternatively, these limits can be obtained directly from the triple collinear limits of sect. 5.1, by keeping only terms proportional to $1/w$ and subsequently replacing $1/w$ by $(s_{bd}+s_{cd})/s_{ad}$, $1/(1-w)$ by 1 and y by $1-x$.

In fact, in this limit we find a universal soft factor multiplied by a collinear splitting function,

$$P_{d;abc}(x, s_{ab}, s_{bc}, s_{abc}, s_{ad}, s_{bd}, s_{cd}) = S_{d;abc}(x, s_{ab}, s_{bc}, s_{abc}, s_{ad}, s_{bd}, s_{cd}) P_{bc\to P}(x, s_{bc}), \tag{7.25}$$

where,

$$S_{d;abc}(z, s_{ab}, s_{bc}, s_{abc}, s_{ad}, s_{bd}, s_{cd}) = \frac{2(s_{bd}+s_{cd})}{s_{ab}s_{ad}} \left(z + \frac{(s_{ab}+z s_{bc})}{s_{abc}} \right). \tag{7.26}$$

A similar result holds for gluon c becoming soft,

$$|\mathcal{A}(\ldots, a, b, c, \ldots, e, \ldots)|^2 \to P_{abc;e} |\mathcal{A}(\ldots, P, \ldots, e, \ldots)|^2, \tag{7.27}$$

where,

$$P_{abc;e} = P_{d;abc}(a \leftrightarrow c, d \leftrightarrow e). \tag{7.28}$$

In the case that b is soft the matrix elements do not possess sufficient singularities since the collinear particles a and c are not directly colour-connected,

$$|\mathcal{A}(\ldots, a, b, c, \ldots)|^2 \to \text{less singular.} \tag{7.29}$$

Here, there may be two powers of the small invariants in the denominator, but, when integrated over the appropriate (small) region of phase space this yields a vanishing contribution. On the other hand, for QED-like subamplitudes where the gluons are symmetrised there is a non-zero contribution when either gluon is soft. Note that in all cases where the soft particle is a quark or antiquark, there is also no singular contribution.

Soft/Collinear Limit of $e^+e^- \to 5$ Partons

For the specific case of the two-quark currents, the sum over all soft/collinear limits is easily obtained,

$$\begin{aligned}
\left|\mathcal{S}_\mu(Q_1;1,2,3;\overline{Q}_2)V^\mu\right|^2 &\to \left(P_{Q_1 12;3} + P_{Q_1;123} + P_{123;\overline{Q}_2} + P_{1;23\overline{Q}_2}\right)\left|\mathcal{S}^3_\mu V^\mu\right|^2, \\
\left|\mathcal{S}_\mu(Q_1;1,2,\tilde{3};\overline{Q}_2)V^\mu\right|^2 &\to \left(P_{Q_1;12\overline{Q}_2} + P_{1Q_1\tilde{3};\overline{Q}_2} + P_{\tilde{3}Q_1 1;2}\right. \\
&\quad \left. + P_{Q_1;\tilde{3}\overline{Q}_2 2} + P_{Q_1 12;\overline{Q}_2} + P_{\tilde{3}\overline{Q}_2 2;1}\right)\left|\mathcal{S}^3_\mu V^\mu\right|^2, \\
\left|\mathcal{S}_\mu(Q_1;\tilde{1},\tilde{2},\tilde{3};\overline{Q}_2)V^\mu\right|^2 &\to \sum_{P(1,2,3)} \left(P_{\tilde{1}Q_1\tilde{2};\overline{Q}_2} + P_{Q_1;\tilde{2}\overline{Q}_2\tilde{3}}\right)\left|\mathcal{S}^3_\mu V^\mu\right|^2.
\end{aligned} \tag{7.30}$$

The only non-vanishing contributions in the soft/collinear limit from the four-quark currents are,

$$\begin{aligned}
\left|\mathcal{T}^A_\mu(Q_1,\overline{Q}_2;Q_3,\overline{Q}_4;1)V^\mu\right|^2 &\to \left(P_{Q_1;1\overline{Q}_4 Q_3} + P_{\overline{Q}_2 Q_1 1;\overline{Q}_4}\right)\left|\mathcal{S}^3_\mu V^\mu\right|^2, \\
\left|\overline{\mathcal{T}}_\mu(Q_1,\overline{Q}_2;Q_3,\overline{Q}_4;1)V^\mu\right|^2 &\to \left(S_{Q_1 1\overline{Q}_2} P_{Q_3\overline{Q}_4\to G} + S_{Q_3 1\overline{Q}_4} P_{Q_1\overline{Q}_2\to G}\right. \\
&\quad + P_{Q_1;1\overline{Q}_4 Q_3} - P_{Q_1;1Q_3\overline{Q}_4} - P_{\overline{Q}_2;1\overline{Q}_4 Q_3} + P_{\overline{Q}_2;1Q_3\overline{Q}_4} \\
&\quad \left. + P_{Q_3;1\overline{Q}_2 Q_1} - P_{Q_3;1Q_1\overline{Q}_2} - P_{\overline{Q}_4;1\overline{Q}_2 Q_1} + P_{\overline{Q}_4;1Q_1\overline{Q}_2}\right)\left|\mathcal{S}^3_\mu V^\mu\right|^2,
\end{aligned} \tag{7.31}$$

where the second term also includes both the unconnected soft/collinear contribution and interferences amongst the various subamplitudes. This is akin to the case of single soft gluon

emission where we have,

$$\mathcal{A}(\ldots,a,g,b,\ldots) \to \left(\frac{p_a\cdot\epsilon}{p_a\cdot p_g}-\frac{p_b\cdot\epsilon}{p_b\cdot p_g}\right)\mathcal{A}(\ldots,a,b,\ldots),$$

and therefore,

$$\begin{aligned}&\Re\left(\mathcal{A}(\ldots,a,g,b,\ldots,c,d,\ldots)\right)\left(\mathcal{A}(\ldots,a,b,\ldots,c,g,d,\ldots)\right)^\dagger\\ &\qquad\to -\frac{1}{2}\left(S_{agc}-S_{agd}-S_{bgc}+S_{bgd}\right)\left|\mathcal{A}(\ldots,a,b,\ldots,c,d,\ldots)\right|^2.\end{aligned}$$

Here, the soft factors are generated by the interference of the two eikonal factors.

$$\sum_{\text{pols}}\left(\frac{p_a\cdot\epsilon}{p_a\cdot p_g}-\frac{p_b\cdot\epsilon}{p_b\cdot p_g}\right)\left(\frac{p_c\cdot\epsilon^*}{p_c\cdot p_g}-\frac{p_d\cdot\epsilon^*}{p_d\cdot p_g}\right).$$

Adding up these limits for the five parton squared matrix elements gives,

$$\begin{aligned}&\frac{1}{3!}\left|\widehat{\mathcal{S}}^5_\mu V^\mu\right|^2+\left|\widehat{\mathcal{T}}^5_\mu V^\mu\right|^2=\left(\frac{g^2N}{2}\right)^2\left|\widehat{\mathcal{S}}^3_\mu V^\mu\right|^2\\ &\times\Bigg[P_{Q_1 12;3}+P_{Q_1;123}+P_{123;\overline{Q}_2}+P_{1;23\overline{Q}_2}\\ &\quad-\frac{1}{N^2}\left(P_{Q_1;12\overline{Q}_2}+P_{Q_1 12;\overline{Q}_2}+P_{\tilde{3}Q_1 1;2}+P_{\tilde{3}\overline{Q}_2 2;1}\right)+\frac{1}{N^4}\left(P_{\tilde{1}Q_1\tilde{2};\overline{Q}_2}+P_{Q_1;\tilde{2}\overline{Q}_2\tilde{3}}\right)\\ &\quad+\frac{2n_F}{N}P_{Q_1;1\overline{Q}_4Q_3}\\ &\quad-\frac{2n_F}{N^3}\left(S_{Q_1 1\overline{Q}_2}P_{Q_3\overline{Q}_4\to G}+P_{Q_1;1\overline{Q}_4Q_3}-P_{Q_1;1Q_3\overline{Q}_4}-P_{\overline{Q}_2;1\overline{Q}_4Q_3}+P_{\overline{Q}_2;1Q_3\overline{Q}_4}\right)\Bigg].\end{aligned}\tag{7.32}$$

7.4.3 Two Soft Gluons

Finally, we consider the contributions where two colour connected gluons are simultaneously soft. This was first studied by Berends and Giele [63] and we include this contribution here for the sake of completeness. Similar results have been discussed by Catani [69]. For gluons b and c soft the colour ordered subamplitudes factorise,

$$\left|\mathcal{A}(\ldots,a,b,c,d,\ldots,)\right|^2\to S_{abcd}(s_{ad},s_{ab},s_{cd},s_{bc},s_{abc},s_{bcd})\left|\mathcal{A}(\ldots,a,d,\ldots)\right|^2.\tag{7.33}$$

where the connected double soft gluon function is given by,

$$S_{abcd}(s_{ad}, s_{ab}, s_{cd}, s_{bc}, s_{abc}, s_{bcd}) = \frac{8s_{ad}^2}{s_{ab}s_{bcd}s_{abc}s_{cd}} + \frac{8s_{ad}}{s_{bc}}\left(\frac{1}{s_{ab}s_{cd}} + \frac{1}{s_{ab}s_{bcd}} + \frac{1}{s_{cd}s_{abc}} - \frac{4}{s_{abc}s_{bcd}}\right) + \frac{8(1-\epsilon)}{s_{bc}^2}\left(\frac{s_{ab}}{s_{abc}} + \frac{s_{cd}}{s_{bcd}} - 1\right)^2. \quad (7.34)$$

Here a and d are the hard partons surrounding the soft pair and may either be gluons or quark/antiquarks. In four dimensions, the double soft factor can be extracted from [63] by squaring and summing the helicity amplitudes for two adjacent soft gluons. Alternatively, it can be obtained by explicitly taking the double soft limit of squared matrix elements for processes involving more than two gluons.

Double Soft Limit of $e^+e^- \to 5$ Partons

As before, for the specific case of the two-quark currents, the connected double soft limit is easily obtained and summing over all contributions we find,

$$\begin{aligned}
\left|\mathcal{S}_\mu(Q_1;1,2,3;\overline{Q}_2)V^\mu\right|^2 &\to \left(S_{Q_1123} + S_{123\overline{Q}_2}\right)\left|\mathcal{S}_\mu^3 V^\mu\right|^2, \\
\left|\mathcal{S}_\mu(Q_1;1,2,\tilde{3};\overline{Q}_2)V^\mu\right|^2 &\to S_{Q_112\overline{Q}_2}\left|\mathcal{S}_\mu^3 V^\mu\right|^2, \\
\left|\mathcal{S}_\mu(Q_1;\tilde{1},\tilde{2},\tilde{3};\overline{Q}_2)V^\mu\right|^2 &\to \text{less singular.}
\end{aligned} \quad (7.35)$$

Combining these limits yields the double soft singular factor for the full squared matrix elements,

$$\frac{1}{3!}\left|\widehat{\mathcal{S}}_\mu^5 V^\mu\right|^2 + \left|\widehat{\mathcal{T}}_\mu^5 V^\mu\right|^2 = \left(\frac{g^2N}{2}\right)^2 \left|\widehat{\mathcal{S}}_\mu^3 V^\mu\right|^2 \left[S_{Q_1123} + S_{123\overline{Q}_2} - \frac{1}{N^2}S_{Q_112\overline{Q}_2}\right]. \quad (7.36)$$

7.5 Summary

In this chapter we have discussed the factorisation properties of squared tree level QCD matrix elements when two particles are unresolved. These properties allow the analytic isolation of the infrared singularities from $(n+2)$ parton scattering processes that would be vital in a next-next-to-leading order calculation of a n-jet-like quantity.

At next-to-next-to-leading order, this knowledge is required for the analytic isolation of infrared singularities of $(n+2)$ parton scattering processes and subsequent numerical combination with the one-loop $(n+1)$ parton (single unresolved particle) and two-loop n parton contributions.

The unresolved particles may be either soft gluons or groups of collinear particles or combinations of both. There are four double unresolved cases; two soft gluons, three simultaneously collinear particles, two independent pairs of collinear particles and one soft gluon together with a collinear pair. In section 7.3 we reviewed the (trivial) factorisation that occurs when the unresolved particles are colour "unconnected". Such factorisation is well known and involves only the familar eikonal and Altarelli-Parisi splitting kernels used to describe single unresolved emission (see the introduction).

When the unresolved particles are all colour "connected", we find a similar factorisation. In section 7.4 we introduced new functions to describe the triple collinear and soft/collinear limits in addition to recalling the known double soft gluon limits of Berends and Giele [63]. These functions are universal and apply to general multiparton scattering amplitudes. As a check on our results, we find that the triple collinear splitting functions obey an expected $N=1$ SUSY identity. In addition, in the strong ordered limit, where one particle is much more unresolved than the other, these factors become simple products of single unresolved factors, one associated with each unresolved particle.

To illustrate the use of these double unresolved approximations, we have examined the singular limits of the tree level matrix elements for $e^+e^- \to 5$ partons [70]. In each case, we find that in the singular limit, the matrix elements can be approximated by a singular factor multiplying the tree level $e^+e^- \to 3$ parton matrix elements. As we discussed in section 7.2, these approximations are part of the ingredients in the calculation of the $\mathcal{O}(\alpha_S^3)$ corrections to the three jet rate in electron positron annihilation. However, much work still remains to be carried out. One important ingredient is to analytically integrate the approximations over the unresolved regions of phase space. A first step in this direction has been carried out in ref. [68] where the hybrid subtraction method of [71] has been used to evaluate the double

unresolved singular contributions associated with a photon-gluon-quark cluster. There is in principle no reason why this approach should not be extended to the more general cases discussed here.

Chapter 8

Conclusions

8.1 Summary

In this thesis we have provided a number of calculational techniques that are relevant for a wide variety of QCD corrections in electron-positron annihilation (and other related processes). In addition we have shown how some of these methods may be implemented by detailing the calculation of the next-to-leading order corrections in four-jet production.

For such a calculation, where the number of contributing Feynman diagrams is large and the tensor structure of each very complex, performing the necessary one-loop integrals provides potential difficulties. In particular, the tensor structure of the matrix elements means that a decomposition into scalar integrals multiplied by kinematical coefficients is very lengthy and algebraically complex. Moreover, such a process results in spurious singularities – with zero residue – when both certain invariants and Gram determinants vanish. In order to control these singularities, we have seen in chapter 3 that it is natural to work with a basis of integrals larger than the set of scalar ones. By extending the basis to include also integrals in higher dimensions and integrals with additional factors of Feynman parameters in the numerator, we automatically protect the spurious poles. These integrals are simply obtained from the scalar integrals and a tensor decomposition in terms of them is straightforward.

In chapter 4 we have outlined the calculation of all the matrix elements necessary for

calculating four-jet observables at next-to-leading order. This comprises the four parton matrix elements at both lowest ($\mathcal{O}(\alpha_S^2)$) and one-loop ($\mathcal{O}(\alpha_S^3)$) orders for the sub-processes $\gamma^* \to q\bar{q}gg$ and $\gamma^* \to q\bar{q}Q\overline{Q}$ and the five parton $\mathcal{O}(\alpha_S^3)$ amplitudes squared where we include an additional gluon. In each case it is convenient to use a colour decomposition to re-write the matrix elements in terms of colourless subamplitudes. For the virtual terms we used the integrals of chapter 3, which appear as terms in the 14 independent functions $\hat{\mathcal{L}}_i$ that are sufficient to describe the one-loop finite contribution. Each of these functions is rather lengthy, but suitable for FORTRAN encoding in an analytic form.

With the matrix elements calculated, it remains to implement them in a suitable phase space Monte Carlo. By making use of the symmetries of the four and five parton contributions of chapter 4, we wrote down more compact expressions in chapter 5. Before any integration can take place, ultraviolet and infrared poles must be isolated and either absorbed into the running coupling or cancelled. Using a hybrid of the commonly-used subtraction and slicing techniques, we exposed the five parton singularities as poles in ϵ and showed that they cancelled with the corresponding four parton infrared divergences of chapter 4. This approach relies on a factorization of the matrix elements in terms of antennae of particles, where a soft gluon is radiated from two colour-adjacent hard partons.

To complete our discussion of the 4 jet calculation, in chapter 6 we presented results obtained using the numerical approach described in chapter 5. This program – `EERAD2` – yielded results for known 4 jet observables, such as the D-parameter and the four-jet fraction, that are consistent with those of other available Monte Carlos. We also presented some new results for distributions that have so far not been considered, such as the narrow jet broadening ($B_{\min}$) and light jet mass (m_l^2/s). In general, using the renormalization scale equal to the physical scale yields next-to-leading order corrections of approximately 100%, which still lie significantly below the data.

Finally, as a further use of the five parton matrix elements, we investigated the factorization that occurs when two particles become unresolved simultaneously. After suitable azimuthal integration, we discovered a set of universal factorization functions that are the

natural extensions of the eikonal and Altarelli-Parisi factors describing soft and collinear single unresolved emission. There are a variety of configurations where two particles are unresolved, the most new and interesting of which are those where three particles are collinear and those where two are collinear and one gluon is soft. Such double unresolved contributions would be relevant in any QCD calculation at next-to-next-to-leading order. As an example, we showed the singular contributions to the process $e^+e^- \to 5$ partons, which could be used in a NNLO analysis of 3 jet production.

8.2 Outlook

This thesis has primarily been concerned with the theoretical, technical aspects of next-to-leading order calculations. Although this culminates with physical predictions of various observables, much work still remains to be done in order to fully take advantage of these results.

In particular, the phenomenology of four jet production is still under-developed. With the next-to-leading order corrections appearing so large – at the physical scale – and yet (for the most part) so unsuccessful in describing the data, we may question the merit of our results. Yet this is no different from the situation for 3 jet-like observables, such as thrust. There, by choosing a smaller scale or by including non-perturbative power corrections, the apparent discrepancy was remedied and even held up as a triumph of QCD. Such studies have yet to be carried out for four jet-like observables.

It now appears that the next-to-leading order QCD corrections for virtually all interesting processes have been calculated. Naturally then, attention turns toward the next step up the perturbative ladder. It is as yet unclear whether extensions of existing technology will suffice, or whether this next step will require the introduction of novel calculational methods. Whichever proves to be the case, much progress is to be expected in this direction in the near future.

Appendix A

Feynman Parametrization

In this appendix we shall derive the form of the scalar integrals assumed throughout chapter 3. We consider a one-loop integral with n external legs carrying momenta p_i and n internal propagators of mass M_i. We shall always work in dimensional regularization by continuing away from 4 and into D dimensions. Note that the calculations performed in this thesis are carried out with the simplifying assumption of M_i=0 for all propagators. This is valid for a wide range of QCD calculations involving loops of gluons and massless quarks (or, more precisely, at sufficiently high centre-of-mass energy s that $m_q^2/s \ll 1$).

Straightforward application of the Feynman rules to an n-point diagram yields the starting form of the scalar integral,

$$\mathrm{I}_n^D[1] = \int \frac{d^D\ell}{i\pi^{D/2}} \frac{1}{(\ell^2 - M_1^2)((\ell+q_1)^2 - M_2^2)\cdots((\ell+q_{n-1})^2 - M_n^2)}, \tag{A.1}$$

where,

$$q_i^\mu = \sum_{j=1}^{i} p_j^\mu, \qquad\qquad q_0^\mu = q_n^\mu = 0.$$

The normalization factor of $i\pi^{D/2}$ is chosen for later convenience. We begin by using Feynman parametrization to combine all the propagator factors into a single denominator. The general identity which we wish to use is,

$$\frac{1}{A_1^{\nu_1}\ldots A_n^{\nu_n}} = \frac{\Gamma(\nu)}{\prod_i \Gamma(\nu_i)} \int_0^1 d^n x_i\, \delta\left(\sum_i x_i - 1\right) \frac{\prod_i x_i^{\nu_i - 1}}{(\sum_i x_i A_i)^{\sum_i \nu_i}}, \tag{A.2}$$

where each of the A_i is one of the propagators and $\nu_i = 1$ for all i. Each propagator corresponds to one of the Feynman parameters x_i, which are constrained by $\sum_i x_i = 1$. Direct application of this identity then yields,

$$\mathrm{I}_n^D[1] = \Gamma(n) \int \frac{d^D L}{i\pi^{D/2}} \int_0^1 d^n x_i \, \delta\left(\sum_i x_i - 1\right) \frac{1}{(L^2 - \Delta)^n}, \tag{A.3}$$

where we have used the constraint on the Feynman parameters where necessary and performed a shift in the loop momentum,

$$\ell^\mu \to L^\mu = \ell^\mu + \mathcal{P}^\mu. \tag{A.4}$$

The auxiliary momentum $\mathcal{P}^\mu = -\sum_{i=1}^n x_{i+1} q_i^\mu$ is exactly that introduced in chapter 3 to decompose the tensor structure of loop integrals, whose origins are seen in the change of variables here. After completing the square in this fashion, the remainder can be written as a quadratic in the Feynman parameters,

$$\begin{aligned} \Delta &= \sum_{i,j} x_i x_j q_{i-1} \cdot q_{j-1} - \sum_i x_i q_{i-1}^2 + \sum_i x_i M_i^2 \\ &= \frac{1}{2} \sum_{i,j} x_i x_j \left(M_i^2 + M_j^2 - (q_{i-1} - q_{j-1})^2 \right) \\ &\equiv \sum_{i,j} x_i x_j S_{ij}. \end{aligned} \tag{A.5}$$

Integrations of the form in equation (A.3) can easily be evaluated by performing a Wick rotation to Euclidean space. This is equivalent to using the identity,

$$\int \frac{d^D l}{i\pi^{D/2}} \frac{1}{(l^2 - \Delta)^n} = (-1)^n \frac{\Gamma(n - D/2)}{\Gamma(n)} \Delta^{D/2-n}. \tag{A.6}$$

The desired form of the scalar integral (eq. 3.6) is then directly obtained,

$$\mathrm{I}_n^D[1] = (-1)^n \Gamma(n - D/2) \int_0^1 d^n x_i \delta(1 - \sum_i x_i) \left[\sum_{i,j=1}^n S_{ij} x_i x_j \right]^{D/2-n}. \tag{A.7}$$

Appendix B

Finite Functions

This appendix collects explicit forms for all the finite functions of chapter 3 which are relevant for the calculation of the matrix elements for $\gamma^* \to 4$ jets at next-to-leading order.

B.1 Triangle Integrals

In this section, we collect together explicit forms for the triangle graphs which appear as building blocks in the box graphs. We fix the kinematics according to fig. 1, so that momenta p_1 and p_2 are exiting, with p_3 determined by momentum conservation. There are two distinct cases, according to whether one or two of the external masses are zero.

B.1.1 The One-Mass Triangle

Here we provide explicit results for the case $p_1^2 = p_2^2 = 0$. There is an additional symmetry under the exchange $p_1 \leftrightarrow p_2$ and $x_1 \leftrightarrow x_3$. Insertions involving x_2 can be eliminated using $x_1 + x_2 + x_3 = 1$.

The $D = 4 - 2\epsilon$ scalar and tensor integrals are given by,

$$\mathrm{I}_3^{1m}[1] \;=\; \frac{c_\Gamma}{\epsilon^2}\frac{(-s_{12})^{-\epsilon}}{s_{12}}, \tag{B.1}$$

$$\mathrm{I}_3^{1m}[x_1] = \mathrm{I}_3^{1m}[x_3] = 2\mathrm{I}_3^{1m}[x_1^2] = 2\mathrm{I}_3^{1m}[x_3^2] = -\frac{1}{s_{12}}\left(\frac{(-s_{12})^{-\epsilon}}{\epsilon} + 2\right) c_\Gamma, \tag{B.2}$$

$$\mathrm{I}_3^{1m}[x_1x_3] = 3\mathrm{I}_3^{1m}[x_1^2x_3] = 3\mathrm{I}_3^{1m}[x_1x_3^2] = \frac{1}{2s_{12}}, \tag{B.3}$$

$$\mathrm{I}_3^{1m}[x_1^3] = \mathrm{I}_3^{1m}[x_3^3] = -\frac{1}{3s_{12}}\left(\frac{(-s_{12})^{-\epsilon}}{\epsilon} + \frac{13}{6}\right) c_\Gamma, \tag{B.4}$$

while, the necessary integrals in $D = 6 - 2\epsilon$ dimensions read,

$$\mathrm{I}_3^{1m,D=6-2\epsilon}[1] = -\frac{1}{2}\left(\frac{(-s_{12})^{-\epsilon}}{\epsilon} + 3\right) c_\Gamma, \tag{B.5}$$

$$\mathrm{I}_3^{1m,D=6-2\epsilon}[x_1] = \mathrm{I}_3^{1m,D=6-2\epsilon}[x_3] = -\frac{1}{6}\left(\frac{(-s_{12})^{-\epsilon}}{\epsilon} + \frac{8}{3}\right) c_\Gamma. \tag{B.6}$$

B.1.2 The Two-Mass Triangle

When two of the external legs are massive, $p_2^2 = 0$ but s_{12}, $p_1^2 \neq 0$, the divergent integrals read,

$$\mathrm{I}_3^{2m}[1] = \frac{c_\Gamma}{\epsilon^2}\left(\frac{(-s_{12})^{-\epsilon} - (-p_1^2)^{-\epsilon}}{s_{12} - p_1^2}\right), \tag{B.7}$$

$$\mathrm{I}_3^{2m}[x_3] = -2\mathrm{Lc}_2^{2m}(p_1,p_2) - \frac{c_\Gamma}{\epsilon}\frac{(-s_{12})^{-\epsilon}}{(s_{12}-p_1^2)} - \frac{p_1^2}{(s_{12}-p_1^2)}\mathrm{I}_3^{2m}[1], \tag{B.8}$$

$$\mathrm{I}_3^{2m}[x_3^2] = -3\mathrm{Lc}_3^{2m}(p_1,p_2) + \frac{1}{2(s_{12}-p_1^2)} - c_\Gamma\frac{(-s_{12})^{-\epsilon}}{\epsilon}\frac{(s_{12}-3p_1^2)}{2(s_{12}-p_1^2)^2} + \frac{p_1^4}{(s_{12}-p_1^2)^2}\mathrm{I}_3^{2m}[1], \tag{B.9}$$

$$\mathrm{I}_3^{2m}[x_3^3] = -\frac{11}{3}\mathrm{Lc}_4^{2m}(p_1,p_2) + \frac{(s_{12}-2p_1^2)}{2(s_{12}-p_1^2)^2} - \frac{p_1^6}{(s_{12}-p_1^2)^3}\mathrm{I}_3^{2m}[1] - \frac{(-s_{12})^{-\epsilon}}{\epsilon}\left(\frac{1}{3(s_{12}-p_1^2)} - \frac{p_1^2}{2(s_{12}-p_1^2)^2} + \frac{p_1^4}{(s_{12}-p_1^2)^3}\right) c_\Gamma, \tag{B.10}$$

while,

$$\mathrm{I}_3^{2m}[x_1] = 2\mathrm{I}_3^{2m}[x_1^2] = 3\mathrm{I}_3^{2m}[x_1^3] = \mathrm{Lc}_1^{2m}(p_1,p_2), \tag{B.11}$$

$$\mathrm{I}_3^{2m}[x_1x_3] = 3\mathrm{I}_3^{2m}[x_1^2x_3] = \frac{1}{2}\mathrm{Lc}_2^{2m}(p_1,p_2), \tag{B.12}$$

$$\mathrm{I}_3^{2m}[x_1x_3^2] = \frac{1}{3}\mathrm{Lc}_3^{2m}(p_1,p_2). \tag{B.13}$$

The functions $\mathrm{Lc}_n^{2m}(p_1,p_2)$ are defined by equations (3.37,3.38).

The $D = 6 - 2\epsilon$ dimension integrals read,

$$\mathrm{I}_3^{2m,D=6-2\epsilon}[1] = \frac{1}{2}\left(p_1^2\mathrm{Lc}_1^{2m}(p_1,p_2) - \left(\frac{(-s_{12})^{-\epsilon}}{\epsilon} + 3\right)c_\Gamma\right), \tag{B.14}$$

$$\mathrm{I}_3^{2m,D=6-2\epsilon}[x_1] = \frac{1}{6}\left(p_1^2\mathrm{Lc}_1^{2m}(p_1,p_2) - \left(\frac{(-s_{12})^{-\epsilon}}{\epsilon} + \frac{8}{3}\right)c_\Gamma\right), \tag{B.15}$$

$$\mathrm{I}_3^{2m,D=6-2\epsilon}[x_3] = \frac{1}{6}\left(p_1^2\mathrm{Lc}_2^{2m}(p_1,p_2) - \left(\frac{(-s_{12})^{-\epsilon}}{\epsilon} + \frac{8}{3}\right)c_\Gamma\right). \tag{B.16}$$

The corresponding integrals for the case $p_1^2 = 0$, $p_2^2 \neq 0$ can be obtained by using the above formulae with the substitutions,

$$p_1 \leftrightarrow p_2, \qquad x_1 \leftrightarrow x_3. \tag{B.17}$$

The limit $p_1^2 \to 0$ may also be safely taken. For example, using the fact that in this limit $\mathrm{Lc}_n^{2m}(p_1,p_2) \to 1/(n-1)/s_{12}$ and observing that all of the triangle loop integral contributions proportional to $1/\epsilon^2$ trivially drop out in eqs. (B.8)-(B.10), we see that,

$$\mathrm{I}_3^{2m}[x_3^n] \to \mathrm{I}_3^{1m}[x_3^n].$$

B.2 Box Integrals

Here we collect together explicit forms for the the finite functions appearing in the box integrals. We fix the kinematics according to fig. 3.5, so that momenta p_1, p_2 and p_3 are exiting, with p_4 determined by momentum conservation.

B.2.1 The Adjacent Two-Mass Box

We first focus on the case where two of the adjacent external legs are massive, $p_4^2 \neq 0$ and $p_1^2 \neq 0$.

For integrals with a single Feynman parameter in the numerator, we have,

$$\mathrm{Ld}_1(p_1,p_2,p_3) = -\left(\mathrm{Ld}_{1S}(p_1,p_2,p_3) + \mathrm{Lc}_0(p_1,p_{23})\right), \tag{B.1}$$

where the box function in $D = 6$, Ld_{1S} is given by equation (3.41). When there are two Feynman parameters in the numerator, we eliminate x_3 using $x_1 + x_2 + x_3 + x_4 = 1$ so there are only three relevant functions. Explicitly, we find,

$$\mathrm{Ld}_{21}(p_1,p_2,p_3) = -\frac{2}{s_{12}}\left(3\mathrm{Ld}_{2S}(p_1,p_2,p_3) + \mathrm{Lc}_{1S}(p_1,p_{23})\right) - \mathrm{Lc}_1(p_{23},p_1), \tag{B.2}$$

$$\begin{aligned}\mathrm{Ld}_{22}(p_1,p_2,p_3) = {} & \frac{2(s_{123}-s_{12})}{s_{12}s_{23}}\left(3\mathrm{Ld}_{2S}(p_1,p_2,p_3) + \mathrm{Lc}_{1S}(p_1,p_{23})\right) \\ & -\frac{s_{12}}{s_{23}}\mathrm{Lc}_1^{2m}(p_1,p_2) + \frac{s_{123}}{s_{23}}\mathrm{Lc}_1(p_{23},p_1),\end{aligned} \tag{B.3}$$

$$\begin{aligned}\mathrm{Ld}_{24}(p_1,p_2,p_3) = {} & \frac{2(p_1^2-s_{12})}{s_{12}s_{23}}\left(3\mathrm{Ld}_{2S}(p_1,p_2,p_3) + \mathrm{Lc}_{1S}(p_1,p_{23})\right) \\ & -\frac{s_{12}}{s_{23}}\mathrm{Lc}_1^{2m}(p_{12},p_3) + \frac{p_1^2}{s_{23}}\mathrm{Lc}_1(p_{23},p_1).\end{aligned} \tag{B.4}$$

The all massive triangle integral function in $D = 6-2\epsilon$, Lc_{1S} is given by equation (3.28), the box integral function in $D = 8-2\epsilon$ is given in equation (3.45) while the remaining triangle functions are given in Appendix B and equations (3.21–3.26). The functions for adjacent box integrals with three insertions of Feynman parameters contain the box in $D = 10-2\epsilon$ (3.46) and triangle in $D = 8-2\epsilon$ (3.31). All integrals can be obtained in terms of the following

four functions,

$$\begin{aligned}
\mathrm{Ld}_{311}(p_1,p_2,p_3) &= -\Bigg(\frac{12}{s_{12}^2}\left(5\mathrm{Ld}_{3S}(p_1,p_2,p_3)+\mathrm{Lc}_{2S}(p_1,p_{23})\right) \\
&\quad +\frac{(s_{12}+p_1^2)}{s_{12}}\mathrm{Lc}_3(p_{23},p_1)+\frac{s_{23}}{s_{12}}\mathrm{Lc}_2(p_1,p_{23})\Bigg), \qquad \text{(B.5)} \\
\mathrm{Ld}_{314}(p_1,p_2,p_3) &= \frac{12(p_1^2-s_{12})}{s_{12}^2 s_{23}}\left(5\mathrm{Ld}_{3S}(p_1,p_2,p_3)+\mathrm{Lc}_{2S}(p_1,p_{23})\right) \\
&\quad +\frac{p_1^4}{s_{12}s_{23}}\mathrm{Lc}_3(p_{23},p_1)-\frac{(s_{12}-p_1^2)}{s_{12}}\mathrm{Lc}_2(p_1,p_{23}) \\
&\quad -\frac{s_{12}}{2s_{23}}\mathrm{Lc}_1^{2m}(p_{12},p_3), \qquad \text{(B.6)} \\
\mathrm{Ld}_{322}(p_1,p_2,p_3) &= -\Bigg(\frac{12(s_{123}-s_{12})^2}{s_{12}^2 s_{23}^2}\left(5\mathrm{Ld}_{3S}(p_1,p_2,p_3)+\mathrm{Lc}_{2S}(p_1,p_{23})\right) \\
&\quad +\frac{s_{123}(s_{12}s_{123}+p_1^2 s_{123}-2p_1^2 s_{12})}{s_{12}s_{23}^2}\mathrm{Lc}_3(p_{23},p_1)-\frac{s_{12}}{2s_{23}}\mathrm{Lc}_2^{2m}(p_1,p_2) \\
&\quad +\frac{s_{12}(s_{12}-s_{123})}{2s_{23}^2}\mathrm{Lc}_1^{2m}(p_{12},p_3)+\frac{s_{123}(s_{123}-2s_{12})}{s_{12}s_{23}}\mathrm{Lc}_2(p_1,p_{23}) \\
&\quad +\frac{(p_1^2 s_{12}+s_{12}s_{23}-s_{12}s_{123})}{2s_{23}^2}\mathrm{Lc}_1^{2m}(p_1,p_2)\Bigg), \qquad \text{(B.7)} \\
\mathrm{Ld}_{344}(p_1,p_2,p_3) &= -\Bigg(\frac{12(s_{12}-p_1^2)^2}{s_{12}^2 s_{23}^2}\left(5\mathrm{Ld}_{3S}(p_1,p_2,p_3)+\mathrm{Lc}_{2S}(p_1,p_{23})\right) \\
&\quad +\frac{p_1^2(p_1^2-2s_{12})}{s_{12}s_{23}}\mathrm{Lc}_2(p_1,p_{23})+\frac{p_1^4(p_1^2-s_{12})}{s_{12}s_{23}^2}\mathrm{Lc}_3(p_{23},p_1) \\
&\quad +\frac{s_{12}(s_{12}-p_1^2)}{2s_{23}^2}\mathrm{Lc}_1^{2m}(p_{12},p_3)+\frac{s_{12}}{2s_{23}}\mathrm{Lc}_2^{2m}(p_{12},p_3)\Bigg). \qquad \text{(B.8)}
\end{aligned}$$

B.2.2 The One-Mass Box

For this kinematic configuration, only $p_4^2 \neq 0$ and there is a 'flip' symmetry, so that functions related to the parameter x_4 are obtained from those related to x_1, by $p_1 \longleftrightarrow p_3$. The box integrals in higher dimension are given by equations (3.56–3.59), and,

$$\mathrm{Ld}_1^{1m}(p_1,p_2,p_3) = -\mathrm{Ld}_{1S}^{1m}(p_1,p_2,p_3). \qquad \text{(B.9)}$$

For two and three insertions, we find,

$$\mathrm{Ld}^{1m}_{21}(p_1,p_2,p_3) = -\frac{1}{s_{12}}\left(6\mathrm{Ld}^{1m}_{2S}(p_1,p_2,p_3)+s_{23}\mathrm{Lc}^{2m}_{1}(p_{23},p_1)\right), \tag{B.10}$$

$$\mathrm{Ld}^{1m}_{22}(p_1,p_2,p_3) = \mathrm{Ld}^{1m}_{1}(p_1,p_2,p_3)-\mathrm{Ld}^{1m}_{21}(p_1,p_2,p_3), \tag{B.11}$$

and,

$$\mathrm{Ld}^{1m}_{311}(p_1,p_2,p_3) = -\frac{1}{s_{12}^2}\Bigg(60\mathrm{Ld}^{1m}_{3S}(p_1,p_2,p_3)+\frac{1}{2}s_{23}^2\mathrm{Lc}^{2m}_{1}(p_{23},p_1) + \frac{1}{2}s_{12}s_{23}\mathrm{Lc}^{2m}_{2}(p_{23},p_1)\Bigg), \tag{B.12}$$

$$\mathrm{Ld}^{1m}_{314}(p_1,p_2,p_3) = -\frac{1}{s_{12}s_{23}}\Bigg(60\mathrm{Ld}^{1m}_{3S}(p_1,p_2,p_3)+\frac{1}{2}s_{23}^2\mathrm{Lc}^{2m}_{1}(p_{23},p_1) + \frac{1}{2}s_{12}^2\mathrm{Lc}^{2m}_{1}(p_{12},p_3)\Bigg), \tag{B.13}$$

$$\mathrm{Ld}^{1m}_{322}(p_1,p_2,p_3) = \mathrm{Ld}^{1m}_{311}(p_1,p_2,p_3)+\mathrm{Ld}^{1m}_{1}(p_1,p_2,p_3)-2\mathrm{Ld}^{1m}_{21}(p_1,p_2,p_3). \tag{B.14}$$

B.2.3 The Opposite-Mass Box

Again, this kinematic configuration possesses a 'flip' symmetry, so that functions related to the parameter x_4 are obtained from those related to x_1, by $p_1 \longleftrightarrow p_3$. In addition, we find that any insertion involving the factor x_1x_4 may be manipulated so as to cancel off the protected factor of $(1-\lambda)$. Therefore the only required box functions are,

$$\mathrm{Ld}^{opp}_{1}(p_1,p_2,p_3) = \frac{1}{s_{13}}\mathrm{Ld}^{opp}_{0}(p_1,p_2,p_3), \tag{B.15}$$

$$\mathrm{Ld}^{opp}_{21}(p_1,p_2,p_3) = \frac{1}{s_{13}}\left((p_2^2-s_{23})\mathrm{Ld}^{opp}_{1}(p_1,p_2,p_3)+s_{23}\mathrm{Lc}^{2m}_{1}(p_{23},p_1) - p_2^2\mathrm{Lc}^{2m}_{1}(p_2,p_1)+\log\left(\frac{s_{123}}{s_{12}}\right)\right), \tag{B.16}$$

$$\mathrm{Ld}^{opp}_{311}(p_1,p_2,p_3) = \frac{1}{s_{13}}\left((p_2^2-s_{23})\mathrm{Ld}^{opp}_{21}(p_1,p_2,p_3)+\frac{1}{2}s_{23}\mathrm{Lc}^{2m}_{2}(p_{23},p_1) - \frac{1}{2}p_2^2\mathrm{Lc}^{2m}_{2}(p_2,p_1)+\frac{1}{2}\log\left(\frac{s_{123}}{s_{12}}\right)\right). \tag{B.17}$$

Appendix C

Limits

In this appendix, we collect together suitable expansions of the various functions presented in chapter 3 in the limit $\Delta_n \to 0$. These expressions represent the leading term in the expansion of the functions as a Taylor series in Δ_n and should be evaluated for $\Delta_n < \delta$, where δ can be determined numerically. Typically, $\delta \sim 10^{-4}\Delta_n^{\max}$ where $\Delta_n^{\max}$ is the largest value the Gram determinant can achieve. In general, for a given numerical precision, *acc* the numerical problems occur when $\Delta \sim (acc)^{1/N}$ where N is the number of Gram determinants in the denominator of the function.

C.1 The Three-Mass Triangle

In the limit that $\Delta_3 \to 0$, we have,

$$\mathrm{Lc}_0(p_1,p_2) \to \frac{1}{2p_1^2p_2^2s_{12}}\left(p_1^2(s_{12}+p_2^2-p_1^2)\log\left(\frac{s_{12}}{p_1^2}\right)+p_2^2(s_{12}+p_1^2-p_2^2)\log\left(\frac{s_{12}}{p_2^2}\right)\right), \tag{C.1}$$

$$\mathrm{Lc}_{1S}(p_1,p_2) \to \frac{1}{12p_1^2p_2^2s_{12}}\left(p_1^4(s_{12}+p_2^2-p_1^2)\log\left(\frac{s_{12}}{p_1^2}\right)+p_2^4(s_{12}+p_1^2-p_2^2)\log\left(\frac{s_{12}}{p_2^2}\right)\right.$$
$$\left.+2p_1^2p_2^2s_{12}\right), \tag{C.2}$$

$$\mathrm{Lc}_{2S}(p_1,p_2) \to \frac{1}{120p_1^2p_2^2s_{12}}\left(p_1^6(s_{12}+p_2^2-p_1^2)\log\left(\frac{s_{12}}{p_1^2}\right)+p_2^6(s_{12}+p_1^2-p_2^2)\log\left(\frac{s_{12}}{p_2^2}\right)\right.$$

$$+\frac{p_1^2 p_2^2 s_{12}}{2}(s_{12}+p_1^2+p_2^2)\Bigg), \tag{C.3}$$

$$\mathrm{Lc}_{3S}(p_1,p_2) \rightarrow \frac{1}{1680 p_1^2 p_2^2 s_{12}}\Bigg(p_1^8(s_{12}+p_2^2-p_1^2)\log\left(\frac{s_{12}}{p_1^2}\right)+p_2^8(s_{12}+p_1^2-p_2^2)\log\left(\frac{s_{12}}{p_2^2}\right)$$
$$+\frac{2p_1^2p_2^2s_{12}}{9}(s_{12}^2+p_1^4+p_2^4+s_{12}p_1^2+s_{12}p_2^2+p_1^2p_2^2)\Bigg), \tag{C.4}$$

$$\mathrm{Lc}_1(p_1,p_2) \rightarrow \frac{1}{3p_1^2(s_{12}+p_2^2-p_1^2)}\left((s_{12}-p_2^2)\log\left(\frac{s_{12}}{p_2^2}\right)+2p_1^2-p_1^4\mathrm{Lc}_0(p_1,p_2)\right), \tag{C.5}$$

$$\mathrm{Lc}_2(p_1,p_2) \rightarrow \frac{1}{6p_2^2(s_{12}+p_1^2-p_2^2)}\Bigg(-4p_2^2(s_{12}+p_1^2-p_2^2)\mathrm{Lc}_3(p_1,p_2)$$
$$+s_{12}-p_2^2+3p_1^2p_2^2\mathrm{Lc}_1(p_1,p_2)-p_1^4\mathrm{Lc}_1(p_2,p_1)+p_2^2\log\left(\frac{s_{12}}{p_2^2}\right)\Bigg), \tag{C.6}$$

$$\mathrm{Lc}_3(p_1,p_2) \rightarrow \frac{1}{5p_1^2(s_{12}+p_2^2-p_1^2)}\left((s_{12}-p_2^2)\log\left(\frac{s_{12}}{p_2^2}\right)+p_1^2-2p_1^4\mathrm{Lc}_1(p_1,p_2)\right), \tag{C.7}$$

$$\mathrm{Lc}_4(p_1,p_2) \rightarrow \frac{1}{15p_2^2(s_{12}+p_1^2-p_2^2)}\Bigg(-6p_2^2(s_{12}+p_1^2-p_2^2)\mathrm{Lc}_5(p_1,p_2)$$
$$+s_{12}-p_2^2+5p_1^2p_2^2\mathrm{Lc}_3(p_1,p_2)-4p_1^4\mathrm{Lc}_2(p_1,p_2)+p_2^2\log\left(\frac{s_{12}}{p_2^2}\right)\Bigg), \tag{C.8}$$

$$\mathrm{Lc}_5(p_1,p_2) \rightarrow \frac{1}{7p_1^2(s_{12}+p_2^2-p_1^2)}\left((s_{12}-p_2^2)\log\left(\frac{s_{12}}{p_2^2}\right)+\frac{2p_1^2}{3}-3p_1^4\mathrm{Lc}_3(p_1,p_2)\right). \tag{C.9}$$

C.2 The Adjacent Two-Mass Box

In the limit $\Delta_4 \rightarrow 0$, we have,

$$\mathrm{Ld}_0(p_1,p_2,p_3) \rightarrow -\frac{1}{2}\left(s_{123}+p_1^2-s_{23}-\frac{2p_1^2s_{123}}{s_{12}}\right)\mathrm{Lc}_0(p_1,p_{23}), \tag{C.10}$$

$$\mathrm{Ld}_{1S}(p_1,p_2,p_3) \rightarrow \frac{-1}{s_{12}s_{23}}\Bigg(\left(s_{123}+p_1^2-s_{23}-\frac{2p_1^2s_{123}}{s_{12}}\right)\mathrm{Lc}_{1S}(p_1,p_{23})$$
$$+\frac{s_{23}}{2}\log\left(\frac{s_{123}}{s_{23}}\right)+s_{12}\log\left(\frac{s_{123}}{s_{12}}\right)-\frac{p_1^2}{2}\log\left(\frac{s_{123}}{p_1^2}\right)\Bigg), \tag{C.11}$$

$$\mathrm{Ld}_{2S}(p_1,p_2,p_3) \rightarrow \frac{-1}{12s_{12}s_{23}}\Bigg(\left(s_{123}+p_1^2-s_{23}-\frac{2p_1^2s_{123}}{s_{12}}\right)\mathrm{Lc}_{2S}(p_1,p_{23})$$
$$+\frac{s_{23}^2}{2}\log\left(\frac{s_{123}}{s_{23}}\right)+s_{12}^2\log\left(\frac{s_{123}}{s_{12}}\right)-\frac{p_1^4}{2}\log\left(\frac{s_{123}}{p_1^2}\right)+s_{12}s_{23}\Bigg),$$

(C.12)

$$\begin{aligned}
\mathrm{Ld}_{3S}(p_1,p_2,p_3) \;\to\; & \frac{-1}{180 s_{12}s_{23}}\left(\left(s_{123}+p_1^2-s_{23}-\frac{2p_1^2 s_{123}}{s_{12}}\right)\mathrm{Lc}_{3S}(p_1,p_{23})\right. \\
& +\frac{s_{23}^3}{2}\log\left(\frac{s_{123}}{s_{23}}\right)+s_{12}^3\log\left(\frac{s_{123}}{s_{12}}\right)-\frac{p_1^6}{2}\log\left(\frac{s_{123}}{p_1^2}\right) \\
& \left.+\frac{1}{4}s_{12}s_{23}(s_{123}+s_{12}+s_{23}+p_1^2)\right), \qquad \text{(C.13)} \\
\mathrm{Ld}_{4S}(p_1,p_2,p_3) \;\to\; & \frac{-1}{840 s_{12}s_{23}}\left(\left(s_{123}+p_1^2-s_{23}-\frac{2p_1^2 s_{123}}{s_{12}}\right)\mathrm{Lc}_{4S}(p_1,p_{23})\right. \\
& +\frac{s_{23}^4}{2}\log\left(\frac{s_{123}}{s_{23}}\right)+s_{12}^4\log\left(\frac{s_{123}}{s_{12}}\right)-\frac{p_1^8}{2}\log\left(\frac{s_{123}}{p_1^2}\right) \\
& +\frac{1}{9}s_{12}s_{23}(s_{123}^2+s_{12}^2+s_{23}^2+p_1^4+s_{123}s_{12}+s_{123}s_{23} \\
& \left.+s_{123}p_1^2+s_{12}p_1^2+s_{23}p_1^2+\frac{s_{12}s_{23}}{2})\right). \qquad \text{(C.14)}
\end{aligned}$$

In this last equation, we have used the finite part of the three mass triangle graph in $D = 12-2\epsilon$. For $p_1^2,\ p_2^2 \neq 0$,

$$\begin{aligned}
\mathrm{Lc}_{4S}(p_1,p_2) \;=\; & \frac{1}{8\Delta_3}\left(2p_1^2p_2^2 s_{12}\mathrm{Lc}_{3S}(p_1,p_2)-\frac{1}{840}\left(p_1^8(s_{12}+p_2^2-p_1^2)\log\left(\frac{s_{12}}{p_1^2}\right)\right.\right. \\
& +p_2^8(s_{12}+p_1^2-p_2^2)\log\left(\frac{s_{12}}{p_2^2}\right) \\
& \left.\left.+\frac{2p_1^2p_2^2s_{12}}{9}(p_1^4+p_2^4+s_{12}^2+p_1^2s_{12}+p_2^2s_{12}+p_1^2p_2^2)\right)\right). \qquad \text{(C.15)}
\end{aligned}$$

C.3 The One-Mass Box

Finally, in the limit $\Delta_4^{1m} \to 0$, we have,

$$\begin{aligned}
\mathrm{Ld}_0^{1m}(p_1,p_2,p_3) \;\to\; & 0, \qquad \text{(C.16)} \\
\mathrm{Ld}_{1S}^{1m}(p_1,p_2,p_3) \;\to\; & \frac{-1}{s_{12}s_{23}}\left(s_{23}\log\left(\frac{s_{123}}{s_{23}}\right)+s_{12}\log\left(\frac{s_{123}}{s_{12}}\right)\right), \qquad \text{(C.17)} \\
\mathrm{Ld}_{2S}^{1m}(p_1,p_2,p_3) \;\to\; & \frac{-1}{12 s_{12}s_{23}}\left(s_{23}^2\log\left(\frac{s_{123}}{s_{23}}\right)+s_{12}^2\log\left(\frac{s_{123}}{s_{12}}\right)+s_{12}s_{23}\right), \qquad \text{(C.18)} \\
\mathrm{Ld}_{3S}^{1m}(p_1,p_2,p_3) \;\to\; & \frac{-1}{180 s_{12}s_{23}}\left(s_{23}^3\log\left(\frac{s_{123}}{s_{23}}\right)+s_{12}^3\log\left(\frac{s_{123}}{s_{12}}\right)\right.
\end{aligned}$$

$$+\frac{1}{4}s_{12}s_{23}(s_{123}+s_{12}+s_{23})\Big)\,, \tag{C.19}$$

$$\mathrm{Ld}_{4S}^{1m}(p_1,p_2,p_3) \;\to\; \frac{-1}{840s_{12}s_{23}}\left(s_{23}^4\log\left(\frac{s_{123}}{s_{23}}\right)+s_{12}^4\log\left(\frac{s_{123}}{s_{12}}\right)\right.$$
$$\left.+\frac{1}{9}s_{12}s_{23}\left(s_{123}^2+s_{12}^2+s_{23}^2+s_{123}s_{12}+s_{123}s_{23}+\frac{s_{12}s_{23}}{2}\right)\right). \tag{C.20}$$

Appendix D

Reduction Relations

After all the reductions of the one-loop integrals are complete, and the relevant expressions have been inserted into the matrix elements, several relations between the functions may be exploited to further reduce the algebraic size of the answer. A simple example of this is given by the symmetry relation for the box integral with two opposite massive external legs,

$$\mathrm{Ld}_0^{\mathrm{opp}}(p_1, p_2, p_3) = \mathrm{Ld}_0^{\mathrm{opp}}(p_3, p_2, p_1).$$

Although this is not useful in an individual tensor reduction, it can obviously lead to cancellation of terms in the matrix element where integrals with $p_1 \leftrightarrow p_3$ may also be present. Compactification may also arise from cancellation of Gram determinants when integrals from different sources are combined. Useful identities are straightforwardly obtained by repeated use of equations (3.14)–(3.17) or by inspection.

D.1 The Three-Mass Triangle

The two symmetry identities relevant for these integrals are,

$$\begin{aligned} \mathrm{Lc}_2(p_2, p_1) &= \mathrm{Lc}_2(p_1, p_2), \\ \mathrm{Lc}_0(p_2, p_1) &= \mathrm{Lc}_0(p_1, p_2). \end{aligned} \tag{D.1}$$

There are also a number of identities which relate the triangle functions when multiplied by a partial Gram determinant,

$$
\begin{aligned}
(s_{12}-p_1^2-p_2^2)\,\mathrm{Lc}_3(p_1,p_2) &= 2p_1^2\,\mathrm{Lc}_2(p_1,p_2)-p_1^2\,\mathrm{Lc}_1(p_1,p_2)+\frac{1}{2}\log\left(\frac{s_{12}}{p_2^2}\right),\\
(s_{12}-p_1^2-p_2^2)\,\mathrm{Lc}_2(p_1,p_2) &= 2p_2^2\,\mathrm{Lc}_3(p_1,p_2)-\frac{3}{2}p_2^2\,\mathrm{Lc}_1(p_1,p_2)-\frac{1}{2}p_1^2\,\mathrm{Lc}_1(p_2,p_1)+\frac{1}{2},\\
(s_{12}-p_1^2-p_2^2)\,\mathrm{Lc}_1(p_2,p_1) &= 2p_2^2\,\mathrm{Lc}_1(p_1,p_2)-p_2^2\,\mathrm{Lc}_0(p_1,p_2)+\log\left(\frac{s_{12}}{p_1^2}\right), \qquad \text{(D.2)}\\
p_1^2\,\mathrm{Lc}_1(p_2,p_1) &= \frac{1}{2}\left((s_{12}-p_1^2-p_2^2)\,\mathrm{Lc}_1(p_1,p_2)+p_1^2\,\mathrm{Lc}_0(p_1,p_2)-\log\left(\frac{s_{12}}{p_2^2}\right)\right).
\end{aligned}
$$

D.2 The Adjacent Two-Mass Box

This configuration of masses has no symmetry relations. The identities for cancelling factors of the Gram determinant read,

$$
\begin{aligned}
&(s_{12}-p_1^2)(s_{13}-p_1^2)\mathrm{Ld}_{344}(p_1,p_2,p_3)=p_1^2 s_{23}\mathrm{Ld}_{344}(p_1,p_2,p_3)+s_{12}\times\Big(\\
&\quad(s_{12}-p_1^2)(\mathrm{Lc}_3(p_1,p_{23})-\mathrm{Lc}_1(p_1,p_{23})\\
&\qquad -\mathrm{Ld}_{24}(p_1,p_2,p_3))-p_1^2\mathrm{Lc}_2(p_{23},p_1)+\frac{s_{12}}{2}\mathrm{Lc}_2^{1m}(p_{12},p_3)\Big),\\
&(s_{12}-p_1^2)(s_{13}-p_1^2)\mathrm{Ld}_{322}(p_1,p_2,p_3)=p_1^2 s_{23}\mathrm{Ld}_{322}(p_1,p_2,p_3)+s_{12}\times\Big(\\
&\quad(s_{13}-p_1^2)\times\Big(\mathrm{Ld}_{22}(p_1,p_2,p_3)-\mathrm{Lc}_3(p_1,p_{23})-\mathrm{Lc}_3(p_{23},p_1)\\
&\qquad -2\mathrm{Lc}_2(p_1,p_{23})+\mathrm{Lc}_1(p_1,p_{23})+\mathrm{Lc}_1(p_{23},p_1)\Big)\\
&\quad +s_{23}\Big(\mathrm{Ld}_{22}(p_1,p_2,p_3)+2\mathrm{Lc}_3(p_1,p_{23})\\
&\qquad +2\mathrm{Lc}_2(p_1,p_{23})-3\mathrm{Lc}_1(p_1,p_{23})-\mathrm{Lc}_1(p_{23},p_1)+\mathrm{Lc}_0(p_1,p_{23})\Big)\\
&\quad +p_1^2\Big(\mathrm{Lc}_2(p_1,p_{23})-\mathrm{Lc}_1(p_{23},p_1)-\frac{1}{2}\mathrm{Lc}_2^{1m}(p_1,p_2)+\mathrm{Lc}_1^{1m}(p_1,p_2)-\frac{1}{2}\log\left(\frac{p_{123}}{p_{12}}\right)\Big)\Big),\\
&(s_{12}-p_1^2)(s_{13}-p_1^2)\mathrm{Ld}_{314}(p_1,p_2,p_3)=p_1^2 s_{23}\mathrm{Ld}_{314}(p_1,p_2,p_3)+s_{12}\times\Big(\\
&\quad s_{23}\left(-\mathrm{Ld}_{24}(p_1,p_2,p_3)+\mathrm{Lc}_3(p_1,p_{23})+\mathrm{Lc}_2(p_1,p_{23})-\mathrm{Lc}_1(p_1,p_{23})\right)
\end{aligned}
$$

$$-(s_{123}-s_{12})\mathrm{Lc}_2(p_1,p_{23})-\frac{1}{2}s_{12}\mathrm{Lc}_1^{1m}(p_{12},p_3)+\frac{1}{2}\Big),$$

$$(s_{12}-p_1^2)(s_{13}-p_1^2)\mathrm{Ld}_{311}(p_1,p_2,p_3)=p_1^2 s_{23}\mathrm{Ld}_{311}(p_1,p_2,p_3)+s_{12}\times\Big($$

$$-s_{23}\left(\mathrm{Ld}_{21}(p_1,p_2,p_3)+\mathrm{Lc}_2(p_1,p_{23})\right)+(s_{12}-p_1^2)\mathrm{Lc}_3(p_{23},p_1)-\frac{1}{2}\log\left(\frac{p_{12}}{p_1^2}\right)\Big),$$

$$(s_{12}-p_1^2)(s_{13}-p_1^2)\mathrm{Ld}_1(p_1,p_2,p_3)=p_1^2 s_{23}\mathrm{Ld}_1(p_1,p_2,p_3)+s_{12}\times\Big($$

$$\mathrm{Ld}_0(p_1,p_2,p_3)+(s_{12}-s_{13})\mathrm{Lc}_0(p_{23},p_1)\Big). \tag{D.3}$$

The functions representing one insertion of a Feynman parameter may be more simply related by partial factors of the Gram determinant,

$$\begin{aligned}
(s_{13}-p_1^2)\mathrm{Ld}_{24}(p_1,p_2,p_3) &= -(s_{12}-p_1^2)\mathrm{Ld}_{22}(p_1,p_2,p_3)-s_{23}\mathrm{Ld}_{24}(p_1,p_2,p_3)\\
&\quad+\frac{s_{12}}{2}\left(2\mathrm{Lc}_1(p_1,p_{23})+\mathrm{Lc}_1(p_{23},p_1)-\mathrm{Lc}_0(p_1,p_{23})\right),\\
(s_{12}-p_1^2)\mathrm{Ld}_{22}(p_1,p_2,p_3) &= s_{12}\left(-\mathrm{Ld}_{21}(p_1,p_2,p_3)+\mathrm{Ld}_1(p_1,p_2,p_3)+\mathrm{Lc}_1(p_1,p_{23})\right),\\
(s_{13}-p_1^2)\mathrm{Ld}_{21}(p_1,p_2,p_3) &= -s_{23}\left(\mathrm{Ld}_{22}(p_1,p_2,p_3)+\mathrm{Ld}_{21}(p_1,p_2,p_3)\right)\\
&\quad+s_{12}\left(\mathrm{Lc}_1(p_{23},p_1)-\mathrm{Lc}_1^{1m}(p_1,p_2)\right),\\
(s_{12}-p_1^2)\mathrm{Ld}_{21}(p_1,p_2,p_3) &= s_{23}\mathrm{Ld}_{24}(p_1,p_2,p_3)-s_{12}\left(\mathrm{Lc}_1(p_{23},p_1)-\mathrm{Lc}_1^{1m}(p_{12},p_3)\right)
\end{aligned} \tag{D.4}$$

D.3 The One-Mass Box

The straightforward symmetry identities which follow directly from the definitions (3.5.2) and (3.60) are,

$$\begin{aligned}
\mathrm{Ld}_{344}^{1m}(p_3,p_2,p_1) &= \mathrm{Ld}_{311}^{1m}(p_1,p_2,p_3),\\
\mathrm{Ld}_{314}^{1m}(p_3,p_2,p_1) &= \mathrm{Ld}_{314}^{1m}(p_1,p_2,p_3),\\
\mathrm{Ld}_{24}^{1m}(p_3,p_2,p_1) &= \mathrm{Ld}_{21}^{1m}(p_1,p_2,p_3),\\
\mathrm{Ld}_{1}^{1m}(p_3,p_2,p_1) &= \mathrm{Ld}_{1}^{1m}(p_1,p_2,p_3),\\
\mathrm{Ld}_{0}^{1m}(p_3,p_2,p_1) &= \mathrm{Ld}_{0}^{1m}(p_1,p_2,p_3).
\end{aligned} \tag{D.5}$$

The further relations useful when a relevant invariant multiplies one of the finite functions are given by,

$$\begin{aligned}
s_{13}\mathrm{Ld}^{1m}_{314}(p_1,p_2,p_3) &= -s_{12}\mathrm{Ld}^{1m}_{21}(p_1,p_2,p_3) + \frac{1}{2}\left(s_{12}\mathrm{Lc}^{2m}_{1}(p_{12},p_3) - s_{23}\mathrm{Lc}^{2m}_{1}(p_{23},p_1) + 1\right),\\
s_{13}\mathrm{Ld}^{1m}_{311}(p_1,p_2,p_3) &= -s_{23}\mathrm{Ld}^{1m}_{21}(p_1,p_2,p_3) + \frac{1}{2}\left(s_{23}\mathrm{Lc}^{2m}_{2}(p_{23},p_1) + \log\left(\frac{s_{123}}{s_{12}}\right)\right),\\
s_{13}\mathrm{Ld}^{1m}_{21}(p_1,p_2,p_3) &= -s_{23}\mathrm{Ld}^{1m}_{1}(p_1,p_2,p_3) + s_{23}\mathrm{Lc}^{2m}_{1}(p_{23},p_1) + \log\left(\frac{s_{123}}{s_{12}}\right),\\
s_{23}\mathrm{Ld}^{1m}_{21}(p_3,p_2,p_1) &= s_{12}\mathrm{Ld}^{1m}_{21}(p_1,p_2,p_3) + s_{23}\mathrm{Lc}^{2m}_{1}(p_{23},p_1) - s_{12}\mathrm{Lc}^{2m}_{1}(p_{12},p_3),\\
s_{13}\mathrm{Ld}^{1m}_{1}(p_1,p_2,p_3) &= \frac{1}{2}\mathrm{Ld}^{1m}_{0}(p_1,p_2,p_3).
\end{aligned} \tag{D.6}$$

D.4 The Opposite Two-Mass Box

The scalar integral possesses symmetry under exchange of the two light-like external legs. Therefore we have,

$$\begin{aligned}
\mathrm{Ld}^{\mathrm{opp}}_{0}(p_3,p_2,p_1) &= \mathrm{Ld}^{\mathrm{opp}}_{0}(p_1,p_2,p_3),\\
\mathrm{Lcd}_{0}(p_3,p_2,p_1) &= \mathrm{Lcd}_{0}(p_1,p_2,p_3).
\end{aligned} \tag{D.7}$$

Recall that there are two types of function specifically introduced to describe the tensor decomposition of this configuration of box. One type of reduction relation relates only one set of these,

$$s_{13}\mathrm{Lcd}_n(p_1,p_2,p_3) = -(s_{12}-p_2^2)\,\mathrm{Lcd}_{n-1}(p_1,p_2,p_3) + \mathrm{Lc}^{2m}_{n}(p_2,p_3) - \mathrm{Lc}^{2m}_{n}(p_{12},p_3), \tag{D.8}$$

for $n = 1,\ldots,4$. Partial cancellation of factors of the Gram determinant yields the identities,

$$\begin{aligned}
\frac{2s_{13}^2}{\Delta_4^{\mathrm{opp}}}\mathrm{Ld}_{311}(p_1,p_2,p_3) &= \frac{2s_{13}}{\Delta_4^{\mathrm{opp}}}\left(-(s_{23}-p_2^2)\,\mathrm{Ld}_{21}(p_1,p_2,p_3) + \frac{1}{2}\log\left(\frac{p_{123}}{p_{12}}\right)\right)\\
&\qquad + \frac{1}{2}\mathrm{Lcd}_2(p_3,p_2,p_1),\\
\frac{2s_{13}^2}{\Delta_4^{\mathrm{opp}}}\mathrm{Ld}_{21}(p_1,p_2,p_3) &= \frac{2s_{13}}{\Delta_4^{\mathrm{opp}}}\left(-(s_{23}-p_2^2)\,\mathrm{Ld}_{1}(p_1,p_2,p_3) + \log\left(\frac{p_{123}}{p_{12}}\right)\right)\\
&\qquad + \mathrm{Lcd}_1(p_3,p_2,p_1),\\
(s_{12}-p_1^2)\,\mathrm{Ld}_{21}(p_1,p_2,p_3) &= (s_{23}-p_2^2)\,\mathrm{Ld}_{21}(p_3,p_2,p_1) + s_{12}\mathrm{Lc}^{2m}_{1}(p_{12},p_3)\\
&\qquad - s_{23}\mathrm{Lc}^{2m}_{1}(p_{23},p_1).
\end{aligned} \tag{D.9}$$

D.5 The One-Mass Pentagon

The pentagon function which arises in the scalar and first-rank tensor integrals changes sign under reversal of order of the legs,

$$\mathrm{Le}_1(p_4, p_3, p_2, p_1) = -\mathrm{Le}_1(p_1, p_2, p_3, p_4). \tag{D.10}$$

Appendix E

Explicit Form of $\mathcal{L}_C(1,2;1,2)$

This appendix gives the explicit form of one of the four-quark finite functions. In contrast to the notation adopted throughout Chapter 3 and Appendices B, C, D here all the particle momenta are light-like, $p_i^2 = 0$ for $i = 1, \ldots 4$. For this reason, the superscripts on the finite functions have been dropped, with the arguments of the functions themselves indicating the relevant mass configuration.

This example also explicitly demonstrates the correspondence of the singularity structure to the tree-level matrix elements. The relevant tree-level ampitude squared is $\mathcal{T}(1,2;1,2)$, which contains only double poles (at most) in the invariants s_{34}, s_{134} and s_{234}. Therefore these are the only denominators allowed in $\mathcal{L}_C(1,2;1,2)$.

$$
\begin{aligned}
&\mathcal{L}_C(1,2;1,2) = \\
&(-96\, s_{12}\, s_{13} - 136\, s_{12}\, s_{34} + 40\, s_{13}^2 - 40\, s_{13}\, s_{14} - 272\, s_{13}\, s_{23} - 40\, s_{13}\, s_{24} - 56\, s_{13}\, s_{34} + 40\, s_{14}\, s_{23} \\
&\quad +16\, s_{14}\, s_{34} - 80\, s_{23}\ s34 - 80\, s_{24}\, s_{34}) \Big/ (\, s_{34}^2\, s_{134}\,) \ + (160\, s_{12}\, s_{13}^2 + 160\, s_{12}\, s_{13}\, s_{34} \\
&\quad +80\, s_{12}\, s_{34}^2 + 160\, s_{13}^2\, s_{23} + 160\, s_{13}^2\, s_{24} + 160\, s_{13}\, s_{23}\, s_{34} + 160\, s_{13}\, s_{24}\, s_{34} + 80\, s_{23}\, s_{34}^2 \\
&\quad +80\, s_{24}\, s_{34}^2) \Big/ (\, s_{34}^2\, s_{134}^2\,) \ + \mathrm{Ld}_0(p_1,p_4,p_{23})(32\, s_{12}\, s_{13} - 64\, s_{12}\, s_{14} + 16\, s_{13}^2 \\
&\quad -16\, s_{13}\, s_{14} + 64\, s_{13}\ s_{23} + 48\, s_{13}\, s_{24} + 32\, s_{13}\, s_{34} - 80\, s_{14}\, s_{23} - 64\, s_{14}\, s_{24} - 32\, s_{14}\, s_{34} \\
&\quad +16\, s_{24}\, s_{34} + 16\, s_{34}^2) \Big/ (\, s_{34}^2\, s_{134}\,) \ + \mathrm{Ld}_0(p_2,p_3,p_4)(-64\, s_{12}^2\, s_{34} + 64\ s_{12}\, s_{13}\, s_{24} \\
&\quad +64\, s_{12}\, s_{14}\, s_{23} - 16\ s_{12}\, s_{14}\, s_{34} - 32\, s_{12}\, s_{23}\, s_{34} - 32\, s_{12}\, s_{24}\, s_{34} - 48\, s_{12}\, s_{34}^2 + 32\, s_{13}^2\, s_{24}
\end{aligned}
$$

$$
\begin{aligned}
&-16\,s_{13}\,s_{14}\,s_{23} - 16\;\,s_{13}\,s_{14}\,s_{24} - 32\,s_{13}\,s_{23}\,s_{24} - 16\,s_{13}\,s_{23}\,s_{34} + 32\,s_{13}\,s_{24}^2 \\
&+16\,s_{13}\,s_{24}\,s_{34} + 16\,s_{14}^2\,s_{23} + 32\,s_{14}\,s_{23}^2 - 32\,s_{14}\,s_{23}\,s_{24} - 16\,s_{14}\,s_{23}\,s_{34})\,/(\,s_{34}^2\,s_{234}s_{134}\,) \\
&+(-80\,s_{12}^2\,s_{34} - 80\,s_{12}\,s_{13}\,s_{23} - 120\,s_{12}\,s_{13}\,s_{34} + 80\,s_{12}\,s_{14}\,s_{23} - 40\,s_{12}\,s_{14}\,s_{34} \\
&-40\,s_{12}\,s_{34}^2 - 40\,s_{13}^2\,s_{23} - 40\,s_{13}^2\,s_{34} + 40\,s_{13}\;\,s_{14}\,s_{34} + 80\,s_{13}\,s_{23}^2 + 120\,s_{13}\,s_{23}\,s_{34} \\
&+40\,s_{13}\,s_{34}^2 + 40\,s_{14}^2\,s_{23} + 80\,s_{14}\,s_{23}^2 + 40\,s_{14}\;\,s_{23}\,s_{34})\,/(\,s_{34}^2\,s_{234}\,s_{134}\,) \\
&+\mathrm{Ld}_0(p_1,p_4,p_3)(32\,s_{12}\,s_{13} + 64\,s_{12}\,s_{14} + 32\,s_{12}\,s_{34} + 16\,s_{13}^2 - 16\,s_{13}\,s_{14} - 32\,s_{13}\,s_{23} \\
&+48\,s_{13}\,s_{24} + 32\,s_{13}\;\,s_{34} + 80\,s_{14}\,s_{23} + 64\,s_{14}\,s_{24} + 64\,s_{24}\,s_{34} + 16\,s_{34}^2)\,/(\,s_{34}^2\,s_{134}\,) \\
&+\mathrm{Lc}_1(p_{23},p_{14})(16\,s_{12}^2\;\,s_{34} + 16\,s_{12}\,s_{13}\,s_{34} + 16\,s_{12}\;\,s_{14}\,s_{34} - 32\,s_{12}\,s_{24}\,s_{34} - 16\;\,s_{12}\,s_{34}^2 \\
&+16\,s_{13}\,s_{14}\,s_{34} + 16\;\,s_{13}\,s_{24}\,s_{34} + 16\,s_{14}\,s_{24}\,s_{34} + 16\,s_{14}\,s_{34}^2 - 16\,s_{24}^2\,s_{34} - 16\,s_{24}\,s_{34}^2)\,/ \\
&(\,s_{34}^2\,s_{134}\,) + \mathrm{Ld}_0(p_2,p_3,p_{14})(32\,s_{12}\,s_{13} + 16\;\,{s_{13}}^2 + 16\,s_{13}\,s_{14} - 32\,s_{13}\,s_{23} + 48\,s_{13}\,s_{24} \\
&+32\,s_{13}\,s_{34} - 32\,s_{14}^2 - 16\,s_{14}\,s_{23} + 32\,s_{14}\,s_{24} + 32\,s_{14}\,s_{34} - 32\,s_{23}\,s_{34} + 16\,s_{24}\,s_{34} \\
&+16\,s_{34}^2)\,/(\,s_{34}^2\,s_{134}\,) + \mathrm{Ld}_0(p_1,p_4,p_3)(-128\,s_{12}\,s_{13}\,s_{14} - 64\,s_{12}\,s_{13}\,s_{34} \\
&-128\,s_{12}\,s_{14}\,s_{34} - 32\;\,s_{12}\,s_{34}^2 - 128\,s_{13}\,s_{14}\,s_{23} - 128\,s_{13}\,s_{14}\,s_{24} - 64\,s_{13}\,s_{23}\,s_{34} \\
&-64\,s_{13}\,s_{24}\,s_{34} - 128\;\,s_{14}\,s_{23}\,s_{34} - 128\,s_{14}\,s_{24}\,s_{34} - 32\,s_{23}\,s_{34}^2 - 32\,s_{24}\,s_{34}^2)\,/(\,s_{34}^2\,s_{134}^2\,) \\
&+\mathrm{Ld}_0(p_2,p_3,p_{14})(-64\,s_{12}\,s_{13}\,s_{14} - 32\,s_{12}\,s_{13}\,s_{34} + 64\,s_{12}\,s_{14}^2 + 32\,s_{12}\;\,s_{14}\,s_{34} \\
&+32\,s_{12}\,s_{34}^2 - 32\,s_{13}^2\,s_{14} - 32\,s_{13}^2\,s_{34} - 32\,s_{13}\;\,s_{14}\,s_{23} - 96\,s_{13}\,s_{14}\,s_{24} - 64\;\,s_{13}\,s_{14}\,s_{34} \\
&-32\,s_{13}\,s_{23}\,s_{34} - 64\;\,s_{13}\,s_{24}\,s_{34} - 32\,s_{13}\,s_{34}^2 + 32\,s_{14}^3 + 96\,s_{14}^2\,s_{23} + 32\,s_{14}^2\,s_{24} \\
&+32\,s_{14}^2\,s_{34} + 64\,s_{14}\,s_{23}\,s_{34} - 32\,s_{14}\,s_{24}\,s_{34} + 32\,s_{23}\,s_{34}^2)\,/(\,s_{34}^2\,s_{134}^2\,) + \mathrm{Lc}_1(p_1,p_{34}) \\
&(-96\,s_{12}\,s_{13}^2 + 24\,s_{12}\,s_{34}^2 - 96\,s_{13}^2\,s_{23} - 96\,s_{13}^2\,s_{24} - 128\,s_{13}^2\,s_{34} + 56\,s_{13}\,s_{23}\,s_{34} \\
&-56\,s_{13}\,s_{24}\,s_{34})\,/(\,s_{34}^2\,s_{134}\,) \\
&+\mathrm{Lc}_2(p_1,p_{234})\,(\,32\,s_{13}^2\,s_{23} + 32\,s_{13}^2\,s_{24} - 16\,s_{13}^2\,s_{34} - 16\,s_{14}^2\,s_{34}\,)\,/\,(s_{34}^2\,s_{134}) + \mathrm{Lc}_2(p_2,p_{34}) \\
&(\,-16\,s_{12}^2\,s_{34} - 16\,s_{12}\;\,s_{13}\,s_{23} + 16\,s_{12}\,s_{14}\,s_{23} + 16\;\,s_{13}\,s_{23}^2 + 16\,s_{14}\,s_{23}^2\,)\,/(\,s_{34}^2\,s_{134}\,) \\
&+\mathrm{Ld}_1(p_1,p_4,p_{23}) \\
&(-32\,s_{12}^2\,s_{34} - 16\,s_{12}\,s_{13}\,s_{34} - 16\,s_{12}\,s_{14}\,s_{34} - 32\,s_{12}\,s_{23}\,s_{34} + 32\,s_{12}\,s_{24}\,s_{34} + 16\,s_{12}\,s_{34}^2\,) \\
&/(\,s_{34}^2\,s_{134}\,) + \mathrm{Ld}_1(p_2,p_3,p_4)(-32\,s_{12}^2\;\,{s_{34}}^2 + 16\,s_{12}\,s_{13}\,s_{34}^2 + 48\,s_{12}\,s_{14}\,s_{23}\,s_{34} \\
&-16\,s_{12}\,s_{23}\,s_{34}^2 + 16\,s_{13}\,s_{14}\,s_{23}\,s_{34} - 16\,s_{14}^2\,s_{23}^2 + 16\,s_{14}\,s_{23}^2\,s_{34})\,/(\,s_{34}^2\,s_{234}\,s_{134}\,)
\end{aligned}
$$

$$+\mathrm{Lcd}_2(p_1,p_{34},p_2)\,(-32\,s_{13}\,s_{23}^3-32\;\;s_{13}\,s_{23}^2\,s_{24}-32\,s_{14}\,s_{23}^3-32\,s_{14}\,s_{23}^2\,s_{24})\,/\,s_{34}^2\;\;s_{134}$$

$$+\mathrm{Ld}_{21}(p_4,p_3,p_2)\,(-32\,s_{12}\,s_{14}\,s_{34}^2+16\,s_{14}^2\,s_{23}\,s_{34})\,/\,s_{34}^2\,s_{234}\,s_{134}+\mathrm{Ld}_{22}(p_1,p_4,p_{23})$$

$$(-16\,s_{12}\,s_{24}^2\,s_{34}-16\;\;s_{13}\,s_{24}^2\,s_{34}+32\,s_{14}\,s_{23}\,s_{24}\,s_{34}+16\,s_{14}\,s_{24}^2\,s_{34})\,/(\,s_{34}^2\,s_{234}\,s_{134})$$

$$+\mathrm{Ld}_1(p_1,p_4,p_3)\,(-16\,s_{12}\,s_{34}^2+16\;\;s_{14}\,s_{23}\,s_{34})\,/\,s_{34}^2\,s_{134}+\mathrm{Ld}_0(p_2,p_3,p_4)(-32\,s_{12}\,s_{13}$$

$$-64\,s_{12}\,s_{14}-32\,s_{12}\;\;s_{34}-16\,s_{13}^2+32\,s_{13}\,s_{23}+16\,s_{13}\,s_{24}-16\,s_{13}\,s_{34}-16\,s_{14}\,s_{23}$$

$$-64\,s_{14}\,s_{24}-32\,s_{14}\;\;s_{34}-16\,s_{24}\,s_{34}-16\,s_{34}^2)\,/(\,s_{34}^2\,s_{134})\;+\mathrm{Ld}_1(p_1,p_4,p_{23})$$

$$(32\,s_{12}^2\,s_{23}\,s_{34}-32\,s_{12}^2\,s_{24}\,s_{34}+16\,s_{12}\,s_{13}\,s_{23}\,s_{34}-48\,s_{12}\,s_{13}\,s_{24}\,s_{34}$$

$$+48\,s_{12}\,s_{14}\,s_{23}\,s_{34}-16\,s_{12}\,s_{14}\,s_{24}\,s_{34}+32\,s_{12}\,s_{23}^2\,s_{34}+32\,s_{12}\,s_{23}\,s_{24}\,s_{34}$$

$$+16\,s_{12}\,s_{23}\,s_{34}^2+64\,s_{12}\,s_{24}^2\,s_{34}+48\,s_{12}\,s_{24}\,s_{34}^2-16\,s_{13}^2\,s_{24}\,s_{34}+16\,s_{13}\,s_{14}\,s_{23}\,s_{34}$$

$$-16\,s_{13}\,s_{14}\,s_{24}\,s_{34}+32\,s_{13}\,s_{24}^2\,s_{34}+16\,s_{13}\;\;s_{24}\,s_{34}^2+16\,s_{14}^2\,s_{23}\,s_{34}$$

$$-32\,s_{14}\,s_{23}\,s_{24}\,s_{34}-16\,s_{14}\,s_{23}\,s_{34}^2)\,/(\,s_{34}^2\,s_{234}\,s_{134})\;+\mathrm{Lc}_0(p_{14},p_{23})(-32\,s_{12}^2\,s_{34}$$

$$-16\,s_{12}\,s_{13}\,s_{34}-16\;\;s_{12}\,s_{14}\,s_{34}+96\,s_{12}\,s_{24}\,s_{34}+48\,s_{12}\,s_{34}^2-16\,s_{13}^2\,s_{34}-16\,s_{13}\,s_{23}\,s_{34}$$

$$-16\,s_{13}\,s_{24}\,s_{34}-16\;\;s_{13}\,s_{34}^2+16\,s_{14}\,s_{23}\,s_{34}+16\,s_{14}\,s_{24}\,s_{34}+16\,s_{14}\,s_{34}^2+16\,s_{23}\,s_{34}^2$$

$$-16\,s_{24}^2\,s_{34}-16\,s_{24}\,s_{34}^2)\,/(\,s_{34}^2\,s_{134})\;+\mathrm{Lc}_1(p_1,p_{234})(16\,s_{13}^2\,s_{23}+32\,s_{13}^2\,s_{24}$$

$$+48\,s_{13}^2\,s_{34}-32\,s_{13}\,s_{14}\,s_{34}+32\,s_{13}\,s_{23}\,s_{34}+96\,s_{13}\,s_{24}\,s_{34}+16\,s_{14}^2\,s_{23}+48\,s_{14}^2\,s_{34}$$

$$+16\,s_{14}\,s_{23}\,s_{34}-16\;\;s_{14}\,s_{24}\,s_{34}-32\,s_{14}\,s_{34}^2)\,/(\,s_{34}^2\,s_{134})\;+\mathrm{Lc}_1(p_2,p_{34})(48\,s_{12}^2\,s_{34}$$

$$+48\,s_{12}\,s_{13}\,s_{23}-8\,s_{12}\,s_{13}\,s_{34}-48\,s_{12}\,s_{14}\,s_{23}+40\,s_{12}\,s_{14}\,s_{34}+40\,s_{12}\,s_{34}^2+24\,s_{13}^2\,s_{23}$$

$$-48\,s_{13}\,s_{23}^2+40\,s_{13}\,s_{23}\,s_{34}-24\,s_{14}^2\,s_{23}-48\;\;s_{14}\,s_{23}^2+24\,s_{14}\,s_{23}\,s_{34})\,/(\,s_{34}^2\,s_{134})$$

$$+\mathrm{Lc}_1(p_2,p_{134})(112\,s_{13}^2\,s_{23}-16\,s_{13}^2\,s_{24}+112\,s_{13}\;\;s_{14}\,s_{23}-16\,s_{13}\,s_{14}\,s_{24}$$

$$+160\,s_{13}\,s_{23}\,s_{34}+80\;\;s_{14}\,s_{23}\,s_{34}+16\,s_{14}\,s_{24}\,s_{34}+16\,s_{23}\,s_{34}^2+16\,s_{24}\,s_{34}^2)\,/(\,s_{34}^2\,s_{134})$$

$$+\mathrm{Lc}_1(p_3,p_{14})\,(-16\,s_{12}\,s_{34}^2-16\,s_{14}\,s_{23}\,s_{34}-32\,s_{14}\,s_{34}^2-32\;\;s_{23}\,s_{34}^2-16\,s_{24}\,s_{34}^2)\,/\,s_{34}^2\,s_{134}$$

$$+\mathrm{Lc}_1(p_4,p_{23})$$

$$(-16\,s_{12}\,s_{14}\,s_{34}+32\,s_{12}\,s_{34}^2-16\,s_{13}\,s_{14}\,s_{34}-32\;\;s_{14}\,s_{23}\,s_{34}-48\,s_{23}\,s_{34}^2+16\,s_{34}^3)$$

$$/(s_{34}^2\,s_{134})+\mathrm{Lc}_1(p_{14},p_{23})(-16\,s_{12}\,s_{13}\,s_{34}-16\;\;s_{12}\,s_{34}^2-16\,s_{13}^2\,s_{34}-16\;\;s_{13}\,s_{23}\,s_{34}$$

$$-16\,s_{13}\,s_{34}^2-16\,s_{14}\,s_{23}\,s_{34}+16\,s_{23}\,s_{34}^2-16\;\;{s_{24}}^2\,s_{34})\,/(\,s_{34}^2\,s_{134})$$

$$+\mathrm{Lcd}_2(p_2,p_{34},p_1)\,(-32\,s_{13}^3\,s_{23}-32\;\;{s_{13}}^3\,s_{24}-32\,s_{13}^2\,s_{14}\,s_{23}-32\,s_{13}^2\,s_{14}\,s_{24})\,/\,s_{34}^2\,s_{134}$$

$$
\begin{aligned}
&+\mathrm{Ld}_0(p_1,p_4,p_{23})(-96\ s_{24}\,s_{34}^2-32\,s_{13}\,s_{23}^2-32\,s_{12}\,s_{34}^2-64\,s_{12}^2\,s_{34}-64\,s_{13}\,s_{34}^2\\
&-32\,s_{13}^2\,s_{34}-32\,s_{34}^3-32\,s_{13}^2\,s_{23}+96\,s_{14}\,s_{23}^2+32\,s_{14}^2\,s_{23}-64\,s_{12}\,s_{13}\ s_{23}\\
&-96\,s_{12}\,s_{13}\,s_{34}+64\ s_{12}\,s_{14}\,s_{23}-32\,s_{12}\,s_{14}\,s_{34}+32\,s_{13}\,s_{14}\,s_{34}-96\,s_{13}\,s_{23}\,s_{34}\\
&+96\,s_{14}\,s_{23}\,s_{34}-96\ s_{13}\,s_{24}\,s_{34}+32\,s_{14}\,s_{24}\,s_{34}+32\,s_{14}\,s_{34}^2-64\,s_{24}^2\,s_{34}+32\,s_{23}^2\,s_{34}\\
&-96\,s_{13}\,s_{23}\,s_{24}+32\ s_{14}\,s_{23}\,s_{24}-32\,s_{23}\,s_{24}\,s_{34})\,/(\,s_{34}^2\,s_{234}\,s_{134}\,)\\
&+\mathrm{Lc}_2(p_1,p_{34})\,(\,32\,s_{12}\,s_{13}^2+16\,s_{13}^2\,s_{23}+16\,s_{13}^2\,s_{24}+32\,s_{13}^2\,s_{34}\,)\,/\,s_{34}^2\,s_{134}\\
&+\mathrm{Le}_1(p_1,p_4,p_3,p_2)(32\,s_{13}^2\,s_{23}^2-32\,s_{14}^2\ {s_{23}}^2-16\,s_{13}^3\,s_{23}+32\,s_{12}\ s_{14}\,s_{34}^2-32\,s_{13}^2\,s_{23}\,s_{34}\\
&-16\,s_{13}\,s_{23}\,s_{34}^2-32\,s_{14}^2\,s_{23}\,s_{34}+64\,s_{13}\,s_{14}\,s_{23}^2+32\,s_{13}\,s_{23}^2\,s_{34}-128\,s_{14}^2\,s_{23}\,s_{24}\\
&+16\,s_{14}\,s_{23}^2\,s_{34}-16\,s_{13}^2\,s_{14}\,s_{23}+16\,s_{13}\,s_{14}^2\,s_{23}-32\,s_{13}\,s_{14}\,s_{23}\,s_{34}+16\,s_{14}^3\,s_{23}\\
&-64\ {s_{14}}^2\,s_{24}^2-16\,s_{12}\,s_{23}\,s_{34}^2-16\,s_{12}\,s_{14}^2\,s_{34}+16\,s_{14}\,s_{24}^2\,s_{34}+32\,s_{12}^2\,s_{14}\,s_{34}\\
&-48\,s_{12}\,s_{13}\,s_{23}\,s_{34}+32\,s_{12}\,s_{14}\,s_{23}\,s_{34}+48\,s_{12}\,s_{14}\,s_{24}\,s_{34}-32\,s_{12}\,s_{13}^2\,s_{23}-32\,s_{12}\,s_{14}^2\,s_{23}\\
&-64\,s_{12}\,s_{14}^2\,s_{24}-32\,s_{14}^2\,s_{24}\,s_{34}+16\,s_{14}\,s_{24}\,s_{34}^2+16\,s_{12}\,s_{13}\,s_{14}\,s_{34})\,/(\,s_{34}^2\,s_{134}\,)\\
&+\mathrm{Lc}_2(p_2,p_{134})\,(\,32\,s_{13}\,s_{23}^2+32\,s_{14}\ {s_{23}}^2\,)\,/\,s_{34}^2\,s_{134}+\mathrm{Lcd}_0(p_1,p_{34},p_2)(-48\,s_{12}\,s_{13}\,s_{34}^2\\
&+32\,s_{12}\,s_{14}\,s_{34}^2+32\,s_{12}\,s_{34}^3-48\,s_{13}^2\,s_{23}\ s_{34}+32\,s_{13}^2\,s_{24}\,s_{34}-128\,s_{13}\,s_{14}\,s_{23}\,s_{34}\\
&-192\,s_{13}\,s_{23}\,s_{34}^2-80\,s_{13}\,s_{24}\,s_{34}^2-48\,s_{14}^2\ s_{23}\,s_{34}-112\,s_{14}\,s_{23}\,s_{34}^2)\,/(\,s_{34}^2\,s_{134}\,)\\
&+\mathrm{Lcd}_1(p_1,p_{34},p_2)(-112\ {s_{13}}^2\,s_{23}^2-80\,s_{13}^2\,s_{23}\,s_{24}-128\,s_{13}\,s_{14}\,s_{23}^2-64\,s_{13}\,s_{14}\,s_{23}\,s_{24}\\
&-176\,s_{13}\,s_{23}^2\,s_{34}-112\,s_{13}\,s_{23}\,s_{24}\,s_{34}-16\,s_{14}^2\,s_{23}^2+16\,s_{14}^2\,s_{23}\,s_{24}-112\,s_{14}\,s_{23}^2\,s_{34}\\
&-48\,s_{14}\,s_{23}\,s_{24}\,s_{34})\,/(\,s_{34}^2\,s_{134}\,)\ +\mathrm{Lcd}_1(p_2,p_{34},p_1)(-16\,s_{13}^3\,s_{23}-16\,s_{13}^3\,s_{24}\\
&-32\,s_{13}^2\,s_{14}\,s_{23}-32\,s_{13}^2\,s_{14}\,s_{24}-80\,s_{13}^2\ s_{23}\,s_{34}-80\,s_{13}^2\,s_{24}\,s_{34}-16\,s_{13}\,s_{14}^2\,s_{23}\\
&-16\,s_{13}\,s_{14}^2\,s_{24}-16\,s_{13}\,s_{14}\,s_{23}\,s_{34}-16\,s_{13}\ s_{14}\,s_{24}\,s_{34})\,/(\,s_{34}^2\,s_{134}\,)\\
&+\mathrm{Ld}_1(p_2,p_3,p_4)\,(\,-16\,s_{12}\,s_{14}\,s_{34}-16\,s_{12}\,s_{34}^2+16\,s_{14}^2\,s_{23}+16\,s_{14}\,s_{23}\,s_{34}\,)\,/\,s_{34}^2\,s_{134}\\
&+\mathrm{Ld}_1(p_2,p_3,p_{14})\,(\,16\,s_{12}\,s_{13}\,s_{34}+16\,s_{12}\,s_{14}\,s_{34}+16\,s_{12}\,s_{34}^2\,)\,/\,s_{34}^2\,s_{134}+\mathrm{Ld}_1(p_2,p_3,p_{14})\\
&(16\,s_{12}\,s_{13}^2\,s_{34}+16\,s_{12}\,s_{13}\,s_{34}^2-16\,s_{12}\,s_{14}^2\ s_{34}-16\,s_{12}\,s_{14}\,s_{34}^2+16\,s_{13}^2\,s_{24}\,s_{34}\\
&-16\,s_{13}\,s_{14}\,s_{23}\,s_{34}+16\,s_{13}\,s_{14}\,s_{24}\,s_{34}+16\,s_{13}\,s_{24}\,s_{34}^2-16\,s_{14}^2\,s_{23}\ s_{34}-16\,s_{14}\,s_{23}\,s_{34}^2)\\
&/(\,s_{34}^2\,s_{134}^2\,)\ +\mathrm{Ld}_{24}(p_1,p_4,p_{23})\\
&(\,48\,s_{12}^2\,s_{24}\,s_{34}+16\,s_{12}^2\,s_{34}^2+32\,s_{12}\,s_{13}\,s_{24}\ s_{34}-32\,s_{12}\,s_{14}\,s_{23}\,s_{34}\,)\,/(\,s_{34}^2\,s_{234}\,s_{134}\,)
\end{aligned}
$$

$$+\mathrm{Ld}_{21}(p_1,p_4,p_{23})\,(\,16\,s_{14}\,s_{23}^2\,s_{34}+32\,s_{14}\,s_{23}\,s_{24}\,s_{34}+16\,s_{14}\,s_{24}^2\,s_{34}\,)\,\Big/\,s_{34}^2\,s_{234}\;\;s_{134}$$

$$+16\,\mathrm{Ld}_{21}(p_2,p_3,p_4)\,s_{12}^2\,s_{34}^2\,\Big/\,s_{34}^2\,s_{234}\,s_{134}$$

$$+\log\left(\frac{s_{1234}}{s_{14}}\right)\,(\,16\,s_{12}\,s_{34}+16\,s_{14}\,s_{34}+32\;\;s_{23}\,s_{34}+32\,s_{24}\,s_{34}\,)\,\Big/\,s_{34}^2\,s_{134}$$

$$+\log\left(\frac{s_{1234}}{s_{14}}\right)\,(\,-32\,s_{12}\,s_{13}\,s_{34}-32\,s_{13}\;\;s_{23}\,s_{34}-32\,s_{13}\,s_{24}\,s_{34}\,)\,\Big/\,{s_{34}}^2\,s_{134}^2+\log\left(\frac{s_{1234}}{s_{23}}\right)$$

$$(-16\,s_{12}\,s_{13}\,s_{34}+16\,s_{12}\,s_{14}\,s_{34}-16\,s_{12}\,s_{34}^2+16\;\;s_{13}\,s_{14}\,s_{34}+16\,s_{13}\,s_{23}\,s_{34}+16\,s_{13}\,s_{34}^2$$

$$+16\,s_{14}\,s_{23}\,s_{34})\,\Big/(\,s_{34}^2\,s_{234}\,s_{134}\,)\,\log\left(\frac{s_{1234}}{s_{23}}\right)\,(\,32\,s_{23}\,s_{34}+16\,s_{24}\,s_{34}-16\,s_{34}^2\,)\,\Big/\,s_{34}^2\,s_{134}$$

$$+\log\left(\frac{s_{234}}{s_{34}}\right)\,(16\,s_{12}\,s_{13}\,s_{34}-16\,s_{12}\,s_{14}\,s_{34}+16\,s_{12}\,s_{34}^2-16\,s_{13}\,s_{14}\,s_{34}-16\,s_{13}\,s_{23}\,s_{34}$$

$$-16\,s_{13}\,s_{34}^2-16\,s_{14}\,s_{23}\,s_{34})\,\Big/(\,s_{34}^2\,s_{234}\,s_{134}\,)$$

$$+\log\left(\frac{s_{134}}{s_{34}}\right)\,(\,32\,s_{12}\,s_{13}\,s_{34}+32\,s_{13}\,s_{23}\,s_{34}+32\,s_{13}\,s_{24}\,s_{34}\,)\,\Big/\,s_{34}^2\,s_{134}^2+\log\left(\frac{s_{1234}}{s_{34}}\right)$$

$$(48\,s_{12}\,s_{13}+72\,s_{12}\,s_{34}-24\,s_{13}^2+24\,s_{13}\,s_{14}+144\,s_{13}\,s_{23}+24\;\;s_{13}\,s_{24}+40\,s_{13}\,s_{34}$$

$$-24\,s_{14}\;\;s_{23}-24\,s_{23}\,s_{34}+48\,s_{24}\;\;s_{34}+48\,s_{34}^2)\,\Big/(\,s_{34}^2\,s_{134}\,)\;+\log\left(\frac{s_{1234}}{s_{234}}\right)\,(48\,s_{12}^2\,s_{34}$$

$$+48\,s_{12}\,s_{13}\,s_{23}+88\,s_{12}\,s_{13}\,s_{34}-48\;\;s_{12}\,s_{14}\,s_{23}+8\,s_{12}\,s_{14}\,s_{34}+40\,s_{12}\,s_{34}^2+24\,s_{13}^2\,s_{23}$$

$$+24\,s_{13}^2\,s_{34}-40\,s_{13}\,s_{14}\,s_{34}-48\;\;s_{13}\,s_{23}^2-88\,s_{13}\,s_{23}\,s_{34}-40\,s_{13}\,s_{34}^2-24\,s_{14}^2\,s_{23}$$

$$-48\,s_{14}\,s_{23}^2-40\,s_{14}\,s_{23}\,s_{34})\,\Big/(\,s_{34}^2\,s_{234}\,s_{134}\,)$$

$$+\log\left(\frac{s_{1234}}{s_{234}}\right)\,(\,80\,s_{13}\,s_{34}-48\,s_{14}\,s_{34}-64\;\;s_{23}\,s_{34}-64\,s_{24}\,s_{34}-16\,s_{34}^2\,)\,\Big/\,s_{34}^2\,s_{134}$$

$$-\log\left(\frac{s_{1234}}{s_{134}}\right)\,(\,32\,s_{12}\,s_{34}+64\,s_{13}\,s_{34}+48\,s_{14}\,s_{34}-40\,s_{23}\,s_{34}+16\,s_{24}\,s_{34}+64\,s_{34}^2\,)$$

$$\Big/\,s_{34}^2\,s_{134}+\log\left(\frac{s_{1234}}{s_{134}}\right)\,(-96\,s_{12}\,s_{13}^2-64\,s_{12}\,s_{13}\,s_{34}-48\,s_{12}\,s_{34}^2-96\,s_{13}^2\,s_{23}-96\,s_{13}^2\,s_{24}$$

$$-64\,s_{13}\,s_{23}\,s_{34}-64\;\;s_{13}\,s_{24}\,s_{34}-48\,s_{23}\,s_{34}^2-48\,s_{24}\,s_{34}^2)\,\Big/(\,s_{34}^2\,s_{134}^2\,).$$

Appendix F

Azimuthal Correlations

In considering the triple collinear limits of chapter 7, it is important to consider azimuthal correlations between polarization vectors whenever there is a propagating spin-1 particle. These considerations are even evident at the double collinear level when one considers the splitting $g \to gg$. Universal factorization in this collinear limit is only true after azimuthal averaging.

In such cases, the usual approach to collinear limits is not sufficient. When identifying the singular behaviour of the matrix elements in the collinear region, it is normal simply to introduce a momentum fraction for each collinear particle, $p_i = z_i P$. However, these relations are only true *exactly* in the collinear limit, when all particles travel along a given direction. However, we are really studying the singular behaviour as an invariant $s \to 0$, not the exact limit of $s = 0$. This discrepancy manifests itself as extra powers of invariants in the denominator of the matrix elements squared. By allowing the collinear particles some rotation around the collinear direction we may recover the true behaviour. A proper formalism should suitably expand all factors in the numerator - including angular factors - before the collinear limit is taken. The splitting function factorization of matrix elements is then only true *after all azimuthal integrations have been carried out.*

In this appendix we show explicitly how the azimuthal terms may be implemented - first in the simple case of two collinear particles and then by extending the results to the triple

collinear case of chapter 7.

F.1 Two Collinear Particles

We first consider the case of a collinear pair in a final state of four on-shell particles. The particle momenta will be written p_i, $i = 1, \ldots, 4$ and we use the generalized Mandelstam variables $s_{ij} = (p_i + p_j)^2$. Particles 3 and 4 are chosen to be collinear, with the combined momentum, $p_{(34)}$ in the z-direction in the centre-of-momentum frame,

$$p_{(34)} = (E_{34}, 0, 0, \alpha),$$

where $s_{34} = p_{(34)}^2 = E_{34}^2 - \alpha^2$. By introducing a transverse momentum $p_T = xE_{34}\sin\theta = (1-x)E_{34}\sin\theta'$, we can write the momenta of the individual particles as,

$$\begin{aligned} p_3 &= (xE_{34}, p_T\sin\phi, p_T\cos\phi, xE_{34}\cos\theta)\,, \\ p_4 &= ((1-x)E_{34}, -p_T\sin\phi, -p_T\cos\phi, (1-x)E_{34}\cos\theta')\,. \end{aligned}$$

Here x is the usual momentum fraction and ϕ the azimuthal angle which will be integrated over. Now consider the two other final state particles, which are not collinear. We represent these generically by,

$$\begin{aligned} p_1 &= (E_1, 0, a, b)\,, \\ p_2 &= (E_2, 0, -a, -b-\alpha)\,, \end{aligned}$$

so that the combined momemtum balances $p_{(34)}$ and $s_{1234} = (E_1 + E_2 + E_{34})^2$. The on-shell conditions for p_1 and p_2 require that,

$$E_1^2 = a^2 + b^2, \qquad E_2^2 = a^2 + (b+\alpha)^2. \tag{F.1}$$

To relate the matrix elements to the 3-particle state represented by 1, 2 and (34) we introduce the further variables,

$$\begin{aligned} y_{12} &= (p_1 + p_2)^2 = (E_1 + E_2)^2 - \alpha^2, \\ y_{13} &= (p_1 + p_{(34)})^2 = 2E_1E_{34} - 2b\alpha + s_{34}, \\ y_{23} &= (p_2 + p_{(34)})^2 = 2E_2E_{34} + 2\alpha(b+\alpha) + s_{34}. \end{aligned}$$

It is now simple to re-write the 4-particle variables s_{ij} in terms of these new variables. For example,

$$\begin{aligned} s_{13} &= 2p_1 \cdot p_3 = 2xE_1E_{34} - 2ap_T\cos\phi - 2bxE_{34}\cos\theta \\ &= x(y_{13} - s_{34}) - 2ap_T\cos\phi + 2bx(\alpha - E_{34}\cos\theta), \end{aligned} \tag{F.2}$$

and,

$$\begin{aligned} s_{23} &= 2p_2 \cdot p_3 = 2xE_2E_{34} + 2ap_T\cos\phi + 2(b+\alpha)xE_{34}\cos\theta \\ &= x(y_{23} - s_{34}) + 2ap_T\cos\phi - 2(b+\alpha)x(\alpha - E_{34}\cos\theta). \end{aligned} \tag{F.3}$$

In order to complete the connection between the two sets of variables, we need expressions for p_T, a and b. We first consider θ and θ' small (effectively dropping terms of order p_T^3) to find,

$$\begin{aligned} s_{34} &= 2p_3 \cdot p_4 = E_{34}^2 - [xE_{34}\cos\theta + (1-x)E_{34}\cos\theta']^2 \\ &= E_{34}^2\left(x\theta^2 + (1-x)\theta'^2\right) \\ &= E_{34}p_T\Theta, \end{aligned} \tag{F.4}$$

where we have also introduced the opening angle $\Theta = \theta + \theta'$. This is simply obtained via,

$$\Theta = \frac{p_T}{xE_{34}} + \frac{p_T}{(1-x)E_{34}} = \frac{p_T}{x(1-x)E_{34}},$$

which then yields the simple relation,

$$p_T^2 = x(1-x)s_{34}.$$

By using this equality and the on-shell condition for p_3, namely $p_T^2 = x^2E_{34}^2(1-\cos^2\theta)$ we find that the coefficient of the b term in eq. (F.2) can be re-written as,

$$2x(\alpha - E_{34}\cos\theta) = \frac{s_{34}}{E_{34}}(1-2x).$$

In fact, we find that all the terms which are explicitly of order s_{34} or higher can be dropped when we substitute the limits such as (F.2) or (F.3) into the matrix elements. Therefore we need only concentrate on an expression for a.

When we now take the collinear limit we will have elimated all the double poles in s_{34} in the matrix elements. Therefore in order to derive an expression for a in terms of these variables we are able to neglect further terms of order s_{34}. We first note that we have $\alpha = E_{34} + \mathcal{O}(s_{34})$ and hence that,

$$\begin{aligned} y_{13} &= 2E_{34}(E_1 - b), \\ y_{23} &= 2E_{34}(E_2 + b + E_{34}), \\ y_{13} + y_{23} &= 2E_{34}E_{1234}, \end{aligned}$$

where $E_{1234}^2 = y_{123} = \frac{(y_{13}+y_{23})^2}{4E_{34}^2}$. Equation (F.1) implies that,

$$\begin{aligned} a^2 &= (E_1 - b)(E_1 + b) = \frac{y_{13}}{2E_{34}}(E_1 + b), \\ a^2 &= (E_2 - b - E_{34})(E_2 + b + E_{34}) \\ &= \frac{y_{23}}{2E_{34}}(E_2 - b - E_{34}) \\ &= \frac{y_{23}}{2E_{34}}(E_{1234} - (E_1 + b) - 2E_{34}). \end{aligned}$$

Combining these two equations enables one to solve for a^2, yielding,

$$a^2 = \frac{y_{12}y_{13}y_{23}}{(y_{13} + y_{23})^2}. \tag{F.5}$$

This is a general result, which in particular will also be true when 3 particles are combined to lie collinearly in the z-direction.

F.2 Three Collinear Particles

The generalization of this formalism to 3 collinear particles is straightforward. We introduce a transverse momentum p_{T_i} for each particle $i = 3, 4, 5$, which balances against the cluster of the other two. So, for example, we have,

$$\begin{aligned} p_3 &= (wE_{345}, p_{T3}\sin\phi_3, p_{T3}\cos\phi_3, wE_{345}\cos\theta_3)\,, \\ p_{(45)} &= ((1-w)E_{345}, -p_{T3}\sin\phi_3, -p_{T3}\cos\phi_3, p_{45}\cos\theta_3')\,, \end{aligned}$$

with $p_{T3} = wE_{345}\sin\theta_3 = p_{45}\sin\theta_3'$. The momentum fractions for 3, 4 and 5 are w, x and y $(= 1 - x - w)$ respectively, whilst transverse momentum conservation implies that $\sum_{i=3}^{5} p_{Ti}\cos\phi_i = 0$.

Using $s_{45} = p_{(45)}^2$ we find that, to first order in s_{45},

$$p_{45} = (1-w)E_{345} - \frac{s_{45}}{2(1-w)E_{345}}.$$

Expanding for small θ_3 and θ_3' as before we also have,

$$s_{345} = E_{345}^2 - \left(wE_{345} + p_{45} - \frac{1}{2}p_{T3}\Theta_3\right)^2,$$

where the opening angle $\Theta_3 = \theta_3 + \theta_3'$ is given by,

$$\Theta_3 = \frac{p_{T3}}{wE_{345}} + \frac{p_{T3}}{p_{45}} = \frac{p_{T3}}{w(1-w)E_{345}} + \mathcal{O}(s_{45}).$$

Combining these two equations yields the identity,

$$p_{T3}^2 = w\left((1-w)s_{345} - s_{45}\right). \tag{F.6}$$

We must now relate the 5-particle variables to the 3-particle ones, in analogy to the reduction from 4 to 3 particles in the single unresolved case. These identities are easily obtained and we find, for example,

$$\begin{aligned} s_{13} &= 2p_1\cdot p_3 = 2wE_1E_{345} - 2ap_{T3}\cos\phi_3, \\ y_{13} &= (p_1 + p_{345})^2 = 2p_1\cdot p_{(345)} + s_{345} = 2E_1E_{345} + s_{345}. \end{aligned}$$

When we now take the double unresolved limit of the 5 parton matrix elements we may employ the substitutions,

$$\begin{aligned} s_{13} &= w(y_{13} - s_{345}) - 2ap_{T3}\cos\phi_3, \\ s_{23} &= w(y_{23} - s_{345}) + 2ap_{T3}\cos\phi_3, \end{aligned}$$

where we have here neglected terms proportional to b from the outset.

Bibliography

[1] M. Gell-Mann, Phys. Lett. **8** (1964) 412;
G. Zweig, CERN preprint TH-401.

[2] The SLAC-MIT experiments are reviewed in J. I. Friedman, H. W. Kendall and R. E. Taylor, Rev. Mod. Phys. **63** (1991) 573.

[3] L. D. Faddeev and V. N. Popov, Phys. Lett. **B25** (1967) 29.

[4] W. J. Stirling, 'α_S: From DIS to LEP', DTP-97-80, hep-ph/9709429.

[5] P. M. Stevenson, Phys. Rev. **D23** (1981) 2916.

[6] G. Grunberg, Phys. Lett. **B95** (1980) 70;
G. Grunberg, Phys. Rev. **D29** (1984) 2315.

[7] C. J. Maxwell and J. A. Nicholls, Phys. Lett. **B213** (1988) 217;
J. Chýla, A. Kataev and S. Larin, Phys. Lett. **B267** (1991) 269.

[8] JADE collaboration, S. Bethke et al., Phys. Lett. **B213** (1988) 235.

[9] S. Catani, Yu. L. Dokshitzer, M. Olsson, G. Turnock and B. R. Webber, Phys. Lett. **B269** (1991) 432.

[10] S. Bethke, Z. Kunszt, D. E. Soper and W. J. Stirling, Nucl. Phys. **B370** (1992) 310.

[11] Ya. I. Azimov, Yu. L. Dokshitzer, V. A. Khoze and S. I. Troyan, Phys. Lett. **B165** (1985) 147; Zeit. Phys. **C27** (1985) 65.

[12] F. Bloch and A. Nordsieck, Phys. Rev. **52** (1937) 54.

[13] T. Kinoshita, J. Math. Phys. **3** (1962) 650;
T.D. Lee and M. Nauenberg, Phys. Rev. **133** (1964) 1549.

[14] G. 't Hooft and M. Veltman, Nucl. Phys. **B44** (1972) 189;
C.G. Bollini and J.J. Giambiagi, Phys. Lett. **40B** (1972) 566;
J.F. Ashmore, Nuovo Cim. Lett. **4** (1972) 289;
G.M. Cicuta and E. Montaldi, Nuovo Cim. Lett. **4** (1972) 329.

[15] G. Altarelli and G. Parisi, Nucl. Phys. **B126** (1977) 298.

[16] Z. Kunszt and D. E. Soper, Phys. Rev. **D46** (1992) 196.

[17] R. K. Ellis, D. A. Ross and A. E. Terrano, Nucl. Phys. **B178** (1981) 421.

[18] S. Frixione, Z. Kunszt and A. Signer, Nucl. Phys. **B467** (1996) 399;
S. Catani and M.H. Seymour, Nucl. Phys. **B485** (1997) 291;
Z. Nagy and Z. Trócsányi, Nucl. Phys. **B486** (1997) 189.

[19] S. Catani and M.H. Seymour, Phys. Lett. **B378** (1996) 287; Nucl. Phys. **B485** (1997) 291.

[20] K. Fabricius, I. Schmitt, G. Kramer and G. Schierholz, Z. Phys. **C11** (1981) 315.

[21] W. T. Giele and E. W. N. Glover, Phys. Rev. **D46** (1992) 1980.

[22] R. Barate et al., ALEPH Collaboration, Phys. Rep. **294** (1998) 1.

[23] G. R. Farrar, 'Experimental and Cosmological Implications of Light Gauginos', RU-97-82, hep-ph/9710395.

[24] R. Akers et al., OPAL Collaboration, Z. Phys. **C65** (1995) 367.

[25] Z. Nagy and Z. Trócsányi, hep-ph/9712385.

[26] L. M. Brown and R. P. Feynman, Phys. Rev. **85** (1952) 231;
G. Passarino and M. Veltman, Nucl. Phys. **B160** (1979) 151.

[27] Z. Bern, L. Dixon and D. A. Kosower, Nucl. Phys. **B412** (1994) 751.

[28] Z. Bern, L. Dixon and D. A. Kosower, Phys. Lett. **B302** (1993) 299, *ibid* **B318** (1993) 649.

[29] G.J. van Oldenborgh and J.A.M. Vermaseren, Z. Phys. **C46** (1990) 425.

[30] R. K. Ellis, W. T. Giele and E. Yehudai, private communication.

[31] A. Signer, Ph.D. thesis, 'Helicity method for next-to-leading order corrections in QCD', ETH Zurich (1995).

[32] A. I. Davydychev, Phys. Lett. **B263** (1991) 107.

[33] O. V. Tarasov, Phys. Rev. **D54** (1996) 6479.

[34] R. G. Stuart, Comp. Phys. Comm. **56** (1988) 367.

[35] G. 't Hooft and M. Veltman, Nucl. Phys. **B153** (1979) 365.

[36] Z. Bern, L. Dixon and D. A. Kosower, Phys. Rev. Lett. **70** (1993) 2677.

[37] Z. Bern, L. Dixon and D. A. Kosower, Nucl. Phys. **B437** (1995) 259.

[38] Z. Kunszt, A. Signer and Z. Trocsanyi, Nucl. Phys. **B411** (1994) 397.

[39] D. Kreimer, Int. J. Mod. Phys. **A8** (1993) 1797;
A. Davydychev, J. Phys. **A25** (1992) 5587.

[40] G. P. Lepage, J. Comp. Phys. **27** (1978) 192.

[41] D.B. Melrose, Il Nuovo Cimento, **40A** (1965) 181;
W. van Neerven and J.A.M. Vermaseren, Phys. Lett. **B137** (1984) 241.

[42] Z. Bern, L. Dixon and D. A. Kosower, Nucl. Phys. Proc. Suppl. **51C** (1996) 243.

[43] Z. Bern, L. Dixon and D. A. Kosower, Nucl. Phys. **B513** (1998) 3.

[44] Z. Bern, L. Dixon, D. A. Kosower and S. Weinzierl, Nucl. Phys. **B489** (1997) 3.

[45] E. W. N. Glover and D. J. Miller, Phys. Lett. **B396** (1997) 257.

[46] H. M. Georgi et al, Annals of Physics **114** (1978) 273;
B. L. Combridge, Nucl. Phys. **B151** (1979) 429.

[47] J. A. M. Vermaseren, Symbolic Manipulation with FORM, CAN, Amsterdam, 1991.

[48] A. Signer, Phys. Lett. **B357** (1995) 204.

[49] L. Dixon, private communication.

[50] J.E. Paton and H.-M. Chan, Nucl. Phys. **B10** (1969) 519;
P. Cvitanovic, P.G. Lauwers and P.N. Scharbach, Nucl. Phys. **B186** (1981) 165;
F.A. Berends and W.T. Giele, Nucl. Phys. **B294** (1987) 700;
D.A. Kosower, B.-H. Lee and V.P. Nair, Phys. Lett. **B201** (1988) 85;
M. Mangano, S. Parke and Z. Xu, Nucl. Phys. **B298** (1988) 653;
M. Mangano, Nucl. Phys. **B309** (1988) 461;
D. Zeppenfeld, Int. J. Mod. Phys. **A3** (1988) 2175.

[51] L. Dixon and A. Signer, Phys. Rev. D. **56** (1997) 4031.

[52] D. Kosower, Phys. Rev. **D57** (1998) 5410.

[53] Z. Kunszt, P. Nason, G. Marchesini and B.R. Webber, in *Z Physics at LEP 1*, vol. 1, ed. G. Altarelli, R. Kleiss and C. Verzegnassi, CERN Yellow Report 89-08.

[54] See for example, M. Schmelling, Proc. 28th International Conference on High Energy Physics, Warsaw, Poland, July 1996, Eds. Z. Ajduk and A.K. Wroblewski, World Scientific 1997, p91.

[55] P.A. Movilla Fernández, O. Biebel, S. Bethke, S. Kluth, P. Pfeifenschneider and the JADE Collaboration, Eur. Phys. J. **C1** (1998) 461;
J. M. Campbell, E. W. N. Glover and C. J. Maxwell, 'Determination of $\Lambda^{(5)}_{\overline{MS}}$ from the measured energy dependence of $< 1 - \text{Thrust} >$', DTP/98/08.

[56] A. Signer and L. Dixon, Phys. Rev. Lett. **78** (1997) 811;
A. Signer, Comput. Phys. Comm. **106** (1997) 125;
A. Signer, hep-ph/9705218, to appear in Proceedings of Moriond: QCD and High-Energy Hadronic Interactions, March 1997.

[57] Z. Nagy and Z. Trócsányi, Phys. Rev. Lett. **79** (1997) 3604.

[58] Z. Nagy and Z. Trócsányi, Nucl. Phys. B, Proc. Suppl. **64** (1998) 63.

[59] P. Abreu et al, DELPHI Collaboration, Z. Phys. **C73** (1996) 11.

[60] Z. Bern, J. S. Rozowsky and B. Yan, Phys. Lett **B401** (1997) 273.

[61] N. I. Ussyukina, talk given at 12th International Workshop on Quantum Field Theory (QFTHEP97), Samara, Russia, Sep. 1997, hep-ph/9801261.

[62] Z. Bern, G. Chalmers, L. Dixon, and D.A. Kosower, Phys. Rev. Letts. **72** (1994) 2134;
Z. Bern, L. Dixon, D.C. Dunbar and D.A. Kosower, Nucl. Phys. **B425** (1994) 217;
Z. Bern, L. Dixon, and D.A. Kosower, Nucl. Phys. **B437** (1995) 259;
Z. Bern and G. Chalmers, Nucl. Phys. **B447** (1995) 465.

[63] F.A. Berends and W.T. Giele, Nucl. Phys. **B313** (1989) 595.

[64] J. Kalinowski, K. Konishi and T.R. Taylor, Nucl. Phys. **B181** (1981) 221, Nucl. Phys. **B181** (1981) 253.

[65] K. Kato and T. Munehisa, Comput. Phys. Commun. **64** (1991) 67.

[66] F.A. Berends and W.T. Giele, Nucl. Phys. **B306** (1988) 759;
W.T. Giele, Ph. D. Thesis, University of Leiden (1989).

[67] I. G. Knowles, Nucl. Phys. **B304** (1988) 767.

[68] A. Gehrmann-De Ridder and E. W. N. Glover, Nucl. Phys. **B517** (1998) 269.

[69] S. Catani, Proceedings of Workshop on 'New Techniques for Calculating Higher Order QCD Corrections', preprint ETH-TH/93-01, Zurich (1992).

[70] K. Hagiwara and D. Zeppenfeld, Nucl. Phys. **B313** (1989) 560;
F. A. Berends, W. T. Giele and H. Kuijf, Nucl. Phys. **B321** (1989) 39;
N. K. Falk, D. Graudenz and G. Kramer, Nucl. Phys. **B328** (1989) 317.

[71] E. W. N. Glover and M. R. Sutton, Phys. Lett. **B342** (1995) 375.